EFHD2 AS A PUTATIVE MODULATOR OF TAU PATHOLOGY

By

Ahlam Soliman Soliman

A DISSERTATION

Submitted to
Michigan State University
in partial fulfillment of the requirements
for the degree of

Neuroscience—Doctor of Philosophy

2024

ABSTRACT

Understanding the pathomechanisms that lead to accumulative protein aggregation in neurodegenerative disorders poses a major challenge in the field. Tauopathies are no exception. Tauopathies encompass a large, diverse group of neurodegenerative disorders characterized by the aberrant aggregation and accumulation of tau protein, the eponym of these conditions, in the brain. Alzheimer's disease (AD) represents the most common tauopathy and the leading cause of dementia worldwide. Other tauopathies include progressive supranuclear palsy, corticobasal degeneration, chronic traumatic encephalopathy, and frontotemporal dementia. Although abnormal tau aggregates unify all tauopathies as the major pathological hallmark, they markedly differ in the affected brain regions, cellular lesions, type of tau aggregates, and, hence, clinical presentations. Pathologically, tau undergoes aberrant conformations and folding promoting its aggregation into dimeric, trimeric, and oligomeric structures. Oligomeric tau aggregates further form filaments that ultimately coalesce into higher order ultrastructure e.g., neurofibrillary tangles in AD. Mounting evidence has confirmed that the accumulation of early pretangle oligomeric tau push neurons over the precipice to toxicity. On the other hand, the formation of neurofibrillary tangles may indicate a neuroprotective pathway against cellular demise. Indeed, demystifying the molecular mechanisms that underlie abnormal sequential aggregation events of tau is paramount to develop effective therapeutic strategies.

Extensive research over the years has pinpointed some factors that could play a role in the biogenesis of pathological tau aggregates. Tau-related factors such as post-translational modifications, mutations, and truncations are proposed to potentially impact pathological tau aggregation. Furthermore, a growing interest has been directed to investigate tau-interacting proteins and the role they play in the pathological trajectory. Some tau interactors may induce the accumulation of oligomeric aggregates whereas others inhibit tau aggregation. Our group discovered EFhd2 as a tau-associated protein in a transgenic model of tauopathy and postmortem tauopathy brains. EFhd2 is a calcium-binding protein that is highly expressed in the central nervous system. Still, the physiological function of EFhd2 in the brain remains poorly understood. Through several studies, we showed that EFhd2 interacts with tau and promotes its aggregation by altering its dynamic properties *in vitro*. Based on our previous findings, a follow-up question that remains unanswered is "What is the role of EFhd2 in tau pathology?"

Herein, we utilized a multidisciplinary approach to answer that question. In particular, we first examined the impact of the recombinant human EFhd2 on monomeric and filamentous recombinant human tau *in vitro* (Chapter Two). The most striking observation was the ability of EFhd2 to entangle *in vitro*-formed tau filaments into larger aggregates without influencing filament formation. It is important to note that this key observation has not been reported for other tau-interacting proteins. Furthermore, using mass spectrometry analysis, we investigated proteome changes in the brain of our novel *Efhd2*$^{-/-}$ mouse model (Chapter Three). Hence, we determined the biological pathways mostly affected by the absence of EFhd2 highlighting the potential physiological significance of EFhd2 in the brain. In the same study, we explored the unstudied brain EFhd2 interactome. Indeed, EFhd2 interactome network and proteome changes in *Efhd2*$^{-/-}$ mice brain underscore the possible, indirect role of EFhd2 in tau pathology and other neurodegenerative diseases. Lastly, we examined the impact of deleting *Efhd2* gene *in vivo* on the progressive pathological phenotype and neuropathological changes of tau in Tau$_{P301L}$ expressing mice by developing the Tau$_{P301L}$/*Efhd2*$^{-/-}$ mouse model (Chapter Four). The results revealed that the absence of EFhd2 induced a moderate-large increase in pretangle oligomeric tau conformations accompanied by a reduction in later tangle markers.

In conclusion, those three interconnected studies complement our previous findings on the association of EFhd2 with tauopathies. The presented data provide cogent evidence to the ability of EFhd2 to modulate the biogenesis of tau aggregates promoting the formation of higher order tangle structures. Moreover, we gained new insights into the possible, multifaceted role of EFhd2 in neurodegeneration, provoking a number of future studies. In essence, this research lays the groundwork to determine the significance of EFhd2 as a therapeutic and/or diagnostic target in neurological disorders, especially tauopathies.

In memory of my late father, whom I wish could be with me now.
For my mother, whose abiding support and encouragement are the reason I am who I am.
For my husband, Mohammed, whose love and care have been the safe harbor for me.
For my beloved son, Malek, who brings joy and sparkle to my life.

ACKNOWLEDGEMENTS

First and foremost, I want to say that all Thanks and Praise are due to Allah Almighty for all His Blessings. Nothing would have been possible without Allah's Support.

A heartfelt gratitude and appreciation go to my major advisor, Dr. Irving Vega. I am thankful to Allah for the opportunity to receive my doctoral training under Dr. Vega's supervision. Not only is Dr. Vega my PhD advisor, but he is also my mentor and educator. It is truly challenging to distill the past four and a half years into a few lines. Indeed, Dr. Vega never alienates himself or his success from my success and achievements. On the contrary, in every action and every gesture, he consistently conveys a clear message: "We are one team having the same vision. I do care about your future as much as I care about mine." This environment undoubtedly has fostered my sense of belonging and motivation to do more. Importantly, Dr. Vega's meritorious mentorship consists in encouraging and advising me to shine and accomplish, using my strengths and embracing my weaknesses without feeling obliged to follow his way. While facing several hardships during my PhD journey, his unwavering support and compassion profoundly lightened the burden. As a future scientist, I learned from Dr. Vega how to read the literature critically, draw conclusions, and generate testable hypotheses. Furthermore, Dr. Vega provided me with a large degree of autonomy in leading the projects, enriching me with the necessary skills for my scientific endeavor. In essence, I am not exaggerating when I say that Dr. Vega exemplifies the mentorship I strive to adopt in my future career.

I want to extend a heartfelt appreciation to my dissertation committee members: Dr. Caryl Sortwell, Dr. Scott Counts, and Dr. Margaret Caulfield. Their suggestions and feedback contributed greatly to my research. Because I tend to delve into the details, the committee consistently encouraged me to think about the big picture and envision how my research aligns with and contributes to the broader field. I am deeply grateful for their unwavering support and encouragement.

I owe immense gratitude to Andrew Umstead, our lab manager, for his continuous technical assistance. Running my experiments could have been much more daunting without his help and his efficient management for the lab resources.

Moreover, I am especially appreciative to Dr. Jared Lamp for his insightful feedback on my research. As the manager of mass spectrometry core, Dr. Lamp taught me the basics of this sophisticated technique. He provided me with the necessary resources that will serve as a

PREFACE

At the time of submission of this dissertation, two chapters had been published. Chapter Two was published in Frontiers in Neuroscience, and Chapter Three was published in the Journal of Neurochemistry. Chapter Four is being prepared for publication. Figures were prepared using Microsoft PowerPoint. All illustrations were created in Biorender.com.

TABLE OF CONTENTS

LIST OF ABBREVIATIONS

α-syn	alpha synuclein
aa	amino acid
ACN	Acetonitrile
AD	Alzheimer's disease
ALS	Amyotrophic Lateral sclerosis
AMBIC	Ammonium bicarbonate
ANOVA	Analysis of variance
ARA	Arachidonic acid
BCR	B cell receptors
BG	Basal ganglia
BS	Brainstem
C-C	Coiled coil domain
C1q	complement component q
C3	complement component 3
C3aR	C3a receptor
CAMK4	Calcium/calmodulin-dependent protein kinas IV
CBD	Corticobasal degeneration
CDK5	Cyclin-dependent kinase 5
CFC	Contextual fear conditioning
CNS	Central nervous system
CTE	Chronic traumatic encephalopathy
CTX	Cortex
DA	Dopamine
DG	Dentate gyrus
DMSO	Dimethyl sulfoxide
DPRs	Dipeptide repeats
EFhd2	EF-hand domain family member 2
EGF	Epidermal growth factor
ELISA	Enzyme-linked immunosorbent assay
EM	Electron microscopy

ER	Endoplasmic reticulum
ES	Embryonic stem cells
EWSR1	EWS RNA binding protein 1
F-actin	filamentous actin
FA	Formic acid
Fishers LSD	Fishers least significant difference
FTD	Frontotemporal dementia
FTDP-17	Frontotemporal dementia and parkinsonism linked to chromosome 17
FTLD	Frontotemporal lobar degeneration
GO	Gene ontology
GSK3β	Glycogen synthase kinase-3 beta
GST	Glutathione S transferase
HCD	High-energy C-trap dissociation
hEFhd2^{WT}	Recombinant human EFhd2 wild type
hEFhd2$^{\Delta CC}$	Recombinant human EFhd2 truncated at C-terminus
hEFhd2$^{\Delta NT}$	Recombinant human EFhd2 truncated at N-terminus
HSP22	Heat shock protein 22
HSP90	Heat shock protein 90
HSPs	Heat shock proteins
hTau40	Human full-length tau
IACUC	Institutional animal care and use committee
IDP	Intrinsically disordered protein
IF	Immunofluorescence
IP	Immunoprecipitation
LB	Lewi bodies
LFQ	Label-free quantification
LLPS	Liquid-liquid phase separation
LPS	Lipopolysaccharide
LRP1	Low-density lipoprotein receptor–related protein 1
LRRK2	Leucine-rich repeat kinase 2
MIS	Motor impairment score

MS	Tandem mass spectrometry
MT	Microtubule
MTBP	Microtubule-binding protein
MTBR	Microtubule-binding repeat
NAc	Nucleus accumbens
NEM	N-ethylmaleimide
NF-κB	Nuclear factor kappa B
NFTs	Neurofibrillary tangles
NS	Nesting score
OGT	O-GlcNAc Transferase
PAD	Phosphatase activating domain
PD	Parkinson's disease
PFC	Prefrontal cortex
PHFs	Paired helical filaments
PiD	Pick's disease
PINK1	PTEN-induced kinase 1
PKA	cAMP-dependent protein kinase
PLCγ	Phospholipase C gamma
PMSF	Phenylmethylsulfonyl fluoride
PP1	Protein phosphatase 1
PPI	protein-protein interaction
ppm	Parts per million
PRM	Parallel reaction monitoring
PSP	Progressive supranuclear palsy
PTMs	Post-translational modifications
RBPs	RNA-binding proteins
RF	Radio frequency
RM-ANOVA	Repeated measures analysis of variance
SDS	Sodium dodecyl sulfate
sELISA	Sandwich enzyme-linked immunosorbent assay
SEM	Standard error of the mean

SLP-65	SH2 domain-containing leukocyte adaptor protein of 65 kDa
SNARE	SNAP receptor
SNP	Single-nucleotide polymorphism
SNpc	Substantia nigra pars compacta
SOD1	Superoxide dismutase 1
SWR	Swiss Webster mice
Syk	Spleen tyrosine kinase
TBS	Tris-buffered saline
TBST-T	Tris-buffered saline plus tween 20
TEM	Transmission electron microscopy
TET	Ten-eleven translocation
ThS	Thioflavin S
TIA1	T-cell intracellular antigen 1
tMS	Targeted mass spectrometry
TNFα	Tumor Necrosis Factor alpha
TNFR	Tumor necrosis factor receptor
TOC1	Tau Oligomeric Complex Antibody
TRAP1	Tumor necrosis factor receptor-associated protein 1
TRiC	T-complex protein 1-Ring complex
UPS	Ubiquitin/proteasome system
VTA	Ventral tegmental area

Chapter One: Introduction

Abstract

Tauopathies are a diverse group of neurodegenerative disorders, and Alzheimer's disease is the most common thereof. As the name implies, tauopathies overlap in the abnormal conformations, folding, and accumulation of tau protein. However, this group of diseases are strikingly diverse with respect to brain regions, cellular lesions, and type of tau aggregates, and, hence, clinical presentations. Over the past three decades, a litany of published studies has been focusing on demystifying the molecular mechanisms that underlie abnormal tau aggregation and subsequent pathology. Admittedly, advances in neurobiology have revolutionized the current understanding of the physicochemical properties of tau, its potential physiological functions, and its pathological changes, but the intricacies that associate with progressive tau accumulation still pose a long-standing challenge. Extensive research over the years has pinpointed some factors that could play a role in tau pathology. However, how these factors initiate, sustain, or inhibit aberrant tau folding and aggregation still elude the scientists. Knowing this is indispensable to develop effective therapeutic approaches for tauopathies. The past decade has witnessed a surge of interest to investigate the role of tau-interacting proteins in pathology. Among those proteins, EFhd2, a calcium-binding protein, is associated with tau *in vitro* and *in vivo*. Our lab conducted a series of studies to examine the interplay between EFhd2 and tau. As such, the overarching research question addressed in this dissertation research is "What is the role of EFhd2 in tau pathology?"

In this chapter, I intend to give a comprehensive, yet brief, literature review on the cumulative knowledge garnered over years about tau and its pathology, highlighting the scientific premise that undergirds my research. The first section is dedicated to providing an overview on tau, including its known physiological functions and pathological implications. In the second section, I conducted a detailed literature review on EFhd2 as a relatively novel tau-associated protein. The chapter will be concluded by the framework and structure of the dissertation research.

Tau protein

Human tau is expressed by *MAPT* gene on chromosome 17q21 (Neve et al., 1986). The gene consists of 16 exons, including 10 exons with constitutive expression (Figure 1.1A). Alternative splicing at exons 2, 3, and 10 generates 6 isoforms of tau protein (352-441 aa) as shown in Figure 1.1A and 1.1B (Wang & Mandelkow, 2016). Exons 2 and 3 encode an N-terminus 29 amino acid (aa) insert each. Hence, by alternative splicing, tau isoforms are formed with either 0N (lack N-terminus inserts), 1N (29 aa N-terminus insert), or 2N (58 aa N-terminus insert) (Figure 1.1B). Likewise, alternative splicing of exon 10 yields tau isoforms comprising either 3 tandem repeats (3R) or 4 tandem repeats (4R) (Figure 1.1B) (Wang & Mandelkow, 2016). Although, physiologically, both 3R and 4R isoforms exist at equivalent ratio in the adult human brain, the fetal brain expresses only the 0N3R isoform (Wang & Mandelkow, 2016).

Figure 1.1B demonstrates the main domains of the longest tau isoform 2N4R that is composed of 441 aa. The two major domains of tau protein are the projection domain and the microtubule-binding domain (Kolarova et al., 2012; Wang & Mandelkow, 2016). The projection domain comprises the N-terminus and the following proline-rich region. On the other hand, microtubule-binding domain spans the tandem repeats (also called microtubule binding repeats, MTBRs) R1-R4 and the C-terminus region (Kolarova et al., 2012; Wang & Mandelkow, 2016). In addition to the 6 tau isoforms in the brain, another tau isoform that is exclusively expressed in the peripheral nervous system called big tau (Fischer, 2023). As yet, this tau isoform has been reported in mice and rat nervous systems with inconclusive evidence for its existence in humans. As the name implies, it is formed by expressing the extra exon 4a, thereby adding 240 aa. Big tau has a higher molecular weight (110 kDa) as opposed to brain tau which is 45-60 kDa (Cleveland et al., 1977a; Fischer, 2023). Despite the considerable progress that has been made, still little is known about the physiological and biological role of big tau.

A recent study has reported a new tau isoform specifically expressed in the human brain; w-Tau isoform (Garcia-Escudero et al., 2021; Cuadros et al., 2022) (Figure 1.1C). This isoform is generated by a unique splicing event that retains intron 12 and excludes exon 13 (Figure 1.1C). As a result, w-Tau protein includes 18 aa residues that correspond to the retained intron 12 as its C-terminal region. In contrast to the rest of the human tau sequence, the 18-residue sequence contains two tryptophan (W) residues, giving the new isoform its name—w-Tau. According to García-Escudero, et al, w-Tau exhibits lower abundance in the brain compared to other tau

isoforms (Garcia-Escudero et al., 2021). Ongoing effort focuses on establishing the physiological and pathological relevance of this newfound tau isoform. Chiefly, w-Tau is less prone to aggregate; a key feature that strongly pertains to tau-mediated neurodegeneration covered in the following sections (Cuadros et al., 2022).
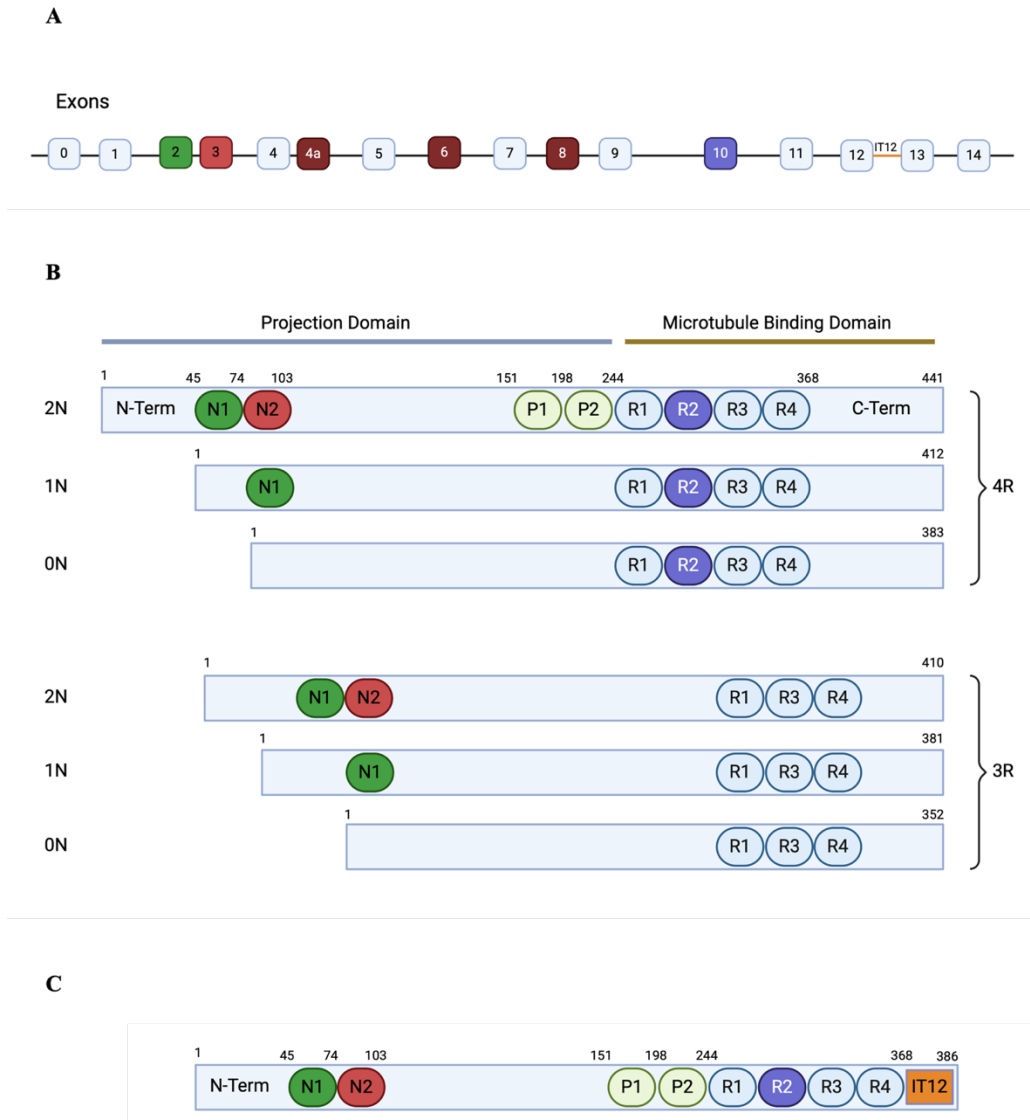
Figure 1.1. Human *MAPT* gene and tau protein splice isoforms. **(A)** The human *MAPT* gene consists of 16 exons. Exons 1, 4, 5, 7, 9, 11, 12, and 13 are constitutive. Exon 0 is part of the promoter, whereas Exon 14 is part of the 3' untranslated region. Exons 2, 3, and 10 are subject to alternative splicing generating the main six tau isoforms. **(B)** Tau protein can be divided into two major domains: the projection domain and the microtubule binding domain. In the projection domain, the two alternatively spliced N-terminal inserts (N1, aa 45-73; N2 aa 74-103) are followed by the highly flexible proline-rich region. The proline-rich region comprises two subdomains: P1 (aa 151-198) and P2 (aa 199-243). The microtubule-binding domain includes

Figure 1.1 (cont'd)
three or four microtubule binding repeats (MTBR) (R1-R4, aa 244-368) with the C-terminal
region at the end (aa 369-441). Alternative splicing of exons 2, 3, and 10 of human *MAPT* yields
the main six tau isoforms. Inclusion or exclusion of exon 10 form 4R or 3R tau isoforms,
respectively. Each of 3R and 4R exists as three isoforms; 2N (N1 and N2), 1N (N1 only), or 0N
(neither N1 nor N2 is included). The longest tau is isoform in 4R2N (441 aa) and the shortest
isoform is 3R0N (352 aa) (Wang & Mandelkow, 2016; Alhadidy & Kanaan, 2024). **(C)**
Recently, a new tau isoform has been reported in human brains generated by retaining intron 12,
which includes a stop codon followed by a canonical polyadenylation sequence, leading to tau
truncation at this location. This isoform excludes exon 13 and retains intron 12 at its C-terminal
region. The additional 18 aa of the translated intron 12 include two tryptophan residues (W) that
do not exist elsewhere in the tau sequence. Hence, this new isoform attained its name as w-Tau
(Garcia-Escudero et al., 2021; Cuadros et al., 2022).

Physicochemical properties of tau

Tau is a thermostable hydrophilic protein (Weingarten et al., 1975; Cleveland et al.,
1977a; Wang & Mandelkow, 2016). Its basic characteristics emanate from the 40 C-terminus
neutral residues and 120 N-terminal acidic residues. This asymmetry in charges presumably
governs protein dynamics and folding (Wang & Mandelkow, 2016). The high content of polar
and charged residues in tau protein imparts a high degree of flexibility, which classifies tau, what
has been known as, intrinsically disordered protein (IDP) (Uversky, 2015; Wang & Mandelkow,
2016).

Historically, the lock-and-key model for proteins prevailed for a long time, which implies
that a protein adopts a unique structure and conformation to bind to a unique target to exert a
specific biological function (Uversky, 2019). That model was challenged by the discovery of
other proteins that are biologically significant, yet they do not adopt a well-defined three-
dimensional structure (Uversky, 2019; Ando, 2022). Accordingly, these proteins attained the
moniker "disordered proteins" because they deviate from their traditional well-structured
counterparts. The lack of defined secondary or tertiary structures in IDPs is ascribed to the low
informational content of its amino acid sequence forming what is known as intrinsically
disordered regions (IDRs) (Uversky, 2019; Ando, 2022). The weak intramolecular interactions
within IDRs drive the exceptional dynamic structure and multiple conformations of IDPs
(Skrabana et al., 2006; Uversky, 2015; Uversky, 2019; Ando, 2022). Thus, IDPs range from
loosely folded, partially folded, completely folded, or unfolded secondary structures.
Furthermore, target-binding residues are widely distributed in space and time (Uversky, 2019).
Such structural malleability enables IDPs to bind to a plethora of unrelated proteins in different

cellular compartments to regulate disparate biological processes (Dyson & Wright, 2005; Skrabana et al., 2006; Uversky, 2015; Uversky, 2019; Mueller et al., 2021). Moreover, the structural flexibility of IDPs is tightly controlled by post-translational modifications (PTMs), whereby protein interactions and cellular localization are regulated (Uversky, 2015; Uversky, 2019). In essence, dynamic conformations and multifunctional nature of IDPs has usurped the traditional viewpoint of "one protein-one structure-one function."

By extrapolating the aforementioned characteristics of IDPs, tau is a highly dynamic protein that lacks a well-defined secondary or tertiary structure. Nonetheless, a seminal study proposed that tau undergoes a global folding in solution, namely a hairpin paperclip structure (Jeganathan et al., 2006). The term paperclip describes the folding state of tau protein as displayed in Figure 1.2A whereby N-terminal, C-terminal, and MTBRs come in proximity to each other (Jeganathan et al., 2006). The current premise states that tau transiently adopts paperclip folding for specific interactions and functions (Kanaan et al., 2011; Mueller et al., 2021).

Additionally, tau is subject to a large array of PTMs, and phosphorylation is the most abundant thereof (Wang & Mandelkow, 2016). In particular, tau protein contains 85 phosphorylation sites (80 serine and threonine and 5 tyrosine residues) that cluster in proline-rich region and MTBRs (Wang & Mandelkow, 2016). Physiologically phosphorylated tau harbors 1-3 phosphates per molecule (Hasegawa et al., 1992; Ksiezak-Reding et al., 1992; Kopke et al., 1993; Wang & Mandelkow, 2016). A plethora of studies have verified tau phosphorylation by several kinases, such as Camk, MAPK, and PKA (Wang & Mandelkow, 2016). Other tau PTMs have garnered research attention in the past years, including acetylation, glycation, ubiquitination, and SUMOylation on lysine; O-GlcNAcylation on serine and threonine, and polyamination on glutamine (Wang & Mandelkow, 2016; Alquezar et al., 2020; Alhadidy & Kanaan, 2024). Various PTMs profiles of tau molecules presumably underpin different tau protein interactions and biological function.

The remarkable diversity of PTMs and their overlap on the same residues attest to a degree of competition or synergy among them on the single tau molecule. If we take ubiquitination as an example, it takes place on lysine residues. Other PTMs on lysine residues, such as glycation and acetylation, preclude tau ubiquitination, thereby preventing tau degradation (Alquezar et al., 2020). On the other hand, *in vitro* studies evince a cooperative manner between

some PTMs. For instance, tau SUMOylation enhanced phosphorylation of certain residues (Alquezar et al., 2020). The question remains, however, how different PTMs interplay on a single tau molecule. In other words, how different are phosphorylated and acetylated tau molecules compared to phosphorylated and SUMOylated molecules in regard to conformations, cellular localization, and interactions? We lack the tools to study the crosstalk among PTMs at the molecular level. Most of the research focuses on studying a single PTM, which does not represent physiological events. The large number of tau's PTMs dictate the presence of unique enciphered PTM codes on a single tau molecule. Each code could represent a unique conformation and function. Demystifying those codes will provide unprecedented insights into tau structures and functions.

Biological role of IDPs, including tau, has been recently associated with liquid-liquid phase separation (LLPS) (Kanaan et al., 2020; Ash et al., 2021). Cell biologists have proposed this nascent concept of phase separation to explain how the cell regulates spatial organization of complex reaction with high efficiency (Hyman et al., 2014). Cellular components are compartmentalized to membraneless structures. Large numbers of membraneless structures behave like liquid droplets of cytoplasm and nucleoplasm (Brangwynne, 2013; Hyman et al., 2014). Prototypical phase-separated molecules are nucleoli (ribosome formation), centrosome (nucleate microtubules), Cajal bodies (spliceosomes), and stress granules (stress conditions) (Brangwynne, 2013; Hyman et al., 2014). These phase-separated liquid-like ensembles control the rate of intracellular reactions by colocalizing cellular molecules at high concentration. Cellular components inside these droplets are highly dynamic and in continuous flux with cytoplasmic/nucleoplasm content (Brangwynne, 2013; Hyman et al., 2014). In fact, few *in vitro* studies have shown that tau phase separates into condensed droplets (Kanaan et al., 2020; Ash et al., 2021). Notwithstanding, the physiological significance of tau LLPS has yet to be fully resolved *in vivo*.

To summarize, the concept of "disordered proteins" emerged to contrast "ordered proteins" that adopt unique static secondary and tertiary structures. After years of laudable research, it became evident that the notion of "disorder" no longer holds water. Instead of describing them as disordered proteins, they are highly dynamic with immensely flexible structures, invoking their versatile interactions and cellular localization. However, the term of "disordered proteins" has not been jettisoned yet despite the evidence that shows otherwise.

Apropos of tau, I can hardly find a paper that does not describe it as an IDP. This term became inextricable from tau. Therefore, I believe that scientists should leverage the current knowledge of the physicochemical properties of proteins to replace IDP with a more accurate term that verily reflects the foldability and dynamicity of these proteins.
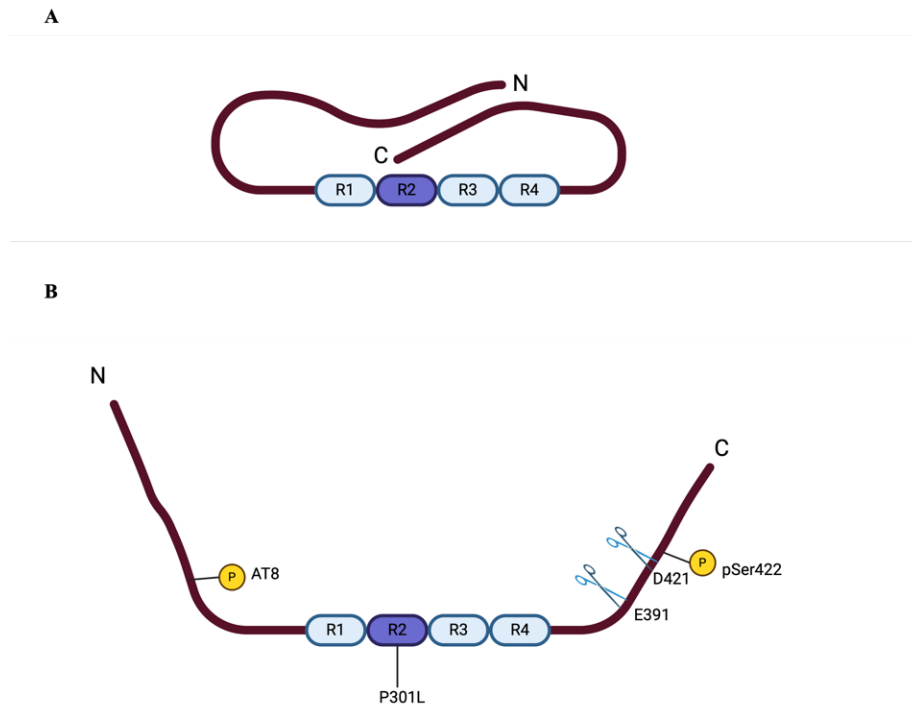
Figure 1.2. The global tau paperclip folding and the factors driving its disruption. **(A)** Tau is highly dynamic with a flexible structure that deviates from conventional proteins that adopt well-defined secondary and tertiary structures. In solution, tau can adopt a global hairpin paperclip-like conformation. In this conformation, the C-terminus folds onto MTBRS whereas the N-terminus folds back over the C-terminus. In this way, the two termini are proximal to each other. Several studies propose that tau transitions from and into paperclip conformation in a continuous dynamic fashion to exert its physiological functions, such as microtubule-mediated axonal transport (Jeganathan et al., 2006; Kanaan et al., 2011). **(B)** Research has endorsed that some molecular events could disrupt paperclip folding and, hence, perturb tau's physiological function. For instance, PTMs, including pSer199/202 (AT8) in the proline-rich region and pSer422 in the C-terminal region, have been reported to interfere with tau folding. In addition, tau truncation at E391 and D421 in the C-terminal region potentially impedes tau's dynamic folding. Several missense mutations in *MAPT* gene, such as P301L, have been reported in familial frontotemporal dementia (FTD) could also disrupt tau folding. The flexible foldability and dynamicity of tau protein are indispensable to exert its physiological functions and interact with other proteins. Therefore, when tau loses this dynamic nature (for example by the aforementioned factors) and adopts a static conformation, it becomes prone to aggregation, promoting subsequent loss-of-function- and gain-of-function-mediated neurotoxicity (Berry et al., 2003; Jeganathan et al., 2008; Wang & Mandelkow, 2016).

Known physiological functions of tau

Tau was first discovered as a microtubule-binding protein (MTBP) in 1975 (Weingarten et al., 1975). In this original study, tau was purified from porcine brain tubulin. Later, tau was proven to enhance tubulin polymerization and microtubule (MT) assembly (Weingarten et al., 1975; Cleveland et al., 1977a, 1977b). Thereafter, tau has been widely propagated as microtubule-binding protein to the extent that microtubule stabilization was deemed the sole function of brain tau.

Tau stabilizes neuronal MT by binding to the interface between α-and β-tubulin heterodimers through MTBR and the intervening dynamic regions (Kadavath et al., 2015; Wang & Mandelkow, 2016). Although it is not yet fully clear how tau impacts tubulin polymerization, earlier research has verified that tau probably nucleates and elongates tubulin for MT assembly and not necessarily exert bundling effect (Gustke et al., 1994). Moreover, the emerging concept of tau LLPS provided the impetus to examine whether phase-separated tau is essential for MT stabilization. In Hernández-Vega, et al, they showed that when tau phase separates into liquid droplets, tubulin partitions in those droplets (Hernandez-Vega et al., 2017). Hence, locally increased tubulin concentration in these droplets facilitates its nucleation to form MT bundles.

For a long time, tau has been described as an axonal protein whose sole function is regulating MT dynamics (Kanaan, 2024). This long-standing perception was fortified by spurious findings from early tau characterization studies using antibodies (Binder et al., 1985). Tau phosphorylation interferes with the binding of these antibodies to their epitopes; therefore, the presence of tau in other neuronal compartments was obfuscated. Shortly afterwards, this technical artifact was identified, yet that misconception became entrenched in the field for decades derailing research to demystify other biological roles of tau (Kanaan, 2024).

As noted in the previous section, tau is a highly dynamic protein carrying a wide range of PTMs, indicating its widespread localization and various interactions. Accordingly, tau cannot be confined to "MT binding and axonal locality " (Uversky, 2015; Mueller et al., 2021). In the past decade, that misconception has been challenged with accruing knowledge derived from several studies that verified de facto distribution of tau in the axons, somatodendritic compartments, nuclei, and synapses (Papasozomenos & Binder, 1987; Kanaan & Grabinski, 2021; Robbins et al., 2021). Evolving insights maintain that tau interacts with various signaling proteins in different cellular compartments to regulates various pathways (Mueller et al., 2021; Zhang et al.,

2022). For instance, nuclear localization of tau has been validated, albeit with unclear physiological role (Camero et al., 2014; Violet et al., 2014). Nuclear tau might regulate and maintain DNA and RNA integrity (Camero et al., 2014; Violet et al., 2014). In fact, the existing literature remains inconclusive in establishing the role of tau in the nucleus.

In addition to regulating MT dynamics, axonal tau controls antero- and retrograde axonal transport by regulating dynein and kinesin (Wang & Mandelkow, 2016). Particularly, tau competes with dynein and kinesin for binding to MT, thereby reducing binding frequency, motile fraction and run length (Stamer et al., 2002). As such, tau governs cargo delivery. Additionally, tau interferes with axonal transport by reducing the number of motors that interact with cargoes (Vershinin et al., 2007). Furthermore, tau regulates kinesin-mediated anterograde transport by activating PP1-GSK3β pathway through its phosphatase activating domain (PAD) (Kanaan et al., 2011). Typically, PAD, which spans the N-terminus 2-18 aa, is not exposed when tau adopts the paperclip folding. If the paperclip opens up, PAD becomes exposed and activates PP1, which then dephosphorylates and activates GSK3β (Kanaan et al., 2011). Accordingly, active GSK3β phosphorylates kinesin motors causing cargo release. These findings attest to a dynamic transition of tau from and into paperclip folding to control anterograde transport. Although it still awaits further investigation, tau impacts axonal elongation and maturation (Caceres & Kosik, 1990; Knops et al., 1991). Particularly, overexpressing tau enhances neurite formation whereas tau knock down inhibits neurite growth.

The tau knockout (TKO) model has been a valuable approach to determine the role of synaptic tau by examining the ramifications of deleting tau. It is worth noting that TKO exhibits undistinguishable phenotypic behavior or developmental irregularities compared to wild type (Harada et al., 1994). Adult hippocampal neurogenesis was impaired in TKO (Fuster-Matanzo et al., 2009; Hong et al., 2010). In addition, two studies reported contrasting outcome of the absence of tau on the hippocampal long-term potentiation and long-term depression (LTP and LTD) in TKO (Ahmed et al., 2014; Kimura et al., 2014). The discrepant results could be attributed to several technical factors; nevertheless, that should not undermine tau's role in synaptic plasticity. Emerging perspective about the biological role of synaptic tau derives from studying tau-interacting proteins (Robbins et al., 2021). Further studies are required to establish the physiological significance of synaptic tau.

Not only is tau a neuronal protein, but it is also expressed in oligodendrocytes and at low levels in astrocytes (LoPresti, 2002; Kubo et al., 2019). Hitherto, no reports have evinced microglial expression for tau. The physiological relevance of tau expression in glial cells has yet to be uncovered.

Tau in pathology

A common feature among highly dynamic proteins is that when they are dysregulated, they lose their structural flexibility and form more ordered, less dynamic structures and aggregates, precipitating a sequela of pathological events (Uversky, 2015). Aberrant accumulation of aggregated proteins is pathognomonic to neurodegenerative diseases that are described as proteinopathies. In this vein, abnormal tau aggregation is the major hallmark in a group of neurological disorders named tauopathies (Sexton et al., 2022). To date, there are around 25 diseases described as tauopathies (Sexton et al., 2022). Despite the common pathological hallmark—tau—tauopathies are a heterogenous group of brain disorders that greatly vary in impacted brain regions, cell types, tau lesions, and, naturally, clinical symptoms (Chung et al., 2021; Sexton et al., 2022).

Alzheimer's disease (AD) is the quintessential tauopathy that was first reported by Dr. Alois Alzheimer describing its primary pathological hallmarks—extracellular amyloid plaques and intracellular neurofibrillary tangles (NFTs) that will be discussed in detail in the next few paragraphs (Alzheimer et al., 1995). The composition of NFTs remained enigmatic for decades until researchers determined that NFTs are indeed formed of paired helical filaments (PHFs) (Kidd, 1963; Terry, 1963). After the discovery of tau in 1975 (Weingarten et al., 1975), several eminent research groups identified tau as the main component of PHFs (Brion et al., 1985; Wood et al., 1986; Goedert et al., 1988; Wischik et al., 1988a; Wischik et al., 1988b). From that time onward, tau has become pivotal in AD-related research to demystify its structure, biological role, and, essentially, factors driving its abnormal aggregation in the brain.

Broadly, tauopathies are classified as primary and secondary based on whether abnormal tau aggregation is the main driver of pathology or not (Chung et al., 2021). Also, tauopathies can be classified according to tau isoforms involved in pathology (3R vs 4R).

Primary Tauopathies

Frontotemporal dementia (FTD) is the major class of primary tauopathies wherein tau is the primary pathological perpetrator. FTD is an inclusive term for a number sporadic and

familial tauopathies that overlap in the progressive neuronal loss in frontal and temporal lobes along with differences in clinical symptoms, tau lesions, and affected cells (Chung et al., 2021).

Pick's disease (PiD)

It is a sporadic 3R FTD with mostly language deterioration and personality and memory disorders. Tau pathology can be detected mainly in the anterior frontal and temporal lobes and medial and inferior temporal cortex (Chung et al., 2021). In addition, PiD is characterized by unique tau lesions called pick's bodies in addition to pick cells detected as ballooned neurons (Combs & Kanaan, 2017). Of note, tau lesions spatially correlate with clinical presentation and neuronal loss (Chung et al., 2021).

Progressive supranuclear palsy (PSP)

It is also referred to as atypical parkinsonism because patients suffer from gait and postural instabilities and oculomotor dysfunction. PSP is a rare sporadic 4R FTD with tau lesions pervading basal ganglia, substantia nigra, and thalamus with overt neuronal loss (Chung et al., 2021). Tau lesions are detected in neurons and glia. Neuronal tau aggregates appear as globose NFTs whereas glial tau aggregates constitute tufted astrocytes and oligodendroglial coiled bodies (Combs & Kanaan, 2017).

Corticobasal degeneration (CBD)

Like PSP, CBD is a rare sporadic 4R atypical parkinsonian FTD. As its name implies, neuronal loss and tau accumulation predominantly impacts cerebral cortex and basal ganglia. CBD patients develop impaired executive skills, unstable movement, parkinsonism, and deteriorated language (Chung et al., 2021). Histologically, tau lesions formed as astrocytes annular clusters of astrocytic processes in addition to astrocytic plaques (Combs & Kanaan, 2017; Chung et al., 2021).

Frontotemporal dementia and parkinsonism linked to chromosome 17 (FTDP-17)

This is a familial FTD caused by autosomal dominant mutations in *MAPT* gene (Goedert & Jakes, 2005; Strang et al., 2019). FTDP-17 are primarily characterized by motor symptoms, behavioral changes, and cognitive impairment. Abnormal tau lesions formed by 3R isoform, 4R isoform, or both accumulate mostly in frontal and temporal lobes (Goedert & Jakes, 2005; Strang et al., 2019; Chung et al., 2021). Similar to other primary tauopathies, neuronal and glial tau lesions are detected in FTDP-17. Heretofore, more than 110 *MAPT* mutations have been identified some of which could be associated with PSP and CBD (Alzforum). The first reported

FTDP-17-related mutation was in 1998 when 13 families with FTDP-17 were screened (Hutton et al., 1998). In this study, 3 missense mutations were discovered (P301L, G272V, and R406W) along with 3 splicing mutations in the 5' splice site of exon 10. The majority of missense mutations cluster in the repeat domains, and they clearly change the sequence of tau protein. On the other hand, splicing mutations do not change the sequence but could change 3R/4R ratio (Hutton et al., 1998). Shortly after the initial discovery of the *MAPT* mutations, the first mutant human tau transgenic mouse was developed overexpressing P301L 0N4R tau under the control of mouse prion promoter—JNPL3 model (Lewis et al., 2001). Subsequently, more transgenic rodent models had been developed overexpressing a variety of FTDP-17- linked tau mutations. Although these models do not represent all tauopathies, they recapitulate some aspects of the common neuropathological features that could enable scientists to investigate molecular mechanisms regulating pathological progression.

Secondary tauopathies

In contrast to primary tauopathies, tau is not the primary pathological culprit in secondary tauopathies; rather, other factors equally contribute to neurodegeneration (Chung et al., 2021; Zhang et al., 2022).

Alzheimer's disease (AD)

It is the most common neurodegenerative disorder and the leading cause of dementia worldwide. AD is a sporadic 3R/4R tauopathy (Wang & Mandelkow, 2016; Chung et al., 2021). Familial early onset AD (FEOAD) is rare and constitutes less than 5% of AD cases. It is caused by fully penetrant mutations in amyloid precursor protein (*APP*), Presenilin 1 (*PS1*), and Presenilin 2 (*PS2*), which yield the 42-aa amyloid β (Aβ). Aβ is prone to fibrillar aggregation forming plaques (Tanzi, 2012). As yet, no *MAPT* mutations have been linked to AD. The principal clinical presentation of AD is incessant memory loss and cognitive impairment leading to pervasive dementia (Goedert, 1993). As the disease progresses, other domains are impaired, such as speech, judgment, and orientation (Goedert, 1993).

The major pathological features of AD are extracellular accumulation of fibrillar Aβ42 forming amyloid plaques and intracellular tau lesions. Intracellular tau lesions include NFTs (in cell bodies and apical dendrites), neuropil threads (in distal dendrites), and neuritic plaques (neurons surrounding amyloid plaques) (Goedert, 1993). Structural analysis of NFTs indicated that they are mainly composed of PHFs and fewer of straight filaments (SF) (Wood et al., 1986;

Goedert, 1993; DeTure & Dickson, 2019; Chung et al., 2021). After neurons die in the late stages, the intracellular NFTs remain as extracellular ghost tangles. Compared to other tauopathies, AD pathology does not involve glial inclusions. However, heightened gliosis and inflammation have been reported in AD (Wang et al., 2023).

The stereotypic progression of NFTs in the brain is the foundation of disease staging (Braak & Braak, 1991; Goedert, 1993). Particularly, pathology starts in the entorhinal cortex (EC) (stage I and II, unnoticed memory impairment) along with prominent neuronal loss in layer II (Gómez-Isla et al., 1996). In fact, several studies have invariably reported noticeable neurodegeneration in EC and hippocampus and synaptic loss in the early stages of AD (Heinonen et al., 1995; Gómez-Isla et al., 1996; Kordower et al., 2001; Price et al., 2001; Scheff & Price, 2006; Scheff et al., 2006; Stoub et al., 2006; Scheff et al., 2007). Likewise, cholinergic basal forebrain neurons in the nucleus basalis start to degenerate significantly in the early stages (Whitehouse et al., 1982; Pearson et al., 1983; Tagliavini & Pilleri, 1983; Mufson et al., 2000; Mufson et al., 2002). The pathology later propagates to the limbic system including hippocampus and thalamus (stage III and IV, mild cognitive impairment). Eventually, profound cognitive dysfunction in stage V and VI accompanies pathology invading isocortical regions including visual cortex. Clearly, the progressive memory loss and cognitive dysfunction correlate perfectly with the topographical progression of NFTs and neuronal loss (Goedert, 1993). On the other hand, the stereotypic progression of fibrillar Aβ deposits shows a nearly contrasting pattern compared to neurofibrillary lesions. Accordingly, AD staging does not rely on the spatial pattern of amyloid deposition as a pathological criterion (Goedert, 1993).

Chronic traumatic encephalopathy (CTE)

This is a sporadic 3R/4R tauopathy that is mainly caused by repetitive traumatic brain injuries or sub-concussions (McKee et al., 2015; McKee et al., 2023). Thus, CTE is common in contact sport players and military (McKee et al., 2015; Kanaan et al., 2016; Combs & Kanaan, 2017; Chung et al., 2021; McKee et al., 2023). Evolving insights have considered CTE as a primary tauopathy since tau is the major driver of neuropathology (Sexton et al., 2022). Pathological tau lesions accumulate in cortical, medial, and temporal lobes, which could then progress to include basal ganglia and brainstem at the sulcal depths (McKee et al., 2015; McKee et al., 2023). These tau lesions typically afflict perivascular neurons and glia. In addition, CTE patients usually develop attention and memory deficit, muscle atrophy, and speech impairment.

Unlike AD, pathological tau accumulation starts as discrete foci in cerebral cortex, which later spread to include other parts of the cortex and medial temporal lobe regions (McKee et al., 2013).

Molecular changes of tau in pathology

Despite the differences among tauopathies with respect to tau lesions, affected cells, brain regions, and symptoms, they all converge on the broad molecular changes of tau. Generally, tau aggregation follows a nucleation elongation mechanism. After losing its dynamic foldability, tau polymerizes to dimers, trimers, and oligomeric structures (Wang & Mandelkow, 2016; Chung et al., 2021). These early oligomeric forms are the rate limiting step that act as a seed recruiting and inducing conformational changes of the normal naïve protein molecules, thereby perpetuating aggregation to form filaments (Kuret et al., 2005; Wang & Mandelkow, 2016; Chung et al., 2021). These filaments further aggregate to PHFs and SF and eventually to NFTs. Decades of research have been dedicated to deciphering the sequential events of tau aggregation and the underlying factors that transition tau from physiologically dynamic protein into pathological aggregates (Kuret et al., 2005; Wang & Mandelkow, 2016; Chung et al., 2021).

Hyperphosphorylation typifies aggregated tau across all tauopathies (6-8 phosphates per molecule vs physiological 1-3 phosphate per molecule) (Hasegawa et al., 1992; Ksiezak-Reding et al., 1992; Kopke et al., 1993). In fact, phosphorylated tau was among the initial detected hallmarks in PHFs of AD (Grundke-Iqbal et al., 1986; Ihara et al., 1986). Several studies have shown that the emergence of some phosphorylated tau epitopes temporally coincides with sequential stages of tau aggregation. For instance, tau phosphorylation at Ser199/202 (AT8) and Th231 (TG-3) signify early tau oligomerization preceding tangles build up (Kanaan et al., 2011; Tiernan et al., 2016; Wang & Mandelkow, 2016). Hitherto, molecular factors that drive tau hyperphosphorylation remain unresolved. Some researchers postulated that phosphorylation sites could disrupt the normal paperclip folding and induce conformation changes, thereby enhancing aggregation (Jeganathan et al., 2008; Wang & Mandelkow, 2016) (Figure 1.2B). Furthermore, tau phosphorylation at Ser422 was demonstrated to inhibit degradation and clearance of aggregated tau by proteasome or autophagy leading to further accumulation (Guillozet-Bongaarts et al., 2006; Uversky, 2015; Wang & Mandelkow, 2016). All in all, several phosphorylation sites of tau could have a combinatorial effect on tau's aggregation-prone conformational changes.

In addition to phosphorylation, truncated tau species have been reported in tau aggregates. Tau cleavage at glutamate 391 (E391), the epitope of MN423 antibody, labels mainly later tangles and PHFs core (Guillozet-Bongaarts et al., 2005). Another cleavage event induced by caspase 3 at aspartate 421 (D421) occurs prior to MN423 (Novak et al., 1993; Guillozet-Bongaarts et al., 2005). As displayed in Figure 1.2B, tau truncation presumably disrupts paperclip folding generating tau forms with higher propensity for aggregation (Berry et al., 2003; Wang & Mandelkow, 2016).

Likewise, accumulating evidence has shown that missense *MAPT* mutations that cluster near MTBRs such as P301L and G272V (Figure 1.2B) impair tau-MT binding and possibly disrupt paperclip folding (Wang & Mandelkow, 2016; Strang et al., 2019; Kanaan et al., 2020). In essence, tau mutants intrinsically promote aberrant conformations and aggregation. It should not escape our attention that tau mutations linked to tauopathies represent a small proportion of pathological tau. Hence, they fall short of explaining the pathological events occurring in sporadic tauopathies.

I alluded earlier to the burgeoning phenomenon of tau phase separation that still awaits further research to reveal its significance *in vivo*. In the past few years, some research groups investigated the link between tau phase separation and aggregation (Wegmann et al., 2018; Kanaan et al., 2020; Ash et al., 2021). Assuming that tau phase separates to dynamic liquid-like droplets, scientists posit that certain factors could diminish dynamicity of phase-separated tau and enhance aggregation. For instance, early events like AT8 phosphorylation or P301L mutation were depicted to enhance tau phase separation forming significantly less dynamic droplets (Kanaan et al., 2020). The formation of more static structures drives oligomerization of phase-separated tau, leading to further fibrillization and filaments formation (Wegmann et al., 2018; Kanaan et al., 2020). Again, these *in vitro* findings have yet to be verified *in vivo*.

By and large, mounting evidence supports that tau undergoes several aberrant molecular events that collectively lead to transitioning into aggregation-prone conformations. These conformations promote polymerization to oligomeric structures that further seed aggregation, and ultimately form filaments and tangles. Hypothetically, a combination of PTMs and, in some cases, mutations initiate pathology-linked conformational changes instantiated by disrupted paperclip structure. Although much has been learned about tau aggregation, still more effort is

currently dedicated to unraveling the crosstalk between all these molecular changes and the upstream driving factors.

Tau-mediated neurotoxicity

The aforementioned abnormal molecular changes of tau that are associated with biogenesis of tau aggregates promote neurotoxicity through two aspects. The first one is loss-of-function-induced neurodegeneration, which is naturally imputed to the inability of tau to undertake its physiological functions discussed in the previous sections (Wang & Mandelkow, 2016). If we take phosphorylation and mutations as an example, they prevent tau binding to MT leading to dysregulated MT dynamics and, hence, impaired axonal transport (Wang & Mandelkow, 2016). Aside from MT binding, tau's pathological conformations (e.g., disrupting paperclip folding) inhibits anterograde axonal transport due to unfettered activation of PP1-GSK3b pathway (Kanaan et al., 2011). Furthermore, several studies reported declined neurite growth, synaptic dysfunction, and deteriorated neurogenesis as manifestation of tau loss-of-function neurodegeneration (Wang & Mandelkow, 2016). The second aspect of tau pathology is the toxic gain-of-function due to the formation of abnormal aggregates that could invoke neurotoxicity.

For a long time, tangles were deemed the principal perpetrator of neurodegeneration (Cowan & Mudher, 2013). This assumption stemmed from the correlation between spatial and temporal load of NFTs in the brain and the symptoms of AD. Notwithstanding, accumulating evidence has underpinned the disconnect between tangle accumulation and neurodegeneration (Cowan & Mudher, 2013). Chiefly, neuronal loss exceeds NFTs' accumulation in superior temporal sulcus by 7-fold, implying that neurons potentially could die before the formation of NFTs (Gomez-Isla et al., 1997). This observation was borne out in animal models of tauopathies (Wittmann et al., 2001; Santacruz et al., 2005; Spires et al., 2006; Sydow et al., 2011). Furthermore, tangle-bearing neurons survive for years and are functionally intact (Morsch et al., 1999; Kuchibhotla et al., 2014). Suppressing mutant tau overexpression in a mouse model halted neuronal loss without changing NFTs burden (Santacruz et al., 2005). In the same vein, neurodegeneration could take place without detectable NFTs (Wittmann et al., 2001). Collectively, these findings, along with more studies reporting similar conclusions, have challenged the widely held assumption that NFTs are the perpetrator, which prodded researchers to indict earlier pretangle tau aggregates.

A substantial body of research has indicated that early pretangle tau forms, especially pre-fibrillar oligomeric tau, could be the true precursor of neurodegeneration in tauopathies (Santacruz et al., 2005; Brunden et al., 2008; Spires-Jones et al., 2009). As explained in the previous section, tau oligomerization is a pivotal event in the early stages of tau aggregation preceding the formation of tangles (Kuret et al., 2005; Patterson et al., 2011a; Lasagna-Reeves et al., 2012). Several research groups interrogated the link between the accumulation of early oligomeric tau forms and neurodegeneration. An evident correlation between age-related cognitive deficit and oligomeric tau load before NFTs formation was reported (Berger et al., 2007). Furthermore, oligomeric tau, and not fibrillar tau forms, induced synaptic dysfunction, memory deterioration, and neuronal loss (Santacruz et al., 2005; Kayed, 2010; Lasagna-Reeves et al., 2011; Jiang et al., 2019). Moreover, oligomeric tau species induced mitochondrial dysfunction by activating apoptotic pathways (Lasagna-Reeves et al., 2011; Niewiadomska et al., 2021). With this increasing evidence, the time-honored hypothesis of NFTs-induced neurotoxicity seems untenable. More scientists now accept NFTs as benign custodians in contrast to oligomeric tau species that wield a potent influence in driving pathological progression in tauopathies.

Additional substantiation to the oligomeric tau's enhanced neurotoxicity emanates from the tenets of seeding and transcellular propagation. The molecular mechanisms underlying the stereotypical progression of tau pathology manifested as sequential spreading to brain regions are not yet clearly understood. These patterns are tally with the severity of diseases, which led to immense effort to elucidate the mechanisms involved (Braak & Braak, 1991; Brettschneider et al., 2015). The most prevailing hypothesis in the field that can explain the relentless stereotyped progression of tau pathology in the brain is seeding and transcellular propagation (Holmes & Diamond, 2014; Holmes et al., 2014; Brettschneider et al., 2015; Sala-Jarque et al., 2022). In seeded aggregation, initial aggregated tau forms recruit native tau monomers and initiate the formation of new aggregates (Holmes & Diamond, 2014; Brettschneider et al., 2015). These aggregates will then propagate to neighbor neurons or glial cells spreading the pathology to further areas (Jucker & Walker, 2013; Holmes & Diamond, 2014; Brettschneider et al., 2015). Several lines of evidence have shown that oligomeric tau exhibits more seeding capacity compared to fibrillar tau and tangles (Usenovic et al., 2015; Jiang et al., 2019; Chung et al., 2021; Zhang et al., 2021). Noteworthy studies demonstrated that tau species smaller than

oligomeric aggregates can induce seeding (Mirbaha et al., 2015; Mirbaha et al., 2018). However, the characteristics of seeding-competent tau species remain poorly understood given the technical challenges to purify specific tau forms. Broadly speaking, it is widely accepted that the notoriety of early pretangle oligomeric tau aggregates arises from their propensity to generate more pathology and propagate to further regions, which also impedes physiological tau interactions. Viewed this way, fibrillar and tangle tau aggregates could represent a safeguard that are formed inside the inflicted cells to prevent further propagation. Although several studies supported this assumption, others have shown the fibrillar tau could induce seeding response and propagation but without detectable neuronal death (Zhang et al., 2021; Sala-Jarque et al., 2022). Hence, the parsimonious model of "more seeding" is commensurate with "more neurotoxicity and neuronal death" still warrants further investigation.

Not only have scientists been examining the toxic forms of tau aggregates, but they also have been intrigued by the stark diversity among tauopathies with respect to clinical presentation, affected brain areas, and tau lesions. Such differences among tauopathies are inexplicable by sharing the same pathological protein, which attracted considerable interest. Recently, important advances have been made in investigating structural and molecular differences in tau aggregates among various tauopathies. The advent of cryo-EM has immensely contributed to unraveling the structural heterogeneity of tau aggregates. Cryo-EM analyses have revealed that the R3-R4 repeat and 12 residues after the R4 repeat region in AD, the R2-R4 repeat and 12 residues after the R4 repeat region in CBD, and the R1, R3–R4 repeat and 12 residues after R4 repeat region in PiD form the cores of the tau filaments (Fitzpatrick et al., 2017; Falcon et al., 2018a; Falcon et al., 2018b; Zhang et al., 2020). In CTE, distinct filamentous tau aggregates are formed constituting a hydrophobic cavity in the core (Falcon et al., 2019). The differences that have been identified thus far in tau aggregates attest to the presence of other various factors that interfere and drive tau aggregation. The identity of these factors is still unknown.

The insights gained thanks to cryo-EM analysis of tau aggregates yielded a number of new avenues of research to reveal the molecular determinants that govern disparate tau conformations and aggregation across tauopathies. Since aberrant PTMs are an inextricable component of tau pathology, a growing number of researchers consider that tau might bear a unique PTMs signature to each tauopathy. Presumably, this PTM signature could serve as a

passcode for tau to transition from physiological monomeric protein into a less dynamic, compactly folded, and pro-aggregant one. In addition, tauopathy-specific PTMs profile might dictate the conformation of tau aggregates. From this standpoint, several studies recently have streamlined mass spectrometry-based methodologies (MS) to compare and contrast tau PTMs among tauopathies (Arakhamia et al., 2020; Kametani et al., 2020; Kyalu Ngoie Zola et al., 2023). These experiments succeeded in showing common and unique PTMs among tauopathies. Broadly speaking, these comparative studies showed consistent results with cryo-EM analysis of tau aggregates. We cannot, however, disregard the inconsistencies among these experiments that are linked to different disease stages of tauopathies' brains and various technical approaches. In particular, using different protocols to extract low (oligomers) and high (fibrils and NFTs) molecular weight tau forms impart unavoidable discrepancies among studies. On the whole, investigating the heterogeneity in tau PTMs has provided further scientific underpinning to the molecular factors that possibly regulate the formation of different tau conformers with various pathogenicity.

Another molecular determinant of tau aggregation that has allured much attention in the past decade is tau-interacting proteins. Although the discovery of tau as a component of PHFs was a major turning point in the realm of tauopathies, particularly AD, initial observations widely suggested that NFTs are solely formed of tau filaments (Castellani et al., 2010). Hence, tau was deemed the sole driver of pathology, undermining the possible role played by other proteins. The past decade has witnessed a surge of interest towards investigating tau protein-protein interactions and their impact on the trajectory of tau pathology (Kavanagh et al., 2022). This growing interest is contemporaneous with our expanding knowledge in regard to tau biology and physicochemical properties. As noted earlier, tau is a highly dynamic protein that interacts with a plethora of proteins in order to exert its physiological functions delineated earlier. Thus, uncontrolled changes in tau interactions with other proteins is a conceivable mechanism whereby aberrant tau aggregation commences. The next section broadens the discussion about advances made lately in studying tau interactome.

Tau interacting proteins

Studying the interactome of a certain protein has become an evolving tool to explore its putative physiological function by investigating the relevant biological network (Snider et al., 2015). In addition, protein-protein interactions signify potential cellular localization.

Furthermore, interactome networks may indicate possible pathological ramifications as a result of protein's dysregulation (Snider et al., 2015). As such, studying tau interactome has lately gained currency to identify its potential interacting partners. By mapping out tau protein-protein interactions (PPI) that are linked to tau aggregation, we will have a better understanding of potential mechanisms that impact tau pathology.

Interactome studies essentially entail coimmunoprecipitation or crosslinking followed by extensive MS-based analysis and data mining to identify proteins purified with tau. In many cases gene ontology is required to classify the identified proteins into their known biological functions, thereby providing a holistic view of cellular processes and molecular pathways associated with tau.

The first large scale study that explored tau interactome was in 2015 using neuroblastoma SH-SY5Y cell line whereby the interactome of both wild type human 2N4R and P301L mutant tau was identified (Gunawardana et al., 2015). The tau interactome network was enriched in RNA-binding proteins (RBPs) , heat shock (HSPs) and proteasomal proteins. Intriguingly, tau association with HSPs and proteasomal was less pronounced with P301L tau. That might imply that P301L tau has higher propensity to aggregate and accumulate due to inefficient degradation of abnormally folded tau by HSPs and proteasomal machinery.

Since tau is subject to aberrant phosphorylation in tauopathies, a study investigated interactome network for phosphorylated tau at Ser396/404 (PHF1) extracted from AD brains (Drummond et al., 2020). Moreover, the researchers conducted localized proteomics on NFTs-bearing neurons using laser capture to microdissect AT8 positive NFTs followed by label-free quantification (LFQ) MS analysis. The results highlighted 542 proteins with abundance change, and the majority thereof are RBPs and HSPs. Among these proteins, 75 were identified in the interactome network of the PHF1 tau. The network was enriched in MTBPs, phagosomes and ubiquitin proteasome system (UPS). Of note, 34 of the identified tau-interacting proteins were also detected in the interactome network of total tau in prior studies. In addition to human tau, few studies explored endogenous rodent tau interactome using total tau antibody (P. Wang et al., 2017). The network included cytoskeletal, synaptic, HSPs, and protein degradation machinery.

Kavanagh, et al. (Kavanagh et al., 2022) elegantly summarized the main tau interactome studies since 2015. Briefly, three studies examined human tau interactome in postmortem tissues of tauopathies by target total or modified tau (Meier et al., 2015; Ayyadevara et al., 2016; Hsieh

et al., 2019; Drummond et al., 2020). In addition, three studies mapped human tau interactome whether wild type or P301L mutation in cell models (Gunawardana et al., 2015; Wang et al., 2019; Tracy et al., 2022). Furthermore, transgenic rodent models that overexpress human mutant tau were leveraged to study tau interactome (P. Wang et al., 2017; Sinsky et al., 2020). Despite the inconsistencies among these studies in regard to individual proteins, the confluence of their results highlights tau interaction with RBPs, ribosomal, cytoskeletal, proteasomal, and synaptic proteins.

   Although much has been learned about tau interactome thanks to those aforementioned studies, a fundamental question has yet to be answered; do these tau-interacting proteins influence and contribute to the biogenesis of tau aggregates and tangles? Or, alternatively, are these proteins indiscriminately sequestered to tau aggregates during pathological progression? In tandem with the great strides made towards revealing pathological tau interactome, another line of research has been devoted to interrogating the impact of individual tau-interacting proteins on its aggregation and conformational changes (Miyata et al., 2011; Patterson et al., 2011b; Voss et al., 2012; Vanderweyde et al., 2016; Apicco et al., 2018; Jiang et al., 2019; Nachman et al., 2020; Ash et al., 2021; Darling et al., 2021; Martinez et al., 2022; Rodriguez Ospina et al., 2022)

   In my dissertation project, I investigated the interplay between tau and a calcium-binding protein; EFhd2. Our lab reported the association between tau and EFhd2 in a tauopathy model and postmortem human tissues. Then we showed that EFhd2 enhanced tau aggregation *in vitro*. In the next section, I will expound on the published research of EFhd2 and its emerging role in neurodegeneration.

EF-hand domain 2 (EFhd2) protein

   EFhd2 protein is encoded by *EFHD2* gene on chromosome 1p36.21 in human and chromosome 4 (4E1;474.75cM) in mouse (Vuadens et al., 2004; Vega, 2016; Kogias et al., 2019). EFhd2 consists of 240 aa with a molecular weight of 27 kDa. Humans and mice share 91% of the EFhd2 protein sequence. First discovered in 2004 after MS-based proteome screening, EFhd2 was identified as a unique protein expressed in CD8^{+} cytotoxic T-cells compared to CD4 and CD19 (B-cells) (Vuadens et al., 2004). In this study, EFhd2 was initially named as Swip1 after Swiss Prot databases used to decipher the identity of this newfound protein. Furthermore, sequencing analysis pinpointed two EF-hand domains; a cardinal domain in all calcium-binding proteins (Nelson et al., 2002). Therefore, by detecting EFhd2 exclusively

in CD8+, this seminal study instigated a number of questions aboutits biological role, especially in T-cells and the functionality of the calcium-binding property.

As depicted in Figure 1.3, EFhd2 protein is composed of N-terminus domain which comprises a flexible region of low complexity and polyalanine (Poly-A) tail motif between 6-9 alanine residues (Avramidou et al., 2007; Kogias et al., 2019). In addition, structural analysis revealed a proline-rich region that spans 70-90 aa followed by two EF-hand domains 91-163aa. The last 50 aa constitute C-terminus coiled-coil domain (C-C) consisting of two or more α helices in parallel or antiparallel orientation and wound around each other to form regular supercoiled bundle (Liu et al., 2006; Park et al., 2016; Szczepaniak et al., 2021). Additionally, EFhd2 has a low isoelectric point with a net negative charge at neutral pH (Ferrer-Acosta et al., 2013b).

Since its discovery, a few research groups have devoted themselves to further examining EFhd2 structure and physicochemical properties as a step towards exploring its biological significance. Although more structural studies are required to deconvolute EFhd2 properties, amino acid sequence and composition, especially in the N-terminus, indicate the highly dynamic properties of EFhd2 (Dyson & Wright, 2005). Importantly, similar to tau, EFhd2 lacks a well-defined tertiary structure that hinders its crystallization. The N-terminus includes mostly helical elements, and the biological relevance of the poly-A motif is not fully understood. Furthermore, C-C domain largely characterizes amyloid proteins that have spontaneous capacity to dimerize and oligomerize and mediates protein interaction (Liu et al., 2006; Ferrer-Acosta et al., 2013a; Ferrer-Acosta et al., 2013b; Szczepaniak et al., 2021). Along similar lines, our lab showed that EFhd2 can form self-oligomeric filaments of 50-500 nm length without external aggregation inducers like heparin (Ferrer-Acosta et al., 2013b). Rather, heparin reduced EFhd2 self-oligomerization—an observation that still awaits further investigation. EFhd2 self-oligomerization was detected by Thioflavin S (ThS), which binds to β-sheet structures as a proxy to protein polymerization.

The initial structural analysis of EFhd2 confirmed the presence of two EF-hand domains that are essentially calcium-binding domains (Vuadens et al., 2004). This early observation prompted further investigation of the capacity of EFhd2 to bind to calcium and its biological significance (Vega et al., 2008; Ferrer-Acosta et al., 2013a). In the general sense, calcium-binding proteins can be categorized to either calcium sensor or calcium modulator (Ababou &

Desjarlais, 2001; Nelson et al., 2002). Calmodulin is the prototype for calcium sensors, where calcium binding induces a conformational change to recruit and bind to downstream effectors. On the other hand, calcium modulators like calbindin bind to calcium without conformational modifications, and their principal role is to regulate intracellular calcium levels (Ababou & Desjarlais, 2001; Nelson et al., 2002). In the calcium-unbound form, EFhd2 exhibits a high degree of structural flexibility. A study reported that calcium-binding to EFhd2, albeit maintaining the core structure of EF-domains, reduces local conformational flexibility and induces a structural stabilization. In other words, calcium-binding drives the formation of more compact folded EFhd2 (Park et al., 2016). By comparison, one could speculate that EFhd2 is a calcium sensor that impacts downstream calcium -mediated signaling pathways. The two calcium-binding domains of EFhd2 have equal binding affinity to calcium in molar ratio of 2 Mol of calcium per 1 Mol of EFhd2 (Hagen et al., 2012). It is postulated that EFhd2 binding to calcium is temporary, indicating that EFhd2 might respond to transient changes in intracellular calcium levels (Hagen et al., 2012). Furthermore, the presence of calcium induced a noticeable attrition in EFhd2 self-oligomerization measured by ThS signal (Ferrer-Acosta et al., 2013b). Calcium-induced conformational changes might hinder C-C domain interactions, impeding EFhd2 self-oligomerization.

Similar to tau, EFhd2 is a thermostable phosphoprotein (Ferrer-Acosta et al., 2013a). Of note, EFhd2 binding with calcium enhances its thermostability (Ferrer-Acosta et al., 2013a; Park et al., 2016). In addition, our group illustrated that CDK5 phosphorylates EFhd2 at Ser74 residue. Intriguingly, we observed that pSer74 EFhd2 exhibited less binding affinity to calcium compared to unphosphorylated EFhd2 (Vazquez-Rosa et al., 2014). Furthermore, EFhd2 is phosphorylated by EGF at Ser183 residue (Huh et al., 2015). Whether EFhd2 is subject to other PTMs is still unknown.

Figure 1.3. EFhd2 protein structure. The N-terminal region of EFhd2 includes a 6-9 polyalanine motif whose function has yet to be determined. A flexible proline-rich region (aa 70-90) is followed by the two EF-hand motifs (EF1 aa 91-127, E2 aa 128-163). The two EF-hand motifs constitute the calcium-binding domain. The two motifs exhibit an equal affinity for

Figure 1.3 (cont'd)
calcium binding. The last 50 aa are part of the C-C coiled-coil domain that characterizes a large family of amyloid proteins, mediating self-oligomerization and protein-protein interactions.

Potential physiological functions of EFhd2

Earlier studies have indicated the ubiquitous expression EFhd2 in the body. Chiefly, EFhd2 was identified in lungs, heart, immune cells, spleen, skeletal muscles, liver, and spinal cord of mice (Avramidou et al., 2007; Vega et al., 2008). However, it is more abundant in CNS; predominantly in the gray matter and mature neurons (Purohit et al., 2014). Furthermore, mouse *Ehfd2* gene is highly expressed in cortical regions, limbic system, amygdala and olfactory bulb as opposed to cerebellum and brainstem that show low lower expression levels (Vega et al., 2008; Purohit et al., 2014). In the neurons, EFhd2 is primarily located in synaptic and somatodendritic compartments in the cytoplasm and proximal to the membrane (Ferrer-Acosta et al., 2013b). Although several studies have proven EFhd2 expression in peripheral immune cells (innate and adaptive), the evidence for its glial expression is yet inconclusive.

The nearly systemic expression of the then novel protein EFhd2 and its highly dynamic properties discussed above imply that EFhd2 associates with and regulates disparate cellular processes and in different cell types. A number of investigators have shown, using *in vitro* cells and cell-free assays, that EFhd2 is linked to cell motility, apoptotic signaling, cancer metastasis, cardiac remodeling, actin organization, and other putative biological activities (Kroczek et al., 2010; Hagen et al., 2012; Huh et al., 2013; Huh et al., 2015; Tu et al., 2018; Zhang et al., 2018; Kogias et al., 2019; Giricz et al., 2020; Peng et al., 2021; Fu et al., 2024; Wu et al., 2024; Zhang et al., 2024).

Most of the early studies demonstrated EFhd2 chiefly as an actin-binding protein that regulates actin dynamics (Huh et al., 2013). These preliminary findings were generated using immune cell lines (B-, T-cells and macrophages) (Ramesh et al., 2009; Huh et al., 2013; Kwon et al., 2013; Tu et al., 2018). Subsequently, the association of EFhd2 with actin was corroborated in cancer cells and cardiac myocytes (Huh et al., 2015; Nippert et al., 2016). EFhd2 binds to actin filaments (F-actin) and enhances its bundling and organization (Huh et al., 2013; Kwon et al., 2013). In addition, EFhd2 colocalized with F-actin in cellular protrusions and lamellipodia *in vitro*, mediating cellular migration and lamellipodia formation (Ramesh et al., 2009; Huh et al., 2013; Kwon et al., 2013; Huh et al., 2015). Furthermore, C-C domain and calcium-binding activity are essential for EFhd2 bundling effect of F-actin (Kwon et al., 2013; Park et al., 2016).

It is postulated that EFhd2 enhances actin bundling by limiting cofilin access and, hence, inhibits actin depolymerization (Huh et al., 2013). Phosphorylation of EFhd2 by EGF at Ser183 impaired EFhd2-induced actin bundling (Huh et al., 2013; Park et al., 2017).

Noteworthy studies have scrutinized the physiological significance of the impact of EFhd2 on actin bundling. EFhd2 colocalized with actin filaments and promoted macrophage recruitment and migration upon stimulation *in vitro* (Tu et al., 2018). The recruitment of macrophages was inhibited by EFhd2 knock down. These results were then validated *in vivo* whereby LPS-injected mice showed augmented macrophage recruitment in lungs associated with increased EFhd2 expression (Tu et al., 2018). The data indicated that actin bundling induced by EFhd2 is necessary for macrophage recruitment. In contrast, injecting LPS to *Efhd2*$^{-/-}$ mice failed to activate and recruit macrophages (Tu et al., 2018). Taken together, these findings shed light on the potential role of EFhd2 in mediating macrophage-induced inflammatory response. A recent study has soundly interrogated EFhd2-mediated macrophage activity in post-atherosclerosis repair (Tong et al., 2021). Consistent with prior results, higher EFhd2 expression was noted in the macrophages surrounding atherosclerotic plaques in an atherosclerosis mouse model. Injecting these mice with peritoneal macrophages of *Efhd2*$^{-/-}$ mice by bone marrow transplantation resulted in alleviated atherosclerosis and promoted atherogenesis in comparison to control macrophage injection (Tong et al., 2021). The confluence of these studies attests to EFhd2 role in macrophage-mediated inflammatory response, thereby delaying repair and promoting apoptosis.

In cancer, EFhd2-mediated actin bundling promoted cancer invasion and metastasis *in vitro* (Huh et al., 2015). Overexpressing EFhd2 enhanced pulmonary metastasis *in vivo*, which was abrogated by EFhd2 knock down (Huh et al., 2015). In addition to regulating actin dynamics, in the same study EFhd2 enhanced cellular migration and metastasis by activating Rho family of small GTPases (Huh et al., 2015). The results indicated that EFhd2 might be a potential therapeutic target to halt metastasis and improve cancer prognosis. This conclusion was reinforced by a recent large scale human cancer data analysis that revealed a link between heightened EFhd2 levels and poor cancer prognosis (Peng et al., 2021).

Not only does EFhd2 regulate actin dynamics in immune cells, but also it mediates cell signaling necessary for survival and life span, especially in B-cells. Through its calcium-binding activity, EFhd2 regulated B-cell receptor (BCR)-induced calcium flux via a calcium-dependent

positive feedback mechanism *in vitro* (Hagen et al., 2012). The same research group detected increased expression levels of EFhd2 in immature B-cells, thereby mediating BCR-apoptotic signaling and regulating cell survival (Avramidou et al., 2007). Particularly, EFhd2 inhibited BCR-activated NF-κB pathway, leading to diminished levels of antiapoptotic Bcl-x (an NF-κB target protein). Accordingly, the authors concluded that EFhd2 regulates apoptosis of B-cells *in vitro*, which implies that uncontrolled increase in EFhd2 abundance may potentially reduce cell survival. Furthermore, *in vitro*, EFhd2 acts as a scaffold in the membrane raft of B-cells (Kroczek et al., 2010). It amplified BCR-induced calcium flux by inducing constitutive association of BCR, Syk, and PLCγ with membrane rafts—a required interaction for downstream signaling events.

EFhd2 and brain disorders

In addition to the above-mentioned findings regarding the role of EFhd2 in regulating actin dynamics and related cellular processes, a different line of research has revealed a strong association between EFhd2 and some psychiatric and personality disorders. Particularly, screening of postmortem brains of suicide victims showed low EFhd2 abundance in the prefrontal cortex (PFC) whereas EFhd2 was high in the amygdala (Kekesi et al., 2012). This finding instigated the practicality of using EFhd2 as a biomarker for suicidal risk. However, that has not been further investigated. Likewise, proteomic MS analysis revealed high EFhd2 levels in the mediodorsal thalamus and dorsolateral PFC of schizophrenic postmortem brains (Martins-de-Souza et al., 2009; Martins-de-Souza et al., 2010).

In essence, these early observations provided the underpinning for researchers to explore the biological role of EFhd2 in CNS wherein EFhd2 expression predominates. One approach that helped in this pursuit was developing a *Efhd2$^{-/-}$* mouse model. This model has provided insights on the physiologic function of EFhd2 in the brain by examining the ramifications of its absence—on the behavior and molecular levels.

In primary hippocampal neurons of *Efhd2$^{-/-}$* mice, enhanced kinesin-mediated MT gliding was observed (Purohit et al., 2014). In other words, EFhd2 impeded kinesin-mediated MT transport *in vitro*. That implies that EFhd2 might regulate cargo transport of neuronal MT. In addition, spine formations and dendritic growth of newborn neurons were declined in *Efhd2$^{-/-}$* mice (Regensburger et al., 2018). Similarly, *Efhd2$^{-/-}$* mice brain displayed a remarkable impairment in dendritic morphology of the adult hippocampal neurons. Furthermore, knocking

down EFhd2 in primary cultured neurons enhanced the number of synapses without noticeable change in the neurite growth (Borger et al., 2014). These results collectively provided convincing evidence that EFhd2 potentially regulates neuronal growth and morphology. In addition, synaptic EFhd2 may be necessary for synaptic pruning during brain development. Still, the molecular mechanism by which EFhd2 regulates those putative processes has yet to be examined.

Behavioral changes in *Efhd2*^{-/-} mice have been investigated in a few studies. One study reported enhanced motion disturbance *in Efhd2*^{-/-} mice; a proxy to motion sickness behavior (Z. B. Wang et al., 2017). It is worth noting that EFhd2 exists at low levels in the vestibular nuclei (VN) of mice that are sensitive to motion sickness (SMS). Conversely, VN of mice that are resistant to motion sickness (RMS) has higher levels of EFhd2. Moreover, overexpressing EFhd2 in VN of SMS rescued motion sickness behavior. Importantly, the results of this study established that changes in EFhd2 levels are downstream to glutamate activation of NMDA receptors (Z. B. Wang et al., 2017). All in all, these results propose EFhd2 as a potential contributing factor in the susceptibility level to motion sickness.

A link between EFhd2 and alcohol consumption was established by an initial study showing increased EFhd2 levels in the cerebellum of inbred long sleep (ILS) mice as opposed to inbred short sleep (ISS) mice (MacLaren & Sikela, 2005). In fact, ISS mice were more sensitive to alcohol sedating effects. The results from this study pointed out a possible role of EFhd2 in mediating alcohol resilience. In the same vein, another study reported a positive association between EFhd2 single-nucleotide polymorphism with lifetime drinking in healthy adolescents (Mielenz et al., 2018). To further interrogate the influence of EFhd2 on alcoholism and alcohol resilience, a study compared alcohol consumption between *Efhd2*^{-/-} and wilt type mice (Mielenz et al., 2018). As expected, *Efhd2*^{-/-} mice demonstrated significantly high levels of alcohol consumption. Furthermore, EFhd2 intensified the alcohol-induced sedating effect, which could explain why control mice have limited alcohol consumption. On the molecular level, basal dopamine (DA) levels significantly abated in nucleus accumbens (NAc) and not in PFC of *Efhd2*^{-/-} mice brains (Mielenz et al., 2018). After alcohol consumption, DA levels increased in NAc and not PFC compared to controls. The data suggest that EFhd2 regulates the reward circuitry that drives addictive behavior.

To expand on the putative role of EFhd2 in building resilience against drug abuse and alcoholism, the same research group sought to the test behavioral changes in *Efhd2*^{-/-} mice in

response to psychostimulants (Kogias et al., 2020). In general, methamphetamine and cocaine enhanced DA and serotonin levels in NAc of *Efhd2*^-/- mice. On the other hand, EFhd2 dampened psychostimulants-induced DA and serotonin levels, thereby developing resilience mainly in NAc and not PFC. The data further suggested that EFhd2 by and large regulates the reward circuitry and protects against addictive behavior and tolerance.

EFhd2 and neurodegeneration

I mentioned in the previous sections that highly dynamic proteins that lack well-defined tertiary structures are prone to abnormal aggregation when they lose their structural dynamicity. These proteins (e.g., tau and EFhd2) are sensitive to cellular environment, protein interactions, and PTMs. Any disruption in the cellular milieu could impede the dynamic foldability of these proteins, adopting an abnormal static more compact structure and promoting aggregation. These abnormal structural and conformational changes in this group of dynamic proteins can promote neurodegeneration. Along this line of thinking, it is plausible to speculate the possible association between EFhd2 and neurodegenerative diseases. In fact, a handful of studies have provisionally established the link between EFhd2 and some neurodegenerative disorders.

<u>EFhd2 and Parkinson's disease (PD)</u>

PD is characterized by progressive loss of dopaminergic neurons in the substantia nigra pars compacta (SNpc) and their projections to the caudate-putamen of the basal ganglia (BG) (Hodaie et al., 2007). Fibrillar α-synuclein (α-Syn) inclusions known as Lewy bodies (LB) is the pathological hallmark of PD, particularly in the SN associated with degenerating neurons (Hodaie et al., 2007). Late stages of the disease are characterized by motor dysfunction, such as tremors, akinesia, and rigidity (Hodaie et al., 2007). Still the molecular mechanisms that drive neuropathology and abnormal accumulation of α-Syn in PD remain under active investigation. A corpus of evidence has linked heightened inflammatory response to neurotoxicity, particularly activated microglia and resultant secreted inflammatory cytokines (Cinar et al., 2022). The current premise is that activated microglia and neuroinflammation could be a double-edged sword; neurotoxic or neuroprotective. Which edge prevails during pathology is a long-standing question in the field. A proteomic study examined the response of murine microglia when stimulated by nitrated α-Syn (a modified α-Syn that causes neuronal death and activates microglia during the disease) (Reynolds et al., 2008; He et al., 2019). In particular, a secretome profile of activated microglia was developed. The results showed that EFhd2 was among the

secreted proteins from activated microglia compared to unchallenged microglia. I want here to point out that this was the first study that established a potential glial expression of EFhd2 (Reynolds et al., 2008). The secretion of EFhd2 from stimulated microglia is in agreement with the role that EFhd2 plays in peripheral immune cells. Therefore, more studies are critical to delve into physiological and pathological significance of EFhd2 in microglia.

Another MS-based screening demonstrated low abundance of EFhd2 in SN of PINK1 KO transgenic mouse model of PD (Diedrich et al., 2011). Of note, *PINK1* gene encodes Pink1 protein (PTEN-induced kinase 1), which is a mitochondrial protein that putatively protects against oxidative stress-induced apoptosis (Deas et al., 2009). Indeed, *PINK1* loss-of-function autosomal recessive mutation is linked to familial early onset PD (Deas et al., 2009). The results of that study contrasts with a microarray correlation study that detected high EFhd2 level in SN of postmortem sporadic PD (Liscovitch & French, 2014). Increased EFhd2 level was associated with positive co-expression of α-Syn and IFN-γ (Liscovitch & French, 2014). The disparity between results may be due to differences between sporadic and familial PD. Furthermore, the data generated using a rodent model in the former study may not necessarily be generalized to the human disease. Taking this on board, the association between differential EFhd2 levels and PD pathology warrants further investigation.

Mutations in human leucine-rich repeat kinase 2 (*LRRK2*) gene has been identified as the most common causative gene of autosomal-dominant familial and sporadic PD (Rui et al., 2018). Lrrk2 interactome was explored *in vitro* using fibroblast cell line (Meixner et al., 2011). MS data analysis identified EFhd2 as a potential Lrrk2 interactor. Interestingly, Lrrk2 co-sediments with F-actin and decreases actin polymerization *in vitro* (Meixner et al., 2011). As discussed in the prior section, EFhd2 is a potential actin-binding protein that possibly enhances acting bundling and polymerization. Hence, it is conceivable to speculate that Lrrk2 regulates actin dynamics by inhibiting EFhd2. Further experiments should verify this speculation.

EFhd2 and Amyotrophic lateral sclerosis (ALS)

ALS is a chronic neuromuscular disorder characterized primarily by muscle wasting and weakness (Hughes, 1982). It is described as motor neuron disease because neurodegeneration notably pervades motor neurons in the cerebral cortex, brainstem, and spinal cord, sparing other brain areas that regulate intellectual and executive domains (Hughes, 1982). Like other neurodegenerative disorders, the etiology of ALS still eludes scientists given the fact that the

majority of cases are sporadic. A small proportion of ALS cases have a familial cause by autosomal dominant mutation in superoxide dismutase 1 (*SOD1*) gene. SOD1 protein accounts for clearing free radicals (Rosen et al., 1993). Proteomic analysis was conducted to examine the differences in the proteome of spinal cord lipid raft between mice expressing either wild type SOD1 or G93A mutant SOD1 (Zhai et al., 2009). G93A is one of the missense mutations that are linked to familial human ALS (Rosen et al., 1993). In fact, lipid raft is a microdomain platform of the cellular plasma membrane wherein scaffold proteins interact with their partners to regulate downstream signaling pathways, vesicle trafficking, neurotransmitter release, and receptor recycling in addition to other important cellular processes (Benarroch, 2007; Zhai et al., 2009). Hence, studying proteomic changes in spinal cord lipid rafts of ALS model could shed light on molecular mechanisms that contribute to pathology. In this study, EFhd2 was uniquely identified in the lipid raft of SOD1 mutant mice, attesting to an association with familial ALS. It should not escape one's attention that among the early proposed biological functions of EFhd2 was serving as a scaffold protein in B-cell lipid raft *in vitro* (see above) whereby it facilitates the association of BCR, Syk, and PLC-γ for calcium-mediated signaling pathways. Therefore, identifying EFhd2 in the spinal cord lipid raft of ALS model lends credence to its role as a scaffold protein regulating cellular processes. Clearly, more research seems imperative to reveal whether EFhd2 acts as a neuronal scaffold protein to regulate linked cellular pathways and, hence, determine the pathological outcomes resulting from its dysregulation.

A mutation in the non-coding region of *C9ORF72* gene represents the most common genetic mutation in both ALS and FTLD (Freibaum & Taylor, 2017). This mutation engenders GGGGCC hexanucleotide repeat expansion. Abnormal translation of this hexanucleotide repeats generate 5 species of dipeptide repeats (DPRs), and PolyGA is the most abundant thereof (Freibaum & Taylor, 2017). A thorough examination of PolyGA interactome was undertaken by coimmunoprecipitation from primary neuronal cultures overexpressing PolyGA followed by MS-analysis (May et al., 2014). Of particular interest is the researchers' findings that EFhd2 was identified among PolyGA interacting partners. Taken together, these studies provide a framework to further investigate whether EFhd2 plays a role during the pathological progression of ALS.

EFhd2 in tauopathies

Few years after the initial discovery of EFhd2 as a uniquely expressed protein in CD8^{+} cells, our lab identified EFhd2 for the first time as a tau-associated protein (Vega et al., 2008). Long before the recent surge of interest in studying tau interactome (discussed above), our research group was convinced that tau aggregation is influenced by the interaction with other proteins. As such, we examined possible tau-associated proteins in a tauopathy mouse model and postmortem brains.

Tau was immunoprecipitated from the brains of JNPL3 mice, a transgenic mouse model for FTDP-17 overexpressing P301L mutant human tau (Lewis et al., 2001; Vega et al., 2008). This model shows overt pathology and behavioral phenotype (mainly motor impairment) that increases with age (Lewis et al., 2001; Vega et al., 2008). MS analysis was employed to identify proteins co-purified with tau, which revealed EFhd2 as a tau-associated protein. In agreement with other published results, Hsc70 co-purified with tau in our study. It is important to note that EFhd2 preferentially coimmunoprecipitated with tau from old terminally ill mice (with severe motor impairment) as opposed to young mice that do not exhibit pathological phenotype (Vega et al., 2008). Furthermore, EFhd2 co-purified with high molecular weight tau from old mice and not young mice. That implies that the EFhd2-tau association is tightly linked to neurodegeneration. To determine EFhd2 domains required for its association with tau, *in vitro* interaction assay was conducted. We reported that the association between EFhd2 and pathological tau extracted from JNPL3 mice required EFhd2 C-C and not N-terminus domain (Ferrer-Acosta et al., 2013b).

These early results were borne out in postmortem AD and FTD brains where EFhd2 coimmunoprecipitated with tau (Vega et al., 2008; Ferrer-Acosta et al., 2013b). In addition, we further confirmed phosphorylated tau (PHF1) and EFhd2 colocalization in somatodendritic compartments in the frontal cortex of postmortem brains of advanced AD cases (Ferrer-Acosta et al., 2013b). Likewise, immunogold labeling of EFhd2 and tau demonstrated their colocalization in filamentous structures of high molecular weight tau extracts (Ferrer-Acosta et al., 2013b).

In the preceding section, I explained that EFhd2 is a phosphoprotein, and our group discovered Ser74 that is specifically phosphorylated by CDK5 (Vazquez-Rosa et al., 2014). In addition, pSer74 of EFhd2 precluded calcium-binding behavior (Vazquez-Rosa et al., 2014). It is well known that Cdk5 activity rises in tauopathies, and it is, in fact, one of the kinases that

play a major role in tau hyperphosphorylation (Liu et al., 2016). Therefore, one would anticipate increased levels of pSer74 EFhd2 in AD brains, for example. Surprisingly, we noticed high abundance of total EFhd2 in postmortem AD brains compared to normal aged controls; however, pSer74 EFhd2 was significantly reduced in AD brains (Vazquez-Rosa et al., 2014). Comparing theoretical predictions and actual observations revealed that other molecular factors could interfere/interact with EFhd2 inhibiting its phosphorylation. Whether these molecular factors are related to dysregulated calcium levels in tauopathies or conformational changes in EFhd2 that took place during pathology is still unknown. Furthermore, the relation between low pSer74 EFhd2 and tau-EFhd2 association in tauopathies merits thorough examination.

To investigate the direct association of EFhd2 and tau, EFhd2 and microtubule 3R repeat tau fragment (K19) were incubated *in vitro,* and β-sheet formation was measured by ThS (Vega et al., 2018). The results showed that ThS signal surpassed that generated by incubating K19 with heparin (a known tau aggregation inducer). Furthermore, ThS signal attenuated with C-C domain deleted-EFhd2, corroborating previous findings that C-C domain is necessary for EFhd2-tau interaction (Vega et al., 2018).

Our lab investigated EFhd2 phase separation *in vitro* and the subsequent changes induced on phase-separated tau (Vega et al., 2019). A new and interesting finding was EFhd2 phase separation in the presence of a crowding agent into static solid-like structures. On the other hand, the presence of calcium promoted EFhd2 separation into dynamic liquid droplets (Vega et al., 2019). In addition, EFhd2 phase separation whether in the presence or absence of calcium was abrogated by deleting C-C domain (Vega et al., 2019). When EFhd2 and tau co-incubated in the presence of a crowding agent, they colocalized to solid-like structures, and FRAP analysis revealed that these structures are not dynamic (Vega et al., 2019). In the presence of calcium, both EFhd2 and tau are still colocalized but in more dynamic phase-separated liquid droplets as verified by FRAP analysis. As expected, neither EFhd2-tau liquid droplets nor solid-like structures was formed upon deleting C-C domain (Vega et al., 2019). These findings speak to a possible direct effect of EFhd2 on tau protein dynamics and phase separation, and, naturally, tau aggregation. In essence, gleaned knowledge about the putative impact of EFhd2 on tau aggregation *in vitro* provides the framework to further investigate whether this impact is reflected on tau aggregation *in vivo* and how that could change our perception about the pathological progression.

An independent transcriptomic analysis for distinct regions of AD brains using RNA-Seq next generation sequencing identified significant alternative splicing of *EFHD2* gene in the frontal lobe of AD compared to controls (Twine et al., 2011). These findings provide further support to the link between EFhd2 and AD. One point worth noting here is that researchers in this study did not specify Braak stages of AD brains examined, nor did they report whether sporadic or familial cases were used.

Recently, Xue, et al thoroughly examined the role of a small noncoding RNA in memory impairment of AD (Xue et al., 2022). In particular, they focused on miR-126, which is downregulated in AD brains. This study in fact made several positive contributions. The researchers, successfully in my view, demonstrated that miR-126 regulates hippocampus-dependent contextual fear conditioning (CFC) (Xue et al., 2022). One hour after CFC, miR-126 is upregulated in hippocampal dentate gyrus (DG), which is essential for contextual memory formation and consolidation, not memory acquisition. Furthermore, knocking down miR-126 attenuated CFC long-term consolidation, and that was reversed with overexpressing miR-126 (Xue et al., 2022). Of particular interest is Xue, et al's finding that EFhd2 is a target gene of miR-126. Moreover, the findings illustrated that EFhd2 mediates the biological role of miR-126 on memory consolidation. Using the transgenic APP/PS1 mice model of AD, the study also confirmed that EFhd2 is a target gene for miR-126 where high and low levels of EFhd2 and miR-126 were noticed, respectively. Importantly, overexpressing miR-126 in the brain resulted in reduced EFhd2 levels along with improved spatial memory of APP/PS1 mice (Xue et al., 2022). In general, the results of this paper are in line with the putative role of EFhd2 in adult hippocampus neurogenesis and synaptic function (explained in previous section) (Regensburger et al., 2018). Previously, the colocalization of EFhd2 with synaptic markers and impaired synaptic function in *Efhd2-/-* mice provide persuasive evidence that EFhd2 impacts synaptic plasticity, an integral process for memory consolidation. Above all, identifying EFhd2 as a target gene to miR-126, which is downregulated in AD, align with our previous findings of higher EFhd2 levels in AD brains (Ferrer-Acosta et al., 2013b).

Besides EFhd2's potential influence on tau aggregation, evolving insights allude to its role in memory impairment in AD. As such, this area requires more research to weave all the threads together and generate a conclusive model of the, possibly, multifaceted role of EFhd2 in pathological progression in tauopathies, especially AD.

Concluding remarks

      In this chapter, I merely scratch the surface in regard to published tau-related research. In fact, the literature abounds with yearslong laudable work that has been trying relentlessly to demystify the intricacies of tau pathology and associated factors, aiming to uncover a reliable therapeutic candidate. Our lab, among others, has been intrigued by studying other factors that could mediate or prevent the biogenesis of tau aggregates, especially interacting proteins. Over the past years, we have provided compelling evidence to the potential association between EFhd2 and tau. However, the impact of this association on tau aggregation and pathological progression has yet to be investigated. This dissertation project extends our previous research by addressing the fundamental question "*What is the role of EFhd2 in tau pathology?*

Dissertation objective and structure

      The main objective of this research is to investigate in-depth the role of EFhd2 on tau aggregation and, hence, pathological progression. To this end, the dissertation project is divided into three experimental chapters as illustrated in Figure 1.4 wherein a multidisciplinary approach was undertaken to address the main question.

      Prior research from our lab has established the association between EFhd2 and tau in a tauopathy model and postmortem tauopathies brains. The association between the two proteins was mainly prominent in the high molecular weight tangle aggregates. After these observations, we wondered whether EFhd2 randomly binds to and gets sequestered by tau aggregates, or it influences the formation of these aggregates. We partly addressed this question by measuring ThS signal (β-sheet formation) of EFhd2-K19 tau fragment co-incubation. EFhd2 enhanced β-sheet formation without aggregation inducer. These data showed that EFhd2 can induce tau aggregation. Furthermore, we investigated whether EFhd2 can change the dynamic properties of tau by assessing tau liquid phase separation in the presence of EFhd2. EFhd2 transformed tau's dynamic liquid droplets into static solid-like structures. Collectively, the results suggest that EFhd2 potentially interacts with tau, changes its dynamic, and induces aggregation. The question remains whether EFhd2 could promote the formation of specific tau aggregates, especially tangles. To address this question, I opted to use recombinant proteins to verify the direct association between EFhd2 and full-length human tau (hTau40/2N4R) and visualize the endpoint aggregates formed (Figure 1.4, <u>Chapter Two</u>). By using techniques, such as electron microscopy, immunogold labeling, and sandwich ELISA, I demonstrated the capacity of recombinant of

EFhd2 to co-aggregate with both monomeric tau and *in vitro*-produced filamentous tau. The results of this experiment lend further support to previous studies, thereby demonstrating the potential direct association between EFhd2 and tau.

We previously reported higher EFhd2 levels in AD brains compared to normal nondemented cases. These data parallel Xue, et al's findings that EFhd2 is a target gene to miR-126, which is downregulated in AD. The association of EFhd2 and pathological tau along with increased EFhd2 levels in AD provided the impetus to closely examine how manipulating EFhd2 expression in the brain could change the progression of tau pathology *in vivo*. Hereto, our lab developed a new model (Tau$_{P301L}$/*Efhd2$^{-/-}$*) by crossing *Efhd2$^{-/-}$* mice with a transgenic tauopathy model overexpressing P301L mutant tau (JNPL3) that exhibits age-dependent overt pathology and behavioral deficit (Figure 1.4). This new model provides a valuable approach to investigate changes in tau pathology in the absence of EFhd2. One point worth noting is that little is still known about the biological functions of EFhd2 in CNS. Therefore, before exploring the behavioral and pathological changes in Tau$_{P301L}$/*Efhd2$^{-/-}$* mice, I sought, using MS-based proteomics, to investigate the global proteome changes in *Efhd2$^{-/-}$* mice brains compared to control wild type mice (*Efhd2$^{+/+}$*) (Figure 1.4, Chapter Three). Furthermore, I examined EFhd2 brain interactome by immunoprecipitating EFhd2 from *Efhd2$^{+/+}$* mice brains followed by tandem MS. The results of this study provide better understanding of the possible physiological role of EFhd2 in CNS by mapping a holistic network of its interacting proteins, especially proteins whose abundance changed with *Efhd2* gene deletion. Above all, the insights gained from this study enabled me to discern the biological context of *Efhd2$^{-/-}$* mice brains wherein tau pathology develops in Tau$_{P301L}$/*Efhd2$^{-/-}$* mice (Figure 1.4, Chapter Four).

Afterwards, I executed a longitudinal behavioral assessment on Tau$_{P301L}$/*Efhd2$^{-/-}$* mice with in-depth cross-sectional histological and biochemical analysis to determine changes in behavioral deficit and pathological tau markers (Figure 1.4, Chapter Four). It is worth noting that results from Chapter Three not only provide the biological context of tau pathology, but also, they provide a framework for possible indirect association of EFhd2 and tau pathology. In other words, deleting *Efhd2* gene induced differential changes in the abundance of some proteins (Chapter Three), which in turn could impact the progression of tau pathology (Chapter Four).

To conclude, the successful execution of this dissertation project offers a more comprehensive understanding of the direct (Chapter Two) and indirect (Chapter Three and Four) role of EFhd2 in the biogenesis of tau aggregates and pathological progression.
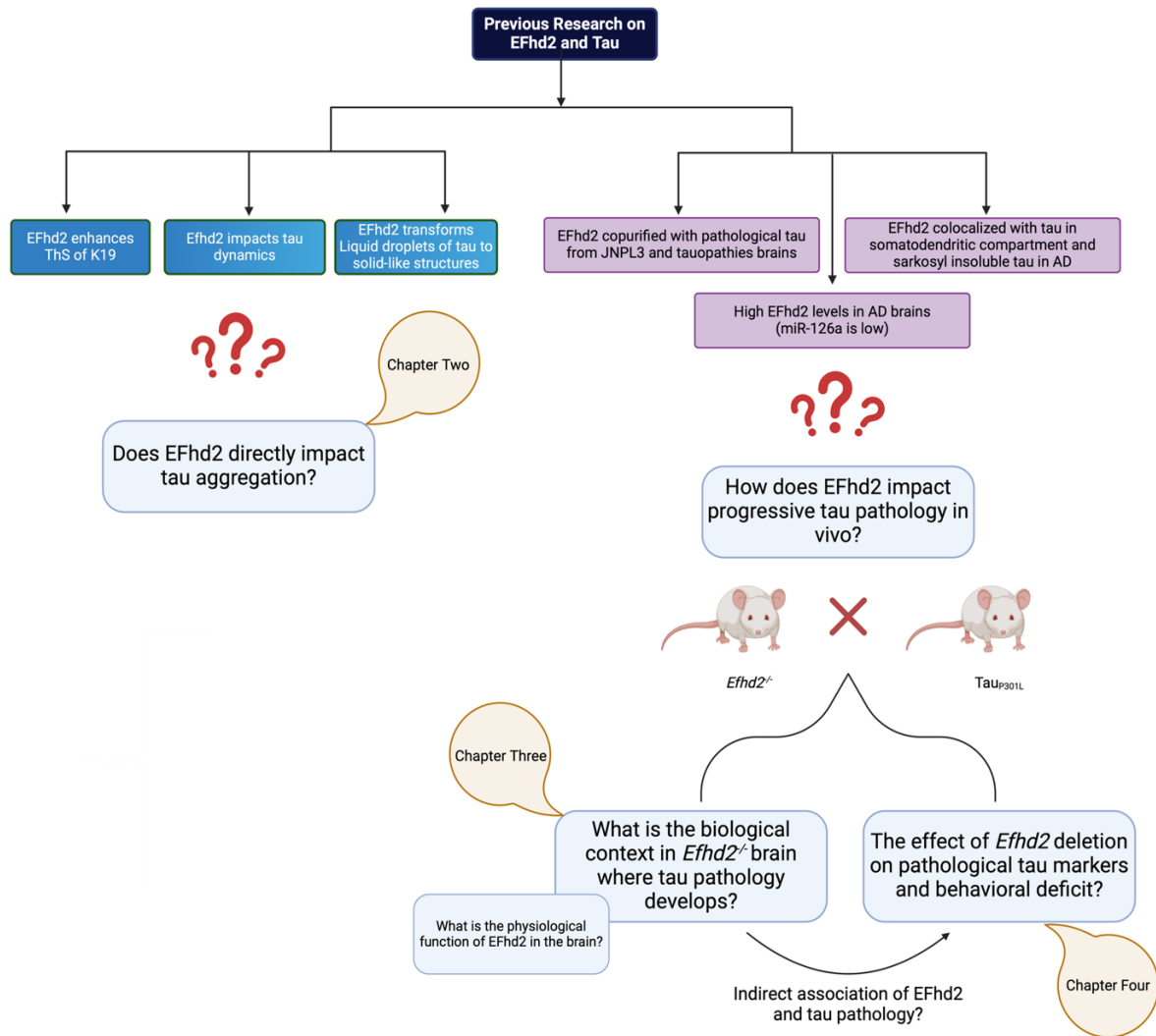
Figure 1.4. Structure and framework of the dissertation. Our group has reported that EFhd2 enhanced ThS when incubated with K19 tau fragment, indicating an increase in β-sheet formation by EFhd2. Furthermore, EFhd2 changed tau dynamics by transforming its dynamic liquid droplets into static solid-like structures. Therefore, in **Chapter Two**, I specifically investigated whether EFhd2 can induce the formation of certain species of tau aggregates when it interacts with monomeric and filamentous tau. To this end, a set of *in vitro* experiments was conducted, including EM, sELISA, and immunogold labeling. Previous research has established

Figure 1.4 (cont'd)

the association of EFhd2 and pathological tau in animal models and postmortem tauopathies along with elevated levels of EFhd2 levels in AD. In addition, EFhd2 is particularly localized with filamentous tau extracted from AD brains. These findings instigated the question of how EFhd2 could change the pathological progression of tau *in vivo*. Hence, we developed the Tau$_{P301L}$/*Efhd2$^{-/-}$* mouse model to study the changes in tau aggregation and behavioral deficit in the absence of EFhd2 (**Chapter Four**). Before addressing this focal point, I used an MS-based approach to elucidate the unstudied EFhd2 interactome in the brain of *Efhd2$^{+/+}$* mice and the global proteome changes in the *Efhd2$^{-/-}$* mice brain (**Chapter Three**). This study provided the foundation to deduce the possible indirect effect of EFhd2 on tau pathology examined in **Chapter Four**. Collectively, the three main studies of my dissertation project will add further support to the possible role of EFhd2 in tau pathology leading to a trove of questions to be addressed in the future.

REFERENCES

Ababou, A., & Desjarlais, J. R. (2001). Solvation energetics and conformational change in EF-hand proteins. *Protein Sci*, *10*(2), 301-312. https://doi.org/10.1110/ps.33601

Ahmed, T., Van der Jeugd, A., Blum, D., Galas, M. C., D'Hooge, R., Buee, L., & Balschun, D. (2014). Cognition and hippocampal synaptic plasticity in mice with a homozygous tau deletion. *Neurobiol Aging*, *35*(11), 2474-2478. https://doi.org/10.1016/j.neurobiolaging.2014.05.005

Alhadidy, M. M., & Kanaan, N. M. (2024). Biochemical approaches to assess the impact of post-translational modifications on pathogenic tau conformations using recombinant protein. *Biochem Soc Trans*, *52*(1), 301-318. https://doi.org/10.1042/BST20230596

Alquezar, C., Arya, S., & Kao, A. W. (2020). Tau Post-translational Modifications: Dynamic Transformers of Tau Function, Degradation, and Aggregation. *Front Neurol*, *11*, 595532. https://doi.org/10.3389/fneur.2020.595532

Alzheimer, A., Stelzmann, R. A., Schnitzlein, H. N., & Murtagh, F. R. (1995). An English translation of Alzheimer's 1907 paper, "Uber eine eigenartige Erkankung der Hirnrinde". *Clin Anat*, *8*(6), 429-431. https://doi.org/10.1002/ca.980080612

Ando, T. (2022). Functional Implications of Dynamic Structures of Intrinsically Disordered Proteins Revealed by High-Speed AFM Imaging. *Biomolecules*, *12*(12), 1876. https://doi.org/10.3390/biom12121876

Apicco, D. J., Ash, P. E. A., Maziuk, B., LeBlang, C., Medalla, M., Al Abdullatif, A., Ferragud, A., Botelho, E., Ballance, H. I., Dhawan, U., Boudeau, S., Cruz, A. L., Kashy, D., Wong, A., Goldberg, L. R., Yazdani, N., Zhang, C., Ung, C. Y., Tripodis, Y., . . . Wolozin, B. (2018). Reducing the RNA binding protein TIA1 protects against tau-mediated neurodegeneration in vivo. *Nat Neurosci*, *21*(1), 72-80. https://doi.org/10.1038/s41593-017-0022-z

Arakhamia, T., Lee, C. E., Carlomagno, Y., Duong, D. M., Kundinger, S. R., Wang, K., Williams, D., DeTure, M., Dickson, D. W., Cook, C. N., Seyfried, N. T., Petrucelli, L., & Fitzpatrick, A. W. P. (2020). Posttranslational Modifications Mediate the Structural Diversity of Tauopathy Strains. *Cell*, *180*(4), 633-644 e612. https://doi.org/10.1016/j.cell.2020.01.027

Ash, P. E. A., Lei, S., Shattuck, J., Boudeau, S., Carlomagno, Y., Medalla, M., Mashimo, B. L., Socorro, G., Al-Mohanna, L. F. A., Jiang, L., Ozturk, M. M., Knobel, M., Ivanov, P., Petrucelli, L., Wegmann, S., Kanaan, N. M., & Wolozin, B. (2021). TIA1 potentiates tau phase separation and promotes generation of toxic oligomeric tau. *Proc Natl Acad Sci U S A*, *118*(9). https://doi.org/10.1073/pnas.2014188118

Avramidou, A., Kroczek, C., Lang, C., Schuh, W., Jack, H. M., & Mielenz, D. (2007). The novel adaptor protein Swiprosin-1 enhances BCR signals and contributes to BCR-induced apoptosis. *Cell Death Differ*, *14*(11), 1936-1947. https://doi.org/10.1038/sj.cdd.4402206

Ayyadevara, S., Balasubramaniam, M., Parcon, P. A., Barger, S. W., Griffin, W. S., Alla, R., Tackett, A. J., Mackintosh, S. G., Petricoin, E., Zhou, W., & Shmookler Reis, R. J. (2016).

Proteins that mediate protein aggregation and cytotoxicity distinguish Alzheimer's hippocampus from normal controls. *Aging Cell*, *15*(5), 924-939. https://doi.org/10.1111/acel.12501

Benarroch, E. E. (2007). Lipid rafts, protein scaffolds, and neurologic disease. *Neurology*, *69*(16), 1635-1639. https://doi.org/10.1212/01.wnl.0000279590.22544.c3

Berger, Z., Roder, H., Hanna, A., Carlson, A., Rangachari, V., Yue, M., Wszolek, Z., Ashe, K., Knight, J., Dickson, D., Andorfer, C., Rosenberry, T. L., Lewis, J., Hutton, M., & Janus, C. (2007). Accumulation of pathological tau species and memory loss in a conditional model of tauopathy. *J Neurosci*, *27*(14), 3650-3662. https://doi.org/10.1523/JNEUROSCI.0587-07.2007

Berry, R. W., Abraha, A., Lagalwar, S., LaPointe, N., Gamblin, T. C., Cryns, V. L., & Binder, L. I. (2003). Inhibition of tau polymerization by its carboxy-terminal caspase cleavage fragment. *Biochemistry*, *42*(27), 8325-8331. https://doi.org/10.1021/bi027348m

Binder, L. I., Frankfurter, A., & Rebhun, L. I. (1985). The distribution of tau in the mammalian central nervous system. *J Cell Biol*, *101*(4), 1371-1378. https://doi.org/10.1083/jcb.101.4.1371

Borger, E., Herrmann, A., Mann, D. A., Spires-Jones, T., & Gunn-Moore, F. (2014). The calcium-binding protein EFhd2 modulates synapse formation in vitro and is linked to human dementia. *J Neuropathol Exp Neurol*, *73*(12), 1166-1182. https://doi.org/10.1097/NEN.0000000000000138

Braak, H., & Braak, E. (1991). Neuropathological stageing of Alzheimer-related changes. *Acta Neuropathol*, *82*(4), 239-259. https://doi.org/10.1007/BF00308809

Brangwynne, C. P. (2013). Phase transitions and size scaling of membrane-less organelles. *J Cell Biol*, *203*(6), 875-881. https://doi.org/10.1083/jcb.201308087

Brettschneider, J., Del Tredici, K., Lee, V. M., & Trojanowski, J. Q. (2015). Spreading of pathology in neurodegenerative diseases: a focus on human studies. *Nat Rev Neurosci*, *16*(2), 109-120. https://doi.org/10.1038/nrn3887

Brion, J. P., Passareiro, H., Nunez, J., & Flament-Durand, J. (1985). Immunological detection of tau protein in neurofibrillary tangles of Alzheimer's disease [Article]. *Archives de Biologie*, *96*(2), 229-235. https://www.scopus.com/inward/record.uri?eid=2-s2.0-0022257253&partnerID=40&md5=5b992ca7839b7995bf29fc0ca499e90c

Brunden, K. R., Trojanowski, J. Q., & Lee, V. M. (2008). Evidence that non-fibrillar tau causes pathology linked to neurodegeneration and behavioral impairments. *J Alzheimers Dis*, *14*(4), 393-399. https://doi.org/10.3233/jad-2008-14406

Caceres, A., & Kosik, K. S. (1990). Inhibition of neurite polarity by tau antisense oligonucleotides in primary cerebellar neurons. *Nature*, *343*(6257), 461-463. https://doi.org/10.1038/343461a0

Camero, S., Benitez, M. J., Barrantes, A., Ayuso, J. M., Cuadros, R., Avila, J., & Jimenez, J. S. (2014). Tau protein provides DNA with thermodynamic and structural features which are similar

to those found in histone-DNA complex. *J Alzheimers Dis*, *39*(3), 649-660. https://doi.org/10.3233/JAD-131415

Castellani, R. J., Rolston, R. K., & Smith, M. A. (2010). Alzheimer disease. *Dis Mon*, *56*(9), 484-546. https://doi.org/10.1016/j.disamonth.2010.06.001

Chung, D. C., Roemer, S., Petrucelli, L., & Dickson, D. W. (2021). Cellular and pathological heterogeneity of primary tauopathies. *Mol Neurodegener*, *16*(1), 57. https://doi.org/10.1186/s13024-021-00476-x

Cinar, E., Tel, B. C., & Sahin, G. (2022). Neuroinflammation in Parkinson's Disease and its Treatment Opportunities. *Balkan Med J*, *39*(5), 318-333. https://doi.org/10.4274/balkanmedj.galenos.2022.2022-7-100

Cleveland, D. W., Hwo, S. Y., & Kirschner, M. W. (1977a). Physical and chemical properties of purified tau factor and the role of tau in microtubule assembly. *J Mol Biol*, *116*(2), 227-247. https://doi.org/10.1016/0022-2836(77)90214-5

Cleveland, D. W., Hwo, S. Y., & Kirschner, M. W. (1977b). Purification of tau, a microtubule-associated protein that induces assembly of microtubules from purified tubulin. *J Mol Biol*, *116*(2), 207-225. https://doi.org/10.1016/0022-2836(77)90213-3

Combs, B., & Kanaan, N. M. (2017). Exposure of the Amino Terminus of Tau Is a Pathological Event in Multiple Tauopathies. *Am J Pathol*, *187*(6), 1222-1229. https://doi.org/10.1016/j.ajpath.2017.01.019

Cowan, C. M., & Mudher, A. (2013). Are tau aggregates toxic or protective in tauopathies? *Front Neurol*, *4*, 114. https://doi.org/10.3389/fneur.2013.00114

Cuadros, R., Perez, M., Ruiz-Gabarre, D., Hernandez, F., Garcia-Escudero, V., & Avila, J. (2022). Specific Peptide from the Novel W-Tau Isoform Inhibits Tau and Amyloid beta Peptide Aggregation In Vitro. *ACS Chem Neurosci*, *13*(13), 1974-1978. https://doi.org/10.1021/acschemneuro.2c00188

Darling, A. L., Dahrendorff, J., Creodore, S. G., Dickey, C. A., Blair, L. J., & Uversky, V. N. (2021). Small heat shock protein 22 kDa can modulate the aggregation and liquid-liquid phase separation behavior of tau. *Protein Sci*, *30*(7), 1350-1359. https://doi.org/10.1002/pro.4060

Deas, E., Plun-Favreau, H., & Wood, N. W. (2009). PINK1 function in health and disease. *EMBO Mol Med*, *1*(3), 152-165. https://doi.org/10.1002/emmm.200900024

DeTure, M. A., & Dickson, D. W. (2019). The neuropathological diagnosis of Alzheimer's disease. *Mol Neurodegener*, *14*(1), 32. https://doi.org/10.1186/s13024-019-0333-5

Diedrich, M., Kitada, T., Nebrich, G., Koppelstaetter, A., Shen, J., Zabel, C., Klose, J., & Mao, L. (2011). Brain region specific mitophagy capacity could contribute to selective neuronal vulnerability in Parkinson's disease. *Proteome Sci*, *9*, 59. https://doi.org/10.1186/1477-5956-9-59

Drummond, E., Pires, G., MacMurray, C., Askenazi, M., Nayak, S., Bourdon, M., Safar, J., Ueberheide, B., & Wisniewski, T. (2020). Phosphorylated tau interactome in the human Alzheimer's disease brain. *Brain*, *143*(9), 2803-2817. https://doi.org/10.1093/brain/awaa223

Dyson, H. J., & Wright, P. E. (2005). Intrinsically unstructured proteins and their functions. *Nat Rev Mol Cell Biol*, *6*(3), 197-208. https://doi.org/10.1038/nrm1589

Falcon, B., Zhang, W., Murzin, A. G., Murshudov, G., Garringer, H. J., Vidal, R., Crowther, R. A., Ghetti, B., Scheres, S. H. W., & Goedert, M. (2018a). Structures of filaments from Pick's disease reveal a novel tau protein fold. *Nature*, *561*(7721), 137-140. https://doi.org/10.1038/s41586-018-0454-y

Falcon, B., Zhang, W., Schweighauser, M., Murzin, A. G., Vidal, R., Garringer, H. J., Ghetti, B., Scheres, S. H. W., & Goedert, M. (2018b). Tau filaments from multiple cases of sporadic and inherited Alzheimer's disease adopt a common fold. *Acta Neuropathol*, *136*(5), 699-708. https://doi.org/10.1007/s00401-018-1914-z

Falcon, B., Zivanov, J., Zhang, W., Murzin, A. G., Garringer, H. J., Vidal, R., Crowther, R. A., Newell, K. L., Ghetti, B., Goedert, M., & Scheres, S. H. W. (2019). Novel tau filament fold in chronic traumatic encephalopathy encloses hydrophobic molecules. *Nature*, *568*(7752), 420-423. https://doi.org/10.1038/s41586-019-1026-5

Ferrer-Acosta, Y., Rodriguez Cruz, E. N., Vaquer Adel, C., & Vega, I. E. (2013a). Functional and structural analysis of the conserved EFhd2 protein. *Protein Pept Lett*, *20*(5), 573-583. https://doi.org/10.2174/0929866511320050011

Ferrer-Acosta, Y., Rodriguez-Cruz, E. N., Orange, F., De Jesus-Cortes, H., Madera, B., Vaquer-Alicea, J., Ballester, J., Guinel, M. J., Bloom, G. S., & Vega, I. E. (2013b). EFhd2 is a novel amyloid protein associated with pathological tau in Alzheimer's disease. *J Neurochem*, *125*(6), 921-931. https://doi.org/10.1111/jnc.12155

Fischer, I. (2023). Big Tau: What We Know, and We Need to Know. *eNeuro*, *10*(5). https://doi.org/10.1523/ENEURO.0052-23.2023

Fitzpatrick, A. W. P., Falcon, B., He, S., Murzin, A. G., Murshudov, G., Garringer, H. J., Crowther, R. A., Ghetti, B., Goedert, M., & Scheres, S. H. W. (2017). Cryo-EM structures of tau filaments from Alzheimer's disease. *Nature*, *547*(7662), 185-190. https://doi.org/10.1038/nature23002

Freibaum, B. D., & Taylor, J. P. (2017). The Role of Dipeptide Repeats in C9ORF72-Related ALS-FTD. *Front Mol Neurosci*, *10*, 35. https://doi.org/10.3389/fnmol.2017.00035

Fu, J. T., Liu, J., Wu, W. B., Chen, Y. T., Lu, G. D., Cao, Q., Meng, H. B., Tong, J., Zhu, J. H., Wang, X. J., Liu, Y., Zhuang, C., Sheng, C., Shen, F. M., Liu, X., Wang, H., Yu, Y., Zhang, Y., Liang, H. Y., . . . Wang, P. (2024). Targeting EFHD2 inhibits interferon-gamma signaling and ameliorates non-alcoholic steatohepatitis. *J Hepatol*. https://doi.org/10.1016/j.jhep.2024.04.009

Fuster-Matanzo, A., de Barreda, E. G., Dawson, H. N., Vitek, M. P., Avila, J., & Hernandez, F. (2009). Function of tau protein in adult newborn neurons. *FEBS Lett*, *583*(18), 3063-3068. https://doi.org/10.1016/j.febslet.2009.08.017

Garcia-Escudero, V., Ruiz-Gabarre, D., Gargini, R., Perez, M., Garcia, E., Cuadros, R., Hernandez, I. H., Cabrera, J. R., Garcia-Escudero, R., Lucas, J. J., Hernandez, F., & Avila, J. (2021). A new non-aggregative splicing isoform of human Tau is decreased in Alzheimer's disease. *Acta Neuropathol*, *142*(1), 159-177. https://doi.org/10.1007/s00401-021-02317-z

Giricz, Z., Makkos, A., Schreckenberg, R., Poling, J., Lorchner, H., Kiss, K., Bencsik, P., Braun, T., Schulz, R., Ferdinandy, P., & Schluter, K. D. (2020). Swiprosin-1/EFhD-2 Expression in Cardiac Remodeling and Post-Infarct Repair: Effect of Ischemic Conditioning. *Int J Mol Sci*, *21*(9). https://doi.org/10.3390/ijms21093359

Goedert, M. (1993). Tau protein and the neurofibrillary pathology of Alzheimer's disease. *Trends Neurosci*, *16*(11), 460-465. https://doi.org/10.1016/0166-2236(93)90078-z

Goedert, M., & Jakes, R. (2005). Mutations causing neurodegenerative tauopathies. *Biochim Biophys Acta*, *1739*(2-3), 240-250. https://doi.org/10.1016/j.bbadis.2004.08.007

Goedert, M., Wischik, C. M., Crowther, R. A., Walker, J. E., & Klug, A. (1988). Cloning and sequencing of the cDNA encoding a core protein of the paired helical filament of Alzheimer disease: identification as the microtubule-associated protein tau. *Proc Natl Acad Sci U S A*, *85*(11), 4051-4055. https://doi.org/10.1073/pnas.85.11.4051

Gomez-Isla, T., Hollister, R., West, H., Mui, S., Growdon, J. H., Petersen, R. C., Parisi, J. E., & Hyman, B. T. (1997). Neuronal loss correlates with but exceeds neurofibrillary tangles in Alzheimer's disease. *Ann Neurol*, *41*(1), 17-24. https://doi.org/10.1002/ana.410410106

Gómez-Isla, T., Price, J. L., McKeel, D. W., Jr., Morris, J. C., Growdon, J. H., & Hyman, B. T. (1996). Profound loss of layer II entorhinal cortex neurons occurs in very mild Alzheimer's disease. *J Neurosci*, *16*(14), 4491-4500. https://doi.org/10.1523/JNEUROSCI.16-14-04491.1996

Grundke-Iqbal, I., Iqbal, K., Tung, Y. C., Quinlan, M., Wisniewski, H. M., & Binder, L. I. (1986). Abnormal phosphorylation of the microtubule-associated protein tau (tau) in Alzheimer cytoskeletal pathology. *Proc Natl Acad Sci U S A*, *83*(13), 4913-4917. https://doi.org/10.1073/pnas.83.13.4913

Guillozet-Bongaarts, A. L., Cahill, M. E., Cryns, V. L., Reynolds, M. R., Berry, R. W., & Binder, L. I. (2006). Pseudophosphorylation of tau at serine 422 inhibits caspase cleavage: in vitro evidence and implications for tangle formation in vivo. *J Neurochem*, *97*(4), 1005-1014. https://doi.org/10.1111/j.1471-4159.2006.03784.x

Guillozet-Bongaarts, A. L., Garcia-Sierra, F., Reynolds, M. R., Horowitz, P. M., Fu, Y., Wang, T., Cahill, M. E., Bigio, E. H., Berry, R. W., & Binder, L. I. (2005). Tau truncation during neurofibrillary tangle evolution in Alzheimer's disease. *Neurobiol Aging*, *26*(7), 1015-1022. https://doi.org/10.1016/j.neurobiolaging.2004.09.019

Gunawardana, C. G., Mehrabian, M., Wang, X., Mueller, I., Lubambo, I. B., Jonkman, J. E., Wang, H., & Schmitt-Ulms, G. (2015). The Human Tau Interactome: Binding to the Ribonucleoproteome, and Impaired Binding of the Proline-to-Leucine Mutant at Position 301 (P301L) to Chaperones and the Proteasome. *Mol Cell Proteomics*, *14*(11), 3000-3014. https://doi.org/10.1074/mcp.M115.050724

Gustke, N., Trinczek, B., Biernat, J., Mandelkow, E. M., & Mandelkow, E. (1994). Domains of tau protein and interactions with microtubules. *Biochemistry*, *33*(32), 9511-9522. https://doi.org/10.1021/bi00198a017

Hagen, S., Brachs, S., Kroczek, C., Furnrohr, B. G., Lang, C., & Mielenz, D. (2012). The B cell receptor-induced calcium flux involves a calcium mediated positive feedback loop. *Cell Calcium*, *51*(5), 411-417. https://doi.org/10.1016/j.ceca.2012.01.004

Harada, A., Oguchi, K., Okabe, S., Kuno, J., Terada, S., Ohshima, T., Sato-Yoshitake, R., Takei, Y., Noda, T., & Hirokawa, N. (1994). Altered microtubule organization in small-calibre axons of mice lacking tau protein. *Nature*, *369*(6480), 488-491. https://doi.org/10.1038/369488a0

Hasegawa, M., Morishima-Kawashima, M., Takio, K., Suzuki, M., Titani, K., & Ihara, Y. (1992). Protein sequence and mass spectrometric analyses of tau in the Alzheimer's disease brain. *J Biol Chem*, *267*(24), 17047-17054. https://doi.org/10.1016/S0021-9258(18)41890-X

He, Y., Yu, Z., & Chen, S. (2019). Alpha-Synuclein Nitration and Its Implications in Parkinson's Disease. *ACS Chem Neurosci*, *10*(2), 777-782. https://doi.org/10.1021/acschemneuro.8b00288

Heinonen, O., Soininen, H., Sorvari, H., Kosunen, O., Paljarvi, L., Koivisto, E., & Riekkinen, P. J., Sr. (1995). Loss of synaptophysin-like immunoreactivity in the hippocampal formation is an early phenomenon in Alzheimer's disease. *Neuroscience*, *64*(2), 375-384. https://doi.org/10.1016/0306-4522(94)00422-2

Hernandez-Vega, A., Braun, M., Scharrel, L., Jahnel, M., Wegmann, S., Hyman, B. T., Alberti, S., Diez, S., & Hyman, A. A. (2017). Local Nucleation of Microtubule Bundles through Tubulin Concentration into a Condensed Tau Phase. *Cell Rep*, *20*(10), 2304-2312. https://doi.org/10.1016/j.celrep.2017.08.042

Hodaie, M., Neimat, J. S., & Lozano, A. M. (2007). The dopaminergic nigrostriatal system and Parkinson's disease: molecular events in development, disease, and cell death, and new therapeutic strategies. *Neurosurgery*, *60*(1), 17-28; discussion 28-30. https://doi.org/10.1227/01.NEU.0000249209.11967.CB

Holmes, B. B., & Diamond, M. I. (2014). Prion-like properties of Tau protein: the importance of extracellular Tau as a therapeutic target. *J Biol Chem*, *289*(29), 19855-19861. https://doi.org/10.1074/jbc.R114.549295

Holmes, B. B., Furman, J. L., Mahan, T. E., Yamasaki, T. R., Mirbaha, H., Eades, W. C., Belaygorod, L., Cairns, N. J., Holtzman, D. M., & Diamond, M. I. (2014). Proteopathic tau seeding predicts tauopathy in vivo. *Proc Natl Acad Sci U S A*, *111*(41), E4376-4385. https://doi.org/10.1073/pnas.1411649111

Hong, X. P., Peng, C. X., Wei, W., Tian, Q., Liu, Y. H., Yao, X. Q., Zhang, Y., Cao, F. Y., Wang, Q., & Wang, J. Z. (2010). Essential role of tau phosphorylation in adult hippocampal neurogenesis. *Hippocampus*, *20*(12), 1339-1349. https://doi.org/10.1002/hipo.20712

Hsieh, Y. C., Guo, C., Yalamanchili, H. K., Abreha, M., Al-Ouran, R., Li, Y., Dammer, E. B., Lah, J. J., Levey, A. I., Bennett, D. A., De Jager, P. L., Seyfried, N. T., Liu, Z., & Shulman, J. M. (2019). Tau-Mediated Disruption of the Spliceosome Triggers Cryptic RNA Splicing and Neurodegeneration in Alzheimer's Disease. *Cell Rep*, *29*(2), 301-316 e310. https://doi.org/10.1016/j.celrep.2019.08.104

Hughes, J. T. (1982). Pathology of amyotrophic lateral sclerosis. *Adv Neurol*, *36*, 61-74. https://www.ncbi.nlm.nih.gov/pubmed/7180695

Huh, Y. H., Kim, S. H., Chung, K. H., Oh, S., Kwon, M. S., Choi, H. W., Rhee, S., Ryu, J. H., Park, Z. Y., Jun, C. D., & Song, W. K. (2013). Swiprosin-1 modulates actin dynamics by regulating the F-actin accessibility to cofilin. *Cell Mol Life Sci*, *70*(24), 4841-4854. https://doi.org/10.1007/s00018-013-1447-5

Huh, Y. H., Oh, S., Yeo, Y. R., Chae, I. H., Kim, S. H., Lee, J. S., Yun, S. J., Choi, K. Y., Ryu, J. H., Jun, C. D., & Song, W. K. (2015). Swiprosin-1 stimulates cancer invasion and metastasis by increasing the Rho family of GTPase signaling. *Oncotarget*, *6*(15), 13060-13071. https://doi.org/10.18632/oncotarget.3637

Hutton, M., Lendon, C. L., Rizzu, P., Baker, M., Froelich, S., Houlden, H., Pickering-Brown, S., Chakraverty, S., Isaacs, A., Grover, A., Hackett, J., Adamson, J., Lincoln, S., Dickson, D., Davies, P., Petersen, R. C., Stevens, M., de Graaff, E., Wauters, E., . . . Heutink, P. (1998). Association of missense and 5'-splice-site mutations in tau with the inherited dementia FTDP-17. *Nature*, *393*(6686), 702-705. https://doi.org/10.1038/31508

Hyman, A. A., Weber, C. A., & Julicher, F. (2014). Liquid-liquid phase separation in biology. *Annu Rev Cell Dev Biol*, *30*(1), 39-58. https://doi.org/10.1146/annurev-cellbio-100913-013325

Ihara, Y., Nukina, N., Miura, R., & Ogawara, M. (1986). Phosphorylated tau protein is integrated into paired helical filaments in Alzheimer's disease. *J Biochem*, *99*(6), 1807-1810. https://doi.org/10.1093/oxfordjournals.jbchem.a135662

Jeganathan, S., Hascher, A., Chinnathambi, S., Biernat, J., Mandelkow, E. M., & Mandelkow, E. (2008). Proline-directed pseudo-phosphorylation at AT8 and PHF1 epitopes induces a compaction of the paperclip folding of Tau and generates a pathological (MC-1) conformation. *J Biol Chem*, *283*(46), 32066-32076. https://doi.org/10.1074/jbc.M805300200

Jeganathan, S., von Bergen, M., Brutlach, H., Steinhoff, H. J., & Mandelkow, E. (2006). Global hairpin folding of tau in solution. *Biochemistry*, *45*(7), 2283-2293. https://doi.org/10.1021/bi0521543

Jiang, L., Ash, P. E. A., Maziuk, B. F., Ballance, H. I., Boudeau, S., Abdullatif, A. A., Orlando, M., Petrucelli, L., Ikezu, T., & Wolozin, B. (2019). TIA1 regulates the generation and response

to toxic tau oligomers. *Acta Neuropathol*, *137*(2), 259-277. https://doi.org/10.1007/s00401-018-1937-5

Jucker, M., & Walker, L. C. (2013). Self-propagation of pathogenic protein aggregates in neurodegenerative diseases. *Nature*, *501*(7465), 45-51. https://doi.org/10.1038/nature12481

Kadavath, H., Hofele, R. V., Biernat, J., Kumar, S., Tepper, K., Urlaub, H., Mandelkow, E., & Zweckstetter, M. (2015). Tau stabilizes microtubules by binding at the interface between tubulin heterodimers. *Proc Natl Acad Sci U S A*, *112*(24), 7501-7506. https://doi.org/10.1073/pnas.1504081112

Kametani, F., Yoshida, M., Matsubara, T., Murayama, S., Saito, Y., Kawakami, I., Onaya, M., Tanaka, H., Kakita, A., Robinson, A. C., Mann, D. M. A., & Hasegawa, M. (2020). Comparison of Common and Disease-Specific Post-translational Modifications of Pathological Tau Associated With a Wide Range of Tauopathies. *Front Neurosci*, *14*, 581936. https://doi.org/10.3389/fnins.2020.581936

Kanaan, N. M. (2024). Tau here, tau there, tau almost everywhere: Clarifying the distribution of tau in the adult CNS. *Cytoskeleton (Hoboken)*, *81*(1), 107-115. https://doi.org/10.1002/cm.21820

Kanaan, N. M., Cox, K., Alvarez, V. E., Stein, T. D., Poncil, S., & McKee, A. C. (2016). Characterization of Early Pathological Tau Conformations and Phosphorylation in Chronic Traumatic Encephalopathy. *J Neuropathol Exp Neurol*, *75*(1), 19-34. https://doi.org/10.1093/jnen/nlv001

Kanaan, N. M., & Grabinski, T. (2021). Neuronal and Glial Distribution of Tau Protein in the Adult Rat and Monkey. *Front Mol Neurosci*, *14*, 607303. https://doi.org/10.3389/fnmol.2021.607303

Kanaan, N. M., Hamel, C., Grabinski, T., & Combs, B. (2020). Liquid-liquid phase separation induces pathogenic tau conformations in vitro. *Nat Commun*, *11*(1), 2809. https://doi.org/10.1038/s41467-020-16580-3

Kanaan, N. M., Morfini, G. A., LaPointe, N. E., Pigino, G. F., Patterson, K. R., Song, Y., Andreadis, A., Fu, Y., Brady, S. T., & Binder, L. I. (2011). Pathogenic forms of tau inhibit kinesin-dependent axonal transport through a mechanism involving activation of axonal phosphotransferases. *J Neurosci*, *31*(27), 9858-9868. https://doi.org/10.1523/JNEUROSCI.0560-11.2011

Kavanagh, T., Halder, A., & Drummond, E. (2022). Tau interactome and RNA binding proteins in neurodegenerative diseases. *Mol Neurodegener*, *17*(1), 66. https://doi.org/10.1186/s13024-022-00572-6

Kayed, R. (2010). Anti-tau oligomers passive vaccination for the treatment of Alzheimer disease. *Hum Vaccin*, *6*(11), 931-935. https://doi.org/10.4161/hv.6.11.12689

Kekesi, K. A., Juhasz, G., Simor, A., Gulyassy, P., Szego, E. M., Hunyadi-Gulyas, E., Darula, Z., Medzihradszky, K. F., Palkovits, M., Penke, B., & Czurko, A. (2012). Altered functional

protein networks in the prefrontal cortex and amygdala of victims of suicide. *PLoS One*, *7*(12), e50532. https://doi.org/10.1371/journal.pone.0050532

Kidd, M. (1963). Paired helical filaments in electron microscopy of Alzheimer's disease. *Nature*, *197*(4863), 192-193. https://doi.org/10.1038/197192b0

Kimura, T., Whitcomb, D. J., Jo, J., Regan, P., Piers, T., Heo, S., Brown, C., Hashikawa, T., Murayama, M., Seok, H., Sotiropoulos, I., Kim, E., Collingridge, G. L., Takashima, A., & Cho, K. (2014). Microtubule-associated protein tau is essential for long-term depression in the hippocampus. *Philos Trans R Soc Lond B Biol Sci*, *369*(1633), 20130144. https://doi.org/10.1098/rstb.2013.0144

Knops, J., Kosik, K. S., Lee, G., Pardee, J. D., Cohen-Gould, L., & McConlogue, L. (1991). Overexpression of tau in a nonneuronal cell induces long cellular processes. *J Cell Biol*, *114*(4), 725-733. https://doi.org/10.1083/jcb.114.4.725

Kogias, G., Kornhuber, J., Reimer, D., Mielenz, D., & Muller, C. P. (2019). Swiprosin-1/ EFhd2: from Immune Regulator to Personality and Brain Disorders. *Neurosignals*, *27*(S1), 1-19. https://doi.org/10.33594/000000179

Kogias, G., Zheng, F., Kalinichenko, L. S., Kornhuber, J., Alzheimer, C., Mielenz, D., & Muller, C. P. (2020). Swiprosin1/EFhd2 is involved in the monoaminergic and locomotor responses of psychostimulant drugs. *J Neurochem*, *154*(4), 424-440. https://doi.org/10.1111/jnc.14959

Kolarova, M., Garcia-Sierra, F., Bartos, A., Ricny, J., & Ripova, D. (2012). Structure and pathology of tau protein in Alzheimer disease. *Int J Alzheimers Dis*, *2012*, 731526. https://doi.org/10.1155/2012/731526

Kopke, E., Tung, Y. C., Shaikh, S., Alonso, A. C., Iqbal, K., & Grundke-Iqbal, I. (1993). Microtubule-associated protein tau. Abnormal phosphorylation of a non-paired helical filament pool in Alzheimer disease. *J Biol Chem*, *268*(32), 24374-24384. https://doi.org/10.1016/S0021-9258(20)80536-5

Kordower, J. H., Chu, Y., Stebbins, G. T., DeKosky, S. T., Cochran, E. J., Bennett, D., & Mufson, E. J. (2001). Loss and atrophy of layer II entorhinal cortex neurons in elderly people with mild cognitive impairment. *Ann Neurol*, *49*(2), 202-213. https://www.ncbi.nlm.nih.gov/pubmed/11220740

Kroczek, C., Lang, C., Brachs, S., Grohmann, M., Dutting, S., Schweizer, A., Nitschke, L., Feller, S. M., Jack, H. M., & Mielenz, D. (2010). Swiprosin-1/EFhd2 controls B cell receptor signaling through the assembly of the B cell receptor, Syk, and phospholipase C gamma2 in membrane rafts. *J Immunol*, *184*(7), 3665-3676. https://doi.org/10.4049/jimmunol.0903642

Ksiezak-Reding, H., Liu, W. K., & Yen, S. H. (1992). Phosphate analysis and dephosphorylation of modified tau associated with paired helical filaments. *Brain Res*, *597*(2), 209-219. https://doi.org/10.1016/0006-8993(92)91476-u

Kubo, A., Misonou, H., Matsuyama, M., Nomori, A., Wada-Kakuda, S., Takashima, A., Kawata, M., Murayama, S., Ihara, Y., & Miyasaka, T. (2019). Distribution of endogenous normal tau in the mouse brain. *J Comp Neurol*, *527*(5), 985-998. https://doi.org/10.1002/cne.24577

Kuchibhotla, K. V., Wegmann, S., Kopeikina, K. J., Hawkes, J., Rudinskiy, N., Andermann, M. L., Spires-Jones, T. L., Bacskai, B. J., & Hyman, B. T. (2014). Neurofibrillary tangle-bearing neurons are functionally integrated in cortical circuits in vivo. *Proc Natl Acad Sci U S A*, *111*(1), 510-514. https://doi.org/10.1073/pnas.1318807111

Kuret, J., Chirita, C. N., Congdon, E. E., Kannanayakal, T., Li, G., Necula, M., Yin, H., & Zhong, Q. (2005). Pathways of tau fibrillization. *Biochim Biophys Acta*, *1739*(2-3), 167-178. https://doi.org/10.1016/j.bbadis.2004.06.016

Kwon, M. S., Park, K. R., Kim, Y. D., Na, B. R., Kim, H. R., Choi, H. J., Piragyte, I., Jeon, H., Chung, K. H., Song, W. K., Eom, S. H., & Jun, C. D. (2013). Swiprosin-1 is a novel actin bundling protein that regulates cell spreading and migration. *PLoS One*, *8*(8), e71626. https://doi.org/10.1371/journal.pone.0071626

Kyalu Ngoie Zola, N., Balty, C., Pyr Dit Ruys, S., Vanparys, A. A. T., Huyghe, N. D. G., Herinckx, G., Johanns, M., Boyer, E., Kienlen-Campard, P., Rider, M. H., Vertommen, D., & Hanseeuw, B. J. (2023). Specific post-translational modifications of soluble tau protein distinguishes Alzheimer's disease and primary tauopathies. *Nat Commun*, *14*(1), 3706. https://doi.org/10.1038/s41467-023-39328-1

Lasagna-Reeves, C. A., Castillo-Carranza, D. L., Sengupta, U., Clos, A. L., Jackson, G. R., & Kayed, R. (2011). Tau oligomers impair memory and induce synaptic and mitochondrial dysfunction in wild-type mice. *Mol Neurodegener*, *6*, 39. https://doi.org/10.1186/1750-1326-6-39

Lasagna-Reeves, C. A., Castillo-Carranza, D. L., Sengupta, U., Sarmiento, J., Troncoso, J., Jackson, G. R., & Kayed, R. (2012). Identification of oligomers at early stages of tau aggregation in Alzheimer's disease. *Faseb j*, *26*(5), 1946-1959. https://doi.org/10.1096/fj.11-199851

Lewis, J., Dickson, D. W., Lin, W. L., Chisholm, L., Corral, A., Jones, G., Yen, S. H., Sahara, N., Skipper, L., Yager, D., Eckman, C., Hardy, J., Hutton, M., & McGowan, E. (2001). Enhanced neurofibrillary degeneration in transgenic mice expressing mutant tau and APP. *Science*, *293*(5534), 1487-1491. https://doi.org/10.1126/science.1058189

Liscovitch, N., & French, L. (2014). Differential Co-Expression between alpha-Synuclein and IFN-gamma Signaling Genes across Development and in Parkinson's Disease. *PLoS One*, *9*(12), e115029. https://doi.org/10.1371/journal.pone.0115029

Liu, J., Zheng, Q., Deng, Y., Cheng, C. S., Kallenbach, N. R., & Lu, M. (2006). A seven-helix coiled coil. *Proc Natl Acad Sci U S A*, *103*(42), 15457-15462. https://doi.org/10.1073/pnas.0604871103

Liu, S. L., Wang, C., Jiang, T., Tan, L., Xing, A., & Yu, J. T. (2016). The Role of Cdk5 in Alzheimer's Disease. *Mol Neurobiol*, *53*(7), 4328-4342. https://doi.org/10.1007/s12035-015-9369-x

LoPresti, P. (2002). Regulation and differential expression of tau mRNA isoforms as oligodendrocytes mature in vivo: implications for myelination. *Glia*, *37*(3), 250-257. https://doi.org/10.1002/glia.10035

MacLaren, E. J., & Sikela, J. M. (2005). Cerebellar gene expression profiling and eQTL analysis in inbred mouse strains selected for ethanol sensitivity. *Alcohol Clin Exp Res*, *29*(9), 1568-1579. https://doi.org/10.1097/01.alc.0000179376.27331.ac

Martinez, P., Patel, H., You, Y., Jury, N., Perkins, A., Lee-Gosselin, A., Taylor, X., You, Y., Viana Di Prisco, G., Huang, X., Dutta, S., Wijeratne, A. B., Redding-Ochoa, J., Shahid, S. S., Codocedo, J. F., Min, S., Landreth, G. E., Mosley, A. L., Wu, Y. C., . . . Lasagna-Reeves, C. A. (2022). Bassoon contributes to tau-seed propagation and neurotoxicity. *Nat Neurosci*, *25*(12), 1597-1607. https://doi.org/10.1038/s41593-022-01191-6

Martins-de-Souza, D., Gattaz, W. F., Schmitt, A., Rewerts, C., Maccarrone, G., Dias-Neto, E., & Turck, C. W. (2009). Prefrontal cortex shotgun proteome analysis reveals altered calcium homeostasis and immune system imbalance in schizophrenia. *Eur Arch Psychiatry Clin Neurosci*, *259*(3), 151-163. https://doi.org/10.1007/s00406-008-0847-2

Martins-de-Souza, D., Maccarrone, G., Wobrock, T., Zerr, I., Gormanns, P., Reckow, S., Falkai, P., Schmitt, A., & Turck, C. W. (2010). Proteome analysis of the thalamus and cerebrospinal fluid reveals glycolysis dysfunction and potential biomarkers candidates for schizophrenia. *J Psychiatr Res*, *44*(16), 1176-1189. https://doi.org/10.1016/j.jpsychires.2010.04.014

May, S., Hornburg, D., Schludi, M. H., Arzberger, T., Rentzsch, K., Schwenk, B. M., Grasser, F. A., Mori, K., Kremmer, E., Banzhaf-Strathmann, J., Mann, M., Meissner, F., & Edbauer, D. (2014). C9orf72 FTLD/ALS-associated Gly-Ala dipeptide repeat proteins cause neuronal toxicity and Unc119 sequestration. *Acta Neuropathol*, *128*(4), 485-503. https://doi.org/10.1007/s00401-014-1329-4

McKee, A. C., Stein, T. D., Huber, B. R., Crary, J. F., Bieniek, K., Dickson, D., Alvarez, V. E., Cherry, J. D., Farrell, K., Butler, M., Uretsky, M., Abdolmohammadi, B., Alosco, M. L., Tripodis, Y., Mez, J., & Daneshvar, D. H. (2023). Chronic traumatic encephalopathy (CTE): criteria for neuropathological diagnosis and relationship to repetitive head impacts. *Acta neuropathologica*, *145*(4), 371-394. https://doi.org/10.1007/s00401-023-02540-w

McKee, A. C., Stein, T. D., Kiernan, P. T., & Alvarez, V. E. (2015). The neuropathology of chronic traumatic encephalopathy. *Brain Pathol*, *25*(3), 350-364. https://doi.org/10.1111/bpa.12248

McKee, A. C., Stern, R. A., Nowinski, C. J., Stein, T. D., Alvarez, V. E., Daneshvar, D. H., Lee, H. S., Wojtowicz, S. M., Hall, G., Baugh, C. M., Riley, D. O., Kubilus, C. A., Cormier, K. A., Jacobs, M. A., Martin, B. R., Abraham, C. R., Ikezu, T., Reichard, R. R., Wolozin, B. L., . . .

Cantu, R. C. (2013). The spectrum of disease in chronic traumatic encephalopathy. *Brain*, *136*(Pt 1), 43-64. https://doi.org/10.1093/brain/aws307

Meier, S., Bell, M., Lyons, D. N., Ingram, A., Chen, J., Gensel, J. C., Zhu, H., Nelson, P. T., & Abisambra, J. F. (2015). Identification of Novel Tau Interactions with Endoplasmic Reticulum Proteins in Alzheimer's Disease Brain. *J Alzheimers Dis*, *48*(3), 687-702. https://doi.org/10.3233/JAD-150298

Meixner, A., Boldt, K., Van Troys, M., Askenazi, M., Gloeckner, C. J., Bauer, M., Marto, J. A., Ampe, C., Kinkl, N., & Ueffing, M. (2011). A QUICK screen for Lrrk2 interaction partners--leucine-rich repeat kinase 2 is involved in actin cytoskeleton dynamics. *Mol Cell Proteomics*, *10*(1), M110 001172. https://doi.org/10.1074/mcp.M110.001172

Mielenz, D., Reichel, M., Jia, T., Quinlan, E. B., Stockl, T., Mettang, M., Zilske, D., Kirmizi-Alsan, E., Schonberger, P., Praetner, M., Huber, S. E., Amato, D., Schwarz, M., Purohit, P., Brachs, S., Spranger, J., Hess, A., Buttner, C., Ekici, A. B., . . . Muller, C. P. (2018). EFhd2/Swiprosin-1 is a common genetic determinator for sensation-seeking/low anxiety and alcohol addiction. *Mol Psychiatry*, *23*(5), 1303-1319. https://doi.org/10.1038/mp.2017.63

Mirbaha, H., Chen, D., Morazova, O. A., Ruff, K. M., Sharma, A. M., Liu, X., Goodarzi, M., Pappu, R. V., Colby, D. W., Mirzaei, H., Joachimiak, L. A., & Diamond, M. I. (2018). Inert and seed-competent tau monomers suggest structural origins of aggregation. *eLife*, *7*, e36584. https://doi.org/10.7554/eLife.36584

Mirbaha, H., Holmes, B. B., Sanders, D. W., Bieschke, J., & Diamond, M. I. (2015). Tau Trimers Are the Minimal Propagation Unit Spontaneously Internalized to Seed Intracellular Aggregation. *J Biol Chem*, *290*(24), 14893-14903. https://doi.org/10.1074/jbc.M115.652693

Miyata, Y., Koren, J., Kiray, J., Dickey, C. A., & Gestwicki, J. E. (2011). Molecular chaperones and regulation of tau quality control: strategies for drug discovery in tauopathies. *Future Med Chem*, *3*(12), 1523-1537. https://doi.org/10.4155/fmc.11.88

Morsch, R., Simon, W., & Coleman, P. D. (1999). Neurons may live for decades with neurofibrillary tangles. *J Neuropathol Exp Neurol*, *58*(2), 188-197. https://doi.org/10.1097/00005072-199902000-00008

Mueller, R. L., Combs, B., Alhadidy, M. M., Brady, S. T., Morfini, G. A., & Kanaan, N. M. (2021). Tau: A Signaling Hub Protein. *Front Mol Neurosci*, *14*, 647054. https://doi.org/10.3389/fnmol.2021.647054

Mufson, E. J., Ma, S. Y., Cochran, E. J., Bennett, D. A., Beckett, L. A., Jaffar, S., Saragovi, H. U., & Kordower, J. H. (2000). Loss of nucleus basalis neurons containing trkA immunoreactivity in individuals with mild cognitive impairment and early Alzheimer's disease. *J Comp Neurol*, *427*(1), 19-30. https://doi.org/10.1002/1096-9861(20001106)427:1<19::aid-cne2>3.0.co;2-a

Mufson, E. J., Ma, S. Y., Dills, J., Cochran, E. J., Leurgans, S., Wuu, J., Bennett, D. A., Jaffar, S., Gilmor, M. L., Levey, A. I., & Kordower, J. H. (2002). Loss of basal forebrain P75(NTR)

immunoreactivity in subjects with mild cognitive impairment and Alzheimer's disease. *J Comp Neurol*, *443*(2), 136-153. https://doi.org/10.1002/cne.10122

Nachman, E., Wentink, A. S., Madiona, K., Bousset, L., Katsinelos, T., Allinson, K., Kampinga, H., McEwan, W. A., Jahn, T. R., Melki, R., Mogk, A., Bukau, B., & Nussbaum-Krammer, C. (2020). Disassembly of Tau fibrils by the human Hsp70 disaggregation machinery generates small seeding-competent species. *J Biol Chem*, *295*(28), 9676-9690. https://doi.org/10.1074/jbc.RA120.013478

Nelson, M. R., Thulin, E., Fagan, P. A., Forsen, S., & Chazin, W. J. (2002). The EF-hand domain: a globally cooperative structural unit. *Protein Sci*, *11*(2), 198-205. https://doi.org/10.1110/ps.33302

Neve, R. L., Harris, P., Kosik, K. S., Kurnit, D. M., & Donlon, T. A. (1986). Identification of cDNA clones for the human microtubule-associated protein tau and chromosomal localization of the genes for tau and microtubule-associated protein 2. *Brain Res*, *387*(3), 271-280. https://doi.org/10.1016/0169-328x(86)90033-1

Niewiadomska, G., Niewiadomski, W., Steczkowska, M., & Gasiorowska, A. (2021). Tau Oligomers Neurotoxicity. *Life (Basel)*, *11*(1). https://doi.org/10.3390/life11010028

Nippert, F., Schreckenberg, R., Hess, A., Weber, M., & Schluter, K. D. (2016). The Effects of Swiprosin-1 on the Formation of Pseudopodia-Like Structures and beta-Adrenoceptor Coupling in Cultured Adult Rat Ventricular Cardiomyocytes. *PLoS One*, *11*(12), e0167655. https://doi.org/10.1371/journal.pone.0167655

Novak, M., Kabat, J., & Wischik, C. M. (1993). Molecular characterization of the minimal protease resistant tau unit of the Alzheimer's disease paired helical filament. *Embo j*, *12*(1), 365-370. https://doi.org/10.1002/j.1460-2075.1993.tb05665.x

Papasozomenos, S. C., & Binder, L. I. (1987). Phosphorylation determines two distinct species of Tau in the central nervous system. *Cell Motil Cytoskeleton*, *8*(3), 210-226. https://doi.org/10.1002/cm.970080303

Park, K. R., An, J. Y., Kang, J. Y., Lee, J. G., Lee, Y., Mun, S. A., Jun, C. D., Song, W. K., & Eom, S. H. (2017). Structural mechanism underlying regulation of human EFhd2/Swiprosin-1 actin-bundling activity by Ser183 phosphorylation. *Biochem Biophys Res Commun*, *483*(1), 442-448. https://doi.org/10.1016/j.bbrc.2016.12.124

Park, K. R., Kwon, M. S., An, J. Y., Lee, J. G., Youn, H. S., Lee, Y., Kang, J. Y., Kim, T. G., Lim, J. J., Park, J. S., Lee, S. H., Song, W. K., Cheong, H. K., Jun, C. D., & Eom, S. H. (2016). Structural implications of Ca(2+)-dependent actin-bundling function of human EFhd2/Swiprosin-1. *Sci Rep*, *6*(1), 39095. https://doi.org/10.1038/srep39095

Patterson, K. R., Remmers, C., Fu, Y., Brooker, S., Kanaan, N. M., Vana, L., Ward, S., Reyes, J. F., Philibert, K., Glucksman, M. J., & Binder, L. I. (2011a). Characterization of prefibrillar Tau oligomers in vitro and in Alzheimer disease. *J Biol Chem*, *286*(26), 23063-23076. https://doi.org/10.1074/jbc.M111.237974

Patterson, K. R., Ward, S. M., Combs, B., Voss, K., Kanaan, N. M., Morfini, G., Brady, S. T., Gamblin, T. C., & Binder, L. I. (2011b). Heat shock protein 70 prevents both tau aggregation and the inhibitory effects of preexisting tau aggregates on fast axonal transport. *Biochemistry*, *50*(47), 10300-10310. https://doi.org/10.1021/bi2009147

Pearson, R. C., Sofroniew, M. V., Cuello, A. C., Powell, T. P., Eckenstein, F., Esiri, M. M., & Wilcock, G. K. (1983). Persistence of cholinergic neurons in the basal nucleus in a brain with senile dementia of the Alzheimer's type demonstrated by immunohistochemical staining for choline acetyltransferase. *Brain Res*, *289*(1-2), 375-379. https://doi.org/10.1016/0006-8993(83)90046-x

Peng, Y., Meng, G., Sheng, X., & Gao, H. (2021). Transcriptome and DNA methylation analysis reveals molecular mechanisms underlying intrahepatic cholangiocarcinoma progression. *J Cell Mol Med*, *25*(13), 6373-6387. https://doi.org/10.1111/jcmm.16615

Price, J. L., Ko, A. I., Wade, M. J., Tsou, S. K., McKeel, D. W., & Morris, J. C. (2001). Neuron number in the entorhinal cortex and CA1 in preclinical Alzheimer disease. *Arch Neurol*, *58*(9), 1395-1402. https://doi.org/10.1001/archneur.58.9.1395

Purohit, P., Perez-Branguli, F., Prots, I., Borger, E., Gunn-Moore, F., Welzel, O., Loy, K., Wenzel, E. M., Gromer, T. W., Brachs, S., Holzer, M., Buslei, R., Fritsch, K., Regensburger, M., Bohm, K. J., Winner, B., & Mielenz, D. (2014). The Ca2+ sensor protein swiprosin-1/EFhd2 is present in neurites and involved in kinesin-mediated transport in neurons. *PLoS One*, *9*(8), e103976. https://doi.org/10.1371/journal.pone.0103976

Ramesh, T., Kim, Y.-D., Kwon, M.-S., Jun, C.-D., & Kim, S.-W. (2009). Swiprosin-1 regulates cytokine expression of human mast cell line HMC-1 through actin remodeling. *Immune network*, *9*(6), 274-284. https://doi.org/10.4110/in.2009.9.6.274

Regensburger, M., Prots, I., Reimer, D., Brachs, S., Loskarn, S., Lie, D. C., Mielenz, D., & Winner, B. (2018). Impact of Swiprosin-1/Efhd2 on Adult Hippocampal Neurogenesis. *Stem Cell Reports*, *10*(2), 347-355. https://doi.org/10.1016/j.stemcr.2017.12.010

Reynolds, A. D., Kadiu, I., Garg, S. K., Glanzer, J. G., Nordgren, T., Ciborowski, P., Banerjee, R., & Gendelman, H. E. (2008). Nitrated alpha-synuclein and microglial neuroregulatory activities. *J Neuroimmune Pharmacol*, *3*(2), 59-74. https://doi.org/10.1007/s11481-008-9100-z

Robbins, M., Clayton, E., & Kaminski Schierle, G. S. (2021). Synaptic tau: A pathological or physiological phenomenon? *Acta Neuropathol Commun*, *9*(1), 149. https://doi.org/10.1186/s40478-021-01246-y

Rodriguez Ospina, S., Blazier, D. M., Criado-Marrero, M., Gould, L. A., Gebru, N. T., Beaulieu-Abdelahad, D., Wang, X., Remily-Wood, E., Chaput, D., Stevens, S., Uversky, V. N., Bickford, P. C., Dickey, C. A., & Blair, L. J. (2022). Small Heat Shock Protein 22 Improves Cognition and Learning in the Tauopathic Brain. *Int J Mol Sci*, *23*(2), 851. https://doi.org/10.3390/ijms23020851

Rosen, D. R., Siddique, T., Patterson, D., Figlewicz, D. A., Sapp, P., Hentati, A., Donaldson, D., Goto, J., O'Regan, J. P., Deng, H. X., & et al. (1993). Mutations in Cu/Zn superoxide dismutase gene are associated with familial amyotrophic lateral sclerosis. *Nature*, *362*(6415), 59-62. https://doi.org/10.1038/362059a0

Rui, Q., Ni, H., Li, D., Gao, R., & Chen, G. (2018). The Role of LRRK2 in Neurodegeneration of Parkinson Disease. *Curr Neuropharmacol*, *16*(9), 1348-1357. https://doi.org/10.2174/1570159X16666180222165418

Sala-Jarque, J., Zimkowska, K., Avila, J., Ferrer, I., & Del Rio, J. A. (2022). Towards a Mechanistic Model of Tau-Mediated Pathology in Tauopathies: What Can We Learn from Cell-Based In Vitro Assays? *Int J Mol Sci*, *23*(19). https://doi.org/10.3390/ijms231911527

Santacruz, K., Lewis, J., Spires, T., Paulson, J., Kotilinek, L., Ingelsson, M., Guimaraes, A., DeTure, M., Ramsden, M., McGowan, E., Forster, C., Yue, M., Orne, J., Janus, C., Mariash, A., Kuskowski, M., Hyman, B., Hutton, M., & Ashe, K. H. (2005). Tau suppression in a neurodegenerative mouse model improves memory function. *Science*, *309*(5733), 476-481. https://doi.org/10.1126/science.1113694

Scheff, S. W., & Price, D. A. (2006). Alzheimer's disease-related alterations in synaptic density: neocortex and hippocampus. *J Alzheimers Dis*, *9*(3 Suppl), 101-115. https://doi.org/10.3233/jad-2006-9s312

Scheff, S. W., Price, D. A., Schmitt, F. A., DeKosky, S. T., & Mufson, E. J. (2007). Synaptic alterations in CA1 in mild Alzheimer disease and mild cognitive impairment. *Neurology*, *68*(18), 1501-1508. https://doi.org/10.1212/01.wnl.0000260698.46517.8f

Scheff, S. W., Price, D. A., Schmitt, F. A., & Mufson, E. J. (2006). Hippocampal synaptic loss in early Alzheimer's disease and mild cognitive impairment. *Neurobiol Aging*, *27*(10), 1372-1384. https://doi.org/10.1016/j.neurobiolaging.2005.09.012

Sexton, C., Snyder, H., Beher, D., Boxer, A. L., Brannelly, P., Brion, J. P., Buee, L., Cacace, A. M., Chetelat, G., Citron, M., DeVos, S. L., Diaz, K., Feldman, H. H., Frost, B., Goate, A. M., Gold, M., Hyman, B., Johnson, K., Karch, C. M., . . . Carrillo, M. C. (2022). Current directions in tau research: Highlights from Tau 2020. *Alzheimers Dement*, *18*(5), 988-1007. https://doi.org/10.1002/alz.12452

Sinsky, J., Majerova, P., Kovac, A., Kotlyar, M., Jurisica, I., & Hanes, J. (2020). Physiological Tau Interactome in Brain and Its Link to Tauopathies. *J Proteome Res*, *19*(6), 2429-2442. https://doi.org/10.1021/acs.jproteome.0c00137

Skrabana, R., Skrabanova, M., Csokova, N., Sevcik, J., & Novak, M. (2006). Intrinsically disordered tau protein in Alzheimer's tangles: a coincidence or a rule? *Bratisl Lek Listy*, *107*(9-10), 354-358. https://www.ncbi.nlm.nih.gov/pubmed/17262987

Snider, J., Kotlyar, M., Saraon, P., Yao, Z., Jurisica, I., & Stagljar, I. (2015). Fundamentals of protein interaction network mapping. *Mol Syst Biol*, *11*(12), 848. https://doi.org/10.15252/msb.20156351

Spires, T. L., Orne, J. D., SantaCruz, K., Pitstick, R., Carlson, G. A., Ashe, K. H., & Hyman, B. T. (2006). Region-specific dissociation of neuronal loss and neurofibrillary pathology in a mouse model of tauopathy. *Am J Pathol*, *168*(5), 1598-1607. https://doi.org/10.2353/ajpath.2006.050840

Spires-Jones, T. L., Stoothoff, W. H., de Calignon, A., Jones, P. B., & Hyman, B. T. (2009). Tau pathophysiology in neurodegeneration: a tangled issue. *Trends Neurosci*, *32*(3), 150-159. https://doi.org/10.1016/j.tins.2008.11.007

Stamer, K., Vogel, R., Thies, E., Mandelkow, E., & Mandelkow, E. M. (2002). Tau blocks traffic of organelles, neurofilaments, and APP vesicles in neurons and enhances oxidative stress. *J Cell Biol*, *156*(6), 1051-1063. https://doi.org/10.1083/jcb.200108057

Stoub, T. R., deToledo-Morrell, L., Stebbins, G. T., Leurgans, S., Bennett, D. A., & Shah, R. C. (2006). Hippocampal disconnection contributes to memory dysfunction in individuals at risk for Alzheimer's disease. *Proc Natl Acad Sci U S A*, *103*(26), 10041-10045. https://doi.org/10.1073/pnas.0603414103

Strang, K. H., Golde, T. E., & Giasson, B. I. (2019). MAPT mutations, tauopathy, and mechanisms of neurodegeneration. *Lab Invest*, *99*(7), 912-928. https://doi.org/10.1038/s41374-019-0197-x

Sydow, A., Van der Jeugd, A., Zheng, F., Ahmed, T., Balschun, D., Petrova, O., Drexler, D., Zhou, L., Rune, G., Mandelkow, E., D'Hooge, R., Alzheimer, C., & Mandelkow, E. M. (2011). Tau-induced defects in synaptic plasticity, learning, and memory are reversible in transgenic mice after switching off the toxic Tau mutant. *J Neurosci*, *31*(7), 2511-2525. https://doi.org/10.1523/JNEUROSCI.5245-10.2011

Szczepaniak, K., Bukala, A., da Silva Neto, A. M., Ludwiczak, J., & Dunin-Horkawicz, S. (2021). A library of coiled-coil domains: from regular bundles to peculiar twists. *Bioinformatics*, *36*(22-23), 5368-5376. https://doi.org/10.1093/bioinformatics/btaa1041

Tagliavini, F., & Pilleri, G. (1983). Neuronal counts in basal nucleus of Meynert in Alzheimer disease and in simple senile dementia. *Lancet*, *1*(8322), 469-470. https://doi.org/10.1016/s0140-6736(83)91462-9

Tanzi, R. E. (2012). The genetics of Alzheimer disease. *Cold Spring Harb Perspect Med*, *2*(10). https://doi.org/10.1101/cshperspect.a006296

Terry, R. D. (1963). The Fine Structure of Neurofibrillary Tangles in Alzheimer's Disease. *J Neuropathol Exp Neurol*, *22*(4), 629-642. https://doi.org/10.1097/00005072-196310000-00005

Tiernan, C. T., Combs, B., Cox, K., Morfini, G., Brady, S. T., Counts, S. E., & Kanaan, N. M. (2016). Pseudophosphorylation of tau at S422 enhances SDS-stable dimer formation and impairs both anterograde and retrograde fast axonal transport. *Exp Neurol*, *283*(Pt A), 318-329. https://doi.org/10.1016/j.expneurol.2016.06.030

Tong, L. C., Wang, Z. B., Zhang, J. Q., Wang, Y., Liu, W. Y., Yin, H., Li, J. C., Su, D. F., Cao, Y. B., Zhang, L. C., & Li, L. (2021). Swiprosin-1 deficiency in macrophages alleviated atherogenesis. *Cell Death Discov*, 7(1), 344. https://doi.org/10.1038/s41420-021-00739-y

Tracy, T. E., Madero-Perez, J., Swaney, D. L., Chang, T. S., Moritz, M., Konrad, C., Ward, M. E., Stevenson, E., Huttenhain, R., Kauwe, G., Mercedes, M., Sweetland-Martin, L., Chen, X., Mok, S. A., Wong, M. Y., Telpoukhovskaia, M., Min, S. W., Wang, C., Sohn, P. D., . . . Gan, L. (2022). Tau interactome maps synaptic and mitochondrial processes associated with neurodegeneration. *Cell*, 185(4), 712-728 e714. https://doi.org/10.1016/j.cell.2021.12.041

Tu, Y., Zhang, L., Tong, L., Wang, Y., Zhang, S., Wang, R., Li, L., & Wang, Z. (2018). EFhd2/swiprosin-1 regulates LPS-induced macrophage recruitment via enhancing actin polymerization and cell migration. *Int Immunopharmacol*, 55, 263-271. https://doi.org/10.1016/j.intimp.2017.12.030

Twine, N. A., Janitz, K., Wilkins, M. R., & Janitz, M. (2011). Whole transcriptome sequencing reveals gene expression and splicing differences in brain regions affected by Alzheimer's disease. *PLoS One*, 6(1), e16266. https://doi.org/10.1371/journal.pone.0016266

Usenovic, M., Niroomand, S., Drolet, R. E., Yao, L., Gaspar, R. C., Hatcher, N. G., Schachter, J., Renger, J. J., & Parmentier-Batteur, S. (2015). Internalized Tau Oligomers Cause Neurodegeneration by Inducing Accumulation of Pathogenic Tau in Human Neurons Derived from Induced Pluripotent Stem Cells. *J Neurosci*, 35(42), 14234-14250. https://doi.org/10.1523/JNEUROSCI.1523-15.2015

Uversky, V. N. (2015). Intrinsically disordered proteins and their (disordered) proteomes in neurodegenerative disorders [Opinion]. *Front Aging Neurosci*, 7, 18. https://doi.org/10.3389/fnagi.2015.00018

Uversky, V. N. (2019). Intrinsically Disordered Proteins and Their "Mysterious" (Meta)Physics [Review]. *Frontiers in Physics*, 7. https://doi.org/10.3389/fphy.2019.00010

Vanderweyde, T., Apicco, D. J., Youmans-Kidder, K., Ash, P. E. A., Cook, C., Lummertz da Rocha, E., Jansen-West, K., Frame, A. A., Citro, A., Leszyk, J. D., Ivanov, P., Abisambra, J. F., Steffen, M., Li, H., Petrucelli, L., & Wolozin, B. (2016). Interaction of tau with the RNA-Binding Protein TIA1 Regulates tau Pathophysiology and Toxicity. *Cell Rep*, 15(7), 1455-1466. https://doi.org/10.1016/j.celrep.2016.04.045

Vazquez-Rosa, E., Rodriguez-Cruz, E. N., Serrano, S., Rodriguez-Laureano, L., & Vega, I. E. (2014). Cdk5 phosphorylation of EFhd2 at S74 affects its calcium binding activity. *Protein Sci*, 23(9), 1197-1207. https://doi.org/10.1002/pro.2499

Vega, I. E. (2016). EFhd2, a Protein Linked to Alzheimer's Disease and Other Neurological Disorders. *Front Neurosci*, 10, 150. https://doi.org/10.3389/fnins.2016.00150

Vega, I. E., Sutter, A., Parks, L., Umstead, A., & Ivanova, M. I. (2018). Tau's Three-Repeat Domain and EFhd2 Co-incubation Leads to Increased Thioflavin Signal. *Front Neurosci*, 12, 879. https://doi.org/10.3389/fnins.2018.00879

Vega, I. E., Traverso, E. E., Ferrer-Acosta, Y., Matos, E., Colon, M., Gonzalez, J., Dickson, D., Hutton, M., Lewis, J., & Yen, S. H. (2008). A novel calcium-binding protein is associated with tau proteins in tauopathy. *J Neurochem*, *106*(1), 96-106. https://doi.org/10.1111/j.1471-4159.2008.05339.x

Vega, I. E., Umstead, A., & Kanaan, N. M. (2019). EFhd2 Affects Tau Liquid-Liquid Phase Separation. *Front Neurosci*, *13*, 845. https://doi.org/10.3389/fnins.2019.00845

Vershinin, M., Carter, B. C., Razafsky, D. S., King, S. J., & Gross, S. P. (2007). Multiple-motor based transport and its regulation by Tau. *Proc Natl Acad Sci U S A*, *104*(1), 87-92. https://doi.org/10.1073/pnas.0607919104

Violet, M., Delattre, L., Tardivel, M., Sultan, A., Chauderlier, A., Caillierez, R., Talahari, S., Nesslany, F., Lefebvre, B., Bonnefoy, E., Buee, L., & Galas, M. C. (2014). A major role for Tau in neuronal DNA and RNA protection in vivo under physiological and hyperthermic conditions. *Front Cell Neurosci*, *8*, 84. https://doi.org/10.3389/fncel.2014.00084

Voss, K., Combs, B., Patterson, K. R., Binder, L. I., & Gamblin, T. C. (2012). Hsp70 alters tau function and aggregation in an isoform specific manner. *Biochemistry*, *51*(4), 888-898. https://doi.org/10.1021/bi2018078

Vuadens, F., Rufer, N., Kress, A., Corthesy, P., Schneider, P., & Tissot, J. D. (2004). Identification of swiprosin 1 in human lymphocytes. *Proteomics*, *4*(8), 2216-2220. https://doi.org/10.1002/pmic.200300779

Wang, C., Zong, S., Cui, X., Wang, X., Wu, S., Wang, L., Liu, Y., & Lu, Z. (2023). The effects of microglia-associated neuroinflammation on Alzheimer's disease [Review]. *Front Immunol*, *14*, 1117172. https://doi.org/10.3389/fimmu.2023.1117172

Wang, P., Joberty, G., Buist, A., Vanoosthuyse, A., Stancu, I. C., Vasconcelos, B., Pierrot, N., Faelth-Savitski, M., Kienlen-Campard, P., Octave, J. N., Bantscheff, M., Drewes, G., Moechars, D., & Dewachter, I. (2017). Tau interactome mapping based identification of Otub1 as Tau deubiquitinase involved in accumulation of pathological Tau forms in vitro and in vivo. *Acta Neuropathol*, *133*(5), 731-749. https://doi.org/10.1007/s00401-016-1663-9

Wang, X., Williams, D., Muller, I., Lemieux, M., Dukart, R., Maia, I. B. L., Wang, H., Woerman, A. L., & Schmitt-Ulms, G. (2019). Tau interactome analyses in CRISPR-Cas9 engineered neuronal cells reveal ATPase-dependent binding of wild-type but not P301L Tau to non-muscle myosins. *Sci Rep*, *9*(1), 16238. https://doi.org/10.1038/s41598-019-52543-5

Wang, Y., & Mandelkow, E. (2016). Tau in physiology and pathology. *Nat Rev Neurosci*, *17*(1), 5-21. https://doi.org/10.1038/nrn.2015.1

Wang, Z. B., Han, P., Tong, L. C., Luo, Y., Su, W. H., Wei, X., Yu, X. H., Liu, W. Y., Zhang, X. H., Lei, H., Li, Z. Z., Wang, F., Chen, J. G., Ma, T. H., Su, D. F., & Li, L. (2017). Low level of swiprosin-1/EFhd2 in vestibular nuclei of spontaneously hypersensitive motion sickness mice. *Sci Rep*, *7*(1), 40986. https://doi.org/10.1038/srep40986

Wegmann, S., Eftekharzadeh, B., Tepper, K., Zoltowska, K. M., Bennett, R. E., Dujardin, S., Laskowski, P. R., MacKenzie, D., Kamath, T., Commins, C., Vanderburg, C., Roe, A. D., Fan, Z., Molliex, A. M., Hernandez-Vega, A., Muller, D., Hyman, A. A., Mandelkow, E., Taylor, J. P., & Hyman, B. T. (2018). Tau protein liquid-liquid phase separation can initiate tau aggregation. *Embo j*, *37*(7). https://doi.org/10.15252/embj.201798049

Weingarten, M. D., Lockwood, A. H., Hwo, S. Y., & Kirschner, M. W. (1975). A protein factor essential for microtubule assembly. *Proc Natl Acad Sci U S A*, *72*(5), 1858-1862. https://doi.org/10.1073/pnas.72.5.1858

Whitehouse, P. J., Price, D. L., Struble, R. G., Clark, A. W., Coyle, J. T., & Delon, M. R. (1982). Alzheimer's disease and senile dementia: loss of neurons in the basal forebrain. *Science*, *215*(4537), 1237-1239. https://doi.org/10.1126/science.7058341

Wischik, C. M., Novak, M., Edwards, P. C., Klug, A., Tichelaar, W., & Crowther, R. A. (1988a). Structural characterization of the core of the paired helical filament of Alzheimer disease. *Proc Natl Acad Sci U S A*, *85*(13), 4884-4888. https://doi.org/10.1073/pnas.85.13.4884

Wischik, C. M., Novak, M., Thogersen, H. C., Edwards, P. C., Runswick, M. J., Jakes, R., Walker, J. E., Milstein, C., Roth, M., & Klug, A. (1988b). Isolation of a fragment of tau derived from the core of the paired helical filament of Alzheimer disease. *Proc Natl Acad Sci U S A*, *85*(12), 4506-4510. https://doi.org/10.1073/pnas.85.12.4506

Wittmann, C. W., Wszolek, M. F., Shulman, J. M., Salvaterra, P. M., Lewis, J., Hutton, M., & Feany, M. B. (2001). Tauopathy in Drosophila: neurodegeneration without neurofibrillary tangles. *Science*, *293*(5530), 711-714. https://doi.org/10.1126/science.1062382

Wood, J. G., Mirra, S. S., Pollock, N. J., & Binder, L. I. (1986). Neurofibrillary tangles of Alzheimer disease share antigenic determinants with the axonal microtubule-associated protein tau (tau). *Proc Natl Acad Sci U S A*, *83*(11), 4040-4043. https://doi.org/10.1073/pnas.83.11.4040

Wu, J., Xu, X., Duan, J., Chai, Y., Song, J., Gong, D., Wang, B., Hu, Y., Han, T., Ding, Y., Liu, Y., Li, J., & Cao, X. (2024). EFHD2 suppresses intestinal inflammation by blocking intestinal epithelial cell TNFR1 internalization and cell death. *Nat Commun*, *15*(1), 1282. https://doi.org/10.1038/s41467-024-45539-x

Xue, B., Qu, Y., Zhang, X., & Xu, X. F. (2022). miRNA-126a-3p participates in hippocampal memory via alzheimer's disease-related proteins. *Cereb Cortex*, *32*(21), 4763-4781. https://doi.org/10.1093/cercor/bhab515

Zhai, J., Strom, A. L., Kilty, R., Venkatakrishnan, P., White, J., Everson, W. V., Smart, E. J., & Zhu, H. (2009). Proteomic characterization of lipid raft proteins in amyotrophic lateral sclerosis mouse spinal cord. *Febs j*, *276*(12), 3308-3323. https://doi.org/10.1111/j.1742-4658.2009.07057.x

Zhang, H., Cao, Y., Ma, L., Wei, Y., & Li, H. (2021). Possible Mechanisms of Tau Spread and Toxicity in Alzheimer's Disease. *Front Cell Dev Biol*, *9*, 707268. https://doi.org/10.3389/fcell.2021.707268

Zhang, S., Tu, Y., Sun, Y. M., Li, Y., Wang, R. M., Cao, Y., Li, L., Zhang, L. C., & Wang, Z. B. (2018). Swiprosin-1 deficiency impairs macrophage immune response of septic mice. *JCI Insight*, *3*(3). https://doi.org/10.1172/jci.insight.95396

Zhang, W., Chen, L., Lu, X., Dong, X., Feng, M., Tu, Y., & Wang, Z. (2024). EFHD2 regulates T cell receptor signaling and modulates T helper cell activation in early sepsis. *Int Immunopharmacol*, *133*, 112087. https://doi.org/10.1016/j.intimp.2024.112087

Zhang, W., Tarutani, A., Newell, K. L., Murzin, A. G., Matsubara, T., Falcon, B., Vidal, R., Garringer, H. J., Shi, Y., Ikeuchi, T., Murayama, S., Ghetti, B., Hasegawa, M., Goedert, M., & Scheres, S. H. W. (2020). Novel tau filament fold in corticobasal degeneration. *Nature*, *580*(7802), 283-287. https://doi.org/10.1038/s41586-020-2043-0

Zhang, Y., Wu, K. M., Yang, L., Dong, Q., & Yu, J. T. (2022). Tauopathies: new perspectives and challenges. *Mol Neurodegener*, *17*(1), 28. https://doi.org/10.1186/s13024-022-00533-z

Chapter Two: EFhd2 co-aggregates with monomeric and filamentous tau *in vitro*

Abstract

Tauopathies are characterized by the abnormal buildup of tau protein, with early oligomeric forms associated with neurodegeneration and the later neurofibrillary tangles possibly conferring neuroprotection. The molecular mechanisms governing the formation of these tau species remain elusive. Recently, more attention has been paid to investigating interactions between tau and other proteins along with their impact on tau aggregation. Our previous work revealed EFhd2's association with pathological tau in animal models and tauopathy brains. Herein, we examined the impact of EFhd2 on monomeric and filamentous tau *in vitro*. The results demonstrated that EFhd2 incubation with monomeric full length human tau (hTau40) formed amorphous aggregates, where both EFhd2 and hTau40 colocalized. Moreover, EFhd2 entangled with arachidonic acid (ARA)-induced filamentous tau. Furthermore, EFhd2-induced aggregation with monomeric and filamentous hTau40 is EFhd2 concentration dependent. Using sandwich ELISA assays, we assessed the reactivity of TOC1 and Alz50—two conformation-specific tau antibodies—to EFhd2-hTau40 aggregates (in the absence and presence of ARA). No TOC1 signal was detected in EFhd2 aggregates with monomeric hTau40 whereas EFhd2 aggregates with hTau40 in the presence of ARA showed a higher signal compared to hTau40 filaments. In contrast, EFhd2 aggregates with both monomeric and filamentous hTau40 reduced Alz50 reactivity. Taken together, our results illustrate for the first time that EFhd2, a tau-associated protein, interacts with monomeric and filamentous tau to form large aggregates that are starkly different from tau oligomers and filaments. Given these findings and previous research, we propose that EFhd2 may play a role in the formation of pathological tau aggregates. Nevertheless, further studies seem vital to test this putative EFhd2's role *in vivo*.

Introduction

The quest to treat tauopathies has fueled a drive to understand the formation of pathological tau aggregates and their effects on neurodegenerative conditions. Tau proteins, known for their dynamic and flexible nature, interact with various cellular components, which makes them central players in many cellular processes (Uversky, 2015; Wang & Mandelkow, 2016; Chung et al., 2021; Mueller et al., 2021). Tau function is regulated by post-translational modifications and interactions with other proteins (Uversky, 2015; Wang & Mandelkow, 2016; Chung et al., 2021). The dynamic structure of tau, coupled with these modifications, is believed to trigger the development of pathological tau variants (Nachman et al., 2020). While neurofibrillary tangles (NFTs) were long considered the primary culprits of neurodegeneration, research has uncovered a disconnect between tangle accumulation and neuronal loss (Morsch et al., 1999; Wittmann et al., 2001; Kuret et al., 2005; Santacruz et al., 2005; Spires et al., 2006; Sydow et al., 2011; Cowan & Mudher, 2013; Kuchibhotla et al., 2014). In tandem with this evolving insight, oligomeric tau forms have emerged as potential instigators of neurodegeneration, and their accumulation correlates with cognitive decline (Berger et al., 2007; Brunden et al., 2008; Spires-Jones et al., 2009; Kayed, 2010; Cowan & Mudher, 2013). Still, identifying the toxic tau species remains a focal point of research, as does understanding the mechanisms behind tau aggregation.

Tau activity relies heavily on its interactions with other proteins, and these interactions shed light on tau pathology (Uversky, 2015; Kavanagh et al., 2022). For instance, T-cell intracellular antigen 1 (TIA1) is an RNA-binding protein that nucleates RNA stress granules. TIA1 has been demonstrated to interact with tau and induce its aberrant folding and neurodegeneration. TIA1 knockdown rescued tau-mediated neurotoxicity (Vanderweyde et al., 2016). In fact, reducing TIA1 mitigated tau oligomerization at the expense of increasing tangle accumulation, which accompanied a marked increase in neuronal survival (Apicco et al., 2018). Along similar lines, the interaction between chaperones and tau has been largely investigated by several research groups using *in vitro* and *in vivo* models (Miyata et al., 2011). Recently a small heat shock protein 22 (HSP22) has been shown to prevent heparin-induced tau aggregation and reduced oligomeric tau build up (Darling et al., 2021).

Previously, we identified EFhd2 as a novel protein associated with tau in the brains of JNPL3 mouse model and postmortem Alzheimer's disease (AD) and frontotemporal lobar degeneration (FTLD) cases (Vega et al., 2008). EFhd2 is a calcium-binding protein expressed in various organs, including the central nervous system (Vega et al., 2008; Purohit et al., 2014; Vega, 2016). In AD brains, we showed that EFhd2 existed at higher levels, co-purified with tau in the sarkosyl-insoluble fraction, and colocalized with pathological tau in the somatodendritic compartment (Ferrer-Acosta et al., 2013b). Using immunogold electron microscopy, we found that EFhd2 and tau colocalized in filamentous structures, indicating that EFhd2 co-aggregates with tau (Ferrer-Acosta et al., 2013b).

In our quest to further understand EFhd2's interactions with tau, we demonstrated that EFhd2 induces a conformational change in tau. When EFhd2 was incubated with the microtubule binding region of 3R tau (K19) without external aggregation inducers, an increased Thioflavin S signal (ThS) was detected (Vega et al., 2018). We also showed that EFhd2's coiled-coil (C-C) domain facilitates its direct protein-protein interaction with tau *in vitro* (Ferrer-Acosta et al., 2013a). Furthermore, we reported that EFhd2 affects tau's liquid-liquid phase separation by promoting the formation of solid-like structures (Vega et al., 2019). The convergence of these data sparked the hypothesis that EFhd2 plays a role in the biogenesis of pathological tau aggregates in tauopathies. This hypothesis is supported by the elevated EFhd2 levels in AD brains. An independent study confirmed that *Efhd2* is a target gene of miR-126a-3p, a microRNA that is downregulated in AD (Pichler et al., 2017; Xue et al., 2022). The downregulation of EFhd2 by miR-126-3p enhanced memory consolidation and rescued cognitive deficits in a transgenic mouse model of AD (Xue et al., 2022).

Herein, we tested the hypothesis that EFhd2 associates with tau and promotes the formation of tau aggregates. We examined the impact of recombinant human EFhd2 (hEFhd2) on monomeric and filamentous full-length human tau (hTau40) *in vitro*. Electron microscopy analysis revealed that hEFhd2 interacted with monomeric hTau40, forming amorphous aggregates. Furthermore, when hEFhd2 was combined with *in vitro*-formed hTau40 filaments/oligomers, hEFhd2 and hTau40 filaments became entangled forming unique larger aggregates. Immunogold labeling confirmed the colocalization of hEFhd2 and hTau40 in these distinct structures. Furthermore, these aggregates showed differential reactivity to conformation-specific tau antibodies; TOC1 and Alz50. Indeed, our study is the first to report the capacity of a

protein, EFhd2, to interact with tau *in vitro*, promoting the formation of higher order structures where they colocalize. Hence, this study provides the basis for further *in vivo* experiments to explore how EFhd2 modulates the biogenesis of tau aggregates in various tauopathies.

Materials and Methods

Recombinant protein production

Recombinant EFhd2 and GST

The wild type human EFhd2 genes tagged with N-terminal 6x histidine or GST was subcloned into chemically competent BL21 (DE3) *E. Coli* (New England Biolabs, cat #C2527H) cells as detailed in (Vega et al., 2008; Vega et al., 2019). Protein purification protocol was adapted from (Vega et al., 2019). Briefly, bacteria were inoculated from the frozen glycerol stock in a starter culture of 50 ml LB/Ampicillin (50 μg/ml) overnight at 37 ºC with constant shaking at 200 rpm. The next day, the saturated starter culture was diluted to 300 ml LB/Ampicillin (50 μg/ml) to 0.2-0.3 OD600 nm and incubated at 37 ºC with constant shaking at 250 rpm. When the culture reached 0.5–0.7 OD600 nm, a final concentration of 0.5 mM IPTG was added to induce protein expression. The culture was incubated for 1.5 h (hEFhd2) or 1 h (GST) at 37 ºC with constant shaking at 250 rpm. Immediately after the induction, OD600 was recorded to verify bacterial growth. The culture was centrifuged at 30,000g for 10 min at 4 ºC. Then, the bacterial pellet was frozen at -80 ºC for 20 min. Afterwards, the pellet was resuspended in 10 ml lysis buffer (1X PBS with 5 mM imidazole). With respect to GST, the pellet was resuspended in 1X PBS. The resuspended pellet was further sonicated by using Misonix XL-2000 set at 4 on ice four times 20 seconds pulses, which was shortly followed by centrifugation at 33,000g for 10 min at 4 ºC. The supernatant was rapidly separated and incubated with 1 ml of pre-equilibrated fresh HIS-select Nickel resin (Sigma, cat #H0537-25ML) or fresh GST Sepharose beads (GE Healthcare, cat #17-0756-01) overnight at 4 ºC with constant rotation. Next, the beads were allowed to settle by gravity on ice, and the supernatant was discarded. The beads were then resuspended in 1 mL Lysis buffer (or 1X PBS for GST) and carefully transferred to 10 ml column (Bio-Rad, cat #731-1550). The Lysis buffer was allowed to flow through. As soon as the lysis buffer reaches the top of the beads bed, fresh 10 ml lysis buffer (or 1X PBS) was added to wash the beads. The recombinant protein was eluted with 500 μL of 1x PBS containing 250 mM Imidazole (pH 8.0) (or 50 mM glutathione for GST). Two fractions were collected for each protein and checked on SDS-PAGE. Then, the fractions were pooled and underwent three buffer

exchange cycles with 1X PBS using centricon spin filters 3 kDa cutoff at 18,000 xg for 10 min (Sigma, cat #UFC500324). Protein concentration was determined by Pierce Rapid Gold BCA protein assay kit (Thermo Scientific, cat #A53225). To prevent hEFhd2 spontaneous self-aggregation, the final concentration was quickly brought to 2-2.5 μg/μl. For simplicity, GST final concentration was 2.3 μg/μl. The purified proteins were digested with trypsin and subjected to tandem mass spectrometry to identify potential post-translational modifications and bacterial protein contaminants (Umstead et al., 2020).

Recombinant Tau protein

Recombinant tau production and purification protocol was adapted from (Combs et al., 2017) with modifications. DNA plasmid of full-length human tau (hTau40) with C-terminal 6x histidine tag (PT7CHT40) was transformed to chemically competent BL21 *E. coli* (New England Biolabs, cat #C2527H) cells. In particular, 10 ng of DNA was added to bacterial cells and mixed by gentle swirling followed by incubation on ice for 30 min. Then, the bacteria were exposed to heat shock at 42 ºC for exactly 30 s immediately followed by incubation on ice for 10 min. Then, transformed cells were allowed to recover by growing in 250 μl of antibiotic-free S.O.C medium at 37 ºC with constant shaking at 225 rpm for 1 h. Afterwards, cells were plated on prewarmed LB agar/Ampicillin (100 μg/ml) and incubated overnight at 37 ºC in an inverted position. The next day, a single colony was picked and inoculated in a pre-culture of 50 mL LB/Ampicillin (100 μg/ml), which was incubated overnight at 30 ºC with constant shaking at 100 rpm. The saturated pre-culture was diluted to 300 ml with LB/Ampicillin (100 μg/mL) to <0.1 OD600 nm and incubated at 37 ºC with constant shaking at 250 rpm. When the culture reached 0.8–1 OD600 nm, a final concentration of 1 mM IPTG was added to induce protein expression. The culture was incubated for 2 h at 37 ºC with constant shaking at 250 rpm. The culture was centrifuged at 8000 g for 10 min at 4 ºC. The pellet was resuspended/ washed in 40 ml ice-cold STE buffer (0.1 M NaCl + 10 mM Tris Base + 1 mM EDTA, PH= 8.0). The cell suspension was carefully transferred to a pre-weighed tube and centrifuged at 8000 xg for 10 min at 4 ºC. The pellet weight was recorded. Afterwards, the pellet was resuspended in 5x volumes of ice-cold lysis D buffer (0.5 M NaCl + 10 mM tris base + 5 mM imidazole, pH= 8.0) containing 1x protease inhibitors cocktail (Thermo Fisher, cat #78437) and 1 mM PMSF (Sigma, cat #78830-5G). Then the pellet was sonicated by using Misonix XL-2000 set at 4 on ice four times with 20 s pulses. To avoid protein degradation, the protease inhibitors and PMSF were added after

sonication in addition to 0.1 % Brij 35 (Thermo Scientific, cat #20150). The resulting lysate was boiled at 99 ºC for 15 min. This step is important to eliminate bacterial heat shock proteins purified with tau. The boiled lysate was centrifuged at 16,000 g for 10 min at 4 ºC. The supernatant was carefully transferred to a new tube wherein (1x) protease inhibitors and (1 mM) PMSF were added. Subsequently, the supernatant was incubated with 1 ml of pre-equilibrated fresh HIS-select Nickel resin (Sigma, cat #H0537-25ML) overnight at 4 ºC with constant rotation. The beads were allowed to settle by gravity on ice, and the supernatant was carefully removed and discarded. The beads were gently resuspended in 1 ml of Lysis buffer (1X PBS + 5 mM imidazole) and rapidly transferred to a 10 ml column (Bio-Rad, cat #731-1550). As the Lysis buffer reached the top of the beads bed, 10 ml of lysis buffer were added at once to wash the beads. Recombinant tau protein was eluted with 500 μl of 1X PBS containing 250 mM Imidazole (pH = 8.0). Two elution fractions were collected and checked on SDS-PAGE. The two fractions were then pooled and underwent three buffer exchange cycles with tau storage buffer (70 mM Tris, pH 7.4, 75 mM NaCl) using centricon spin filters 3 kDa cutoff at 18,000 xg for 10 min/ cycle at 4 ºC (Sigma, cat #UFC500324). Protein concentration was determined by Pierce Rapid Gold BCA protein assay kit (Thermo Scientific, cat #A53225). The final concentration was brought 2.5-5 μg/μl. Finally, DTT was added for a final concentration of 1 mM to impede the formation of disulfide bonds. The purified proteins were digested with trypsin and subjected to tandem mass spectrometry to identify potential post-translational modifications and bacterial protein contaminants (Umstead et al., 2020).

In vitro tau polymerization and filament formation

Arachidonic acid (ARA) is a well-known polyanion molecule capable of inducing tau filaments _in vitro_. Being a free fatty acid, ARA promotes tau aggregation above critical micelle concentration due to the negative charge on the lipid surface, which acts as a nucleating factor for tau fibrillization (Wilson & Binder, 1997; Chirita et al., 2003). It is important to note that ARA promotes tau aggregation at 2 μM, which similar to the physiological level of tau. Herein, we followed the standard protocol of ARA-induced tau aggregation (Combs et al., 2017) by adding 2 μM of recombinant protein (hTau40, hEFhd2, or GST) to the polymerization buffer (5 mM DTT + 100 mM NaCl + 10 mM HEPEs + 0.1 mM EDTA). The protein is mixed by gentle swirling and tapping. The final concentration of 75 μM ARA (Cayman, cat #900100.1) was added carefully and mixed by gentle swirling to avoid air bubbles, which might change the

aggregation dynamics. A working solution of 2 mM ARA in 100% ethanol is prepared immediately before use. Then, it is discarded due to the oxidation of ARA. After adding ARA to the polymerization reaction, the tubes are tightly wrapped using parafilm to minimize the evaporation that will impact the final concentration. Unless otherwise stated, the polymerization was allowed to proceed overnight (16-18 h) at room temperature. Reactions that do not include ARA, equivalent volume of 100% ethanol is added to the polymerization buffer-protein mixture. Equimolar concentrations (2 μM) were added to the polymerization buffer when recombinant proteins were incubated together. Moreover, to examine the effect of reducing EFhd2 concentration on tau aggregation, 2, 1 or 0.5 μM hEFhd2 was added with 2 μM hTau40 in the polymerization buffer for direct comparison. At the end of polymerization time, samples were subjected to immunogold labeling, or directly processed for imaging using transmission electron microscopy. All the experiments were repeated at least three independent times.

Immunogold labeling

To investigate the colocalization of hTau40 and hEFhd2 in aggregate structures, immunogold labeling and electron microscopy was used. Briefly, a parafilm platform was prepared in a humidifying chamber for all incubation steps. Twenty microliters of each sample were fixed with 2% glutaraldehyde (EMS, cat #16120) for 10 min. Then, a 300-mesh carbon-coated nickel grid (EMS, FCF300NI) was placed on a 5 μl drop of each fixed sample spotted on the parafilm for 1 min. Then each grid was rinsed in one 10 μl drop of sterile water that was then wicked away using Whitman filter paper (Capillary Blotting and Wicking applications, GB003). This step was repeated with a 20 μl drop of blocking solution (5% normal goat serum + 0.1% bovine serum albumin in TBS). Next, the grids were placed over a 20 μl drop blocking solution for 30 min blocking at room temperature. After blocking, each grid was incubated with a 20 μl drop of primary antibodies for 1.5 h at room temperature. Primary antibody solution was a mixture of Tau13 1:2500 (Biolegend, cat #835201 and EFhd2 1:10, rabbit (Prosci, cat #5657) diluted in TBS/ 5% normal goat serum. After incubation, grids were rinsed with sterile filtered TBS three times 1 min each. The grids were then incubated with a 20 μl drop of secondary antibodies mixture for 1 h at room temperature. Secondary antibodies were 15 mm gold-conjugated goat anti-rabbit (EMS, cat #25112) and 6 nm gold-conjugated goat anti-mouse (EMS, cat #25124) diluted in TBS/ 5% NGS 1:20. Subsequently, grids were washed with TBS six times 1 min each. Lastly, the grids were rinsed with a 10 μl drop of water followed by another rinse

with a 10 µl drop of VitroEase (2% methylamine vanadate, Thermo Scientific, cat #A51037)). The last step was staining the grid on a 10 µl drop of VitroEase for 2 min. Grids were stored in grid boxes to fully dry before taking the micrographs.

Transmission electron microscopy (TEM)

TEM was used to visualize the morphological changes of tau aggregates induced by hEFhd2 (Cox et al., 2016). At the end of the polymerization reaction, unless the samples were processed for immunogold, all samples were processed for TEM using the same procedure. Beforehand, a parafilm platform was prepared on which grid handling took place. We used 300 mesh carbon-coated copper grids (EMS, cat #FCF300-CU). First, 20 µl of each sample were fixed with 2% glutaraldehyde for 10 min. Then, a 5 µl drop of each sample was spotted on the parafilm. The grids were placed on the top of sample drops for 1 min. The grids were rinsed by picking up a 10 µl drop of sterile water and wicking it away using Whatman filter paper. The final step was incubating the grids over a 10 µl drop of 2% uranyl acetate (EMS, 22400) for 1 min. The grids were allowed to fully dry in a closed grid box before taking the micrographs using a JEOL JEM-1400 Plus electron microscope at 80 kV and 5,000X and 15,000X magnification (25,000X and 40,000X for immunogold staining). Images were captured with an AMT XR81 digital camera and AMT software version 602.6 (Advanced Microscopy Techniques).

Quantitative TEM analysis

Individual aggregate area for all experiments was quantified using Image J (Fiji 2.3) using the images captured at 5000X magnification. First, the scale on Image J was set at 374 pixels equal to 800 nm to match the scale bar. Auto-threshold was selected to differentiate between aggregates versus background. To ensure unbiased detection of aggregated structures, the images of hTau40^m (no aggregates) were used to establish the minimum area of true aggregates and to eliminate background of detected specks. Data were compiled from at least three replicates of each experiment using three randomly selected fields of each replicate.

Oligomeric EFhd2 short filaments were quantified, and their average area was set as a baseline (1500 nm^2) above which hTau40^m/hEFhd2 aggregate area was analyzed and counted. The reason is that in hTau40^m/hEFhd2 samples we observed amorphous aggregates and short filaments that could be ascribed to hEFhd2 oligomerization. Likewise, average area of hTau40^{ARA} filaments were set as a baseline (2000 nm^2) above which hTau40^{ARA}/hEFhd2

aggregate area were analyzed and counted. It is noteworthy that the data, often, had to be curated manually if the software recognized one object as two separate objects, or if it counted a hole as an object. Micrographs with the lowest number of outliers were selected to make the figures presented in the paper.

Sandwich ELISA

As described in Combs et al, 2017 a nondenaturing sandwich ELISA assay (sELISA) is instrumental to quantify tau oligomeric modifications in disease brains and recombinant protein (Combs et al., 2017). Herein, a slightly modified version of the assay was used to assess EFhd2-induced aggregates formed with hTau40^m and hTau40^{ARA}. Unless stated otherwise, all steps were undertaken at room temperature with shaking at 200 rpm. Washing and blocking were performed using 200μl/well. All other steps performed using 50μl/well. The capture antibodies used were Tau13, TOC1, or Alz50. Tau13 (Biolegend, cat #835201) is a pan-tau monoclonal mouse IgG1antibody that reacts with monomeric and aggregated tau. TOC1 is a monoclonal mouse IgM antibody that was developed against tau dimers. It is a conformation-dependent antibody whose epitope is presumably revealed with dimerization and oligomerization (RRID#: AB_2832939; Kanaan Lab) (Patterson et al., 2011; Ward et al., 2013). Alz50 is another tau conformation-specific antibody. It is monoclonal mouse IgM that recognizes discontinuous epitope in misfolded tau 2-10 aa and 312-342 aa (RRID#: AB_2313937; Davies lab) (Wolozin et al., 1986; Ksiezak-Reding et al., 1988; Goedert et al., 1991; Ksiezak-Reding et al., 1995; Carmel et al., 1996). At the end of overnight incubation of polymerization reaction, samples were initially diluted in 1X PBS to 40 nM (Tau13), 20 nM (TOC1, in presence of ARA), 40 nM (TOC1, in the absence of ARA; and Alz50). High binding 96-well plates (Corning, cat #3590) were coated with TOC1, Tau13, or Alz50 diluted to 2 ng/μl in 1X PBS and incubated overnight at 4 °C. Additional wells were coated with only 1X PBS and were used as a negative antibody control. Sample wells were strictly washed twice with ELISA wash buffer (100 mM borate acid, 25 mM sodium borate, 75 mM NaCl, 0.25 mM thimerosal, 0.4% (w/v) bovine serum albumin, 0.05% (v/v) Tween-20) and then blocked for 1 h with 5% non-fat dry milk (NFDM) prepared in ELISA wash buffer. Then, sample wells were carefully washed twice with ELISA wash buffer followed by adding the diluted samples for 1.5 h. Sample wells were washed 4 times with ELISA wash buffer and incubated with the detection antibodies; rabbit polyclonal pan-tau R1(Kannan lab) at 1:10k for 1.5 h. Afterwards, sample wells were carefully washed 4 times and incubated with goat-anti-

rabbit-HRP at 1:5000 (Vector Labs, cat #PI-1000) for 1 h. Wells were washed 4 times before developing with 3,3′,5,5′-tetramethylbenzidine (TMB, Sigma cat T8665) 8 min (Tau13, Alz50 and TOC1). Reactions were stopped using 3.5% sulfuric acid. Absorbance readings were measured at 450 nm on a SpectraMax Plus 384 microplate reader (Molecular Devices). Absorbance values of no capture negative control were first subtracted for sample values; then, the background-corrected values were converted to percent light absorbed using the equation $\%A = (1 - 10^{-A}) * 100$, where A is equal to absorbance at 450 nm.

Statistical analysis

All data were analyzed using GraphPad Prism v9.5 (San Diego, www.graphpad.com, RRID:SCR_002798). Before running statistical analysis, outliers were detected and removed from the data. ROUT method with a false discovery rate of 1% was used for detection of outliers. Normal distribution was tested using the Shapiro–Wilk test. For comparisons between two groups, unpaired T-test and Mann–Whitney test were used for Gaussian and non-Gaussian distribution samples, respectively. For multiple groups, Kruskal-Wallis test (followed by Dunn's multiple comparison post hoc test) was used for non-Gaussian samples. p-Values were calculated with a 95% confidence interval, if nothing is mentioned, it is nonsignificant: otherwise, $*p < 0.05$, $**p < 0.01$, $***p < 0.001$, $****p < 0.0001$. Data presented were shown as mean ± SEM.

Results

Incubating EFhd2 with monomeric and filamentous tau resulted in aggregate formation

Previously, our research established the connection between EFhd2 and pathological tau in both a transgenic tau model and postmortem brain tissues of tauopathies (Vega et al., 2008; Ferrer-Acosta et al., 2013b). Furthermore, we demonstrated that EFhd2 influences the conformation of tau by increasing its β-sheet structure (Vega et al., 2018). In addition, EFhd2 has been shown to affect tau's liquid-liquid phase separation by promoting the formation of solid-like structures *in vitro* (Vega et al., 2019). However, whether EFhd2 can drive the aggregation of monomeric or filamentous tau has yet to be investigated.

In our experimental approach, we utilized arachidonic acid (ARA)-induced tau fibrillization as an *in vitro* mode of tau filaments and oligomers (Combs et al., 2017). The polymerization reaction proceeded for 16-18 h at room temperature using either a single recombinant protein or by co-incubating equimolar concentrations of a protein mixture. Subsequently, each reaction was fixed and placed on carbon-coated copper grids for

visualization via transmission electron microscopy (TEM). For simplicity, hTau40^m refers to full-length human tau hTau40 incubated overnight at room temperature without an inducer, while hTau40^{ARA} refers to hTau40 incubated overnight with ARA. Additionally, hTau40^m/hEFhd2 and hTau40^{ARA}/hEFhd2 refer to the co-incubation of recombinant human EFhd2 with hTau40 in the absence and presence of ARA, respectively.

To establish a reference to which we could compare the co-incubation of EFhd2 and hTau40, each of the two proteins was first incubated separately both in the absence and presence of ARA. In line with previous research findings, monomeric hTau40 (hTau40^m) incubated overnight at room temperature without ARA exhibited no detectable filaments or aggregates (Figure 2.1A) (Kuret et al., 2005; Patterson et al., 2011; Cox et al., 2016). In contrast, Figure 2.1B shows that overnight incubation of hTau40 in the presence of ARA induced the formation of oligomers (asterisk), as well as short (caret) and long (open arrowhead) filaments (hTau40^{ARA}). Our prior studies established that EFhd2 self-oligomerizes without a nucleation factor or external inducer (Ferrer-Acosta et al., 2013a). Consistently, EFhd2 incubated overnight at room temperature formed short filamentous structures (Figure 2.1C). However, the addition of ARA reduced EFhd2 filament formation, as seen in Figure 2.1D. These findings align with our previously reported observations regarding the impact of heparin on EFhd2 self-oligomerization (Ferrer-Acosta et al., 2013b).

EFhd2 co-incubation with hTau40^m and hTau40^{ARA} led to the formation of distinct protein aggregates (Figure 2.2). EFhd2 induced the formation of amorphous aggregates when added to hTau40^m. Those aggregates were not observed in any of the recombinant proteins alone (Figure 2.2A, arrows; compared with Figure 2.1A and 2.1C). In addition, short filaments were noticed surrounding the larger protein aggregates (Figure 2.2A, arrowheads). These short filaments could represent EFhd2 self-oligomerization, as observed in Fig 2.1C. In contrast, when hEFhd2 was added to hTau40 in the presence of ARA (hTau40^{ARA}/hEFhd2), we detected aggregates that are different from those observed in hTau40^m/hEFhd2 (Figure 2.2A vs Figure 2.2B). The observed aggregates in hTau40^{ARA}/hEFhd2 seem to be formed through entangled or intertwined filaments (arrows in Figure 2.2B). The protein aggregates observed in hTau40^{ARA}/hEFhd2 are clearly different from hTau40^{ARA} filaments (Figure 2.1B).

Quantitatively, hTau40^{ARA}/hEFhd2 and hTau40^m/hEFhd2 aggregates are significantly different in area (Figure 2.2E). As delineated in the methods section, we quantified the average

area for EFhd2 filaments (Figure 2.1C and Figure 2.2E, dotted line) and hTau40^{ARA} filaments (Figure 2.1B and Figure 2.2E, solid line) and used them as a baseline above which we calculated the area of the protein aggregates observed in hTau40^m/hEFhd2 and hTau40^{ARA}/hEFhd2, respectively. We also subtracted the detected electron dense speckles that represent artifacts of the staining process. The distribution of hTau40^{ARA}/hEFhd2 aggregate areas highlights the formation of larger aggregates than the average area of long tau filaments in hTau40^{ARA} (Figure 2.2E, dashed line), indicating that the overnight co-incubation of hEFhd2 and hTau40 in the presence of ARA led to the formation of larger distinct protein aggregates. In addition, the area of hTau40^m/hEFhd2 aggregates is larger than the area of the EFhd2 filaments (Figure 2.2E, dotted line). These results indicate that incubation of EFhd2 with either hTau40^m or hTau40^{ARA} induces the formation of protein aggregates with different structural characteristics.

EFhd2 protein bears a net negative charge. Hence, it was plausible to ascribe the observed protein structures formed by incubating hEFhd2 with hTau40 in the absence or presence of ARA to mere electrostatic interaction between the two proteins. Alternatively, EFhd2 in equimolar concentration might create a crowded environment that could exert changes on tau folding and promote the formation of the observed aggregates. To address those two explanations, we conducted a control experiment using GST protein. We chose GST because it shares some physicochemical properties with EFhd2 (i.e., molecular weight and isoelectric point). Importantly, GST has not been shown to be associated with tau. Thus, we co-incubated recombinant GST with hTau40 in the absence or presence of ARA (Figure 2.2C and 2.2D). GST neither promoted changes in hTau40^m nor did it induce similar structures like those formed with hEFhd2 (Figure 2.2A vs Figure 2.2C). Likewise, adding GST to hTau40 in the presence of ARA did not lead to the formation of large protein aggregates as observed when hEFhd2 (Figure 2.2B vs Figure 2.2D). These results collectively make for a solid case that the protein aggregates observed during the co-incubation of hEFhd2 with hTau40, with or without ARA, can be clearly attributed to protein-protein interaction between EFhd2 and tau.
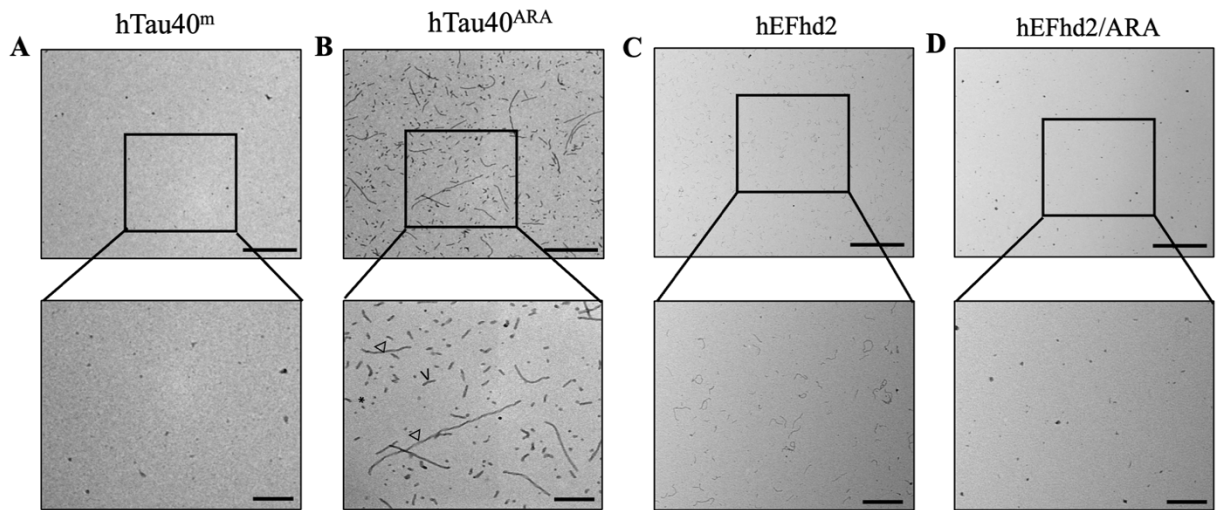
Figure 2.1. hEFhd2 and hTau40 recombinant proteins incubated in absence or presence of Arachidonic acid (ARA). (A) Representative micrograph of monomeric tau incubated overnight in the absence of ARA (hTau40^m); no obvious aggregates or filaments are formed. **(B)** Representative micrograph of filamentous/oligomeric tau (hTau40^{ARA}) by incubating hTau40 with ARA overnight; combination of oligomers (asterisk), short (caret) and long filaments (open arrowheads) are detected. **(C)** Representative micrograph of overnight polymerization of hEFhd2; short filaments are detected. **(D)** Representative micrograph hEFhd2 polymerization overnight in the presence of ARA (hEFhd2/ARA); remarkable reduction in hEFhd2 filaments is noticed. Scale bars 800 and 200 nm for the top and bottom micrographs, respectively. Experiments were repeated at least three independent times.
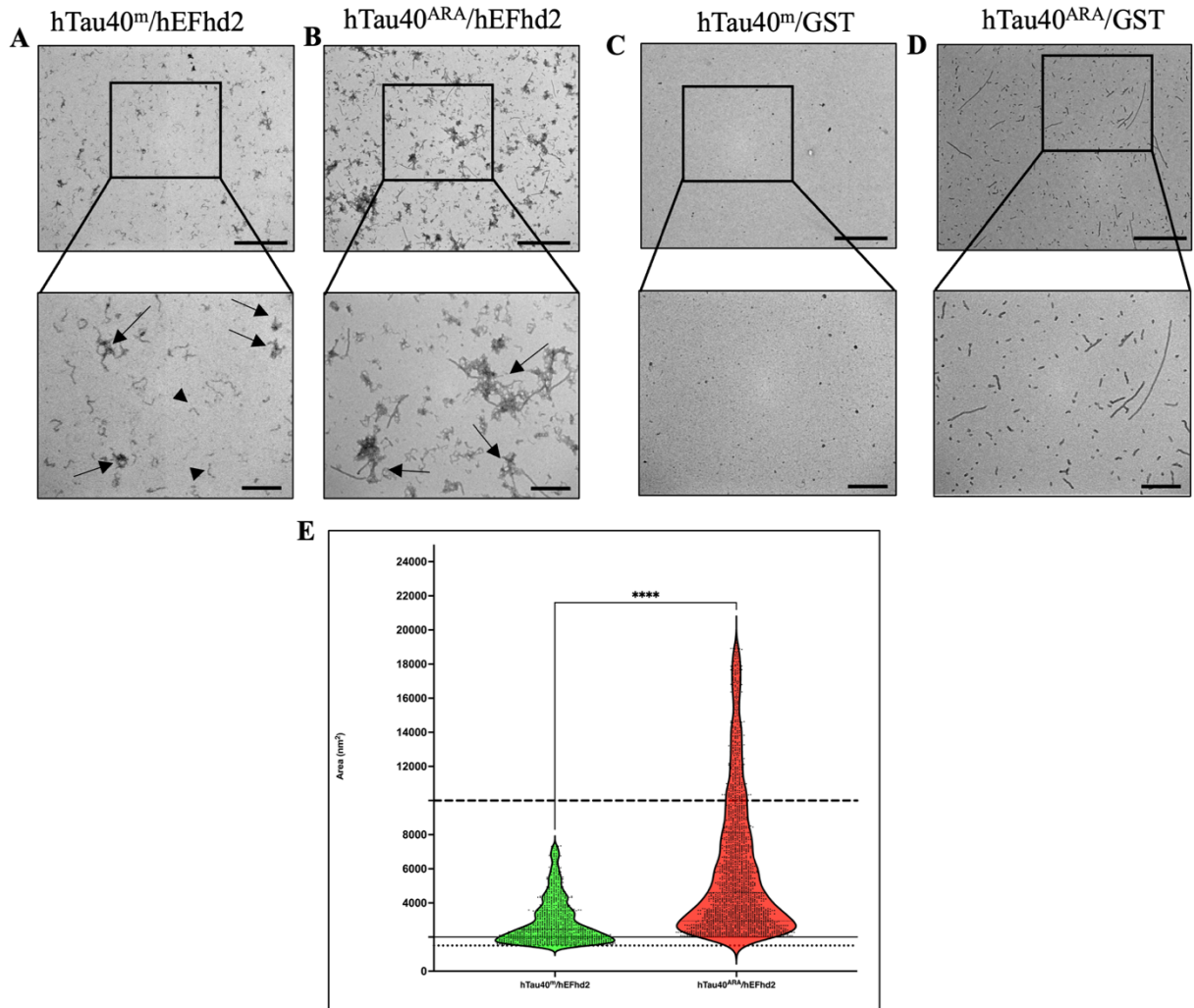
Figure 2.2. hEFhd2 promotes the aggregation of monomeric and filamentous hTau40 *in vitro*. (**A**) Representative micrograph of co-incubation of hEFhd2 (2 μM) hTau40^m (monomeric tau) overnight in the absence of ARA; amorphously shaped aggregates are detected (arrows) while EFhd2 oligomeric filaments can be seen (arrowheads). (**B**) Representative micrograph of overnight co-incubation of hEFhd2 with hTau40 in presence of ARA (hTau40^{ARA}/hEFhd2; filaments are entangled into larger aggregates (arrows). (**C**) Representative micrograph of co-incubation of GST with hTau40^m overnight in the absence of ARA (hTau40^m/GST); no aggregates or filaments were detected. (**D**) Representative micrograph of overnight co-incubation of GST with hTau40 in the presence of ARA (hTau40^{ARA}/GST), similar to hTau40^{ARA}, a combination of oligomeric and filamentous tau exists. Scale bars 800 and 200 nm for the top and bottom micrographs, respectively. Experiments were repeated at least three independent times. (**E**) Quantitative EM analysis of individual aggregate area shows that hTau40^{ARA}/hEFhd2 aggregates are significantly larger than hTau40^m/hEFhd2 aggregates. Data are represented in violin blot to show the distribution of individual aggregate area. Data were drawn from n=3 replicates/group and 3 micrographs for each replicate. Number of outliers detected and excluded are 199 and 380 for hTau40^m/hEFhd2 and hTau40^{ARA}/hEFhd2, respectively. Analysis was conducted by Mann-Whitney test, ****$p<0.0001$. Values are presented as mean ± SEM. The dotted and solid lines represent the average aggregate area of hEFhd2 filaments and hTau40^{ARA}

Figure 2.2 (cont'd)
filaments used as baseline to quantify hTau40^m/hEFhd2 and hTau40^{ARA}/ hEFhd2 aggregates, respectively. The dashed line represents the average individual aggregate area of tau long filaments.

hEFhd2 and hTau40 colocalize in the newly formed protein aggregates

To determine the colocalization of both hEFhd2 and hTau40 within the observed aggregates, immunogold electron microscopy was employed. The detection of hTau40 and hEFhd2 was carried out using Tau13 and anti-EFhd2 antibodies, respectively, immediately after the overnight polymerization reaction. Control experiments were initially conducted to demonstrate the specificity of primary antibodies (Figure A2.1, A-C) and secondary antibodies (Figure A2.1D) used in the immunogold labeling. Figure 2.3A illustrates that both hTau40 (small gold particles, arrowheads) and hEFhd2 (large particles, arrows) colocalize on the same amorphous protein aggregated structure. The electron density of amorphous protein aggregates can be challenging to focus when using immunogold labeling in electron microscopy. The lack of defined structural features and the uneven distribution of electron-dense material within amorphous aggregates affects the clarity of the imaging, including the precise localization of immunogold labels. Therefore, focusing on amorphous aggregates is more challenging compared to well-defined structures with clear boundaries. Consistently, colocalization of hTau40 (small particles, arrowheads) and hEFhd2 (large particles, arrows) was evident in hTau40^{ARA}/hEFhd2 (Figure 2.3B). Interestingly, hEFhd2 imbued the protein dense area where hTau40 filaments coalesce into the aggregates (Figure 2.3B). These results endorse that the observed aggregates comprise hEFhd2 and hTau40.

The aforementioned results along with previous studies confirm the direct association between hEFhd2 and hTau40. Nonetheless, to rule out that antibody binding to protein aggregates are technical artifacts (e.g., due to sample fixation with glutaraldehyde), we opted to use nondenaturing sELISA as an additional approach to verify the association of hEFhd2 and hTau40 on the same structures. The assays were conducted using Tau13 as the capture antibody and anti-EFhd2 as the detection antibody. Control samples were hTau40 in the absence (hTau40^m) or presence (hTau40^{ARA}) of ARA. As demonstrated in Figure 2.3C, EFhd2 signal was not detected in these samples. In contrast, EFhd2 signal was detected in both hTau40^m/hEFhd2 and hTau40^{ARA}/hEFhd2 samples. The data collectively attest to a bona fide interaction between hEFhd2 and hTau40.

hTau40^m/hEFhd2   hTau40^{ARA}/hEFhd2

A

B

C

Tau13-EFhd2 sELISA
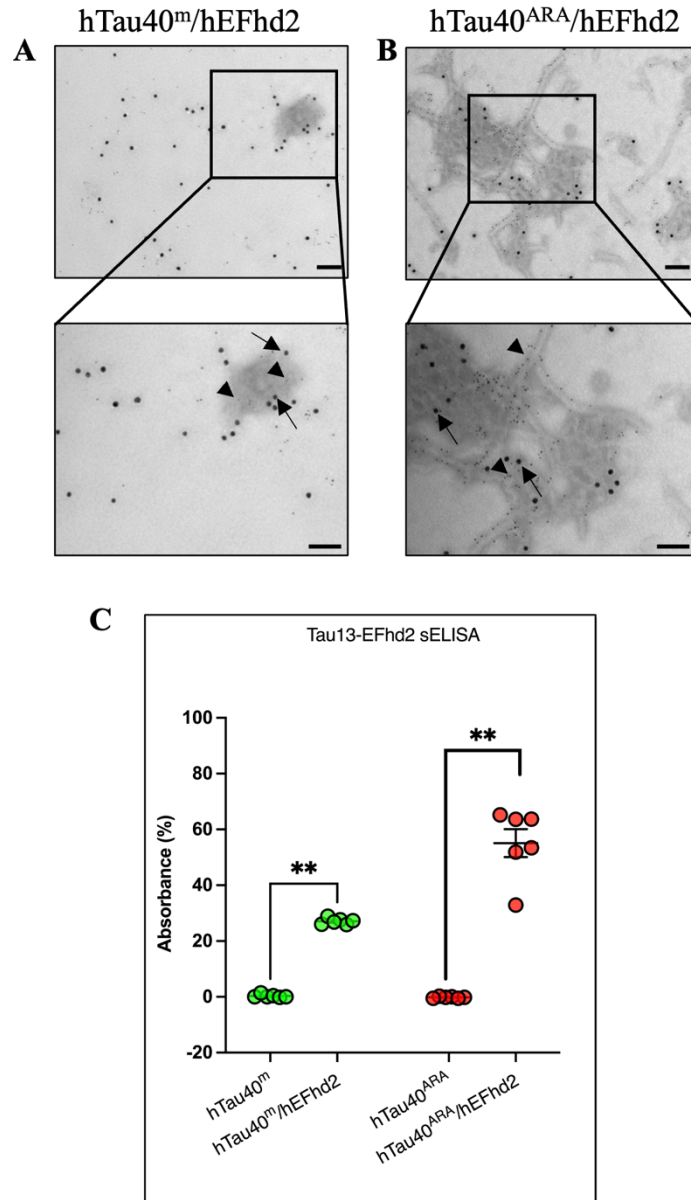
Figure 2.3. hEFhd2 and hTau40 colocalize on hEFhd2-induced aggregates. After overnight polymerization of recombinant proteins, all samples were labeled using both Tau13 antibody (IgG1 mouse antibody) and anti-EFhd2 (rabbit antibody). Distinct co-labeling was confirmed using gold-conjugated secondary antibodies anti-mouse 6 nm (small gold particles) and anti-rabbit 15 nm (large particles). (**A**) Representative micrograph of immunogold labeling conducted on hTau40^m/hEFhd2 (without ARA). Co-labeling of EFhd2 (large particles; arrows) and tau (small particles; arrowheads) was detected on the aggregates. (**B**) Representative micrograph of immunogold labeling conducted on hTau40^{ARA}/hEFhd2 (with ARA). Co-labeling of EFhd2 (large particles; arrows) and tau (small particles; arrowheads) was detected on the observed aggregates of entangled filaments. Scale bar for the top and for the bottom micrographs are 100 nm. Experiments were repeated at least three independent times. (**C**) sELISA was conducted using Tau13 as capture antibody with anti-EFhd2 as detection antibody. hTau40^m/EFhd2 and

Figure 2.3 (cont'd)

hTau40^{ARA}/hEFhd2 samples show increased signals compared to their respective controls using Mann-Whitney test; p**<0.01. Values are presented as mean ± SEM.

<u>The formation of hEFhd2-hTau40 aggregates is contingent on the concentration of EFhd2</u>

To further investigate the extent of hEFhd2/hTau40 aggregation, we explored whether the formation of these aggregates relies on the concentration of hEFhd2. When equimolar hEFhd2 and hTau40^m were used, the expected aggregates formed (compare Figure 2.2A and 2.4A). Reducing hEFhd2 concentration by half to 1 μM showed minimal differences in the aggregate structure of hTau40^m/hEFhd2 (Figure 2.4B). However, quantitative analysis revealed that 1 μM hEFhd2 led to the formation of aggregates with significantly smaller areas compared to 2 μM hEFhd2 (Figure 2.4D). Importantly, it should be noted that, as described earlier (Figure 2.2E), hTau40^m/hEFhd2 aggregates had a larger area than the area of hEFhd2 self-oligomeric filaments baseline (Fig 2.4D, dotted line). Conversely, with 0.5 μM hEFhd2, no aggregates were detected above the baseline (Figure 2.4C). These results indicate that the formation of hTau40^m/hEFhd2 aggregates is indeed hEFhd2 concentration dependent.

We also examined the effect that different hEFhd2 concentrations have on the formation of aggregates when incubated with hTau40^{ARA} (hTau40 in the presence of ARA). EM micrographs in Figures 2.5A and B illustrate unnoticeable structural differences in hTau40^{ARA}/hEFhd2 when 2 and 1 μM hEFhd2 concentrations were used. In contrast, detection of the hTau40^{ARA}/hEFhd2 entangled protein aggregates remarkably diminished when 0.5 μM hEFhd2 was used and short filaments predominated in the fields (Figure 2.5C). Moreover, statistical analysis presented in Figure 2.5D showed a significant difference in aggregate area when either 2 μM or 1 μM hEFhd2 were used in comparison to 0.5 μM hEFhd2. No significant difference was detected in the aggregate area between 2 μM and 1 μM hEFhd2. These results imply that the extent of hEFhd2-hTau aggregation is directly correlated with varying EFhd2 concentrations.
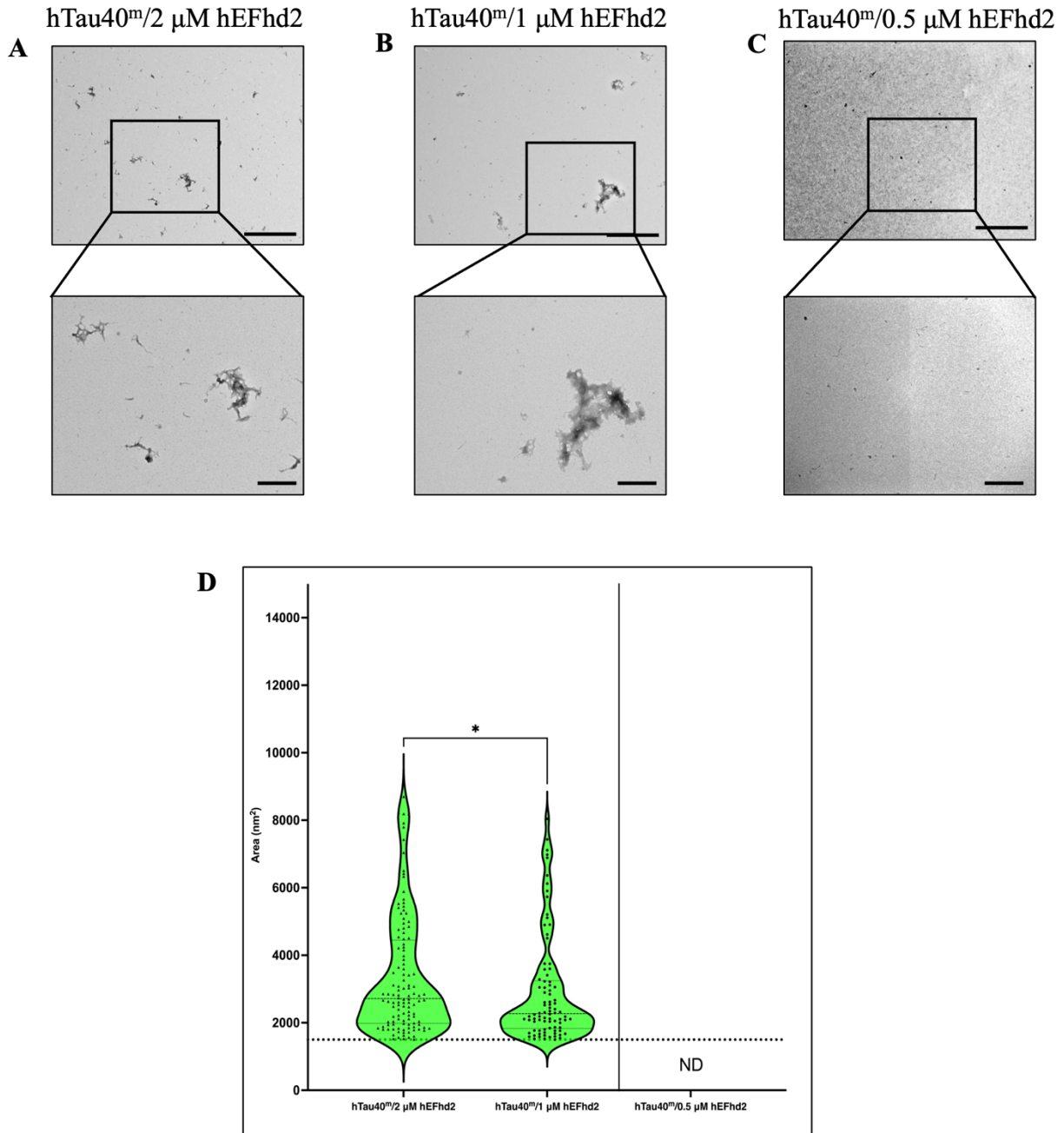
Figure 2.4. The formation of hTau40^m/hEFhd2 amorphous aggregates is hEFhd2 concentration dependent. A-C Representative micrographs of hTau40^m/hEFhd2 (co-incubating 2 μM of hTau40 and 2 μM hEFhd2 (**A**), 1 μM hEFhd2 (**B**), or 0.5 μM hEFhd2 (**C**) overnight in the absence of ARA. (**D**) Quantitative EM analysis of individual aggregate area of hTau40^m/hEFhd2 aggregates represented as violin blot. Because 0.5 μM hEFhd2 failed to promote perceptible aggregation (above the baseline of EFhd2 oligomeric filaments area; dotted line), it was not included in the analysis. The outliers detected and excluded are 23 (hTau40^m/2 μM hEFhd2) and 20 (hTau40^m/1 μM hEFhd2). The comparison between 2 and 1 μM hEFhd2-induced aggregates was conducted by Mann-Whitney test, p*<0.05. Values are presented as

Figure 2.4 (cont'd)
mean ± SEM. Dotted line represents the average individual aggregate area of hEFhd2 filaments. Scale bars are 800 and 200 nm for the top and the bottom micrographs, respectively.
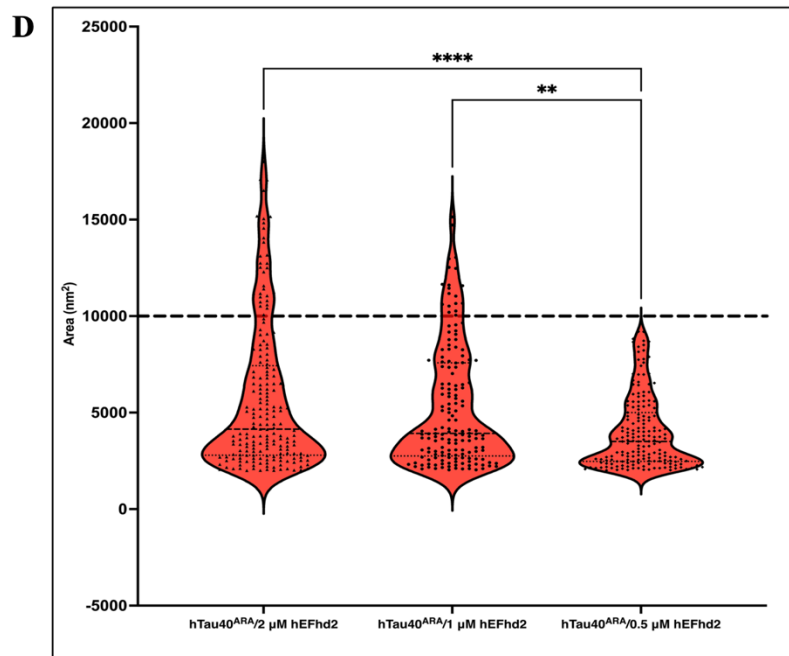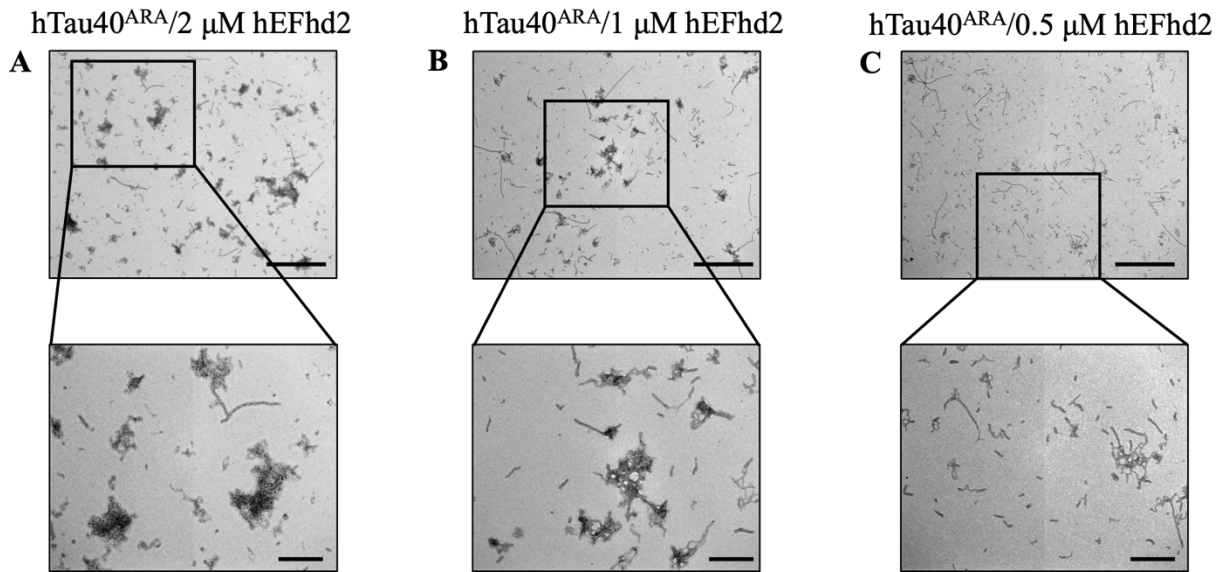
Figure 2.5. hTau40^{ARA}/hEFhd2 entangled structure formed in hEFhd2 concentration-dependent manner. A-C Representative micrographs of hTau40^{ARA}/hEFhd2 by co-incubation of 2 μM of hTau40 and 2 μM hEFhd2 (**A**), 1 μM hEFhd2 (**B**), or 0.5 μM hEFhd2 (**C**) overnight in the presence of ARA. (**D**) Quantitative EM analysis of individual aggregate area of hTau40^{ARA}/hEFhd2 aggregates. The outliers detected and excluded are 40 (hTau40^{ARA}/2 μM hEFhd2), 26 (hTau40^{ARA}/1 μM hEFhd2), and 27 (hTau40^{ARA}/0.5 μM hEFhd2). Kruskal-Wallis was conducted for statistical comparison between groups. Dunn's test was used for post hoc multiple comparison **p<0.01, ***p<0.001. Values are presented as mean ± SEM. Dashed line

Figure 2.5 (cont'd)

represents the average individual aggregate area of tau long filaments. Scale bars are 800 and 200 nm for the top and the bottom micrographs, respectively.

Influence of hEFhd2 at various stages of hTau40 filament formation *in vitro*

The co-incubation of hEFhd2, hTau40, and ARA (a robust inducer of tau fibrillization) elicited the entanglement of hEFhd2 with hTau40 filaments, suggesting that hEFhd2 did not interfere with ARA-induced hTau40 filament formation (Figure 2.2B). Figure 2.6A summarizes the experimental paradigm followed to examine how the addition of hEFhd2 to hTau40 prior to or after ARA impacts the formation of protein aggregates. In Figure 2.6C, hTau40 filaments (hTau40^f) were generated by initially incubating hTau40 with ARA for 24 h, followed by incubation with hEFhd2 for additional 16 h (hTau40^f/hEFhd2). Conversely, in Figure 2.6D, we incubated hEFhd2 and hTau40 (hTau40^m/hEFhd2) for 24 h, followed by ARA for additional 16 h (hTau40^m/hEFhd2/ARA). TEM was used to validate the formation of hTau40 filaments after 24 and 40 h incubation. The micrographs show that hTau40^f at 24 h (before adding hEFhd2) and at 40 h (the total experimental duration) are virtually the same as hTau40^{ARA} formed overnight (Figure A2.2, A-C). Similarly, we did not notice a difference between hTau40^m/hEFhd2 at 24 or 40 h and hTau40^m/hEFhd2 after overnight reaction (Figure A2.2, D-E). From Figure 2.6B, we can observe the consistent formation of hTau40^{ARA}/hEFhd2 aggregates as a reference.

Introducing hEFhd2 after ARA-induced tau filament formation (hTau40^f/hEFhd2) comparatively reduced the formation of intertwined filamentous structures (Figure 2.6B vs Figure 2.6C). Additionally, isolated filaments were visible alongside the intertwined filamentous structures (Figure 2.6C). The quantitative analysis showed a significant decrease in the area of hTau40^f/hEFhd2 entangled filamentous structures in comparison to the area of structures that emerged when all three components were co-incubated simultaneously hTau40^{ARA}/hEFhd2 (Figure 2.6E). It is important to note that despite the differences in area, the observed intertwined filamentous structures seem morphologically similar (Figures 2.6B and 2.6C).

These results indicate that hEFhd2 may be more effective at entangling hTau40 filaments during their formation rather than after they are fully formed. In other words, hEFhd2 may not interfere with the initial formation of hTau40 filaments; rather, it promotes their entanglement as they are being generated. Along this line of thinking, pre-incubation of hTau40 and hEFhd2 (hTau40^m/hEFhd2) did not interfere with ARA-induced hTau40 filament formation (Figure 2.6D). Notably, filamentous structures radiate from the amorphous protein aggregates when

79

hTau40 and hEFhd2 were incubated before the addition of ARA (Figure 2.6D). The observed structures are generally similar to those shown in Figures 2.6B and 2.6C. Moreover, the area of aggregates formed when ARA was added after the incubation of hEFhd2 and hTau40 (hTau40^m/hEFhd2/ARA) showed no significant difference from those observed when all three components were co-incubated (hTau40^{ARA}/hEFhd2) (Figure 2.6E). Taken together, these results signal that hEFhd2 does not interfere with the ARA-induced formation of hTau40 filaments. We can infer that hEFhd2 could be more effective at entangling tau filaments during ARA-induced tau polymerization than after long hTau40 filaments have been fully formed.
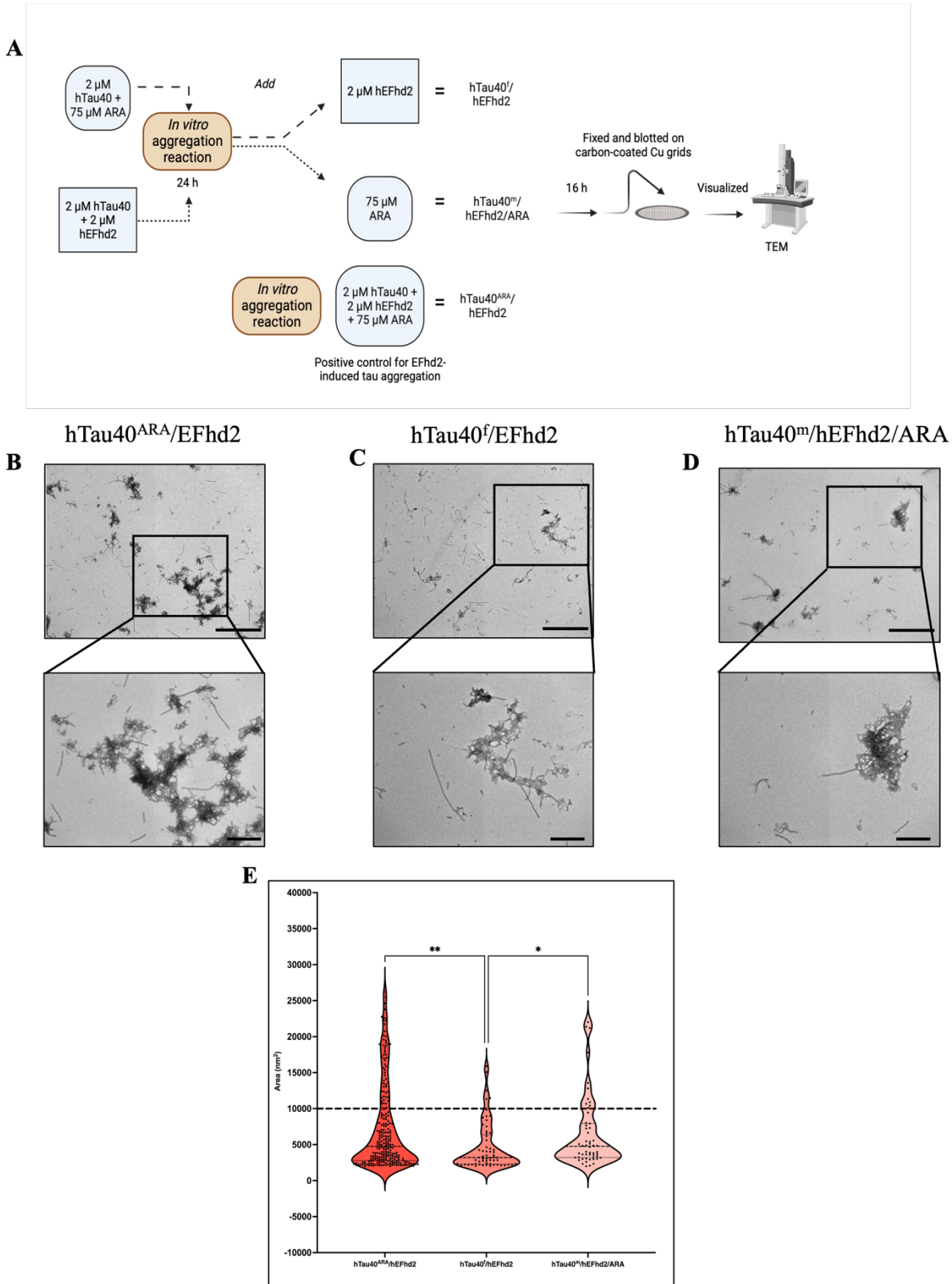
Figure 2.6. Influence of hEFhd2 at various phases of hTau40 filaments formation *in vitro*. **(A)** Summary of experimental paradigm**.** The figure summarizes the polymerization reaction conducted for this experiment and the terminology used to indicate each sample.

Figure 2.6 (cont'd)

All the reactions were conducted using 2 μM of hEFhd2 and hTau40. Arachidonic acid was used at 75 μM. hTau40^f/hEFhd2 sample is incubating hTau40 and ARA for 24 h followed by adding hEFhd2 and let the reaction proceed for another 16 h. hTau40^m/hEFhd2/ARA sample is co-incubating hEFhd2 and hTau40 for 24 h then ARA was added and the reaction proceeded for 16 h. hTau40^{ARA}/hEFhd2 sample is co-incubating hEFhd2 and hTau40 in the presence of ARA for 16 h. Then all samples were fixed on grids and visualized with TEM. This illustration was created with Biorender.com. (**B**) Representative micrograph of hTau40^{ARA}/hEFhd2 showing hTau40 filaments entangled into larger aggregates. (**C**) Representative micrograph of hTau40^f/hEFhd2 where the micrographs were taken after the 40-h reaction. A clear reduction in size and number of aggregates was noticed. (**D**) Representative micrograph of hTau40^m/hEFhd2/ARA where micrographs were taken after the 40-h reaction. A tangible reduction in the size and number of aggregates were observed from the micrographs. (**E**) Quantitative EM analysis of individual aggregate area shows that aggregates of hTau40^{ARA}/hEFhd2 and hTau40^m/hEFhd2/ARA aggregates are significantly higher than hTau40^f/hEFhd2 aggregates. No significant difference was detected between hTau40^{ARA}/hEFhd2 and hTau40^m/hEFhd2/ARA. Outliers were identified first using the ROUT method with false discovery rate of 1%. The outliers detected and excluded are 44 (hTau40^{ARA}/hEFhd2), 12 (hTau40^f/hEFhd2), and 14 (hTau40^m/hEFhd2/ARA). Then, Kruskal-Wallis was conducted for statistical comparison between groups. Dunn's test was used for post hoc multiple comparisons. *<0.05, **<0.01. Values are presented as mean ± SEM. Dashed line represents the average individual aggregate area of tau long filaments. Scale bars are 800 and 200 nm for the top and the bottom micrographs, respectively.

<u>Assessment of hEFhd2-hTau aggregates with tau-conformation specific antibodies</u>

Tau conformational changes are among the pivotal pathological events associated with neuronal toxicity (Brunden et al., 2008; Spires-Jones et al., 2009; Lasagna-Reeves et al., 2012; Cowan & Mudher, 2013; Chung et al., 2021). Hence, several tools have been geared towards characterizing tau conformation associated with its aggregated forms to understand their spatial and temporal evolution during tauopathies. Tau oligomeric complex 1 (TOC1) antibody is a conformation-dependent antibody that recognizes tau oligomers (Patterson et al., 2011; Ward et al., 2013). TOC1 epitope is exposed upon oligomerization and presumably is masked with further tau fibrillization. Sandwich ELISA (sELISA) is used to quantify and characterize TOC1 signal in tauopathies and *in vitro* tau fibrils (Tiernan et al., 2016; Combs et al., 2017). Thus, sELISA was conducted here to determine whether hEFhd2-hTau aggregates have conformational changes detected by TOC1.

hTau40^m/hEFhd2 and hTau40^{ARA}/hEFhd2 aggregates were formed as described earlier and validated using TEM. The protein aggregates were then subjected to sELISA. As illustrated in Figure 2.7A, sELISA using Tau13 as capture antibody and R1 (pan-tau) as detection antibody

was conducted to detect total hTau40 (monomeric and aggregated) levels. The results point to nearly comparable tau levels in hTau40^m/hEFhd2 and hTau40^m. In contrast, a significantly lower hTau40 level is detected in hTau40^{ARA}/hEFhd2 compared to hTau40^{ARA}.

We assessed TOC1 reactivity of aggregated hTau40 in the presence of hEFhd2. As expected, TOC1 showed no affinity for hTau40^m (monomeric tau without ARA), which served as a negative control (Figure 2.7B). Consistent with previous research (Tiernan et al., 2016; Combs et al., 2017), TOC1 successfully captured hTau40^{ARA}, confirming the formation of ARA-induced hTau40 oligomers and the associated conformational changes (Figure 2.7B). Interestingly, hTau40^m/hEFhd2 (hEFhd2 and hTau40 in the absence of ARA) was not captured with TOC1 (Figure 2.7B). This result indicates that the formation of hTau40^m/hEFhd2 aggregates does not involve the conformation change detected by TOC1. Alternatively, amorphous protein aggregate might mask the conformational epitope. Conversely, TOC1 reactivity in hTau40^{ARA}/hEFhd2 (hEFhd2 and hTau40 in the presence of ARA) was significantly higher compared to hTau40^{ARA} (Figure 2.7B). These results indicate that TOC1 captures hTau40^{ARA}/hEFhd2 aggregates more effectively than hTau40^{ARA}. That could imply that ARA-induced hTau40 filament formation in the presence of hEFdh2 leads to greater exposure of the TOC1 specific conformational epitope in comparison to hTau40^{ARA}. It is important to note here that statistical analysis was not conducted to compare between samples in the absence of ARA to samples in the presence of ARA (See Material and Methods).

We also tested if hEFhd2 induces a tau conformational change that could be detected by Alz50. Alz50 antibody recognizes a discontinuous epitope that involves tau's N-terminus and microtubule-binding repeat domains, which is formed due to a conformational change associated with tau oligomer formation (Wolozin et al., 1986; Ksiezak-Reding et al., 1988; Goedert et al., 1991; Ksiezak-Reding et al., 1995; Carmel et al., 1996). Following the same methodology, we conducted sELISA to analyze Alz50 reactivity. Figure 2.7C demonstrates that Alz50 captured hTau40^{ARA}. Alz50 signal was also detected with hTau40^m, suggesting that during the incubation time some monomeric hTau40 adapted the conformational change detected by Alz50. The incubation of hEFhd2 with hTau40 in the absence (hTau40^m/hEFhd2) or presence (hTau40^{ARA}/hEFhd2) of ARA significantly reduced Alz50 reactivity compared to hTau40^m and hTau40^{ARA}, respectively. Reduced Alz50 signal in hTau40^{ARA}/hEFhd2 could be ascribed to the

formation of a different tau conformation that masks Alz50 epitope.

Figure 2.7. Assessment of hTau40/hEFhd2 aggregates with hTau-conformation specific antibodies. Sandwich ELISA was done after overnight polymerization reaction using 2 μM recombinant proteins. It is important to note that samples prepared in the absence of ARA (hTau40^m/hEFhd2 and hTau40^m) were assessed by sELISA separately from those in the presence of ARA (hTau40^{ARA}/hEFhd2 and hTau40$^{ARA)}$. Therefore, no direct statistical comparison between the two sets was conducted. (**A**) Total hTau40 was assessed using Tau13 as capture antibody and R1 as detection antibody. Unpaired T-test revealed no significant difference in tau level between hTau40^m/hEFhd2 and hTau40^m. However, hTau40 level in hTau40^{ARA}/hEFhd2 is significantly lower than hTau40^{ARA} analyzed by unpaired T-test. (**B**) Oligomeric hTau40 conformation was assessed using TOC1 as capture antibody and R1 as detection antibody. Unpaired T-test showed that hTau40^{ARA}/hEFhd2 has higher signal compared to hTau40^{ARA}. (**C**) sELISA using Alz50 as capture antibody and R1 as detection antibody. Unpaired T-test revealed a significant difference between hTau40^m/hEFhd2 and hTau40^m. Likewise, Alz50 reactivity was

Figure 2.7 (cont'd)
significantly lower in hTau40^{ARA}/hEFhd2 compared to hTau40^{ARA}. *p<0.05, ****p<0.0001. Values are presented as mean ± SEM. The data were drawn from n=6.

Discussion

In this study, we unprecedentedly demonstrate that EFhd2 has the capacity to promote tau aggregation forming a unique higher order structure. Currently, the literature abounds with several studies investigating the effect of other proteins on pathological tau formation. Nonetheless, EFhd2 is the first to show the propensity to entangle tau filaments into larger aggregates.

Understanding the biogenesis of pathogenic tau aggregates poses a crucial step towards the identification of effective treatments for tauopathies, such as AD. Indeed, the mechanisms that lead to the formation of pathological tau species *in vivo* remain to be elucidated. *In vitro* studies provided important information about the biochemical properties of tau proteins and their propensity to form aggregates. Tau proteins do not spontaneously oligomerize *in vitro*. Tau requires external inducers that largely serve as nucleation factors to promote the formation of tau oligomers or filaments (Goedert et al., 1996; Wilson & Binder, 1997; Chirita et al., 2003; Lasagna-Reeves et al., 2010). Therefore, we have been convinced that tau association with other proteins could be playing a major role in tau-mediated pathogenesis. Against this backdrop, we discovered the calcium-binding protein EFhd2 as a tau-associated protein in a tauopathy mouse model and AD brains (Vega et al., 2008; Ferrer-Acosta et al., 2013b; Vega, 2016).

In our previous studies, EFhd2 coimmunoprecipitated with pathological tau in brain extracts from AD and other tauopathies (Vega et al., 2008). EFhd2 also colocalized with pathological tau in the somatodendritic compartment (Ferrer-Acosta et al., 2013b). Additionally, immunogold EM analysis of the sarkosyl-insoluble fraction of AD frontal cortex confirmed co-labeling of filamentous structures by tau and EFhd2 (Ferrer-Acosta et al., 2013b). That provided further evidence that EFhd2 is associated with tau filamentous structures. However, whether EFhd2 directly binds to tau filaments or influences their formation remains unclear. Furthermore, EFhd2 tau dynamics demonstrated by enhancing ThS and promoting the formation of solid-like structures in controlled *in vitro* conditions (Vega et al., 2018; Vega et al., 2019).

Thence, we hypothesize that EFhd2 plays a direct role in promoting tau aggregation. To test this hypothesis, we examined EFhd2's capacity to co-aggregate with monomeric (hTau40^m) and ARA-induced filamentous (hTau40^{ARA}) hTau40 *in vitro*. The results indicate that the

presence of hEFhd2 leads to the aggregation of hTau40 even in the absence of ARA. Immunogold analysis revealed that the resulting amorphous protein aggregates consist of both hTau40^m and hEFhd2 intricately connected. Furthermore, adding hEFhd2 did not interfere with the ARA-induced formation of hTau40^{ARA} (filaments and oligomers). Significantly, it intertwined with hTau40 filaments into uniquely formed aggregates. Immunogold labeling also demonstrated that hEFhd2 and hTau40 colocalize within these aggregates wherein hEFhd2 predominantly situated at the core connecting the hTau40 filaments.

To affirm the specificity of hEFhd2, we investigated whether GST, a molecule sharing certain physicochemical characteristics with hEFhd2, triggers hTau40 aggregation in vitro (Figure 2.2). The findings definitively demonstrated that GST did not prompt the formation of aggregates with monomeric or filamentous hTau40. Therefore, we conclude that the impact of EFhd2 on tau aggregation *in vitro* is EFhd2 specific.

EFhd2 self-oligomerizes and forms short filaments without an external aggregation inducer. That sparks the possibility that the observed protein aggregates with monomeric tau comprise solely EFhd2 oligomeric filaments. First, morphologically, EFhd2 filaments are not comparable to hTau40^m/EFhd2 aggregates (Figure 2.1C vs Figure 2.2A). Second, quantitative analysis revealed that EFhd2-induced aggregates with hTau40^m are larger than the average area of EFhd2 filaments (the dotted line in Figure 2.2E). Therefore, it is reasonable to deduce that those protein aggregates comprise EFhd2 and tau together as verified with immunogold labeling and sELISA data (Figure 2.3).

The presented findings beg the question whether EFhd2 filaments are necessary for the formation of aggregates with monomeric and filamentous tau. It should not escape our attention that adding ARA induced a clear reduction on EFhd2 self-oligomerization (Figure 2.1D). In fact, this is in line with our published research on the effect of heparin on EFhd2 (Ferrer-Acosta et al., 2013b). Heparin and ARA broadly induce *in vitro* aggregation via electrostatic interaction with positively charged proteins (e.g., tau). Given the fact that EFhd2 is a negatively charged molecule, we could speculate that a degree of repulsive force exists between EFhd2 and those aggregation inducers that hinder EFhd2 from self-oligomerization. On the whole, the evident reduction in EFhd2 self-oligomerization in the presence of ARA undermines the possibility that the unique entangled hTau40^{ARA}/ hEFhd2 aggregates necessitate EFhd2 filaments.

Previously, Kayed lab established an alternative method for *in vitro* tau fibrillization using amyloid-β (Aβ) peptide oligomers (Lasagna-Reeves et al., 2010). Like EFhd2, Aβ has a spontaneous propensity to aggregate and form fibrils/oligomers *in vitro*. This characteristic was leveraged to generate *in vitro* tau filaments/oligomers instead of using the conventional polyanionic compounds. In this method, the preformed Aβ oligomers, added at substoichiometric concentration, act as a nucleation seed that promotes tau fibrillization. An ad hoc deduction would be that EFhd2 has the same effect on tau fibrillization as Aβ peptides, and that EFhd2 filaments could be seeding tau aggregation *in vitro*. Although we do not rule out this possibility, this argument does not hold water because it overlooks the clear morphological distinction of tau aggregates formed with EFhd2 versus Aβ peptide. Although colocalization was not shown, Aβ oligomers merely act as a nidus to monomeric tau that becomes misfolded and further aggregates to filaments and oligomers. On the other hand, EFhd2 incubation with tau induced the formation of larger unique, amorphous aggregates wherein EFhd2 and tau colocalize.

Earlier, we demonstrated that EFhd2 impacts β-sheet structure formation of tau *in vitro* (Vega et al., 2018). Therefore, we investigated whether hEFhd2 co-aggregation with hTau induces conformational changes detectable by either TOC1 or Alz50 (Figure 2.7). TOC1 targets a linear epitope (209-240 aa) exposed during oligomerization (Patterson et al., 2011; Ward et al., 2013). In contrast, Alz50 recognizes a discontinuous epitope involving distant amino acids that come into proximity as a result of conformational changes associated with tau oligomerization (Ksiezak-Reding et al., 1988; Goedert et al., 1991; Ksiezak-Reding et al., 1995). The results indicated that hTau40^m/hEFhd2 did not expose the TOC1-recognized epitope. Conversely, the signal from hTau40^{ARA}/hEFhd2 samples was significantly higher than that detected with ARA-induced hTau40^{ARA}. On the other hand, Alz50 reactivity diminished in both hTau40^{ARA}/hEFhd2 and hTau40^m/hEFhd2. Another important observation is the reduced Tau13 reactivity to hTau40^{ARA}/hEFhd2 compared to hTau40^{ARA} shown in Figure 2.7A. Taken together, differential reactivity of three tau antibodies that recognize various epitopes speaks to the conformational changes that could be induced by the entanglement of ARA-induced tau filaments in the presence of EFhd2. That leads to enhancing TOC1's epitope exposure while possibly masking Alz50 and Tau13 epitopes.

Previous studies have shown tau-associated proteins that modulate the formation of tau filaments *in vitro*, such as TIA1, Hsp22, FKBP51, S100B and others (Mandelkow &

87

Mandelkow, 2012; Fontaine et al., 2015; Oroz et al., 2018; Jiang et al., 2019; Darling et al., 2021; Moreira et al., 2021; Moreira & Gomes, 2023). The effect of these tau-associated proteins on tau filament formation has been studied in the presence of either heparin or ARA. Generally, these studies examined whether the tau-associated protein had an impact on altering the size of tau filaments induced by heparin or ARA without necessarily assessing any changes in the structure of tau filaments. Our study contrasts with these previous studies in that we showed that EFhd2 induced monomeric hTau40 aggregation and entangled hTau40 filaments into larger clusters. We showed that EFhd2 and hTau40 colocalize in the detected structures. Additionally, we demonstrated that EFhd2 does not affect ARA-induced tau filament formation. Thus, EFhd2 is a tau-associated protein that induces the formation of entangled tau filaments. Nonetheless, it is worth mentioning that pathological tau also undergoes diverse molecular changes, including phosphorylation, acetylation, truncation, and other modifications, which could contribute to its aggregation. Furthermore, EFhd2 is a phosphoprotein and a target of CDK5 (Vazquez-Rosa et al., 2014). Therefore, further inquiry into the impact of phosphorylated EFhd2 on both modified and unmodified tau forms is necessary to further study the effect of EFhd2 on tau protein dynamics. Above all, this study offers an *in vitro* model that could be leveraged to examine the interplay between EFhd2 and different tau isoforms. Nonetheless, assessing the influence of EFhd2 on tau-induced neurotoxicity *in vivo* is a pivotal future direction. These ensuing *in vivo* studies will enhance our understanding of EFhd2's role in tauopathies and its potential as a target for modulating tau-mediated neurodegeneration.

REFERENCES

Apicco, D. J., Ash, P. E. A., Maziuk, B., LeBlang, C., Medalla, M., Al Abdullatif, A., Ferragud, A., Botelho, E., Ballance, H. I., Dhawan, U., Boudeau, S., Cruz, A. L., Kashy, D., Wong, A., Goldberg, L. R., Yazdani, N., Zhang, C., Ung, C. Y., Tripodis, Y., . . . Wolozin, B. (2018). Reducing the RNA binding protein TIA1 protects against tau-mediated neurodegeneration in vivo. *Nat Neurosci*, *21*(1), 72-80. https://doi.org/10.1038/s41593-017-0022-z

Berger, Z., Roder, H., Hanna, A., Carlson, A., Rangachari, V., Yue, M., Wszolek, Z., Ashe, K., Knight, J., Dickson, D., Andorfer, C., Rosenberry, T. L., Lewis, J., Hutton, M., & Janus, C. (2007). Accumulation of pathological tau species and memory loss in a conditional model of tauopathy. *J Neurosci*, *27*(14), 3650-3662. https://doi.org/10.1523/JNEUROSCI.0587-07.2007

Brunden, K. R., Trojanowski, J. Q., & Lee, V. M. (2008). Evidence that non-fibrillar tau causes pathology linked to neurodegeneration and behavioral impairments. *J Alzheimers Dis*, *14*(4), 393-399. https://doi.org/10.3233/jad-2008-14406

Carmel, G., Mager, E. M., Binder, L. I., & Kuret, J. (1996). The structural basis of monoclonal antibody Alz50's selectivity for Alzheimer's disease pathology. *J Biol Chem*, *271*(51), 32789-32795. https://doi.org/10.1074/jbc.271.51.32789

Chirita, C. N., Necula, M., & Kuret, J. (2003). Anionic micelles and vesicles induce tau fibrillization in vitro. *J Biol Chem*, *278*(28), 25644-25650. https://doi.org/10.1074/jbc.M301663200

Chung, D. C., Roemer, S., Petrucelli, L., & Dickson, D. W. (2021). Cellular and pathological heterogeneity of primary tauopathies. *Mol Neurodegener*, *16*(1), 57. https://doi.org/10.1186/s13024-021-00476-x

Combs, B., Tiernan, C. T., Hamel, C., & Kanaan, N. M. (2017). Production of recombinant tau oligomers in vitro. *Methods Cell Biol*, *141*, 45-64. https://doi.org/10.1016/bs.mcb.2017.06.005

Cowan, C. M., & Mudher, A. (2013). Are tau aggregates toxic or protective in tauopathies? *Front Neurol*, *4*, 114. https://doi.org/10.3389/fneur.2013.00114

Cox, K., Combs, B., Abdelmesih, B., Morfini, G., Brady, S. T., & Kanaan, N. M. (2016). Analysis of isoform-specific tau aggregates suggests a common toxic mechanism involving similar pathological conformations and axonal transport inhibition. *Neurobiol Aging*, *47*, 113-126. https://doi.org/10.1016/j.neurobiolaging.2016.07.015

Darling, A. L., Dahrendorff, J., Creodore, S. G., Dickey, C. A., Blair, L. J., & Uversky, V. N. (2021). Small heat shock protein 22 kDa can modulate the aggregation and liquid-liquid phase separation behavior of tau. *Protein Sci*, *30*(7), 1350-1359. https://doi.org/10.1002/pro.4060

Ferrer-Acosta, Y., Rodriguez Cruz, E. N., Vaquer Adel, C., & Vega, I. E. (2013a). Functional and structural analysis of the conserved EFhd2 protein. *Protein Pept Lett*, *20*(5), 573-583. https://doi.org/10.2174/0929866511320050011

Ferrer-Acosta, Y., Rodriguez-Cruz, E. N., Orange, F., De Jesus-Cortes, H., Madera, B., Vaquer-Alicea, J., Ballester, J., Guinel, M. J., Bloom, G. S., & Vega, I. E. (2013b). EFhd2 is a novel amyloid protein associated with pathological tau in Alzheimer's disease. *J Neurochem*, *125*(6), 921-931. https://doi.org/10.1111/jnc.12155

Fontaine, S. N., Sabbagh, J. J., Baker, J., Martinez-Licha, C. R., Darling, A., & Dickey, C. A. (2015). Cellular factors modulating the mechanism of tau protein aggregation. *Cell Mol Life Sci*, *72*(10), 1863-1879. https://doi.org/10.1007/s00018-015-1839-9

Goedert, M., Jakes, R., Spillantini, M. G., Hasegawa, M., Smith, M. J., & Crowther, R. A. (1996). Assembly of microtubule-associated protein tau into Alzheimer-like filaments induced by sulphated glycosaminoglycans. *Nature*, *383*(6600), 550-553. https://doi.org/10.1038/383550a0

Goedert, M., Spillantini, M. G., & Jakes, R. (1991). Localization of the Alz-50 epitope in recombinant human microtubule-associated protein tau. *Neurosci Lett*, *126*(2), 149-154. https://doi.org/10.1016/0304-3940(91)90541-z

Jiang, L., Ash, P. E. A., Maziuk, B. F., Ballance, H. I., Boudeau, S., Abdullatif, A. A., Orlando, M., Petrucelli, L., Ikezu, T., & Wolozin, B. (2019). TIA1 regulates the generation and response to toxic tau oligomers. *Acta Neuropathol*, *137*(2), 259-277. https://doi.org/10.1007/s00401-018-1937-5

Kavanagh, T., Halder, A., & Drummond, E. (2022). Tau interactome and RNA binding proteins in neurodegenerative diseases. *Mol Neurodegener*, *17*(1), 66. https://doi.org/10.1186/s13024-022-00572-6

Kayed, R. (2010). Anti-tau oligomers passive vaccination for the treatment of Alzheimer disease. *Hum Vaccin*, *6*(11), 931-935. https://doi.org/10.4161/hv.6.11.12689

Ksiezak-Reding, H., Davies, P., & Yen, S. H. (1988). Alz 50, a monoclonal antibody to Alzheimer's disease antigen, cross-reacts with tau proteins from bovine and normal human brain. *J Biol Chem*, *263*(17), 7943-7947. https://doi.org/10.1016/S0021-9258(18)68425-X

Ksiezak-Reding, H., Leibowitz, R. L., Bowser, R., & Davies, P. (1995). Binding of Alz 50 depends on Phe8 in tau synthetic peptides and varies between native and denatured tau proteins. *Brain Res*, *697*(1-2), 63-75. https://doi.org/10.1016/0006-8993(95)00785-o

Kuchibhotla, K. V., Wegmann, S., Kopeikina, K. J., Hawkes, J., Rudinskiy, N., Andermann, M. L., Spires-Jones, T. L., Bacskai, B. J., & Hyman, B. T. (2014). Neurofibrillary tangle-bearing neurons are functionally integrated in cortical circuits in vivo. *Proc Natl Acad Sci U S A*, *111*(1), 510-514. https://doi.org/10.1073/pnas.1318807111

Kuret, J., Chirita, C. N., Congdon, E. E., Kannanayakal, T., Li, G., Necula, M., Yin, H., & Zhong, Q. (2005). Pathways of tau fibrillization. *Biochim Biophys Acta*, *1739*(2-3), 167-178. https://doi.org/10.1016/j.bbadis.2004.06.016

Lasagna-Reeves, C. A., Castillo-Carranza, D. L., Guerrero-Muoz, M. J., Jackson, G. R., & Kayed, R. (2010). Preparation and characterization of neurotoxic tau oligomers. *Biochemistry*, *49*(47), 10039-10041. https://doi.org/10.1021/bi1016233

Lasagna-Reeves, C. A., Castillo-Carranza, D. L., Sengupta, U., Guerrero-Munoz, M. J., Kiritoshi, T., Neugebauer, V., Jackson, G. R., & Kayed, R. (2012). Alzheimer brain-derived tau oligomers propagate pathology from endogenous tau. *Sci Rep*, *2*(1), 700. https://doi.org/10.1038/srep00700

Mandelkow, E. M., & Mandelkow, E. (2012). Biochemistry and cell biology of tau protein in neurofibrillary degeneration. *Cold Spring Harb Perspect Med*, *2*(7), a006247. https://doi.org/10.1101/cshperspect.a006247

Miyata, Y., Koren, J., Kiray, J., Dickey, C. A., & Gestwicki, J. E. (2011). Molecular chaperones and regulation of tau quality control: strategies for drug discovery in tauopathies. *Future Med Chem*, *3*(12), 1523-1537. https://doi.org/10.4155/fmc.11.88

Moreira, G. G., Cantrelle, F. X., Quezada, A., Carvalho, F. S., Cristovao, J. S., Sengupta, U., Puangmalai, N., Carapeto, A. P., Rodrigues, M. S., Cardoso, I., Fritz, G., Herrera, F., Kayed, R., Landrieu, I., & Gomes, C. M. (2021). Dynamic interactions and Ca(2+)-binding modulate the holdase-type chaperone activity of S100B preventing tau aggregation and seeding. *Nat Commun*, *12*(1), 6292. https://doi.org/10.1038/s41467-021-26584-2

Moreira, G. G., & Gomes, C. M. (2023). Tau liquid-liquid phase separation is modulated by the Ca(2+) -switched chaperone activity of the S100B protein. *J Neurochem*, *166*(1), 76-86. https://doi.org/10.1111/jnc.15756

Morsch, R., Simon, W., & Coleman, P. D. (1999). Neurons may live for decades with neurofibrillary tangles. *J Neuropathol Exp Neurol*, *58*(2), 188-197. https://doi.org/10.1097/00005072-199902000-00008

Mueller, R. L., Combs, B., Alhadidy, M. M., Brady, S. T., Morfini, G. A., & Kanaan, N. M. (2021). Tau: A Signaling Hub Protein. *Front Mol Neurosci*, *14*, 647054. https://doi.org/10.3389/fnmol.2021.647054

Nachman, E., Wentink, A. S., Madiona, K., Bousset, L., Katsinelos, T., Allinson, K., Kampinga, H., McEwan, W. A., Jahn, T. R., Melki, R., Mogk, A., Bukau, B., & Nussbaum-Krammer, C. (2020). Disassembly of Tau fibrils by the human Hsp70 disaggregation machinery generates small seeding-competent species. *J Biol Chem*, *295*(28), 9676-9690. https://doi.org/10.1074/jbc.RA120.013478

Oroz, J., Chang, B. J., Wysoczanski, P., Lee, C. T., Perez-Lara, A., Chakraborty, P., Hofele, R. V., Baker, J. D., Blair, L. J., Biernat, J., Urlaub, H., Mandelkow, E., Dickey, C. A., & Zweckstetter, M. (2018). Structure and pro-toxic mechanism of the human Hsp90/PPIase/Tau complex. *Nat Commun*, *9*(1), 4532. https://doi.org/10.1038/s41467-018-06880-0

Patterson, K. R., Remmers, C., Fu, Y., Brooker, S., Kanaan, N. M., Vana, L., Ward, S., Reyes, J. F., Philibert, K., Glucksman, M. J., & Binder, L. I. (2011). Characterization of prefibrillar Tau

oligomers in vitro and in Alzheimer disease. *J Biol Chem*, *286*(26), 23063-23076. https://doi.org/10.1074/jbc.M111.237974

Pichler, S., Gu, W., Hartl, D., Gasparoni, G., Leidinger, P., Keller, A., Meese, E., Mayhaus, M., Hampel, H., & Riemenschneider, M. (2017). The miRNome of Alzheimer's disease: consistent downregulation of the miR-132/212 cluster. *Neurobiol Aging*, *50*, 167 e161-167 e110. https://doi.org/10.1016/j.neurobiolaging.2016.09.019

Purohit, P., Perez-Branguli, F., Prots, I., Borger, E., Gunn-Moore, F., Welzel, O., Loy, K., Wenzel, E. M., Gromer, T. W., Brachs, S., Holzer, M., Buslei, R., Fritsch, K., Regensburger, M., Bohm, K. J., Winner, B., & Mielenz, D. (2014). The Ca2+ sensor protein swiprosin-1/EFhd2 is present in neurites and involved in kinesin-mediated transport in neurons. *PLoS One*, *9*(8), e103976. https://doi.org/10.1371/journal.pone.0103976

Santacruz, K., Lewis, J., Spires, T., Paulson, J., Kotilinek, L., Ingelsson, M., Guimaraes, A., DeTure, M., Ramsden, M., McGowan, E., Forster, C., Yue, M., Orne, J., Janus, C., Mariash, A., Kuskowski, M., Hyman, B., Hutton, M., & Ashe, K. H. (2005). Tau suppression in a neurodegenerative mouse model improves memory function. *Science*, *309*(5733), 476-481. https://doi.org/10.1126/science.1113694

Spires, T. L., Orne, J. D., SantaCruz, K., Pitstick, R., Carlson, G. A., Ashe, K. H., & Hyman, B. T. (2006). Region-specific dissociation of neuronal loss and neurofibrillary pathology in a mouse model of tauopathy. *Am J Pathol*, *168*(5), 1598-1607. https://doi.org/10.2353/ajpath.2006.050840

Spires-Jones, T. L., Stoothoff, W. H., de Calignon, A., Jones, P. B., & Hyman, B. T. (2009). Tau pathophysiology in neurodegeneration: a tangled issue. *Trends Neurosci*, *32*(3), 150-159. https://doi.org/10.1016/j.tins.2008.11.007

Sydow, A., Van der Jeugd, A., Zheng, F., Ahmed, T., Balschun, D., Petrova, O., Drexler, D., Zhou, L., Rune, G., Mandelkow, E., D'Hooge, R., Alzheimer, C., & Mandelkow, E. M. (2011). Tau-induced defects in synaptic plasticity, learning, and memory are reversible in transgenic mice after switching off the toxic Tau mutant. *J Neurosci*, *31*(7), 2511-2525. https://doi.org/10.1523/JNEUROSCI.5245-10.2011

Tiernan, C. T., Combs, B., Cox, K., Morfini, G., Brady, S. T., Counts, S. E., & Kanaan, N. M. (2016). Pseudophosphorylation of tau at S422 enhances SDS-stable dimer formation and impairs both anterograde and retrograde fast axonal transport. *Exp Neurol*, *283*(Pt A), 318-329. https://doi.org/10.1016/j.expneurol.2016.06.030

Umstead, A., Soliman, A. S., Lamp, J., & Vega, I. E. (2020). Validation of recombinant human protein purified from bacteria: An important step to increase scientific rigor. *Anal Biochem*, *611*, 113999. https://doi.org/10.1016/j.ab.2020.113999

Uversky, V. N. (2015). Intrinsically disordered proteins and their (disordered) proteomes in neurodegenerative disorders [Opinion]. *Front Aging Neurosci*, *7*, 18. https://doi.org/10.3389/fnagi.2015.00018

Vanderweyde, T., Apicco, D. J., Youmans-Kidder, K., Ash, P. E. A., Cook, C., Lummertz da Rocha, E., Jansen-West, K., Frame, A. A., Citro, A., Leszyk, J. D., Ivanov, P., Abisambra, J. F., Steffen, M., Li, H., Petrucelli, L., & Wolozin, B. (2016). Interaction of tau with the RNA-Binding Protein TIA1 Regulates tau Pathophysiology and Toxicity. *Cell Rep*, *15*(7), 1455-1466. https://doi.org/10.1016/j.celrep.2016.04.045

Vazquez-Rosa, E., Rodriguez-Cruz, E. N., Serrano, S., Rodriguez-Laureano, L., & Vega, I. E. (2014). Cdk5 phosphorylation of EFhd2 at S74 affects its calcium binding activity. *Protein Sci*, *23*(9), 1197-1207. https://doi.org/10.1002/pro.2499

Vega, I. E. (2016). EFhd2, a Protein Linked to Alzheimer's Disease and Other Neurological Disorders. *Front Neurosci*, *10*, 150. https://doi.org/10.3389/fnins.2016.00150

Vega, I. E., Sutter, A., Parks, L., Umstead, A., & Ivanova, M. I. (2018). Tau's Three-Repeat Domain and EFhd2 Co-incubation Leads to Increased Thioflavin Signal. *Front Neurosci*, *12*, 879. https://doi.org/10.3389/fnins.2018.00879

Vega, I. E., Traverso, E. E., Ferrer-Acosta, Y., Matos, E., Colon, M., Gonzalez, J., Dickson, D., Hutton, M., Lewis, J., & Yen, S. H. (2008). A novel calcium-binding protein is associated with tau proteins in tauopathy. *J Neurochem*, *106*(1), 96-106. https://doi.org/10.1111/j.1471-4159.2008.05339.x

Vega, I. E., Umstead, A., & Kanaan, N. M. (2019). EFhd2 Affects Tau Liquid-Liquid Phase Separation. *Front Neurosci*, *13*, 845. https://doi.org/10.3389/fnins.2019.00845

Wang, Y., & Mandelkow, E. (2016). Tau in physiology and pathology. *Nat Rev Neurosci*, *17*(1), 5-21. https://doi.org/10.1038/nrn.2015.1

Ward, S. M., Himmelstein, D. S., Lancia, J. K., Fu, Y., Patterson, K. R., & Binder, L. I. (2013). TOC1: characterization of a selective oligomeric tau antibody. *J Alzheimers Dis*, *37*(3), 593-602. https://doi.org/10.3233/JAD-131235

Wilson, D. M., & Binder, L. I. (1997). Free fatty acids stimulate the polymerization of tau and amyloid beta peptides. In vitro evidence for a common effector of pathogenesis in Alzheimer's disease. *Am J Pathol*, *150*(6), 2181-2195. https://www.ncbi.nlm.nih.gov/pubmed/9176408

Wittmann, C. W., Wszolek, M. F., Shulman, J. M., Salvaterra, P. M., Lewis, J., Hutton, M., & Feany, M. B. (2001). Tauopathy in Drosophila: neurodegeneration without neurofibrillary tangles. *Science*, *293*(5530), 711-714. https://doi.org/10.1126/science.1062382

Wolozin, B. L., Pruchnicki, A., Dickson, D. W., & Davies, P. (1986). A neuronal antigen in the brains of Alzheimer patients. *Science*, *232*(4750), 648-650. https://doi.org/10.1126/science.3083509

Xue, B., Qu, Y., Zhang, X., & Xu, X. F. (2022). miRNA-126a-3p participates in hippocampal memory via alzheimer's disease-related proteins. *Cereb Cortex*, *32*(21), 4763-4781. https://doi.org/10.1093/cercor/bhab515

APPENDIX

No Primary

Figure A2.1. Immunogold labeling tests the specificity of primary and secondary antibodies. After overnight polymerization of recombinant proteins, all samples were labeled using both Tau13 antibody (IgG1 mouse antibody) and anit-EFhd2 (rabbit antibody). Then all samples were labelled with gold-conjugated secondary antibodies anti-mouse 6 nm (small gold particles) and anti-rabbit 15 nm (large particles). **(A)** Representative micrograph of immunogold labeling of hEFhd2 in the absence of ARA. Only labeling with large gold particles for hEFhd2 are detected. **(B)** Representative micrograph of immunogold labeling conducted on hTau40^m in the absence of ARA. Only labeling with small gold particles for tau are detected. Non-specific large gold particles are scarce. **(C)** Representative micrograph of immunogold labeling conducted on hTau40 in the presence of ARA (hTau40^{ARA}). Only labeling of hTau40 filaments and oligomers with small gold particles are observed. **(D)** The primary antibodies for Tau13 and anti-EFhd2 were omitted to show the absence of non-specific binding of secondary antibodies to hTau40^{ARA}/hEFhd2 aggregates. No large or small particles were observed in the field. Data were drawn from n=3 replicates/group and 3 micrographs for each replicate.
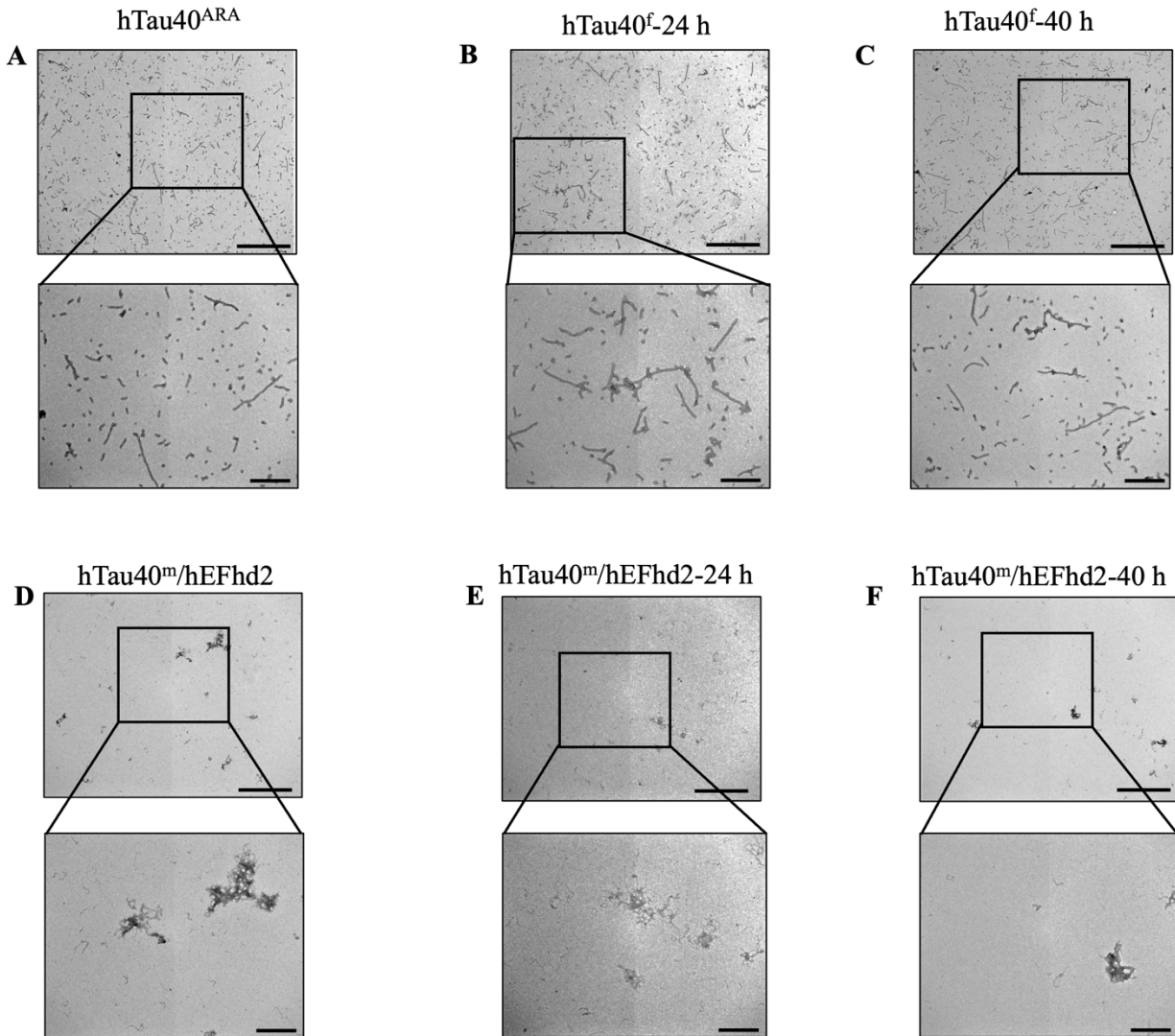
Figure A2.2. Formation of tau filaments and hEFhd2-induced tau aggregates were not impacted by longer duration. (A) Representative micrograph of hTau40^{ARA} (2 μM hTau40 in the presence of ARA for 16 h); typical combination of oligomers, short and long filaments are detected. **(B)** Representative micrograph of hTau40^f 24 h (2 μM hTau40 in the presence of ARA for 24 h before adding 2 μM hEFhd2). **(C)** Representative micrograph of hTau40^f 40 h (adding 2 μM hTau40 in the presence of ARA for 40 h). **(D)** Representative micrograph of hTau40^m/hEFhd2 (co-incubating 2 μM of hTau40 and 2 μM hEFhd2 for 16 h in the absence of ARA). **(E)** Representative micrograph of hTau40^m/hEFhd2-24 h (co-incubating 2 μM of hTau40 and 2 μM hEFhd2 24 h before adding ARA). **(F)** Representative micrograph of hTau40^m/hEFhd2-40 h (co-incubating 2 μM of hTau40 and 2 μM hEFhd2 for 40 h in the absence of ARA). Scale bar for the top micrographs 800 nm and for the bottom micrographs 200 nm.

95

Chapter Three: EFhd2 brain interactome reveals its association with different cellular and molecular processes

Abstract

EFhd2 is a calcium-binding protein that is highly expressed in the central nervous system. We have shown that EFhd2 interacts with tau protein, a key pathological hallmark in Alzheimer's disease and related dementias. However, EFhd2's physiological and pathological functions in the brain remain poorly understood. To gain insights into its physiological function, we identified proteins that coimmunoprecipitated with EFhd2 from mouse forebrain and hindbrain, using tandem mass spectrometry (MS). In addition, quantitative mass spectrometry was used to detect global proteome changes due to deletion of the *Efhd2* gene in mouse forebrain and hindbrain regions. Our data show that mouse EFhd2 is associated with cytoskeleton components, vesicle trafficking modulators, cellular stress response-regulating proteins, and metabolic proteins. Moreover, proteins associated with cytoskeleton, vesicular transport, calcium signaling, stress response, and metabolic pathways showed differential abundance in *Efhd2*$^{-/-}$ mice brain. This study presents, for the first time, an EFhd2 brain interactome that is associated with different cellular and molecular processes. These findings will help prioritize further studies to investigate the mechanisms by which EFhd2 modulates these processes in physiological and pathological conditions of the nervous system.

Introduction

EF-Hand Domain family member 2 (EFhd2), also known as Swiprosin-1, is a calcium-binding protein found across various species from human to nematodes (Vega, 2016; Kogias et al., 2019). In fact, mouse *Efhd2* gene is 91% identical to the human *EFHD2* gene (Vega, 2016; Kogias et al., 2019). EFhd2 is a 240-amino acid protein with a polyalanine motif (6-9 alanine) at the N-terminus, which confers its thermostability (Ferrer-Acosta et al., 2013a). In addition, EFhd2 has two EF-hand calcium-binding domains that span amino acids 95-123 and 131-159. EFhd2 has a dynamic structure with the propensity to self-oligomerize (Ferrer-Acosta et al., 2013b). The coiled-coil domain (C-C) in the C-terminus mediates EFhd2 self-oligomerization (Ferrer-Acosta et al., 2013b). Using proteomic analysis, we reported that EFhd2 is phosphorylated by CDK5 at Ser74. Interestingly, phosphorylated EFhd2 shows low calcium-binding activity (Vazquez-Rosa et al., 2014).

EFhd2 is widely expressed in most organs with predominant levels in the central nervous system (CNS) (Vega et al., 2008). In particular, it is abundant in forebrain regions such as the hippocampus, frontal cortex, and olfactory bulb with lower levels in the cerebellum and brainstem (Purohit et al., 2014). Reportedly, EFhd2 is mainly expressed in the gray matter where it localizes to the somatodendritic compartments (Ferrer-Acosta et al., 2013b; Borger et al., 2014; Purohit et al., 2014). However, the biological role of EFhd2 is still unclear. Previous studies suggested that EFhd2 is involved with different signaling pathways in immune cells (Kogias et al., 2019). For instance, in B cells, EFhd2 inhibits B-cell receptor (BCR)-induced NF-κB signaling, which then downregulates anti-apoptotic protein BCL-XL (Avramidou et al., 2007). Moreover, EFhd2 enhances BCR-induced calcium influx by acting as a scaffold protein for Syk, SLP-65, and PLCγ (Kroczek et al., 2010). Collectively, these data suggest a role of EFhd2 in B cells survival or lifespan. In T cells, EFhd2 is abundant in microvilli-like membrane structures and lamellipodia where it associates with F-actin structures (Kwon et al., 2013). Further characterization of EFhd2 showed that it mediates cell spreading and migration, possibly, by regulating actin bundling and polymerization (Kwon et al., 2013). However, the mechanism by which EFhd2 modulates actin structures and mediates cell migration remains elusive.

EFhd2 has been associated with cancer and neurodegeneration. Consistent with its role in modulating cell migration and survival, EFhd2 exists at higher levels in a multitude of invasive human cancers (Huh et al., 2015). Ectopic overexpression of EFhd2 led to pulmonary metastasis

by activating Rho family of GTPases. Therefore, EFhd2 is associated with cancer invasion and represents a potential therapeutic target (Huh et al., 2015; Peled et al., 2018; Peng et al., 2021). In the CNS, we provided evidence for the association of EFhd2 with tauopathies (Vega et al., 2008). Tauopathies are a heterogeneous group of neurodegenerative diseases that encompass Alzheimer's disease (AD), frontotemporal dementias (FTDs), corticobasal degeneration (CBD), among others (Wang & Mandelkow, 2016; Dujardin et al., 2018; Chung et al., 2021; Zhang et al., 2022). The cardinal pathological hallmark in all tauopathies is the aberrant aggregation of microtubule-associated protein tau. During the disease trajectory, tau undergoes conformational changes and transitions from soluble monomers to oligomeric structure to ultimately insoluble paired helical filaments leading to neurodegeneration (Wang & Mandelkow, 2016; Dujardin et al., 2018; Gotz et al., 2019; Chung et al., 2021; Zhang et al., 2022). The molecular mechanisms that underlie abnormal tau depositions are unknown. We showed that EFhd2 co-purified with pathological tau in a mouse model of tauopathy and postmortem AD human brains (Vega et al., 2008; Ferrer-Acosta et al., 2013b). EFhd2 interacts with the microtubule domain of tau and induces the formation of amyloid structure *in vitro* (Vega et al., 2018). Moreover, EFhd2 transforms the liquid phase behavior of tau to solid-like structures (Vega et al., 2019). Taken together, these findings highlight the potential role of EFhd2 in modulating tau aggregation. However, further studies seem necessary to unravel the role of EFhd2 in tau-mediated neurodegeneration (reviewed in (Vega, 2016)).

To gain insights into EFhd2's biological function, we generated an EFhd2 knockout mouse model (*Efhd2$^{-/-}$*). *Efhd2$^{-/-}$* mice develop without gross anatomical, developmental, or morphological anomalies, despite impaired dendritic morphology in the CNS (Purohit et al., 2014; Regensburger et al., 2018). Other studies suggested that EFhd2 proteins regulate the behavioral response to alcohol and drug addiction (Kogias et al., 2019). *Efhd2$^{-/-}$* mice show increased alcohol consumption (Mielenz et al., 2018) and behavioral changes to psychostimulant drugs invoked by enhanced monoaminergic response in the reward system (Kogias et al., 2020). Moreover, it was demonstrated that EFhd2 impedes kinesin-mediated axonal transport in cultured hippocampal neurons (Purohit et al., 2014). These data indicate that EFhd2 may confer resilience against addiction and play a potential role in neuronal transport and survival. At present, however, the molecular mechanisms by which EFhd2 modulates resilience and neuronal survival have yet to be investigated.

Despite the strides we and other colleagues have made to unveil EFhd2's function in the brain, its biological function remains poorly understood. To broaden our understanding of EFhd2's function in the brain, we sought to identify EFhd2-associated proteins in adult mouse brain. EFhd2 was immunoprecipitated from forebrain (i.e., cerebrum including limbic system, basal ganglia, and diencephalon) and hindbrain (i.e., cerebellum and brainstem) regions of EFhd2 wild type (*Efhd2*$^{+/+}$) mice. The associated proteins were identified by tandem mass spectrometry (MS) (Figure 3.1A). Additionally, to uncover molecular pathways associated with EFhd2 function, label-free quantitative (LFQ) proteomics was used to identify proteome changes in forebrain and hindbrain regions due to the deletion of the *Efhd2* gene (*Efhd2*$^{-/-}$) (Figure 3.1A). Herein, the data indicate that EFhd2 in mice forebrain and hindbrain regions is associated with cytoskeleton components, vesicle trafficking modulators, cellular stress response-regulating proteins, and metabolic proteins. Moreover, *Efhd2* gene deletion affected the abundance of proteins associated with metabolic pathways, transport, stress response and protein localization in forebrain and hindbrain regions. These findings serve as a foundation for further studies directed to uncover the role of EFhd2 in different physiological and pathological pathways.

Materials and Methods

Commercial antibodies

Antibodies were selected to validate pre-determined EFhd2-associated proteins by western blot. Western blot analysis was performed to verify the specificity of commercial antibodies using whole brain extracts (data not shown). We used antibodies that detected a protein band at the expected molecular weight of the targeted protein. Thermo Fisher scientific (Waltham, Massachusetts): Rabbit polyclonal anti-transgelin 3 (cat #12246-1-AP,1:250); Rabbit monoclonal anti-tropomodulin 2 (cat #MA5-36150, 1:250); Rabbit polyclonal anti-coronin 2b (cat #13802-1-AP,1:250). Cell Signaling Technology (Danvers, Massachusetts): Rabbit polyclonal anti-myosin 2a (cat #3403, 1:500), Rabbit monoclonal anti-myosin 2b (cat #8824, 1:500)

Monoclonal Anti-EFhd2 antibody production

A mouse monoclonal anti-EFhd2 (clone 10D6) antibody was generated in *Efhd2*$^{-/-}$ mice using methods similar to those previously described (Grabinski & Kanaan, 2016). Briefly, animals received subcutaneous injections of hEFhd2$^{\Delta CC}$ protein (100 µg protein in adjuvant) every 3 weeks until sufficient titers were achieved (signal above-background at ≥1:2,621,440

dilution). Hybridoma fusion techniques (Binder et al., 1985; Grabinski & Kanaan, 2016) were used, and cultures were screened for reactivity against the hEFhd2$^{\Delta CC}$, hEFhd2$^{\Delta NT}$, and hEFhd2^{WT} protein by indirect enzyme linked immunosorbent assay (ELISA, see below). Positive clones were subcloned at least three times as described (Grabinski & Kanaan, 2016). Antibody isotype was determined using the IsoStrip Mouse Monoclonal Antibody Isotyping Kit (Roche, cat #11493027001), and mycoplasma testing was performed using the Mycoplasma PCR ELISA kit (Roche, cat #11663925910). After the clone was verified as clean, stable, and positive, the line was grown in a CELLine 350 bioreactor (Integra Biosciences), and the antibody was purified by Protein A affinity chromatography (GE Healthcare, cat #17-1279-01) and stored at 1 mg/ml in 10 mM HEPES, 500 mM NaCl, 50% Glycerol. This new anti-EFhd2 antibody will be shared upon reasonable request.

Anti-EFhd2 Antibody validation

ELISAs were performed to determine the binding affinity and specificity of the EFhd2 antibody for EFhd2 protein using previously detailed methods (Grabinski & Kanaan, 2016). Briefly, hEFhd2$^{\Delta CC}$, hEFhd2$^{\Delta NT}$, and hEFhd2^{WT} (50 μl at 2 ng/μl in borate saline) coated onto wells of a 96-well plate (Corning, cat #3590) for 1h. Wells were washed (wash solution: 100 mM boric acid, 25 mM sodium tetraborate decahydrate, 75 mM NaCl, 250 μM thimerosal, 0.4% bovine serum albumin and 0.1% Tween 20), blocked in blocking buffer (5% non-fat dry in wash solution; 200 μl/well) for 1 h, and then incubated in purified anti-EFhd2 clone 10D6 antibody (1 mg/ml stock; serially diluted from 1:100 to 1:17,714,700 – in blocking buffer; 2 h). Wells were washed and incubated in goat anti-mouse HRP conjugated antibody (1:5,000; Jackson ImmunoResearch, cat #15-035-003; 1 h). Wells were washed and then reactivity was detected with 3,3′,5,5′ tetramethylbenzidine substrate (50 μl/well; Sigma, cat #T0440; 8 min development). Reactions were quenched with 50 μl 3.6% H_2SO_4, and then the absorbance was read at 450 nm. All washes were done 3 times with 200 μl/well of wash solution, and antibodies were diluted in blocking buffer. Blank wells were used to obtain background absorbance, which was removed from sample signals. Absorbance values were converted to percent light absorbed and data analyzed using sigmoidal non-linear curve fitting to obtain titer values (Figure A3.1.).

Animals

All animals use protocol was approved by Michigan State University's Institutional Animal Care and Use Committee (IACUC protocol #04-18-052-00). *Efhd2$^{-/-}$* was generated from

targeted embryonic stem (ES) cells for EFhd2 obtained from the KOMP Repository (www.komp.org), an NCRR-NIH supported mouse strain repository (U42-RR024244). The ES cells (C57BL/6N-EFhd2 $^{rm1(KOMP)Vlcg}$) were created by Velocigene (Valenzuela et al., 2003). *Efhd2* gene knockout in ES cells was performed by homologous recombination using a targeting vector (Neo-LacZ) (KOMP Repository, UC Davies (Pettitt et al., 2009). ES cells were electroporated with a neomycin (G418)-Lac Z clones. A 60% euploid clone was injected into C57BL/6 mouse blastocysts, from which chimeric males were obtained. Chimeras were bred with C57BL/6 wild-type females. After establishing *Efhd2$^{-/-}$* mouse colony in the C57BL/6, females and males were crossed with Swiss Webster mice, and the genomic background assessed. To assess genomic background, we used the genomic marker developed by DartMouse^{TM}. This strategy utilizes single-nucleotide polymorphisms (SNP) spread throughout the genome to determine the contribution of genomic DNA when different mouse strains are crossed, providing greater efficiency towards reaching a homogenous genomic background colony. Starting F2, we generated the three main genotypes, namely *Efhd2$^{+/+}$*, *Efhd2$^{+/-}$* and *Efhd2$^{-/-}$*. Based on genomic markers data, from generation F4 forward, the mouse colony shows a stable mixed SW/C57BL/6 genomic background (Figure A3.2.). In this study, age-matched (11-12 months) female *Efhd2$^{+/+}$* and *Efhd2$^{-/-}$* mice were used. Males were excluded from the study. The selected age and sex were based on previous studies that indicated higher EFhd2 abundance in adult mice regardless of sex (Purohit et al., 2014). In addition, Female *Efhd2$^{-/-}$* mice at this age do not show behavior or motor impairment compared to their wild type littermates (Purohit et al., 2014). Their activity level is comparable to age-matched wild type mice. Mice were socially housed (up to 5 mice per cage), and food and water were provided *ad libitum*. Mice were transferred to a clean cage with food and water weekly. No sample calculation was performed. Sample size was determined according to previous studies that indicated the minimum number of samples to achieve a power of 0.90 (Levin, 2011). Six mice per group were used for global proteome discovery of EFhd2-associated proteins and LFQ. Three mice per group were used for the subsequent validation of EFhd2-associated proteins by western blot and targeted mass spectrometry (tMS). Inclusion criteria were defined by genotype and sex. Simple randomization was used to select mice per genotype. Animals were euthanized by CO_2 suffocation, and tissues were extracted as previously described (Vega et al., 2008).

Genotyping

　　Genotyping was performed by extracting DNA from ear punches at weaning (21 days) using Kappa Mouse Genotyping Kit (GE cat #. KK7352) according to manufacturers' recommendations (Figure 3.1B). Amplification of the LacZ gene was performed using the *3' Uni Neo* (5'GCAGCCTCTGTTCCACATACACTTCA3') and *Reg 10032R1 (5' GCCTATAGTTAAGGGGAGTTGGGTGG 3')* primers. For the *Efhd2* gene, *Efhd2 Fwd* (5' CTTGGCCTCGAAGAAGTTCTTGG3') and *Efhd2 Rev* (5'GCCCTCTAAGGCTTTGTGAATGC3') primers were used. Amplification of both genes was performed using cycling conditions recommended by the KOMP consortium. PCR reaction: 12.5 μl 2x Kappa Fast genotyping, 1.25 μl Primer Fwd (100 ng/μl), 1.25 μl primer Rev (100 ng/ μl), 1 μl extracted DNA and 9 μl ddH$_2$0. In Figure 3.1C, western blot was used to confirm the genotyping results.
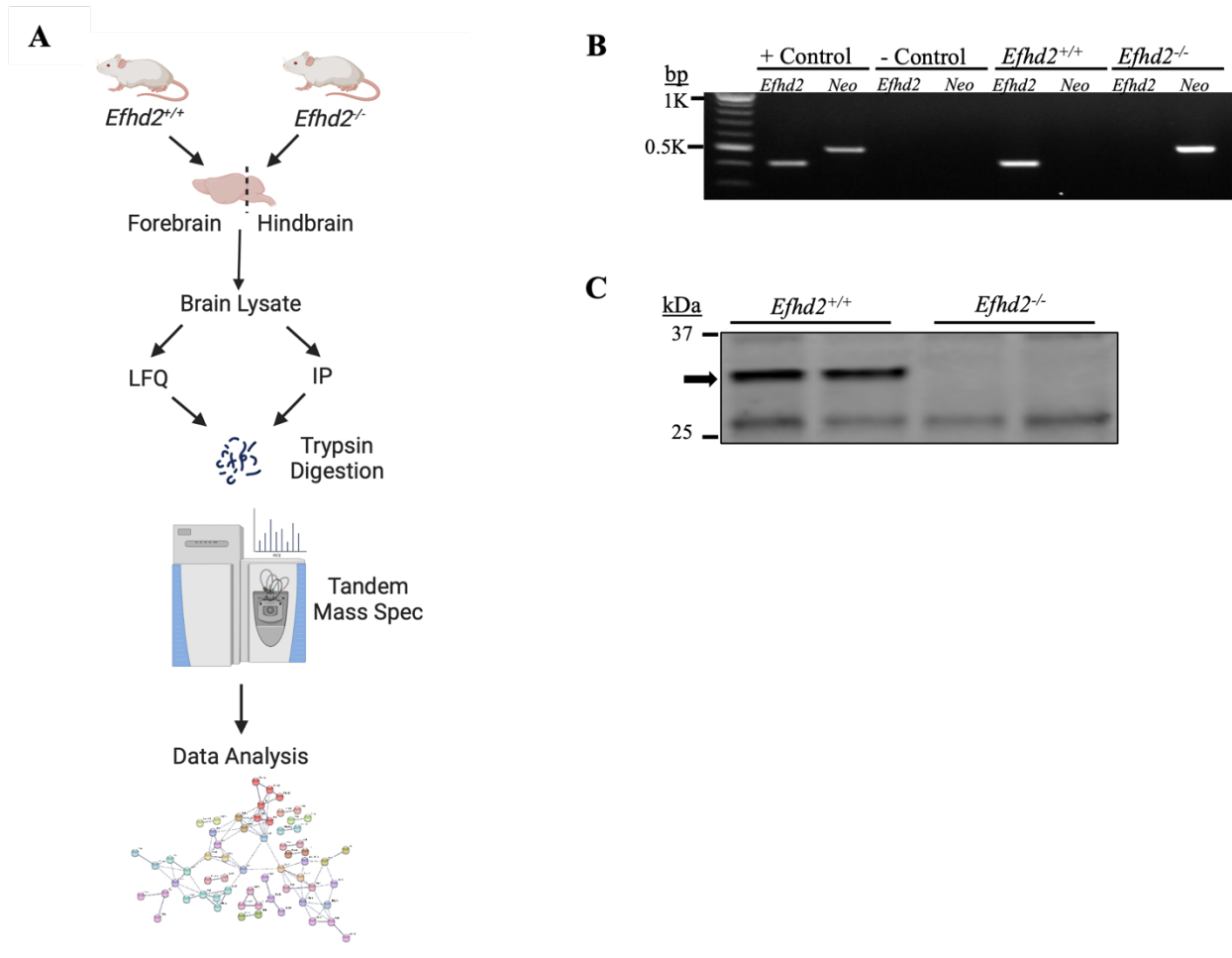
Figure 3.1. Experimental design. (**A**) Workflow for identifying EFhd2-associated proteins in mouse brain tissues and proteome changes in *Efhd2*$^{-/-}$ mice. (**B**) PCR-based genotyping. It shows the presence of *Efhd2* gene in the wild type (*Efhd2*$^{+/+}$) while detection of the Neomycin cassette (*Neo*) verifies the knockout (*Efhd2*$^{-/-}$). DNA base pair (bp) ladder was used. (**C**) Western blot using anti-EFhd2 (clone 10D6) antibody for 45µg of postnuclear brain lysates of *Efhd2*$^{+/+}$ and *Efhd2*$^{-/-}$. The arrow indicates EFhd2 protein band. Molecular weight markers (kDa) are indicated. The figure was created with Biorender.com.

Tissue processing

Experimental design is illustrated in Figure 3.1A *Efhd2*$^{+/+}$ (n=6) and *Efhd2*$^{-/-}$ (n=6) forebrain (i.e., cerebrum including limbic system, basal ganglia, and diencephalon) and hindbrain (i.e., cerebellum and brainstem) regions were homogenized in five volumes of 20 mM Tris Base, pH 7.4, 150 mM NaCl, 1 mM EDTA (Acros Organics, cat #60-00-4), 1 mM EGTA (Acros Organics, cat #67-42-5), 5 mM sodium pyrophosphate (Alfa Aesar, cat #13472-36-1), 30 mM NaF (Acros Organics, cat #7681-49-4), and supplemented with 1X Halt protease inhibitor cocktail (Thermo Scientific, cat #. 78430). Brain homogenate was centrifuged at 18,400 x g, 4 °C

for 10 minutes, and the supernatant (postnuclear lysate) was transferred to a clean tube to estimate its protein concentrations using BCA Assay (Pierce, cat #. 23225). The same tissue protein lysates were used for identification of EFhd2-associated proteins (immunoprecipitation-MS) and LFQ. MS samples processing and tissue processing were conducted by different personnel.

Identification of EFhd2-associated proteins

Immunoprecipitation (IP)

Postnuclear lysates were incubated with Protein A/G-conjugated magnetic beads (Pierce, cat #. 88803) for 3 h at 4 °C with constant rotation. This step is crucial to preclear samples from endogenous immunoglobulins and other proteins that nonspecifically bind to the beads. Afterwards, sample tubes were placed on a magnetic strip, and the supernatant (precleared lysate) was transferred to clean tubes. BCA assay was performed to estimate the precleared lysate protein concentration. Three micrograms of anti-EFhd2 (clone 10D6) were added to 2 mg of precleared lysate and incubated with constant rotation for 17 h at 4 °C. Then, Protein A/G-conjugated magnetic beads were added and incubated at 4 °C for 4 hours. The supernatant was transferred to clean tubes and the beads were washed 4 times with 25 mM ammonium bicarbonate (AMBIC) (VWR, cat #BDH9206), pH 8. After the final wash, beads were split evenly for western blot and MS.

Western Blot

After washing the beads, the wash buffer was completely removed, and beads were resuspended in SDS-loading buffer containing N-ethylmaleimide (2X NEM) instead of β-mercaptoethanol and incubated overnight at 4 °C. Mouse immunoprecipitates along with 45 µg of the respective postnuclear lysates (input) were resolved on 4-20% SDS-PAGE gels and transferred to nitrocellulose membranes (0.45 µm, Bio-Rad, cat #. 1620115). The membranes were blocked by 5% non-fat dry milk in 1X TBST (2.5 mM Tris-Base, 15 mM NaCl, 30 mM KCL, 0.1% Tween 20) for 1 h at room temperature. Then, the membranes were incubated in 1:5000 Anti-EFhd2 (clone 10D6) overnight at 4 °C. After primary incubation, membranes were washed three times in 1X TBST and then incubated in 1:2000 of appropriate secondary antibody (LI-COR) at room temperature for 1 h. Subsequently, membranes were washed three times in 1X TBST. Membranes were visualized by the LI-COR Odyssey Imaging System and analyzed using Image Studio (v5.2).

Protein Digestion

After IP, beads were resuspended in the digestion buffer (25 mM AMBIC/50% acetonitrile (ACN) (Fisher Scientific, cat #A955-4)), and 500 ng rLys-C (Promega, cat #. V1671) was added to each sample and incubated at 37 °C for 1.5 h. Afterwards, 1 µg trypsin (Promega, cat #. V5280) was added to the samples and incubated at 37 °C for 17 h. The digestion solution was transferred to clean tubes and dried completely using a speed vacuum at 30 °C. Finally, samples were resuspended in 50 µL of 25 mM AMBIC/5% ACN.

Liquid Chromatography Tandem Mass Spectrometry

nanoLC-MS/MS separations were performed with a Thermo Scientific™ Ultimate™ 3000 RSLCnano System. Peptides were desalted in-line using a C18 trap cartridge (300 µm x 5 mm) with 2% ACN, 0.1% formic acid (FA) (MilliporeSigma, cat #F0507) for 5 min with a flow rate of 5 µl/min at 40 °C. The trap cartridge was then brought in-line with a 2 µm diameter bead, C18 EASY-Spray™ column (75 µm x 250 mm) for analytical separation over 120 min with a flow rate of 350 nl/min at 40 °C. The mobile phase consisted of 0.1% FA (buffer A) and 0.1% FA in ACN (buffer B). The separation gradient was as follows: 5 min desalting, 95 min 4-40% B, 2 min 40-65% B, 3 min 65-95% B, 11 min 95% B, 1 min 95-4% B, 3 min 4% B. Three microliters of each sample were injected.

Top 20 data dependent mass spectrometric analysis was performed with a Q Exactive™ HF-X Hybrid Quadrupole-Orbitrap™ Mass Spectrometer. MS1 resolution was 60K at 200 m/z with a maximum injection time of 45 ms, AGC target of 3e6, and scan range of 300-1500 m/z. MS2 resolution was 60K at 200 m/z, with a maximum injection time of 118 ms, AGC target of 5e3, and isolation range of 1.3 m/z. HCD normalized collision energy was 28. Only ions with charge states from +2 to +6 were selected for fragmentation, and dynamic exclusion was set to 30 s. The electrospray voltage was 1.9 kV at a 2.0 mm tip to inlet distance. The ion capillary temperature was 280 °C and the RF level was 55.0. All other parameters were set as default.

Protein Identification

Protein identification was conducted by Proteome Discoverer™ Software version 2.2.0.388. Spectra were searched with Sequest HT against the Mus musculus Uniprot protein database (61204 unique sequences). Enzyme specificity was set to trypsin with an MS1 tolerance of 10 ppm and a fragment tolerance of 0.02 Da. Oxidation (M), acetylation (protein N-term), and methionine loss (protein N-term) were set as dynamic modifications. False discovery rates were

set to 0.01 using the Percolator node. Two unique peptides were required for protein identification. All other parameters were set as default. The data was curated to correct discrepancies in the accession number and deleting all proteins that were also identified in the negative control (IP from *Efhd2*$^{-/-}$brain regions).

Validation of EFhd2-*associated proteins*

The proteins selected for validation needed to fulfill the following criteria: 1) detection in both forebrain and hindbrain regions of mouse brain 2) involved in specific molecular processes to which EFhd2 was previously associated, and 3) availability and validation of commercial antibodies. Forebrain and hindbrain from *Efhd2*$^{+/+}$ mice (n=3) and *Efhd2*$^{-/-}$ mice (n=3) were used to validate the EFhd2-associated proteins identified by MS. To take in consideration biological variability, the three tissue samples for each region were pooled and homogenized. Thus, we generated one tissue lysate from the mice forebrains and hindbrains. IP and western blot were performed as explained above. In addition, a targeted mass spectrometry (tMS) approach was developed to account for differences in sensitivity between western blot and MS analyses. Target peptides were selected from the peptides identified in the data dependent mass spectrometry experiments (see *Liquid Chromatography Tandem Mass Spectrometry* section). tMS chromatography was identical to the chromatography described above, except for the following changes. tMS peptides were separated using a C18 trap column (75 µm x 20 mm) in-line with a 3 µm diameter bead, C18 EASY-Spray™ separation column (75 µm x 150 mm) for analytical separation over 130 min. The separation gradient was as follows: 100 min 4-40% B, 2 min 40-65% B, 3 min 65-95% B, 11 min 95% B, 1 min 95-4% B, 13 min 4% B. One microliter of each sample was injected.

Skyline v 4.2 was used to configure peptide isolation lists for parallel reaction monitoring (PRM). Targeted scans were collected using an unscheduled inclusion list. Fragment ion spectra were acquired at 60K at 200 m/z, with a maximum injection time of 100 ms, and AGC target of 2e5. All other parameters were as described above. Skyline was also used to evaluate PRM data. Peptide retention times were manually refined. MS/MS mass tolerance filtering matched the acquisition method (60K at 200 m/z). The top 3 fragment ions as ranked by Skyline were compared to the NIST Mouse HCD Library (maximum library rank of 6) to validate the detected product ions against an established database (CHEMDATA.NIST.GOV, 2021). Peptide dot

products and peak areas were calculated by Skyline. Dot products under 0.7 were not considered a positive identification of the product ions.

Label-Free Quantification (LFQ)

Three 10 µg aliquots of postnuclear lysate from *Efhd2*$^{+/+}$ (n=6) and *Efhd2*$^{-/-}$(n=6)) forebrain and hindbrain were buffer exchanged 4 times into 500 µl 25 mM AMBIC, pH 8.0 using an Amicon ultra 3 kDa centrifugal filter (Millipore, cat #. UFC-500396). Samples were centrifuged at 18,400 x g, 4 °C for 10 min per exchange. After exchanging, samples were dried completely using a speed vacuum at 30 °C and stored at -20 °C before digestion. Samples were digested in sets of nine, each sample consisting of three technical replicates. Samples were resuspended in 50 µl 25 mM AMBIC in 50% ACN containing 500 ng rLys-C (Promega, cat #. V1671), and incubated at 37 °C for 1.5 h. Then, 1 µg trypsin (Promega, cat #. V5280) was added to each sample and incubated at 37°C for 17 h. After digestion, samples were dried completely before resuspension in 50 µl 25 mM AMBIC in 5% ACN. Liquid Chromatography Tandem Mass Spectrometry was performed over 120 minutes using a 2 µm diameter bead, C18 EASY-Spray™ column (75 µm x 250 mm). The separation gradient was as follows: 5 min desalting, 40 min 4-40% B, 2 min 40-65% B, 2 min 65-95% B, 7 min 95% B, 1 min 95-4% B, 3 min 4% B. Protein identification proceeded as previously described for the IP samples. Quantitative ratios were determined using the Precursor Ion Quantitation node. This node calculates the abundance of a peptide as the summation of its quantitative peptide spectral matches. Peptide ratios are determined in a pairwise manner from the geometric median of all combinations of peptide abundance ratios. Protein ratios are determined from the geometric median of all combinations of peptide ratios. P-values were determined by ANOVA (background based) and adjusted for multiple comparisons with the Benjamini-Hochberg procedure. Due to missing values in LFQ, we curated the protein list retaining quantitated proteins with, at least, 80% of normalized values in one experimental group (i.e., *Efhd2*$^{+/+}$ or *Efhd2*$^{-/-}$). The data was not assessed for normality and no test for outliers was conducted. Figure was generated using GraphPad Prism 8.

Gene ontology (GO) enrichment Analysis

Cytoscape (v3.8.0) and the ClueGO application (v2.5.7) with the following selection criteria: Statistical Test Used = Enrichment/Depletion (Two-sided hypergeometric test), Correction Method Used = Benjamini-Hochberg, Min GO Level = 1, Max GO Level = 4, Cluster #1, Number of Genes = 10, Min Percentage = 5.0, GO Fusion = false, GO Group = true, Kappa

Score Threshold = 0.5, Group By Kappa Statistics = true, Initial Group Size = 1, Sharing Group Percentage = 50.0, Organism analyzed: Mus Musculus [10090], Identifier types used: [AccessionID, UniProtKB_AC], Evidence codes used: [All_without_IEA].

Results

EFhd2 interactome in mouse brain

EFhd2's physiological and molecular functions are not yet completely understood. Identification of EFhd2's interactome will unravel its association with specific cellular processes, especially in the brain where it is highly abundant. EFhd2 was immunoprecipitated from forebrain and hindbrain brain regions of $Efhd2^{+/+}$ mice using a novel anti-EFhd2 antibody (as shown in Figure A3.1). $Efhd2^{-/-}$ mice were included as negative control to detect non-specific binding proteins. Immunoprecipitation (IP) of EFhd2 from the forebrain region was confirmed using western blot (Figure 3.2A, lanes 1-6). As expected, no EFhd2 bands were observed in IP samples from $Efhd2^{-/-}$ forebrain samples (Figure 3.2A, lanes 7-12). Likewise, EFhd2 was immunoprecipitated from hindbrain regions of $Efhd2^{+/+}$ mice (Figure 3.2B lanes 1-6), but not from $Efhd2^{-/-}$, as expected (Figure 3.2B lanes 7-12).

Proteins that co-purified with EFhd2 were identified by MS. Data were curated by excluding proteins detected in both $Efhd2^{-/-}$ and $Efhd2^{+/+}$ IPs (see Materials and Methods). After data curation, 53 and 73 proteins were identified coimmunoprecipitating with EFhd2 in forebrain and hindbrain regions, respectively. Fourteen EFhd2-associated proteins were identified in both regions (Myh9, Myh10, Myl12b, Myl6, Myo5a, Tmod2, Coro2b, Tagln3, Capza2, Capzb, Sptbn2, 1, Rpl13, EWSR1). To determine the represented biological functions among the identified EFhd2-associated proteins, we conducted a literature search using keywords "*protein name* and brain" or "*protein name* and neuron". The functional categories represented in Figure 3.3 include at least two proteins per group. Therefore, categories with only one protein are not represented here nor are the proteins of unidentified or not fully investigated biological relevance. However, all proteins are listed in Tables A3.1 and A3.2.

A Forebrain
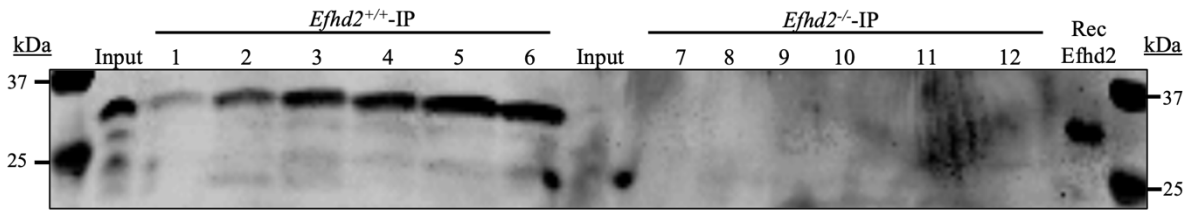
B Hindbrain
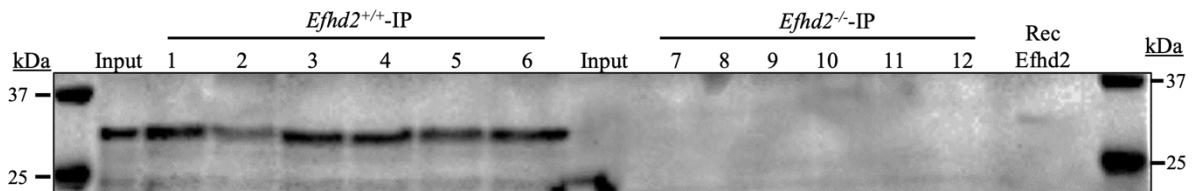
Figure 3.2. EFhd2 immunoprecipitation from forebrain and hindbrain regions of *Efhd2*$^{+/+}$ mice. Western blot using anti-EFhd2 antibody (10D6) confirms EFhd2 IP from *Efhd2*$^{+/+}$ mice (lanes 1-6, n=6) (**A**) forebrain and (**B**) hindbrain regions. No EFhd2 was detected in either input lysates or IP of *Efhd2*$^{-/-}$(lanes 7-12, n=6). Input is 45 μg postnuclear brain lysate. Recombinant hEFhd2 (5ng) was used as positive control.

EFhd2 interactome in the forebrain

EFhd2-associated proteins in forebrain are illustrated in Figure 3.3A. EFhd2 was associated with acting-binding proteins known to regulate actin cytoskeleton dynamics (e.g., Cfl1, Capza2, Dbn1, and Tmod2). Moreover, the data showed that EFhd2 associates with actin-crosslinking proteins like Sptbn1, Sptbn2, Add1, and Ank2. Actin-binding (Myh9, Myh10, Myo5a) and microtubule-binding (Kif5b) motor proteins also coimmunoprecipitated with EFhd2. In addition to actin-binding proteins, intermediate filament proteins in neurons and astrocytes coimmunoprecipitated with EFhd2 (Gfap, Nefh, Nefl, and Nefm) Several proteins that regulate membrane trafficking and cellular transport were also identified (Figure 3.3A). For example, SNARE complex proteins (Vamp2, Snap25, and Stx1b) control synaptic vesicle docking and fusion (Brunger et al., 2009; Sudhof & Rothman, 2009; Jahn & Fasshauer, 2012). Synaptotagmin-like protein Sytl4, its interactor Rab8a and Dnm1 (involved in clathrin-dependent endocytosis) were also identified as EFhd2-associated proteins, suggesting that EFhd2 associates with known protein complex that mediate vesicle trafficking. Based on these results, EFhd2 is associated with proteins involved in cytoskeletal reorganization, vesicle trafficking, and cellular transport likely in both neurons and astrocytes.

The data analysis also revealed the association of EFhd2 with signaling and stress response proteins. Among the identified proteins, Camk2a and Camk2b are α and β isoforms of CamKII (Gaertner et al., 2004). Map2k1 (MEK1) is an upstream activator of the ERK pathway that regulates cell cycle, survival, and apoptosis (Zhu et al., 2002; Zhu et al., 2003). Ogt is responsible for O-GlcNAcylation of proteins that imparts a neuroprotective effect against cellular oxidative stress (Wani et al., 2017). Molecular chaperones of the heat shock proteins family also coimmunoprecipitated with EFhd2. Particularly, Hsp12a and Hsp90aa1 are inducible stress proteins that prevent protein aggregation and enhance cell survival (Wynn et al., 1994). Notably, Hsp12a is an endoplasmic reticulum (ER) stress protein (Kitao et al., 2004). Hsp90aa1 (inducible isoform of Hsp90) mediates nucleus-cytoplasm trafficking of glucocorticoid receptors through interaction with cytoskeletal proteins (Pratt et al., 2006). Of note, Camk2a and Hsp90aa1 directly interact and were identified as hub genes among bipolar disorder risk genes (Li et al., 2019). Taken together, these results suggest that EFhd2 is associated with proteins involved in interrelated molecular pathways that impact neuronal growth, synaptogenesis, and protein homeostasis in forebrain regions.

Along with the cytoskeleton components, trafficking regulators, and stress response proteins, ribosomal proteins (e.g., Rpl13 and Rps15) also co-purified with EFhd2. These proteins represent constituents of ribosomes that mediate and control protein synthesis. EFhd2 was associated with several RNA-binding proteins (RBPs) including Sfpq, Nono, and Ewsr1. Ewsr1 is a TET family multifunctional protein that regulates transcription, RNA metabolism and transport, and cellular signal transduction (Lee et al., 2019). Moreover, Nono and Sfpq are components of neuronal RNA transport granules (Kanai et al., 2004). The transport of RNA granules to axonal ending is indispensable for localized protein synthesis and maintaining RNA and protein homeostasis (Cajigas et al., 2012). It has been shown that Sfpq interacts with Kif5a to regulate RNA granules axonal transport (Fukuda et al., 2020). These findings, together with its association with cell trafficking, indicate that EFhd2 may be involved in the transport of RNA granules and RNA metabolism.

EFhd2 interactome in the hindbrain

In hindbrain regions, EFhd2 was found in association with proteins involved in biological functions like those identified in the forebrain (Figure 3.3B). This included actin filaments regulatory proteins such as Pfn2, Sptbn2, Tmod2, and Capza2. In addition, the α-tubulin isoform

Tubal3 and microtubule-associated protein Map4 co-purified with EFhd2, which suggests an association of EFhd2 with microtubule cytoskeleton dynamics. Furthermore, Dsp is a desmosomal protein that interacts with vimentin to anchor intermediate filaments to the membrane (Meng et al., 1997). Actin- and microtubule-binding motor proteins (Myh9, Myh10, Myl6, and Myo5a) were associated with EFhd2 in both forebrain and hindbrain. Similarly, vesicle trafficking proteins, such as SNARE complex proteins (Snap91) and SNARE interactors (Syt2, Rph3a, and Ehd1) were also found associated with EFhd2 in hindbrain (Sollner et al., 1993; Wei et al., 2010; Ferrer-Orta et al., 2017). Proteins that mediate endocytosis were also identified such as Dnm1, Amph, Tom1l2, and Ap3d1(Cao et al., 1998; Takei et al., 1999; Drasbek et al., 2008; Wang et al., 2010; Farías et al., 2017). These results provide further evidence for the association of EFhd2 with cytoskeleton regulation and trafficking pathways that is consistent in both forebrain and hindbrain.

Hindbrain EFhd2 was associated with cellular homeostasis mechanisms. Specifically, EFhd2 co-purified with EF-hand type calcium-binding proteins like Calb1 and Calm1 that control calcium homeostasis and impact calcium-dependent signaling cascades (Figure 3.3B). Related to calcium homeostasis, EFhd2 was associated with other signaling transduction effectors like Camk4, Mpp6, and Prkcg. Furthermore, Ubiquitin/proteasome system (UPS) components were identified as EFhd2-associated proteins in hindbrain regions (Figure 3.3B). Proteins with ubiquitin ligase or ubiquitin ligase-regulating activity (e.g., Uchl1, Cand1, and Trim2) coimmunoprecipitated with EFhd2 along with a proteasomal protein Psmd5 (Khazaei et al., 2011; Pierce et al., 2013; Gong et al., 2016). Moreover, Prdx6, a predominantly astrocytic antioxidant enzyme that protects the cell against oxidative stress, was also identified as an EFhd2-associated protein (Power et al., 2008). Consistent with the results from the forebrain, EFhd2 is associated with proteins involved in neuronal growth, stress response, and protein turnover in hindbrain.

In hindbrain regions, EFhd2 was also found associated with proteins that regulate a wide range of metabolic pathways (e.g., Idh3g, Aldh6a1, Hadha, and Aldoc). Additionally, EFhd2 associates with Vps13c and Dnm1l that maintain mitochondrial membrane potential and mitochondrial fission, respectively (Lesage et al., 2016; Kamerkar et al., 2018). In fact, Dnm1l (dynamin-related protein 1 Drp1) is a large cytosolic GTPase that is recruited to the mitochondrial outer membrane to mediate mitochondrial fission. Thus, EFhd2 is associated with

mitochondrial and cytosolic proteins that maintain tight control of metabolism and mitochondrial homeostasis. Based on these results, EFhd2 is also associated with mitochondrial and cytosolic proteins that maintain tight control of metabolism and mitochondrial homeostasis, whose disruption in part leads to neurodegeneration.
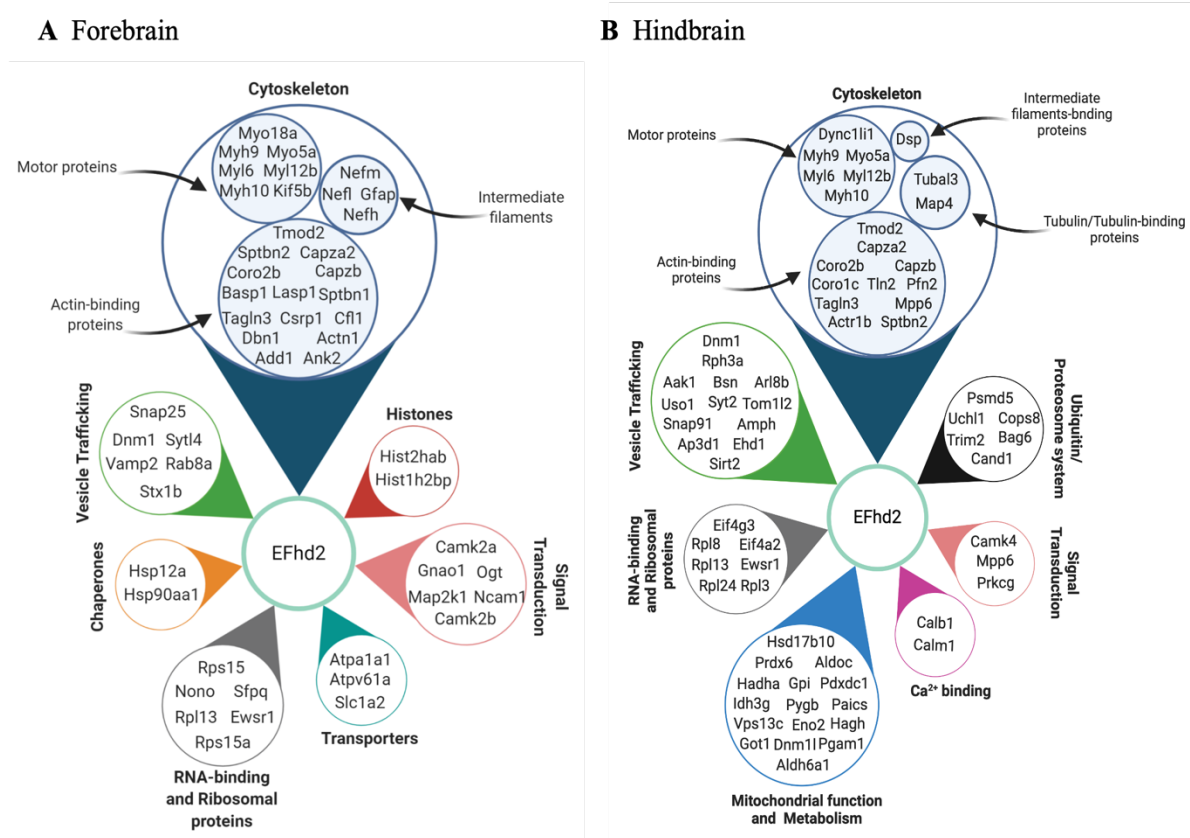
Figure 3.3. EFhd2 interactome in mouse brain. EFhd2-associated proteins in the forebrain region (**A**) and hindbrain (**B**) of *Efhd2*$^{+/+}$ mice (n=6). EFhd2-associated proteins were categorized according to their known biological function. Only the biological functions that contain two or more proteins are represented. This Figure was created with Biorender.com.

Global proteome changes upon deletion of *Efhd2* gene.

Mice that lack EFhd2 develop normally and do not show any phenotype under normal living conditions. However, the absence of the EFhd2 protein may induce proteome changes to compensate for EFhd2's loss of function. To identify proteome changes induced by the deletion of the *Efhd2* gene, we performed global label-free quantitative (LFQ) proteomics analysis in the forebrain and hindbrain regions of *Efhd2*$^{-/-}$ compared to *Efhd2*$^{+/+}$ mice. The data were curated to only assess proteins with abundance changes of at least log2 ± 0.2 (20%) (see Materials and Methods). GO enrichment analysis using ClueGo was conducted to investigate which biological functions changed in the absence of the EFhd2 protein. Out of 281 quantified proteins, 123

proteins were grouped into four main biological functions in the forebrain namely metabolism, stress response, protein regulation, and redox. Similarly, GO analysis of the 762 differentially abundant proteins in the hindbrain region categorized 446 proteins into four main biological functions that include metabolism, stress response, protein localization, and transport. (See Tables A3.3 and A3.4)

Abundance change of categorized proteins is represented as log2 protein change in *Efhd2*$^{-/-}$ vs *Efhd2*$^{+/+}$ mice in Figure 3.4. Most of the forebrain proteins that regulate metabolism showed increased abundance in *Efhd2*$^{-/-}$ mice (Figure 3.4A). Likewise, the protein levels of stress response and redox stress response were generally higher in the forebrain regions of *Efhd2*$^{-/-}$ mice. Regarding protein regulation, the number of proteins with increased abundance were almost equal to those with reduced abundance.

In comparison to forebrain LFQ data, most proteins that regulate metabolism in the hindbrain were more abundant in *Efhd2*$^{-/-}$ with respect to *Efhd2*$^{+/+}$ mice (Figure 3.4B). Conversely, proteins implicated with protein localization, transport, and stress response showed overall decreased abundance in hindbrain regions of *Efhd2*$^{-/--}$ mice.

Taken together, *Efhd2* gene deletion induces changes in proteins that mediate different cellular processes including metabolism, redox, stress response, protein transport, and trafficking. These processes are overrepresented among the identified EFhd2-associated proteins, which led us to examine which novel identified EFhd2-associated proteins also change upon deletion of the *Efhd2* gene. Figure 3.5 shows identified EFhd2-associated proteins in forebrain and hindbrain regions (green nodes indicate increased abundance and red nodes indicate decreased abundance). Eleven proteins differentially abundant in *Efhd2*$^{-/-}$compared to *Efhd2*$^{+/+}$ mice were associated with EFhd2 in both forebrain and hindbrain regions (Figures 3.5A and 3.5B). These proteins include cytoskeletal proteins (Capzb, Coro2b, Myh10, Myh9, Myl12b, Myl6, Sptbn2, and Tmod2), membrane trafficking protein (Dnm1), and RBPs and Ribosomal proteins (Ewsr1 and Rpl13). In addition, 6 unique forebrain EFhd2-associated proteins showed more than log2 ±0.2 change (Figure 3.5A). Primarily, they are cytoskeletal proteins and RBPs. In the hindbrain, we found that 24 unique EFhd2-associated proteins had more than log2 ±0.2 abundance change (Figure 3.5B). These proteins are involved in cytoskeleton dynamics, vesicle trafficking, metabolism, RNA-binding, signal transduction, and UPS (Figure 3.5B). The

convergence of LFQ and EFhd2 interactome data establish an intrinsic relationship between EFhd2 and these specific biological processes.
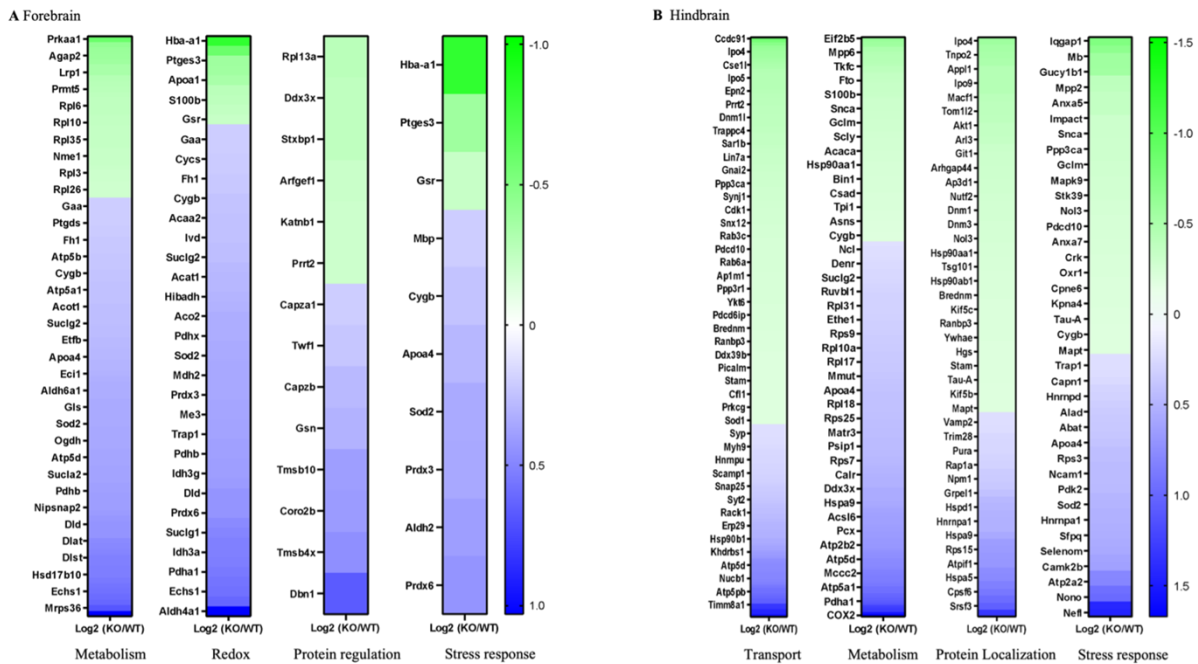
Figure 3.4. Global proteome changes upon *Efhd2* gene deletion. Heatmaps demonstrating abundance change of proteins detected by LFQ in (**A**) forebrain and (**B**) hindbrain. Data are represented as Log2 *Efhd2$^{-/-}$*/*Efhd2$^{+/+}$* ratio of proteins that show ≥ 20% change in *Efhd2$^{-/-}$* mice (n=6) compared to *Efhd2$^{+/+}$* mice (n=6). GO analysis of differentially abundant proteins was conducted using ClueGo in Cytoscape software. ClueGo parameters were >10 proteins/term and Benjamini-Hochberg were used. Kappa score threshold is set to 0.5.
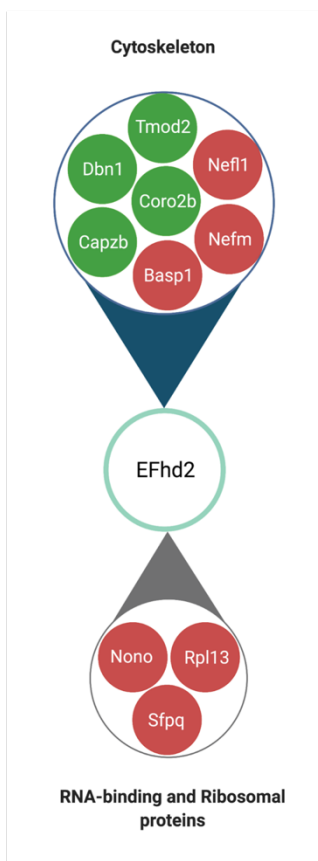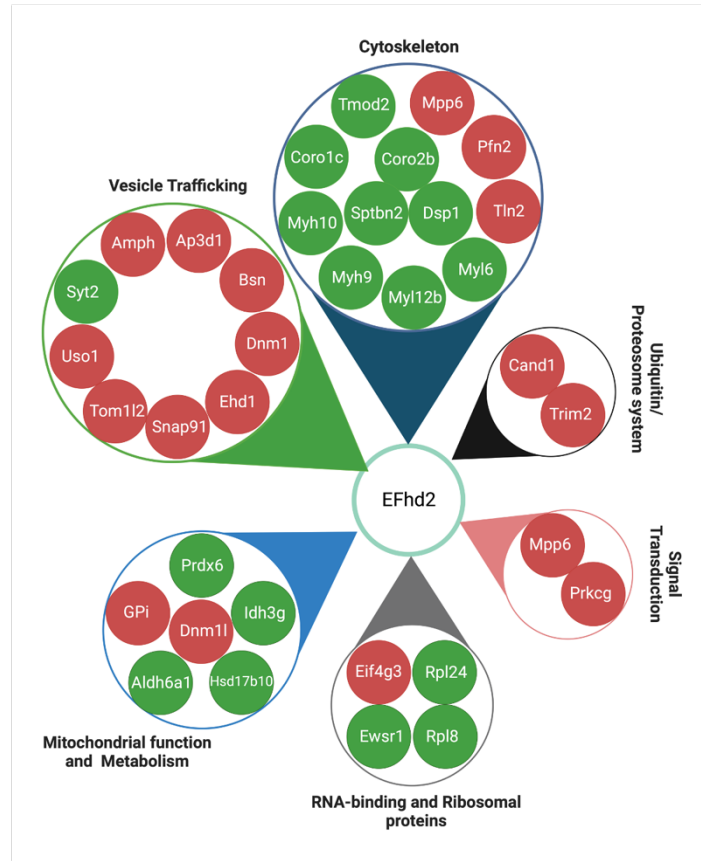
Figure 3.5. EFhd2-associated proteins with abundance change in *Efhd2⁻ᐟ⁻* mice. Identified EFhd2-associated proteins were queried in the label-free quantitative proteomics data. By juxtaposing the detected proteome changes with the identified EFhd2 interactome, we found EFhd2-associated proteins with differential abundance *Efhd2⁻ᐟ⁻* mice. (**A**) In the forebrain, cytoskeleton- and RNA/Ribosome-associated proteins that co-purified with EFhd2 showed differential protein abundance in *Efhd2⁻ᐟ⁻* mice. (**B**) In hindbrain regions, EFhd2-associated proteins linked to cytoskeleton, vesicle trafficking, ubiquitin/proteosome system (UPS), signal transduction, mitochondrial function, and RNA/ ribosomal binding show differential abundance in *Efhd2⁻ᐟ⁻* mice. Green nodes indicate increased abundance and red nodes indicate decreased abundance. The Figure was created with Biorender.com.

Validation of selected EFhd2-associated proteins

   To confirm the identified EFhd2-associated proteins, we selected 5 proteins for validation by western blot. These proteins were chosen based on 1) detection in both forebrain and hindbrain regions of mouse brain, 2) association with molecular processes to which EFhd2 has been previously linked, and 3) availability and validation of commercial antibodies. The selected proteins include transgelin-3 (Tagln3), tropomodulin 2 (Tmod2), and coronin 2b (Coro2b), which are proteins known to regulate actin dynamics and organization. In addition, myosin 2a

(Myh9) and myosin 2b (Myh10) are non-muscle myosin II heavy chain isoforms. Non-muscle myosin II is an actin-binding motor protein that regulates cross-linking and bear contractile properties (Vicente-Manzanares et al., 2009). EFhd2 was immunoprecipitated from forebrain and hindbrain of *Efhd2*$^{+/+}$ mice (n=3). *Efhd2*$^{-/-}$ mice (n=3) were again used as a negative control to ensure that the selected proteins do not bind nonspecifically to either the beads or the antibody. The coimmunoprecipitation of EFhd2 with the five selected proteins was detected by western blot (Figure 3.6). Total lysate from *Efhd2*$^{+/+}$ and *Efhd2*$^{-/-}$ mice brains were used as loading control (Figure 3.6, Input). The result showed that EFhd2 was successfully immunoprecipitated from both forebrain and hindbrain of *Efhd2*$^{+/+}$ mice (Figure 3.6). Tagln3 and Tmod2 coimmunoprecipitated with EFhd2 from both forebrain and hindbrain of *Efhd2*$^{+/+}$ mice (Figure 3.6A). No signal was detected in *Efhd2*$^{-/-}$ control (Figure 3.6A). Despite similar amounts of EFhd2 detected in both regions, the intensity of Tagln3 and Tmod2 signals was higher in the forebrain than the hindbrain samples. In contrast, a similar Coro2b protein signal was detected at the expected molecular weight in both forebrain and hindbrain samples from *Efhd2*$^{+/+}$ mice (Figure 3.6A). A cross-reacting band was also detected in samples from *Efhd2*$^{-/-}$ mice, but the Coro2b signal was much higher in the *Efhd2*$^{+/+}$ samples, suggesting that the signal could be due to cross reaction with a non-specific protein in the sample or background signal from the secondary antibody. Western blot was conducted excluding the anti-Coro2b antibody and incubating with secondary antibody alone. The result showed a protein band at the same molecular weight in the IP samples indicating that the background signal comes from the secondary antibody used (Figure 3.6B). Myh9 and Myh10 also coimmunoprecipitated with EFhd2 in forebrain and hindbrain from *Efhd2*$^{+/+}$ mice. However, their signal was higher in the forebrain samples than the hindbrain samples. Nevertheless, these results confirm the coimmunoprecipitation of EFhd2 with known proteins that modulate actin filaments dynamics and organization.

Targeted mass spectrometry (tMS) is used to detect specific peptides ions from a protein of interest. The IP samples were digested with trypsin and subjected to tMS. To develop a PRM approach, two peptides were selected for each protein that were previously detected by MS. The total area under the curve of the detected peptide ions was calculated from both forebrain and hindbrain immunoprecipitates from *Efhd2*$^{+/+}$ and *Efhd2*$^{-/-}$ samples. Fragmentation product ions were confronted to a mouse library that provided an independent confirmation of the expected

peptide ion fragments (dot product value >0.7). First, we used tMS to validate the five proteins (Tagln3, Tmod2, Coro2b, Myh9 and Myh10) detected by western blot (Table A3.5 and Table A3.6). The selected peptide ions for Tagln3 and Coro2B proteins were detected only in the forebrain and hindbrain of *Efhd2*^{+/+} mice (Table A3.5 and Table A3.6). These results are consistent with the western blot data that shows no detection of Tagln3 and Coro2B protein bands in *Efhd2*^{-/-} (Figure 3.6A). The selected peptides for Tmod2, Myh9 and Myh10 were detected in the forebrain of *Efhd2*^{+/+} mice and not in *Efhd2*^{-/-} as illustrated in Table A3.5. Myh9 and Myh10 selected peptides were detected in the hindbrain of both *Efhd2*^{+/+} and *Efhd2*^{-/-} mice. However, the level of detection for these peptide ions in the hindbrain of *Efhd2*^{+/+} mice was 6 to 10 times higher than the detected in *Efhd2*^{-/-} samples as observed from Table A3.6. These findings also accord with the western blot data that shows a background signal in the *Efhd2*^{-/-} samples (Figure 3.6A). We selected peptide ions for three other proteins, namely Drebrin (Dbn1), F-actin-capping protein subunit alpha-2 (Capza2) and RNA-binding protein EWS (Ewrs1) (summarized in Table A3.5 and A3.6). The selected peptides ions for these three proteins were also detected at a higher level in both the forebrain and hindbrain of *Efhd2*^{+/+} samples than *Efhd2*^{-/-} mice. These results validate the co-purification of Dbn1, Capza2 and Ewrs1 with EFhd2 proteins from both forebrain and hindbrain. Interestingly, these three proteins have been associated with AD pathology (Harigaya et al., 1996; Vanderburg et al., 2010; Lee et al., 2019). Lastly, these results also demonstrate that tMS can be used for validation of novel identified associated proteins.
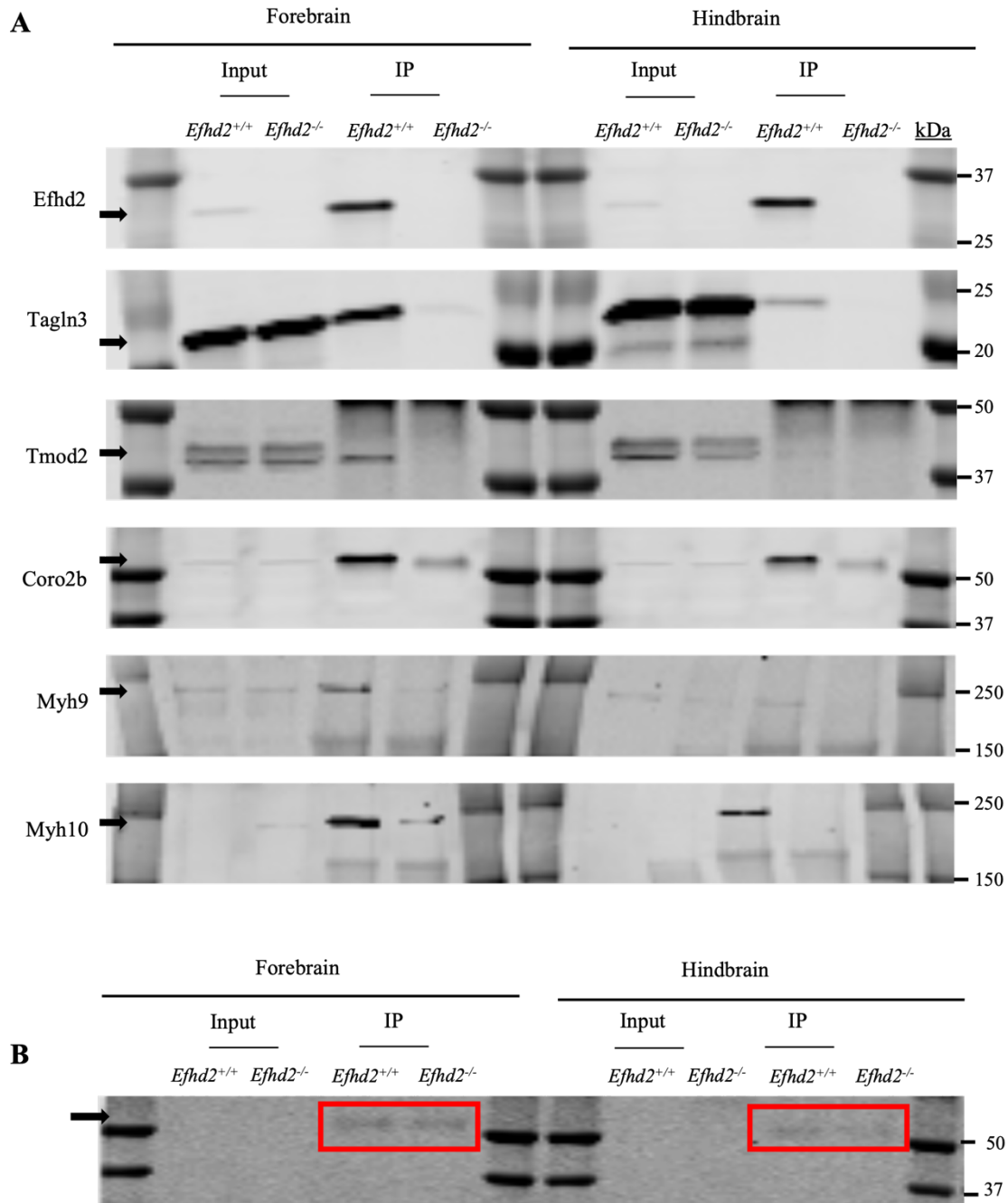
Figure 3.6. Validation of EFhd2-associated proteins. Forebrains and hindbrains from 11-12 months female *Efhd2*$^{+/+}$ (n=3) and *Efhd2*$^{-/-}$ (n=3) mice were homogenized, and EFhd2 was immunoprecipitated by anti-EFhd2 (clone 10D6). (**A**) Western blot was conducted with anti-EFhd2 (1:5000) to verify the IP. Primary antibodies used to validate coimmunoprecipitation of selected proteins are anti-Transgelin 3 (Tagln3), anti-Tropomodulin 2 (Tmod2), anti-Coronin 2b (Coro2b), anti-Myosin 2a (Myh9), and anti-Myosin 2b (Myh10). All the selected EFhd2-associated proteins in the forebrain and hindbrain regions at the expected molecular weight (black arrow). None of them were identified in the IP from *Efhd2*$^{-/-}$ samples. (**B**) Western blot conducted without primary antibody to verify the background signal observed at ~50kDa.

Figure 3.6 (cont'd)
The signal was observed at the same molecular weight (arrow) indicating that corresponds to a secondary antibody cross-reacting band. Input is 45µg of postnuclear brain lysate. Molecular weight marker is indicated by kDa.

Discussion

As yet, little is known about the biological role of EFhd2 in the CNS. In this study, we used MS proteomic analysis to broaden our understanding of the potential molecular pathways that EFhd2 is associated with. The aim of this study is twofold: 1) to characterize, for the first time, EFhd2 interactome network in the brain, 2) to examine the proteome changes upon deleting EFhd2 using *Efhd2*$^{-/-}$ mice.

Physiological significance of EFhd2 brain interactome

Several studies have indicated that EFhd2 colocalizes with F-actin in cell protrusions and lamellipodia *in vitro* using various cell models (Ramesh et al., 2009; Huh et al., 2013; Kwon et al., 2013; Park et al., 2017). Furthermore, EFhd2 overexpression induces cell spreading and lamellipodia formation whereas EFhd2 knock down inhibits cell migration (Kwon et al., 2013; Kogias et al., 2019). Moreover, EFhd2 colocalizes with tau, tubulin, and actin in the leading edge of primary neurons (Purohit et al., 2014). In cell-free assays, EFhd2 increases actin bundling and inhibits cofilin-mediated actin depolymerization (Huh et al., 2013). Here, we identified that EFhd2 is associated with several actin-binding proteins that regulate filament organization, actin polymerization and depolymerization, and cross-linking. A recent study has reported that Coro2b is predominantly expressed in the CNS and is enriched in growth cones wherein it interacts with F-actin to reduce the speed of F-actin filaments (Chen et al., 2020). They showed also that Coro2b is required for dendrite development and its coiled-coil domain mediates self-oligomerization, which is required to inhibit actin polymerization (Chen et al., 2020). We showed that EFhd2's coiled-coil domain is required for its self-oligomerization and association with tau proteins (Ferrer-Acosta et al., 2013b). Thus, it is plausible to speculate that EFhd2 promotes actin filament formation by associating with Coro2b through their coiled-coil domains, which prevents Coro2b from interacting with F-actin. Interestingly, Tmod2, another identified EFhd2-associated protein, serves as an end-actin filament cap to stabilize the filaments, preventing elongation and depolymerization, specifically at the dendrites (Omotade et al., 2018). These findings suggest that EFhd2's role in actin filaments dynamics is through its interaction with known actin-binding proteins. Future studies should reveal molecular pathways that control

the interaction between EFhd2 and actin-binding proteins in CNS. Not only is EFhd2 associated with actin-binding proteins, but it is also associated with microtubules- and intermediate filaments-regulating proteins, as well as known actin-motor proteins (e.g., Myh9 and Myh10) (Woolner et al., 2008; Pecci et al., 2018). Collectively, the data imply that EFhd2 might be a modulator of cytoskeleton dynamics and translocation.

EFhd2 decreases kinesin-mediated microtubule gliding *in vitro* (Purohit et al., 2014). Interestingly, numerous proteins that regulate disparate trafficking pathways co-purified with EFhd2. No previous reports have shown that EFhd2 regulates vesicle trafficking. Although we cannot determine whether EFhd2 directly associates with vesicle trafficking proteins or this association is secondary to its interaction with cytoskeleton, more studies will be required to unveil this molecular aspect of EFhd2 function that has not been studied before. In particular, the mouse forebrain EFhd2 was associated with Sytl4 and its physiological interactor Rab8a that together bind to SNARE complex and regulate vesicle docking and fusion (Hampson et al., 2013). Likewise, EFhd2 in the hindbrain was associated with Amph and Dnm1 that mediate Clathrin-dependent endocytosis (Grabs et al., 1997). Based on these observations, we hypothesize that EFhd2 might act as a scaffold that recruits protein complexes needed for subsequent target interaction. This hypothesis is supported by a previous study that showed EFhd2 as a scaffold recruiting BCR, Syk, and PLCγ to regulate BCR-induced calcium influx in WEHI-231 cells (Kroczek et al., 2010). Therefore, we cannot disregard this possible biological role of EFhd2 in regulating vesicle trafficking.

EFhd2 brain interactome also included calcium -dependent signaling proteins. For instance, we identified Camk2a (αCamkII) in association with EFhd2 in mouse forebrain regions. Previous studies suggested that EFhd2 may modulate signaling pathways in response to calcium oscillations. The identified association between EFhd2 and αCamkII indicates that EFhd2 may exert a direct effect on proteins regulated by changes in calcium levels that are involved in synaptic plasticity. Both EFhd2 and αCamkII play a role in controlling addiction behavior. αCamkII autophosphorylation at T286 mediates the autonomous αCamkII activity independent of calcium/calmodulin (Glazewski et al., 2000). Autophosphorylated αCamkII is important for the induction of long-term potentiation in neocortical experience-dependent plasticity. The autonomous activity of αCamkII due to autophosphorylation amplifies calcium signaling, and it is linked to drug seeking behavior (Anderson et al., 2008; Easton et al., 2013).

Consistently, the expression of αCamkII autophosphorylation mutant (T286A) reduces alcohol consumption in mice and attenuates initial alcohol preference (Easton et al., 2013). Expression of αCamkII mutant (T286A) also subdued dopamine levels upon alcohol challenge (Easton et al., 2013). In another study, the inhibition of αCamkII in the ventral tegmental area (VTA) affected cocaine-evoked synaptic plasticity, suggesting that αCamkII activity is required for cocaine conditioning (Anderson et al., 2008). In contrast, it was shown that *Efhd2*$^{-/-}$ mice consumed more alcohol than wild-type mice and developed increased sensation-seeking behavior and low anxiety (Mielenz et al., 2018). Interestingly, deletion of EFhd2 led to enhanced excitability of dopaminergic neurons in VTA and enhanced extracellular dopamine response upon treatment with psychostimulant drugs (Mielenz et al., 2018; Kogias et al., 2019). These results suggest that EFhd2 may modulate synaptic activity to prevent addictive behavior. Moreover, a SNP (rs112146896) in EFhd2 gene was positively associated with high frequency of alcohol consumption in an adolescent population (European School Survey Project). Taken together, we could infer that EFhd2 protects against addiction by interacting with autophosphorylated αCamkII and possibly preventing its autonomous activity. This speculation merits further investigation. Additionally, future experiments should unravel whether the interaction between EFhd2 and αCamkII is calcium dependent.

Molecular chaperones and UPS components coimmunoprecipitated with EFhd2. These proteins regulate stress response by maintaining proper protein folding, preventing abnormal aggregation, and degrading misfolded proteins. Moreover, several mitochondrial chaperones that mediate mitochondrial homeostasis were also identified. UPS and chaperones machinery are regulated by different signaling pathways. In this regard, signal transduction proteins known to modulate the UPS system, such as ERK1 and 14-3-3 proteins, also coimmunoprecipitated with EFhd2. These signal transduction proteins govern downstream signaling cascades pivotal for cell survival, neuronal growth, and axonal transport (Berg et al., 2003; Cruz & Cruz, 2007).

In this study, we also demonstrate that EFhd2 is associated with RBPs and ribosomal proteins that regulate various stages of transcription and translation. Few identified RBPs mediate RNA granule transport, which also dictates intact cytoskeletal structure and interaction with motor proteins. Not only do the presented data indicate the functional associations of EFhd2, but they also indicate potential EFhd2 cellular localization. In addition to being a

cytosolic protein, the data suggest that EFhd2 is presumably a nuclear, mitochondrial, and ER protein

The impact of *Efhd2* gene deletion on proteome level

Another approach to reveal the potential physiological role of EFhd2 in the brain was by developing *Efhd2$^{-/-}$* mice whereby we could scrutinize the molecular and behavioral ramifications of the absence of EFhd2. Consistent with published reports, *Efhd2$^{-/-}$* mice show normal behavioral phenotype compared to the wild-type control without noticeable developmental anomalies. Herein, we evaluated the global proteome changes in the forebrain and hindbrain brain regions of *Efhd2$^{-/-}$* compared to *Efhd2$^{+/+}$* mice using LFQ mass spectrometry. By grouping the differentially abundant proteins, we found that mainly metabolic processes, stress response, redox response, and protein regulation showed abundance changes upon deleting EFhd2 in the forebrain. In the hindbrain, the overrepresented biological functions of the differential abundant proteins in *Efhd2$^{-/-}$* mice are metabolism, stress response, protein localization, and transport. Moreover, *Efhd2* deletion induced changes in the abundance of several identified EFhd2-associated proteins (Figure 3.5). One may speculate that these changes could be attributed to the putative role of EFhd2 in regulating protein degradation and/or expression. This supposition is based on the association of EFhd2 with protein degradation machinery (chaperones and UPS) and translation and transcription members (RBPs and ribosomes). Alternatively, these changes could be compensatory mechanisms to mitigate the consequences of the *Efhd2* deletion. This could explain, in part, the fact that we and others did not observe developmental or morphological anomalies in *Efhd2$^{-/-}$* mice (Purohit et al., 2014).). Indeed, these data raise a few questions: Do the observed protein changes denote a compensatory mechanism to maintain normal cytoskeleton organization and vesicle trafficking? What are the pathological ramifications of EFhd2 dysregulation? These questions and others are worth examining to better understand the physiological role of EFhd2 in the brain and its role in neurological disorders.

EFhd2 brain interactome and neurodegeneration

In previous studies, we reported the association of EFhd2 with pathological tau in neurodegenerative disorders like AD and FTD. Thus, we investigated the relation between the identified EFhd2-associated proteins and neurodegeneration or neuroprotection and how the dysfunction of these proteins contribute to neuropathology. Take, for example, Ogt, which is

associated with EFhd2 in the forebrain (as illustrated in Figure 3.3A). Ogt is responsible for O-GlcNAcylation of a number of proteins, including tau (Wani et al., 2017). In addition, Ogt expression is induced by cellular oxidative stress, imparting a neuroprotective effect. A recent study demonstrated that Ogt activity is reduced during aging contributing to cognitive impairment, which was rescued upon Ogt overexpression (Zuliani et al., 2021). Importantly, tau O-GlcNAcylation counteracts tau phosphorylation and hinders tau aggregation (Wani et al., 2017). Therefore, Ogt could be playing a neuroprotective role against tau-mediated neurodegeneration.

Bassoon (Bsn) is a presynaptic scaffolding protein that was identified as an EFhd2-interacting partner in the hindbrain region (Figure 3.3B). Importantly, Bassoon level is reduced in the hindbrain of $Efhd2^{-/-}$ mice brains. In fact, bassoon is a large protein in the presynaptic active zone that is critical for normal synaptic functions and networks (Annamneedi et al., 2018). In. addition, it is implicated in spatial and contextual memory (Annamneedi et al., 2018). Recently, bassoon has been identified as a tau interactor (Martinez et al., 2022). Particularly, bassoon interacts with seed-competent misfolded and aggregated tau compared to monomeric tau. Moreover, the absence of bassoon halted tau spreading and progression of pathology in a transgenic tau mouse model (Martinez et al., 2022). The nascent link between bassoon and neurodegenerative disorders, especially tauopathy alludes to its putative role in stabilizing tau aggregation and exacerbating neurotoxicity. Our findings herein spur future research to reveal whether EFhd2 contributes to neuropathology through a direct interaction with bassoon. It should not escape our attention that the EFhd2 interactome presented in this study includes the association of EFhd2 with other synaptic proteins.

Camk4 (Calcium/Calmodulin-dependent protein kinase 4) is associated with EFhd2 in the hindbrain region (Figure 3.3B). Disrupted calcium homeostasis is evident in AD leading to dysregulation of calmodulin, increased activity of downstream Camk4, and tau hyperphosphorylation (Berridge, 2010; Sałaciak et al., 2021). Inhibiting Camk4 reduced phosphorylated tau and improved memory impairment in a transgenic tauopathy model (Ye et al., 2017).

Several molecular chaperones that relate to neurodegenerative diseases were identified in EFhd2 interactome. For instance, Hsp90aa1—identified in the forebrain— interacts with many client proteins like tau, α-synuclein, and kinases and transcription factors to regulate their

function and folding (Bohush et al., 2019). Hsp90 has a neurodegenerative effect as it stabilizes tau kinases and, thus, increases tau phosphorylation and aggregation (Miyata et al., 2011; Bohush et al., 2019).

Notably, UPS dysfunction has been reported in several neurovegetative disorders like AD, PD, and Amyotrophic lateral sclerosis (ALS) (Gong et al., 2016). The disruption of UPS leads to deficit in clearing misfolded proteins and, ultimately, protein aggregation and neuronal death. Uchl1 (Figure 3.3B) is purportedly a neuroprotective protein whose downregulation in AD leads to increased ubiquitination and degradation of proteins responsible for synaptic plasticity and learning (Guglielmotto et al., 2017). Furthermore, previous findings have established the link between mitochondrial dysfunction and UPS disruption in AD (Gong et al., 2016). Presumably, dysfunctional mitochondria produce less ATP that is required for proper UPS function. Additionally, UPS regulates mitochondrial function and acts as a quality control by degrading mitochondrial proteins. Mitochondrial dysfunction in AD manifests as excessive mitochondrial fission (Grimm et al., 2016). Mitochondrial fission-regulating proteins Dnm1l was identified in the EFhd2 interactome. In fact, the levels of Dnm1l (Drp1) increased in AD brains leading to excessive mitochondrial fission and mitochondrial damage (Reddy et al., 2011; Joshi et al., 2018). With this insight, Dnm1l has become a potential target to inhibit excessive mitochondrial fission.

Among the RBPs that co-purified with EFhd2 is Ewsr1 (Figure 3.3). Ewsr1 is a TET family multifunctional protein that regulates transcription, RNA splicing and metabolism (Lee et al., 2019). Few Ewsr1 mutations have been tied to ALS and FTD. Furthermore, Ewsr1 KO mice show neuronal atrophy and abnormal motor behavior. Intriguingly, Ewsr1 levels increased in *Efhd2*$^{-/-}$ mice *in* the hindbrain region.

Limitations and future directions

Several limitations of our data analysis are worth noting. Quantitation after IP was not done due to the technical variability in this approach. To account for sample and technical variability, we grouped biological replicates (e.g., IPs from the same brain region). The rigorous experimental design and stringent data curation criteria used to identify EFhd2-associated proteins may have excluded bona fide EFhd2-associated proteins that tend to bind non-specifically to beads. For example, we could not list actin among the curated EFhd2-associated proteins in mice since it was detected among proteins identified in the negative controls. In

addition, we noticed that the number of detected EFhd2-associated proteins is variable among different regions of mice brains. This variability can be ascribed to the limited efficiency of IP to capture some protein-protein interactions. Nevertheless, we validated several proteins identified as EFhd2-associated proteins using western blot and tMS. Because the fundamental research question in this study was to identify EFhd2 interacting proteins, we did not delve into the interconnections among EFhd2-associated proteins. However, further analysis will be conducted to provide a more comprehensive perspective on EFhd2 biological associations.

Conducting GO of differentially abundant proteins using ClueGo imposes limitation in data analysis by setting a threshold of >10 proteins/term. Therefore, not all the detected proteins were included, which could overlook other biological functions that may be impacted by the deletion of EFhd2. For this reason, we used literature searches to group EFhd2-associated proteins into their biological functions. Finally, even though we report all proteins detected by LFQ, we set a threshold at $\log2\pm0.2$ (20%) to be included in our data analysis, based on expected variations due to median protein half-life. However, proteins that showed change less than 20%, not related to their natural rate of turn over, may also be biologically relevant.

Validating MS proteomics data has specific challenges that need to be acknowledged. The first challenge is the selection of proteins to be validated. Here, the identification of EFhd2-associated proteins is regulated by differential interaction that relies on variable regulation of biological mechanisms needed for these associations. Based on this expected variability, we established a stepwise selection process for validating EFhd2-associated proteins (see Materials and Methods). The second challenge is comparing results from two techniques with different sensitivity levels. Western blot entails using antibodies with different binding constants and specificity to their respective antigen. Therefore, variability in detection sensitivity of the antibodies renders them inefficient regardless of their specificity to the targeted protein. Accordingly, we developed a tMS approach according to pre-determined targeting criteria based on mass, charge state, and retention time. This method has both the sensitivity and specificity required to validate the identified EFhd2-associated proteins. The third challenge was the inadequacy to distinguish between direct and indirect interaction as explained earlier.

Despite the abovementioned limitations, our findings portray for the first time the mouse EFhd2 brain interactome, which bestows an exhaustive view of the putative role of EFhd2 in regulating different cellular processes and molecular pathways. Further work is in progress to

126

determine human EFhd2 brain interactome to substantiate the presented findings. All in all, as depicted in Figure 3.7, the results provide a groundwork to further characterize the physiological role of EFhd2 in regulating inextricable cellular processes and molecular pathways. Future studies will decipher mechanistically how EFhd2 controls these pathways and how they might be implicated in pathological progression of diseases.
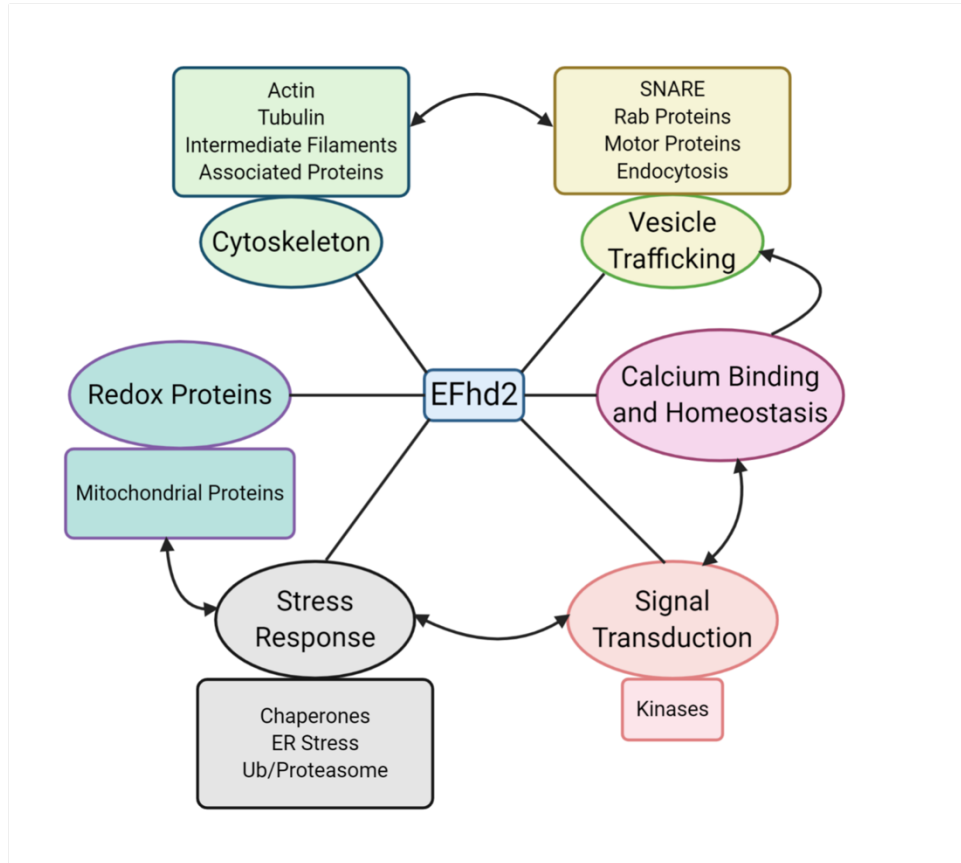
Figure 3.7. EFhd2 is associated with different molecular and cellular processes. EFhd2 protein is highly abundant in the brain, but its physiological function is not well understood. Using a mass spectrometry-based proteomics approach, we found that EFhd2 is associated with numerous proteins implicated in tightly interconnected molecular pathways. These findings suggest that EFhd2 might be a scaffold protein or regulator that coordinates protein-protein interactions to facilitate the regulation and/or crosstalk between different biological processes. The Figure was created with Biorender.com.

REFERENCES

Anderson, S. M., Famous, K. R., Sadri-Vakili, G., Kumaresan, V., Schmidt, H. D., Bass, C. E., Terwilliger, E. F., Cha, J. H., & Pierce, R. C. (2008). CaMKII: a biochemical bridge linking accumbens dopamine and glutamate systems in cocaine seeking. *Nat Neurosci*, *11*(3), 344-353. https://doi.org/10.1038/nn2054

Annamneedi, A., Caliskan, G., Muller, S., Montag, D., Budinger, E., Angenstein, F., Fejtova, A., Tischmeyer, W., Gundelfinger, E. D., & Stork, O. (2018). Ablation of the presynaptic organizer Bassoon in excitatory neurons retards dentate gyrus maturation and enhances learning performance. *Brain Struct Funct*, *223*(7), 3423-3445. https://doi.org/10.1007/s00429-018-1692-3

Avramidou, A., Kroczek, C., Lang, C., Schuh, W., Jack, H. M., & Mielenz, D. (2007). The novel adaptor protein Swiprosin-1 enhances BCR signals and contributes to BCR-induced apoptosis. *Cell Death Differ*, *14*(11), 1936-1947. https://doi.org/10.1038/sj.cdd.4402206

Berg, D., Holzmann, C., & Riess, O. (2003). 14-3-3 proteins in the nervous system. *Nat Rev Neurosci*, *4*(9), 752-762. https://doi.org/10.1038/nrn1197

Berridge, M. J. (2010). Calcium hypothesis of Alzheimer's disease. *Pflugers Arch*, *459*(3), 441-449. https://doi.org/10.1007/s00424-009-0736-1

Binder, L. I., Frankfurter, A., & Rebhun, L. I. (1985). The distribution of tau in the mammalian central nervous system. *J Cell Biol*, *101*(4), 1371-1378. https://doi.org/10.1083/jcb.101.4.1371

Bohush, A., Bieganowski, P., & Filipek, A. (2019). Hsp90 and Its Co-Chaperones in Neurodegenerative Diseases. *Int J Mol Sci*, *20*(20). https://doi.org/10.3390/ijms20204976

Borger, E., Herrmann, A., Mann, D. A., Spires-Jones, T., & Gunn-Moore, F. (2014). The calcium-binding protein EFhd2 modulates synapse formation in vitro and is linked to human dementia. *J Neuropathol Exp Neurol*, *73*(12), 1166-1182. https://doi.org/10.1097/NEN.0000000000000138

Brunger, A. T., Weninger, K., Bowen, M., & Chu, S. (2009). Single-molecule studies of the neuronal SNARE fusion machinery. *Annu Rev Biochem*, *78*, 903-928. https://doi.org/10.1146/annurev.biochem.77.070306.103621

Cajigas, I. J., Tushev, G., Will, T. J., tom Dieck, S., Fuerst, N., & Schuman, E. M. (2012). The local transcriptome in the synaptic neuropil revealed by deep sequencing and high-resolution imaging. *Neuron*, *74*(3), 453-466. https://doi.org/10.1016/j.neuron.2012.02.036

Cao, X., Ballew, N., & Barlowe, C. (1998). Initial docking of ER-derived vesicles requires Uso1p and Ypt1p but is independent of SNARE proteins. *The EMBO Journal*, *17*(8), 2156-2165. https://doi.org/10.1093/emboj/17.8.2156

CHEMDATA.NIST.GOV. (2021). *Libraries of Peptide Tandem Mass Spectra*. Retrieved August 6, 2021 from https://chemdata.nist.gov/dokuwiki/doku.php?id=peptidew:cdownload

Chen, Y., Xu, J., Zhang, Y., Ma, S., Yi, W., Liu, S., Yu, X., Wang, J., & Chen, Y. (2020). Coronin 2B regulates dendrite outgrowth by modulating actin dynamics. *FEBS Letters*, *594*(18), 2975-2987. https://doi.org/10.1002/1873-3468.13886

Chung, D. C., Roemer, S., Petrucelli, L., & Dickson, D. W. (2021). Cellular and pathological heterogeneity of primary tauopathies. *Mol Neurodegener*, *16*(1), 57. https://doi.org/10.1186/s13024-021-00476-x

Cruz, C. D., & Cruz, F. (2007). The ERK 1 and 2 pathway in the nervous system: from basic aspects to possible clinical applications in pain and visceral dysfunction. *Curr Neuropharmacol*, *5*(4), 244-252. https://doi.org/10.2174/157015907782793630

Drasbek, K. R., Holm, M. M., Delenclos, M., & Jensen, K. (2008). Mapping of the spontaneous deletion in the Ap3d1 gene of mocha mice: fast and reliable genotyping. *BMC Res Notes*, *1*(1), 119. https://doi.org/10.1186/1756-0500-1-119

Dujardin, S., Begard, S., Caillierez, R., Lachaud, C., Carrier, S., Lieger, S., Gonzalez, J. A., Deramecourt, V., Deglon, N., Maurage, C. A., Frosch, M. P., Hyman, B. T., Colin, M., & Buee, L. (2018). Different tau species lead to heterogeneous tau pathology propagation and misfolding. *Acta Neuropathol Commun*, *6*(1), 132. https://doi.org/10.1186/s40478-018-0637-7

Easton, A. C., Lucchesi, W., Lourdusamy, A., Lenz, B., Solati, J., Golub, Y., Lewczuk, P., Fernandes, C., Desrivieres, S., & Dawirs, R. R. (2013). α CaMKII Autophosphorylation Controls the Establishment of Alcohol Drinking Behavior. *Neuropsychopharmacology*, *38*(9), 1636-1647. https://doi.org/10.1038/npp.2013.60

Farías, G. G., Guardia, C. M., De Pace, R., Britt, D. J., & Bonifacino, J. S. (2017). BORC/kinesin-1 ensemble drives polarized transport of lysosomes into the axon. *Proceedings of the National Academy of Sciences*, *114*(14), E2955-E2964. https://doi.org/10.1073/pnas.1616363114

Ferrer-Acosta, Y., Rodriguez Cruz, E. N., Vaquer Adel, C., & Vega, I. E. (2013a). Functional and structural analysis of the conserved EFhd2 protein. *Protein Pept Lett*, *20*(5), 573-583. https://doi.org/10.2174/09298665113200050011

Ferrer-Acosta, Y., Rodriguez-Cruz, E. N., Orange, F., De Jesus-Cortes, H., Madera, B., Vaquer-Alicea, J., Ballester, J., Guinel, M. J., Bloom, G. S., & Vega, I. E. (2013b). EFhd2 is a novel amyloid protein associated with pathological tau in Alzheimer's disease. *J Neurochem*, *125*(6), 921-931. https://doi.org/10.1111/jnc.12155

Ferrer-Orta, C., Perez-Sanchez, M. D., Coronado-Parra, T., Silva, C., Lopez-Martinez, D., Baltanas-Copado, J., Gomez-Fernandez, J. C., Corbalan-Garcia, S., & Verdaguer, N. (2017). Structural characterization of the Rabphilin-3A-SNAP25 interaction. *Proc Natl Acad Sci U S A*, *114*(27), E5343-E5351. https://doi.org/10.1073/pnas.1702542114

Fukuda, Y., Pazyra-Murphy, M. F., Silagi, E. S., Tasdemir-Yilmaz, O. E., Li, Y., Rose, L., Yeoh, Z. C., Vangos, N. E., Geffken, E. A., Seo, H.-S., Adelmant, G., Bird, G. H., Walensky, L. D., Marto, J. A., Dhe-Paganon, S., & Segal, R. A. (2020). Binding and transport of SFPQ-RNA

granules by KIF5A/KLC1 motors promotes axon survival. *Journal of Cell Biology*, *220*(1). https://doi.org/10.1083/jcb.202005051

Gaertner, T. R., Kolodziej, S. J., Wang, D., Kobayashi, R., Koomen, J. M., Stoops, J. K., & Waxham, M. N. (2004). Comparative analyses of the three-dimensional structures and enzymatic properties of alpha, beta, gamma and delta isoforms of Ca2+-calmodulin-dependent protein kinase II. *J Biol Chem*, *279*(13), 12484-12494. https://doi.org/10.1074/jbc.M313597200

Glazewski, S., Giese, K. P., Silva, A., & Fox, K. (2000). The role of alpha-CaMKII autophosphorylation in neocortical experience-dependent plasticity. *Nat Neurosci*, *3*(9), 911-918. https://doi.org/10.1038/78820

Gong, B., Radulovic, M., Figueiredo-Pereira, M. E., & Cardozo, C. (2016). The Ubiquitin-Proteasome System: Potential Therapeutic Targets for Alzheimer's Disease and Spinal Cord Injury. *Front Mol Neurosci*, *9*, 4. https://doi.org/10.3389/fnmol.2016.00004

Gotz, J., Halliday, G., & Nisbet, R. M. (2019). Molecular Pathogenesis of the Tauopathies. *Annu Rev Pathol*, *14*, 239-261. https://doi.org/10.1146/annurev-pathmechdis-012418-012936

Grabinski, T., & Kanaan, N. M. (2016). Novel Non-phosphorylated Serine 9/21 GSK3beta/alpha Antibodies: Expanding the Tools for Studying GSK3 Regulation. *Front Mol Neurosci*, *9*, 123. https://doi.org/10.3389/fnmol.2016.00123

Grabs, D., Slepnev, V. I., Zhou, S. Y., David, C., Lynch, M., Cantley, L. C., & DeCamilli, P. (1997). The SH3 domain of amphiphysin binds the proline-rich domain of dynamin at a single site that defines a new SH3 binding consensus sequence. *Journal of Biological Chemistry*, *272*(20), 13419-13425. https://doi.org/10.1074/jbc.272.20.13419

Grimm, A., Friedland, K., & Eckert, A. (2016). Mitochondrial dysfunction: the missing link between aging and sporadic Alzheimer's disease. *Biogerontology*, *17*(2), 281-296. https://doi.org/10.1007/s10522-015-9618-4

Guglielmotto, M., Monteleone, D., Vasciaveo, V., Repetto, I. E., Manassero, G., Tabaton, M., & Tamagno, E. (2017). The Decrease of Uch-L1 Activity Is a Common Mechanism Responsible for Aβ 42 Accumulation in Alzheimer's and Vascular Disease. *Front Aging Neurosci*, *9*, 320. https://doi.org/10.3389/fnagi.2017.00320

Hampson, A., O'Connor, A., & Smolenski, A. (2013). Synaptotagmin-like protein 4 and Rab8 interact and increase dense granule release in platelets. *J Thromb Haemost*, *11*(1), 161-168. https://doi.org/10.1111/jth.12068

Harigaya, Y., Shoji, M., Shirao, T., & Hirai, S. (1996). Disappearance of actin-binding protein, drebrin, from hippocampal synapses in Alzheimer's disease. *J Neurosci Res*, *43*(1), 87-92. https://doi.org/10.1002/jnr.490430111

Huh, Y. H., Kim, S. H., Chung, K. H., Oh, S., Kwon, M. S., Choi, H. W., Rhee, S., Ryu, J. H., Park, Z. Y., Jun, C. D., & Song, W. K. (2013). Swiprosin-1 modulates actin dynamics by

regulating the F-actin accessibility to cofilin. *Cell Mol Life Sci*, *70*(24), 4841-4854. https://doi.org/10.1007/s00018-013-1447-5

Huh, Y. H., Oh, S., Yeo, Y. R., Chae, I. H., Kim, S. H., Lee, J. S., Yun, S. J., Choi, K. Y., Ryu, J. H., Jun, C. D., & Song, W. K. (2015). Swiprosin-1 stimulates cancer invasion and metastasis by increasing the Rho family of GTPase signaling. *Oncotarget*, *6*(15), 13060-13071. https://doi.org/10.18632/oncotarget.3637

Jahn, R., & Fasshauer, D. (2012). Molecular machines governing exocytosis of synaptic vesicles. *Nature*, *490*(7419), 201-207. https://doi.org/10.1038/nature11320

Joshi, A. U., Saw, N. L., Shamloo, M., & Mochly-Rosen, D. (2018). Drp1/Fis1 interaction mediates mitochondrial dysfunction, bioenergetic failure and cognitive decline in Alzheimer's disease. *Oncotarget*, *9*(5), 6128-6143. https://doi.org/10.18632/oncotarget.23640

Kamerkar, S. C., Kraus, F., Sharpe, A. J., Pucadyil, T. J., & Ryan, M. T. (2018). Dynamin-related protein 1 has membrane constricting and severing abilities sufficient for mitochondrial and peroxisomal fission. *Nature Communications*, *9*(1), 1-15. https://doi.org/10.1038/s41467-018-07543-w

Kanai, Y., Dohmae, N., & Hirokawa, N. (2004). Kinesin transports RNA: isolation and characterization of an RNA-transporting granule. *Neuron*, *43*(4), 513-525. https://doi.org/10.1016/j.neuron.2004.07.022

Khazaei, M. R., Bunk, E. C., Hillje, A. L., Jahn, H. M., Riegler, E. M., Knoblich, J. A., Young, P., & Schwamborn, J. C. (2011). The E3-ubiquitin ligase TRIM2 regulates neuronal polarization. *J Neurochem*, *117*(1), 29-37. https://doi.org/10.1111/j.1471-4159.2010.06971.x

Kitao, Y., Hashimoto, K., Matsuyama, T., Iso, H., Tamatani, T., Hori, O., Stern, D. M., Kano, M., Ozawa, K., & Ogawa, S. (2004). ORP150/HSP12A regulates Purkinje cell survival: a role for endoplasmic reticulum stress in cerebellar development. *J Neurosci*, *24*(6), 1486-1496. https://doi.org/10.1523/JNEUROSCI.4029-03.2004

Kogias, G., Kornhuber, J., Reimer, D., Mielenz, D., & Muller, C. P. (2019). Swiprosin-1/ EFhd2: from Immune Regulator to Personality and Brain Disorders. *Neurosignals*, *27*(S1), 1-19. https://doi.org/10.33594/000000179

Kogias, G., Zheng, F., Kalinichenko, L. S., Kornhuber, J., Alzheimer, C., Mielenz, D., & Muller, C. P. (2020). Swiprosin1/EFhd2 is involved in the monoaminergic and locomotor responses of psychostimulant drugs. *J Neurochem*, *154*(4), 424-440. https://doi.org/10.1111/jnc.14959

Kroczek, C., Lang, C., Brachs, S., Grohmann, M., Dutting, S., Schweizer, A., Nitschke, L., Feller, S. M., Jack, H. M., & Mielenz, D. (2010). Swiprosin-1/EFhd2 controls B cell receptor signaling through the assembly of the B cell receptor, Syk, and phospholipase C gamma2 in membrane rafts. *J Immunol*, *184*(7), 3665-3676. https://doi.org/10.4049/jimmunol.0903642

Kwon, M. S., Park, K. R., Kim, Y. D., Na, B. R., Kim, H. R., Choi, H. J., Piragyte, I., Jeon, H., Chung, K. H., Song, W. K., Eom, S. H., & Jun, C. D. (2013). Swiprosin-1 is a novel actin

bundling protein that regulates cell spreading and migration. *PLoS One*, *8*(8), e71626. https://doi.org/10.1371/journal.pone.0071626

Lee, J., Nguyen, P. T., Shim, H. S., Hyeon, S. J., Im, H., Choi, M. H., Chung, S., Kowall, N. W., Lee, S. B., & Ryu, H. (2019). EWSR1, a multifunctional protein, regulates cellular function and aging via genetic and epigenetic pathways. *Biochim Biophys Acta Mol Basis Dis*, *1865*(7), 1938-1945. https://doi.org/10.1016/j.bbadis.2018.10.042

Lesage, S., Drouet, V., Majounie, E., Deramecourt, V., Jacoupy, M., Nicolas, A., Cormier-Dequaire, F., Hassoun, S. M., Pujol, C., Ciura, S., Erpapazoglou, Z., Usenko, T., Maurage, C. A., Sahbatou, M., Liebau, S., Ding, J., Bilgic, B., Emre, M., Erginel-Unaltuna, N., . . . International Parkinson's Disease Genomics, C. (2016). Loss of VPS13C Function in Autosomal-Recessive Parkinsonism Causes Mitochondrial Dysfunction and Increases PINK1/Parkin-Dependent Mitophagy. *Am J Hum Genet*, *98*(3), 500-513. https://doi.org/10.1016/j.ajhg.2016.01.014

Levin, Y. (2011). The role of statistical power analysis in quantitative proteomics. *Proteomics*, *11*(12), 2565-2567. https://doi.org/10.1002/pmic.201100033

Li, H., Zhou, D. S., Chang, H., Wang, L., Liu, W., Dai, S. X., Zhang, C., Cai, J., Liu, W., Li, X., Fan, W., Tang, W., Tang, W., Liu, F., He, Y., Bai, Y., Hu, Z., Xiao, X., Gao, L., & Li, M. (2019). Interactome Analyses implicated CAMK2A in the genetic predisposition and pharmacological mechanism of Bipolar Disorder. *J Psychiatr Res*, *115*, 165-175. https://doi.org/10.1016/j.jpsychires.2019.05.024

Martinez, P., Patel, H., You, Y., Jury, N., Perkins, A., Lee-Gosselin, A., Taylor, X., You, Y., Viana Di Prisco, G., Huang, X., Dutta, S., Wijeratne, A. B., Redding-Ochoa, J., Shahid, S. S., Codocedo, J. F., Min, S., Landreth, G. E., Mosley, A. L., Wu, Y. C., . . . Lasagna-Reeves, C. A. (2022). Bassoon contributes to tau-seed propagation and neurotoxicity. *Nat Neurosci*, *25*(12), 1597-1607. https://doi.org/10.1038/s41593-022-01191-6

Meng, J. J., Bornslaeger, E. A., Green, K. J., Steinert, P. M., & Ip, W. (1997). Two-hybrid analysis reveals fundamental differences in direct interactions between desmoplakin and cell type-specific intermediate filaments. *Journal of Biological Chemistry*, *272*(34), 21495-21503. https://doi.org/10.1074/jbc.272.34.21495

Mielenz, D., Reichel, M., Jia, T., Quinlan, E. B., Stockl, T., Mettang, M., Zilske, D., Kirmizi-Alsan, E., Schonberger, P., Praetner, M., Huber, S. E., Amato, D., Schwarz, M., Purohit, P., Brachs, S., Spranger, J., Hess, A., Buttner, C., Ekici, A. B., . . . Muller, C. P. (2018). EFhd2/Swiprosin-1 is a common genetic determinator for sensation-seeking/low anxiety and alcohol addiction. *Mol Psychiatry*, *23*(5), 1303-1319. https://doi.org/10.1038/mp.2017.63

Miyata, Y., Koren, J., Kiray, J., Dickey, C. A., & Gestwicki, J. E. (2011). Molecular chaperones and regulation of tau quality control: strategies for drug discovery in tauopathies. *Future Med Chem*, *3*(12), 1523-1537. https://doi.org/10.4155/fmc.11.88

Omotade, O. F., Rui, Y., Lei, W., Yu, K., Hartzell, H. C., Fowler, V. M., & Zheng, J. Q. (2018). Tropomodulin Isoform-Specific Regulation of Dendrite Development and Synapse Formation. *J Neurosci*, *38*(48), 10271-10285. https://doi.org/10.1523/jneurosci.3325-17.2018

Park, K. R., An, J. Y., Kang, J. Y., Lee, J. G., Lee, Y., Mun, S. A., Jun, C. D., Song, W. K., & Eom, S. H. (2017). Structural mechanism underlying regulation of human EFhd2/Swiprosin-1 actin-bundling activity by Ser183 phosphorylation. *Biochem Biophys Res Commun*, *483*(1), 442-448. https://doi.org/10.1016/j.bbrc.2016.12.124

Pecci, A., Ma, X., Savoia, A., & Adelstein, R. S. (2018). MYH9: Structure, functions and role of non-muscle myosin IIA in human disease. *Gene*, *664*, 152-167. https://doi.org/10.1016/j.gene.2018.04.048

Peled, M., Dragovich, M. A., Adam, K., Strazza, M., Tocheva, A. S., Vega, I. E., & Mor, A. (2018). EF Hand Domain Family Member D2 Is Required for T Cell Cytotoxicity. *Journal of Immunology*, *201*(9), 2824-2831. https://doi.org/10.4049/jimmunol.1800839

Peng, Y., Meng, G., Sheng, X., & Gao, H. (2021). Transcriptome and DNA methylation analysis reveals molecular mechanisms underlying intrahepatic cholangiocarcinoma progression. *J Cell Mol Med*, *25*(13), 6373-6387. https://doi.org/10.1111/jcmm.16615

Pettitt, S. J., Liang, Q., Rairdan, X. Y., Moran, J. L., Prosser, H. M., Beier, D. R., Lloyd, K. C., Bradley, A., & Skarnes, W. C. (2009). Agouti C57BL/6N embryonic stem cells for mouse genetic resources. *Nat Methods*, *6*(7), 493-495. https://doi.org/10.1038/nmeth.1342

Pierce, N. W., Lee, J. E., Liu, X., Sweredoski, M. J., Graham, R. L. J., Larimore, E. A., Rome, M., Zheng, N., Clurman, B. E., Hess, S., Shan, S. O., & Deshaies, R. J. (2013). Cand1 Promotes Assembly of New SCF Complexes through Dynamic Exchange of F Box Proteins. *Cell*, *153*(1), 206-215. https://doi.org/10.1016/j.cell.2013.02.024

Power, J. H., Asad, S., Chataway, T. K., Chegini, F., Manavis, J., Temlett, J. A., Jensen, P. H., Blumbergs, P. C., & Gai, W. P. (2008). Peroxiredoxin 6 in human brain: molecular forms, cellular distribution and association with Alzheimer's disease pathology. *Acta Neuropathol*, *115*(6), 611-622. https://doi.org/10.1007/s00401-008-0373-3

Pratt, W. B., Morishima, Y., Murphy, M., & Harrell, M. (2006). Chaperoning of glucocorticoid receptors. *Handb Exp Pharmacol*(172), 111-138. https://doi.org/10.1007/3-540-29717-0_5

Purohit, P., Perez-Branguli, F., Prots, I., Borger, E., Gunn-Moore, F., Welzel, O., Loy, K., Wenzel, E. M., Gromer, T. W., Brachs, S., Holzer, M., Buslei, R., Fritsch, K., Regensburger, M., Bohm, K. J., Winner, B., & Mielenz, D. (2014). The Ca2+ sensor protein swiprosin-1/EFhd2 is present in neurites and involved in kinesin-mediated transport in neurons. *PLoS One*, *9*(8), e103976. https://doi.org/10.1371/journal.pone.0103976

Ramesh, T., Kim, Y.-D., Kwon, M.-S., Jun, C.-D., & Kim, S.-W. (2009). Swiprosin-1 regulates cytokine expression of human mast cell line HMC-1 through actin remodeling. *Immune network*, *9*(6), 274-284. https://doi.org/10.4110/in.2009.9.6.274

Reddy, P. H., Reddy, T. P., Manczak, M., Calkins, M. J., Shirendeb, U., & Mao, P. (2011). Dynamin-related protein 1 and mitochondrial fragmentation in neurodegenerative diseases. *Brain Res Rev*, *67*(1-2), 103-118. https://doi.org/10.1016/j.brainresrev.2010.11.004

Regensburger, M., Prots, I., Reimer, D., Brachs, S., Loskarn, S., Lie, D. C., Mielenz, D., & Winner, B. (2018). Impact of Swiprosin-1/Efhd2 on Adult Hippocampal Neurogenesis. *Stem Cell Reports*, *10*(2), 347-355. https://doi.org/10.1016/j.stemcr.2017.12.010

Sałaciak, K., Koszałka, A., Żmudzka, E., & Pytka, K. (2021). The Calcium/Calmodulin-Dependent Kinases II and IV as Therapeutic Targets in Neurodegenerative and Neuropsychiatric Disorders. *International Journal of Molecular Sciences*, *22*(9), 4307. https://doi.org/10.3390/ijms22094307

Sollner, T., Whiteheart, S. W., Brunner, M., Erdjument-Bromage, H., Geromanos, S., Tempst, P., & Rothman, J. E. (1993). SNAP receptors implicated in vesicle targeting and fusion. *Nature*, *362*(6418), 318-324. https://doi.org/10.1038/362318a0

Sudhof, T. C., & Rothman, J. E. (2009). Membrane fusion: grappling with SNARE and SM proteins. *Science*, *323*(5913), 474-477. https://doi.org/10.1126/science.1161748

Takei, K., Slepnev, V. I., Haucke, V., & De Camilli, P. (1999). Functional partnership between amphiphysin and dynamin in clathrin-mediated endocytosis. *Nature Cell Biology*, *1*(1), 33-39. https://doi.org/10.1038/9004

Valenzuela, D. M., Murphy, A. J., Frendewey, D., Gale, N. W., Economides, A. N., Auerbach, W., Poueymirou, W. T., Adams, N. C., Rojas, J., Yasenchak, J., Chernomorsky, R., Boucher, M., Elsasser, A. L., Esau, L., Zheng, J., Griffiths, J. A., Wang, X., Su, H., Xue, Y., . . . Yancopoulos, G. D. (2003). High-throughput engineering of the mouse genome coupled with high-resolution expression analysis. *Nat Biotechnol*, *21*(6), 652-659. https://doi.org/10.1038/nbt822

Vanderburg, C. R., Davis, D. A., Diamond, R. E., Kao, P. F., & Delalle, I. (2010). Capzb2 PROTEIN EXPRESSION IN THE BRAINS OF PATIENTS DIAGNOSED WITH ALZHEIMER'S DISEASE AND HUNTINGTON'S DISEASE. *Transl Neurosci*, *1*(1), 55-58. https://doi.org/10.2478/v10134-010-0008-9

Vazquez-Rosa, E., Rodriguez-Cruz, E. N., Serrano, S., Rodriguez-Laureano, L., & Vega, I. E. (2014). Cdk5 phosphorylation of EFhd2 at S74 affects its calcium binding activity. *Protein Sci*, *23*(9), 1197-1207. https://doi.org/10.1002/pro.2499

Vega, I. E. (2016). EFhd2, a Protein Linked to Alzheimer's Disease and Other Neurological Disorders. *Front Neurosci*, *10*, 150. https://doi.org/10.3389/fnins.2016.00150

Vega, I. E., Sutter, A., Parks, L., Umstead, A., & Ivanova, M. I. (2018). Tau's Three-Repeat Domain and EFhd2 Co-incubation Leads to Increased Thioflavin Signal. *Front Neurosci*, *12*, 879. https://doi.org/10.3389/fnins.2018.00879

Vega, I. E., Traverso, E. E., Ferrer-Acosta, Y., Matos, E., Colon, M., Gonzalez, J., Dickson, D., Hutton, M., Lewis, J., & Yen, S. H. (2008). A novel calcium-binding protein is associated with tau proteins in tauopathy. *J Neurochem*, *106*(1), 96-106. https://doi.org/10.1111/j.1471-4159.2008.05339.x

Vega, I. E., Umstead, A., & Kanaan, N. M. (2019). EFhd2 Affects Tau Liquid-Liquid Phase Separation. *Front Neurosci*, *13*, 845. https://doi.org/10.3389/fnins.2019.00845

Vicente-Manzanares, M., Ma, X., Adelstein, R. S., & Horwitz, A. R. (2009). Non-muscle myosin II takes centre stage in cell adhesion and migration. *Nat Rev Mol Cell Biol*, *10*(11), 778-790. https://doi.org/10.1038/nrm2786

Wang, T., Liu, N. S., Seet, L. F., & Hong, W. (2010). The emerging role of VHS domain-containing Tom1, Tom1L1 and Tom1L2 in membrane trafficking. *Traffic*, *11*(9), 1119-1128. https://doi.org/10.1111/j.1600-0854.2010.01098.x

Wang, Y., & Mandelkow, E. (2016). Tau in physiology and pathology. *Nat Rev Neurosci*, *17*(1), 5-21. https://doi.org/10.1038/nrn.2015.1

Wani, W. Y., Chatham, J. C., Darley-Usmar, V., McMahon, L. L., & Zhang, J. (2017). O-GlcNAcylation and neurodegeneration. *Brain Res Bull*, *133*, 80-87. https://doi.org/10.1016/j.brainresbull.2016.08.002

Wei, S. H., Xu, Y., Shi, H., Wong, S. H., Han, W. P., Talbot, K., Hong, W. J., & Ong, W. Y. (2010). EHD1 is a synaptic protein that modulates exocytosis through binding to snapin. *Molecular and Cellular Neuroscience*, *45*(4), 418-429. https://doi.org/10.1016/j.mcn.2010.07.014

Woolner, S., O'Brien, L. L., Wiese, C., & Bement, W. M. (2008). Myosin-10 and actin filaments are essential for mitotic spindle function. *J Cell Biol*, *182*(1), 77-88. https://doi.org/10.1083/jcb.200804062

Wynn, R. M., Davie, J. R., Cox, R. P., & Chuang, D. T. (1994). Molecular chaperones: heat-shock proteins, foldases, and matchmakers. *J Lab Clin Med*, *124*(1), 31-36. https://doi.org/10.5555/uri:pii:0022214394901511

Ye, S., Wang, T. T., Cai, B., Wang, Y., Li, J., Zhan, J. X., & Shen, G. M. (2017). Genistein protects hippocampal neurons against injury by regulating calcium/calmodulin dependent protein kinase IV protein levels in Alzheimer's disease model rats. *Neural Regen Res*, *12*(9), 1479-1484. https://doi.org/10.4103/1673-5374.215260

Zhang, Y., Wu, K. M., Yang, L., Dong, Q., & Yu, J. T. (2022). Tauopathies: new perspectives and challenges. *Mol Neurodegener*, *17*(1), 28. https://doi.org/10.1186/s13024-022-00533-z

Zhu, X., Lee, H. G., Raina, A. K., Perry, G., & Smith, M. A. (2002). The role of mitogen-activated protein kinase pathways in Alzheimer's disease. *Neurosignals*, *11*(5), 270-281. https://doi.org/10.1159/000067426

Zhu, X., Sun, Z., Lee, H. G., Siedlak, S. L., Perry, G., & Smith, M. A. (2003). Distribution, levels, and activation of MEK1 in Alzheimer's disease. *J Neurochem*, *86*(1), 136-142. https://doi.org/10.1046/j.1471-4159.2003.01820.x

Zuliani, I., Lanzillotta, C., Tramutola, A., Francioso, A., Pagnotta, S., Barone, E., Perluigi, M., & Di Domenico, F. (2021). The Dysregulation of OGT/OGA Cycle Mediates Tau and APP Neuropathology in Down Syndrome. *Neurotherapeutics*, *18*(1), 340-363. https://doi.org/10.1007/s13311-020-00978-4
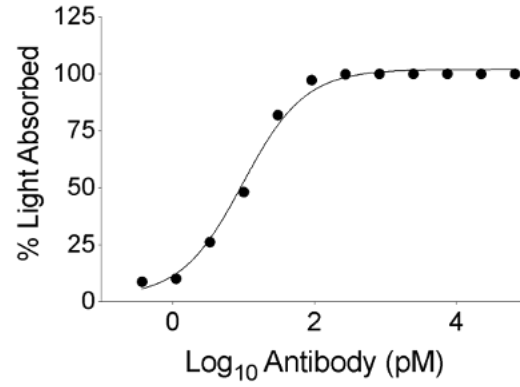
Figure A3.1. EFhd2 antibody titer. Purified mouse anti-EFhd2 antibody (clone 10D6) titer was determined using ELISA with full-length recombinant human EFhd2 protein. The calculated EC_{50} was 10 pM indicating a high affinity antibody.

A

F2

B

F4

C

F8
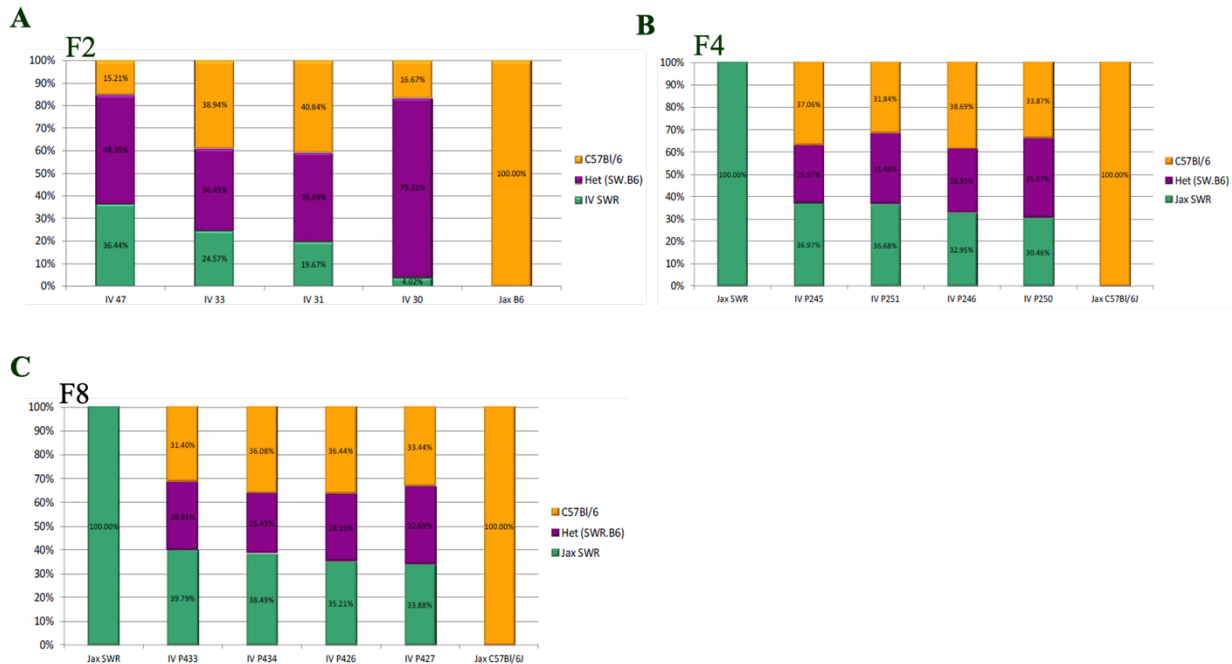
Figure A3.2. Genomic marker background assessment – SNPs. A-C) Illustrates the SNPs associated with either Swiss Webster (SW), C57BL/6J or Mixed (Het(Sw.B6) genomic background. Mice were selected randomly (n=4) from different generations (F2, F4 and F8). The number assigned to each mouse is listed on the graph. Starting F4, we have developed the mouse colony with a stable homogeneous genomic background.

Table A3.1. List of EFhd2-associated proteins in the forebrain

Accession ID	Gene	Protein Description
Q3UH59	*Myh10*	Myosin-10
Q62261	*Sptbn1*	Spectrin beta chain, non-erythrocytic 1
D3Z4J3	*Myo5a*	Unconventional myosin-Va
Q8VDD5	*Myh9*	Myosin-9
Q9JKK7	*Tmod2*	Tropomodulin-2
P39053	*Dnm1*	Dynamin-1
Q68FG2	*Sptbn2*	Spectrin beta chain
Q8BH44	*Coro2b*	Coronin-2B
P47757	*Capzb*	Isoform 3 of F-actin-capping protein subunit beta
E9QAX2	*Myo18a*	Unconventional myosin-XVIIIa
Q60605	*Myl6*	Myosin light polypeptide 6
Q9QXS6	*Dbn1*	Drebrin
P11798	*Camk2a*	Calcium/calmodulin-dependent protein kinase type II subunit alpha
Q8VDN2	*Atp1a1*	Sodium/potassium-transporting ATPase subunit alpha-1
Q3THE2	*Myl12b*	Myosin regulatory light chain 12B
Q9R1Q8	*Tagln3*	Transgelin-3
Q5SVJ0	*Camk2b*	Calcium/calmodulin-dependent protein kinase II, beta, isoform CRA_b
P08553	*Nefm*	Neurofilament 3, medium
P08551	*Nefl*	Neurofilament light polypeptide
P03995	*Gfap*	Glial fibrillary acidic protein
P62843	*Rps15*	40S ribosomal protein S15
P47857	*Pfkm*	Isoform 3 of ATP-dependent 6-phosphofructokinase, muscle type
Q64522	*Hist2h2ab*	Histone H2A type 2-B
Q91XV3	*Basp1*	Brain acid soluble protein 1
P18872	*Gnao1*	Guanine nucleotide-binding protein G(o) subunit alpha
Q9R0Q1	*Sytl4*	Synaptotagmin-like protein 4
Q8K0U4	*Hspa12a*	Heat shock 70 kDa protein 12A
P19246	*Nefh*	Neurofilament heavy polypeptide
B0QZN5	*Vamp2*	Vesicle-associated membrane protein 2
P62245	*Rps15a*	40S ribosomal protein S15a
P97315	*Csrp1*	Cysteine and glycine-rich protein 1
P43006	*Slc1a2*	Excitatory amino acid transporter 2
Q61792	*Lasp1*	LIM and SH3 domain protein 1

Table A3.1 (cont'd)

P60202	*Plp1*	Myelin proteolipid protein
P55258	*Rab8a*	Ras-related protein Rab-8A
P61264	*Stx1b*	Syntaxin-1B
F8WGL3	*Cfl1*	Cofilin-1
P31938	*Map2k1*	Dual specificity mitogen-activated protein kinase kinase 1
P47754	*Capza2*	F-actin-capping protein subunit alpha-2
P60879	*Snap25*	Synaptosomal-associated protein 25
P47963	*Rpl13*	60S ribosomal protein L13
Q7TPR4	*Actn1*	Alpha-actinin-1
Q9QYC0	*Add1*	Alpha-adducin
P07901	*Hsp90aa1*	Heat shock protein HSP 90-alpha
Q8C8R3	*Ank2*	Isoform 2 of Ankyrin-2
Q8CGP2	*Hist1h2bp*	Isoform 2 of Histone H2B type 1-P
Q61768	*Kif5b*	Kinesin-1 heavy chain
P13595	*Ncam1*	Neural cell adhesion molecule 1
Q99K48	*Nono*	Non-POU domain-containing octamer-binding protein
Q5SUS9	*Ewsr1*	RNA-binding protein EWS
Q8VIJ6	*Sfpq*	Splicing factor, proline- and glutamine-rich
Q8CGY8	*Ogt*	UDP-N-acetylglucosamine--peptide N-acetylglucosaminyltransferase 110 kDa subunit
P50516	*Atp6v1a*	V-type proton ATPase catalytic subunit A

Table A3.2. List of EFhd2-associated proteins in the hindbrain

Accession ID	Gene	Protein Description
P39053	*Dnm1*	Isoform 4 of Dynamin-1
Q8K1M6	*Dnm1l*	Dynamin-1-like protein
Q3UH59	*Myh10*	Myosin-10
D3Z4J3	*Myo5a*	Unconventional myosin-Va
Q8VDD5	*Myh9*	Myosin-9
O08709	*Prdx6*	Peroxiredoxin-6
Q8BH44	*Coro2b*	Coronin-2B
P47757	*Capzb*	Isoform 3 of F-actin-capping protein subunit beta
Q9CQW2	*Arl8b*	ADP-ribosylation factor-like protein 8B
Q9R1Q8	*Tagln3*	Transgelin-3
Q60605	*Myl6*	Myosin light polypeptide 6
Q99N15	*Hsd17b10*	17beta-hydroxysteroid dehydrogenase type 10/short chain L-3-hydroxyacyl-CoA dehydrogenase
Q8BX70	*Vps13c*	Vacuolar protein sorting-associated protein 13C
Q3UX10	*Tubal3*	Tubulin alpha chain-like 3
Q3THE2	*Myl12b*	Myosin regulatory light chain 12B
Q71LX4	*Tln2*	Talin-2
Q9JKK7	*Tmod2*	Tropomodulin-2
P05063	*Aldoc*	Fructose-bisphosphate aldolase C
Q9WV92	*Epb41l3*	Isoform 2 of Band 4.1-like protein 3
Q3UKW2	*Calm1*	Calmodulin-1
E9QKC6	*Trim2*	Tripartite motif-containing protein 2
Q8BMS1	*Hadha*	Trifunctional enzyme subunit alpha, mitochondrial
Q9Z1R2	*Bag6*	Large proline-rich protein BAG6
P27546	*Map4*	Microtubule-associated protein 4
P47708	*Rph3a*	Rabphilin-3A
O88737	*Bsn*	Protein bassoon
Q5SRX1	*Tom1l2*	TOM1-like protein 2
P47754	*Capza2*	F-actin-capping protein subunit alpha-2
Q9Z1Z0	*Uso1*	General vesicular transport factor p115
P46097	*Syt2*	Synaptotagmin II
E9QLK9	*Snap91*	Clathrin coat assembly protein AP180
Q80XI3	*Eif4g3*	Eukaryotic translation initiation factor 4 gamma 3
P17183	*Eno2*	Gamma-enolase
Q99K01	*Pdxdc1*	MCG129810, isoform CRA_c

Table A3.2 (cont'd)

P62918	*Rpl8*	60S ribosomal protein L8
P70404	*Idh3g*	Isocitrate dehydrogenase [NAD] subunit gamma 1, mitochondrial
Q8BJY1	*Psmd5*	26S proteasome non-ATPase regulatory subunit 5
P10630	*Eif4a2*	Isoform 2 of Eukaryotic initiation factor 4A-II
Q9EQ20	*Aldh6a1*	Methylmalonate-semialdehyde dehydrogenase [acylating], mitochondrial
P47963	*Rpl13*	60S ribosomal protein L13
Q3UHJ0	*Aak1*	AP2-associated protein kinase 1
P08414	*Camk4*	Calcium/calmodulin-dependent protein kinase type IV
Q8R1Q8	*Dync1li1*	Cytoplasmic dynein 1 light intermediate chain 1
Q7TQF7	*Amph*	Amphiphysin
P05201	*Got1*	Aspartate aminotransferase, cytoplasmic
Q8R5C5	*Actr1b*	Beta-centractin
Q6ZQ38	*Cand1*	Cullin-associated NEDD8-dissociated protein 1
P06745	*Gpi*	Glucose-6-phosphate isomerase
Q8CI94	*Pygb*	Glycogen phosphorylase, brain form
P17742	*Ppia*	Peptidyl-prolyl cis-trans isomerase A
Q5SUS9	*Ewsr1*	RNA-binding protein EWS
Q9R0P9	*Uchl1*	Ubiquitin carboxyl-terminal hydrolase isozyme L1
Q8BP67	*Rpl24*	60S ribosomal protein L24
P12658	*Calb1*	Calbindin
Q9JLB0	*Mpp6*	MAGUK p55 subfamily member 6
Q9DB60	*Fam213b*	Prostamide/prostaglandin F synthase
P63318	*Prkcg*	Protein kinase C gamma type
P27659	*Rpl3*	60S ribosomal protein L3
O54774	*Ap3d1*	AP-3 complex subunit delta-1
P00920	*Ca2*	Carbonic anhydrase 2
Q8BHE3	*Atcay*	Caytaxin
Q02105	*C1qc*	Complement C1q subcomponent subunit C
Q8VBV7	*Cops8*	COP9 signalosome complex subunit 8
Q9WUM4	*Coro1c*	Coronin-1C
E9Q557	*Dsp*	Desmoplakin
Q9WVK4	*Ehd1*	EH domain-containing protein 1
Q921F4	*Hnrnpll*	Heterogeneous nuclear ribonucleoprotein L-like
G5E8T9	*Hagh*	Hydroxyacyl glutathione hydrolase
Q9DCL9	*Paics*	Multifunctional protein ADE2

Table A3.2 (cont'd)

Q8VDQ8	*Sirt2*	NAD-dependent protein deacetylase sirtuin-2
Q9DBJ1	*Pgam1*	Phosphoglycerate mutase 1
Q9JJV2	*Pfn2*	Profilin-2
Q68FG2	*Sptbn2*	Spectrin beta chain

Table A3.3. List of proteins whose abundance changed in the forebrain of *Efhd2⁻ᐟ⁻* mice

Accession ID	Gene	Protein Description	Abundance Ratio (log2): (KO) / (WT)
Q9D8Y0	EFhd2	EF-hand domain-containing protein D2	-2.2
A2AH85	*Eftud2*	116 kDa U5 small nuclear ribonucleoprotein component	-1.12
Q91VB8	*Hba-a1*	Alpha globin 1	-0.84
A2AUK5	*Epb41l1*	Band 4.1-like protein 1	-0.81
O54950	*Prkag1*	5'-AMP-activated protein kinase subunit gamma-1	-0.71
Q792Z1	*Try10*	MCG140784	-0.71
Q9ESM3	*Hapln2*	Hyaluronan and proteoglycan link protein 2	-0.65
Q3TEA8	*Hp1bp3*	Heterochromatin protein 1-binding protein 3	-0.64
Q9Z1W8	*Atp12a*	Potassium-transporting ATPase alpha chain 2	-0.63
Q5EG47	*Prkaa1*	5'-AMP-activated protein kinase catalytic subunit alpha-1	-0.6
P46935	*Nedd4*	E3 ubiquitin-protein ligase NEDD4	-0.59
P43274	*Hist1h1e*	Histone H1.4	-0.58
Q80WM4	*Hapln4*	Hyaluronan and proteoglycan link protein 4	-0.55
P07759	*Serpina3k*	Serine protease inhibitor A3K	-0.47
Q99K48	*Nono*	Non-POU domain-containing octamer-binding protein	-0.46
Q9Z2C4	*Mtmr1*	Myotubularin-related protein 1	-0.44
Q61838	*Pzp*	Pregnancy zone protein	-0.43
Q9ER00	*Stx12*	Syntaxin-12	-0.42
P60202	*Plp1*	Myelin proteolipid protein	-0.41
P08553	*Nefm*	Neurofilament 3, medium	-0.41
Q3UHD9	*Agap2*	Arf-GAP with GTPase, ANK repeat and PH domain-containing protein 2	-0.4
D3YZI9	*Pgbd5*	PiggyBac transposable element-derived protein 5	-0.39
Q9R0Q7	*Ptges3*	Prostaglandin E synthase 3	-0.39
P84228	*Hist2h3c1*	Histone H3.2	-0.38
P62806	*Hist1h4a*	Histone H4	-0.38
Q9Z0P4	*Palm*	Isoform 2 of Paralemmin-1	-0.38
Q08642	*Padi2*	Protein-arginine deiminase type-2	-0.38
P51410	*Rpl9-ps6*	Ribosomal protein L9, pseudogene 6	-0.38
P97493	*Txn2*	Thioredoxin, mitochondrial	-0.38

Table A3.3 (cont'd)

Q9R1R2	*Trim3*	Tripartite motif-containing protein 3	-0.38
Q80X95	*Rraga*	Ras-related GTP-binding protein A	-0.37
Q19LI2	*A1bg*	Alpha-1B-glycoprotein	-0.36
Q9D868	*Ppih*	Isoform 2 of Peptidyl-prolyl cis-trans isomerase H	-0.36
P32848	*Pvalb*	Parvalbumin alpha	-0.36
Q00623	*Apoa1*	Apolipoprotein A-I	-0.35
Q91ZX7	*Lrp1*	Low density lipoprotein receptor-related protein 1	-0.35
P08551	*Nefl*	Neurofilament light polypeptide	-0.35
P01027	*C3*	Complement C3	-0.34
P63328	*Ppp3ca*	Isoform 2 of Serine/threonine-protein phosphatase 2B catalytic subunit alpha isoform	-0.34
Q6W8Q3	*Pcp4l1*	Purkinje cell protein 4-like protein 1	-0.34
Q00896	*Serpina1c*	Alpha-1-antitrypsin 1-3	-0.33
Q62093	*Srsf2*	Serine/arginine-rich splicing factor 2	-0.33
Q60872	*Eif1a*	Eukaryotic translation initiation factor 1A	-0.32
Q8C854	*Myef2*	Myelin expression factor 2	-0.32
G3XA53	*Omg*	Oligodendrocyte-myelin glycoprotein	-0.32
P47915	*Rpl29*	60S ribosomal protein L29	-0.31
Q8BR90	*1 SV*	UPF0600 protein C5orf51 homolog	-0.31
Q9CZX8	*Rps19*	40S ribosomal protein S19	-0.3
D3YZD8	*Aamdc*	Mth938 domain-containing protein	-0.3
Q7TT50	*Cdc42bpb*	Serine/threonine-protein kinase MRCK beta	-0.3
P14869	*Rplp0*	60S acidic ribosomal protein P0	-0.29
P41105	*Rpl28*	60S ribosomal protein L28	-0.29
Q9CX86	*Hnrnpa0*	Heterogeneous nuclear ribonucleoprotein A0	-0.29
Q9CR41	*Hypk*	Huntingtin-interacting protein K	-0.29
Q91V36	*Nrbp2*	Nuclear receptor-binding protein 2	-0.29
P62301	*Rps13*	40S ribosomal protein S13	-0.28
P14115	*Rpl27a*	60S ribosomal protein L27a	-0.28
P46660	*Ina*	Alpha-internexin	-0.28
Q8BGN3	*Enpp6*	Ectonucleotide pyrophosphatase/phosphodiesterase family member 6	-0.28
Q8CIG8	*Prmt5*	Protein arginine N-methyltransferase 5	-0.28
P10639	*Txn*	Thioredoxin	-0.28
Q8BX70	*Vps13c*	Vacuolar protein sorting-associated protein 13C	-0.28
P63248	*Pkia*	cAMP-dependent protein kinase inhibitor alpha	-0.27
Q3U0D9	*Hace1*	E3 ubiquitin-protein ligase HACE1	-0.27

Table A3.3 (cont'd)

P28740	*Kif2a*	Isoform 2 of Kinesin-like protein KIF2A	-0.27
Q8BHL8	*Psmf1*	Proteasome inhibitor PI31 subunit	-0.27
P50114	*S100b*	Protein S100-B	-0.27
B2RQR5	*Sgsm1*	Small G protein signaling modulator 1	-0.27
P47911	*Rpl6*	60S ribosomal protein L6	-0.26
P12970	*Rpl7a*	60S ribosomal protein L7a	-0.26
Q62167	*Ddx3x*	ATP-dependent RNA helicase DDX3X	-0.26
Q8K0E8	*Fgb*	Fibrinogen beta chain	-0.26
O08599	*Stxbp1*	Isoform 2 of Syntaxin-binding protein 1	-0.26
Q91X97	*Ncald*	Neurocalcin-delta	-0.26
Q8VIJ6	*Sfpq*	Splicing factor, proline- and glutamine-rich	-0.26
Q6ZWV3	*Rpl10*	60S ribosomal protein L10	-0.25
P67984	*Rpl22*	60S ribosomal protein L22	-0.25
Q8VEH3	*Arl8a*	ADP-ribosylation factor-like protein 8A	-0.25
Q5XJY5	*Arcn1*	Coatomer subunit delta	-0.25
O88569	*Hnrnpa2b1*	Heterogeneous nuclear ribonucleoproteins A2/B1	-0.25
P61458	*Pcbd1*	Pterin-4-alpha-carbinolamine dehydratase	-0.25
Q62442	*Vamp1*	Vesicle-associated membrane protein 1	-0.25
P47963	*Rpl13*	60S ribosomal protein L13	-0.24
Q6ZWV7	*Rpl35*	60S ribosomal protein L35	-0.24
P47911	*Rpl6*	60S ribosomal protein L6 (Fragment)	-0.24
P84086	*Cplx2*	Complexin-2	-0.24
O55135	*Eif6*	Eukaryotic translation initiation factor 6	-0.24
A6H5Z3	*Exoc6b*	Exocyst complex component 6B	-0.24
Q9QUP5	*Hapln1*	Hyaluronan and proteoglycan link protein 1	-0.24
Q9WV34	*Mpp2*	Isoform 2 of MAGUK p55 subfamily member 2	-0.24
Q9DCS2	*Mettl26*	Methyltransferase-like 26	-0.24
Q3TDD9	*Ppp1r21*	Protein phosphatase 1 regulatory subunit 21	-0.24
Q8K0T0	*Rtn1*	Reticulon (Fragment)	-0.24
Q91VW3	*Sh3bgrl3*	SH3 domain-binding glutamic acid-rich-like protein 3	-0.24
P97351	*Rps3a*	40S ribosomal protein S3a	-0.23
P62754	*Rps6*	40S ribosomal protein S6	-0.23
Q9WUL7	*Arl3*	ADP-ribosylation factor-like protein 3	-0.23
Q8CAB8	*Castor2*	Cytosolic arginine sensor for mTORC1 subunit 2	-0.23
P47791	*Gsr*	Isoform Cytoplasmic of Glutathione reductase, mitochondrial	-0.23

Table A3.3 (cont'd)

P15532	*Nme1*	Nucleoside diphosphate kinase A	-0.23
P12815	*Pdcd6*	Programmed cell death protein 6	-0.23
O35295	*Purb*	Transcriptional activator protein Pur-beta	-0.23
P62761	*Vsnl1*	Visinin-like protein 1	-0.23
P21614	*Gc*	Vitamin D-binding protein	-0.23
O09167	*Rpl21*	60S ribosomal protein L21	-0.22
P61358	*Rpl27*	60S ribosomal protein L27	-0.22
G3X9K3	*Arfgef1*	Brefeldin A-inhibited guanine nucleotide-exchange protein 1	-0.22
Q3UER8	*Fgg*	Fibrinogen gamma chain	-0.22
P62880	*Gnb2*	Guanine nucleotide-binding protein G(I)/G(S)/G(T) subunit beta-2	-0.22
Q5EBP8	*Hnrnpa1*	Heterogeneous nuclear ribonucleoprotein A1	-0.22
P19253	*Gm45713*	Predicted gene 45713	-0.22
Q6ZWU9	*Rps27*	40S ribosomal protein S27	-0.21
P99027	*Rplp2*	60S acidic ribosomal protein P2	-0.21
P27659	*Rpl3*	60S ribosomal protein L3	-0.21
Q91XV3	*Basp1*	Brain acid soluble protein 1	-0.21
Q99KW3	*Trio*	Isoform 4 of Triple functional domain protein	-0.21
Q8BG40	*Katnb1*	Katanin p80 WD40 repeat-containing subunit B1	-0.21
Q80XU3	*Nucks1*	Nuclear ubiquitous casein and cyclin-dependent kinase substrate 1	-0.21
E9PUL5	*Prrt2*	Proline-rich transmembrane protein 2	-0.21
Q9CQ89	*Cuta*	Protein CutA	-0.21
P63325	*Rps10*	40S ribosomal protein S10	-0.2
Q9CR57	*Rpl14*	60S ribosomal protein L14	-0.2
Q9CZM2	*Rpl15*	60S ribosomal protein L15	-0.2
P62717	*Rpl18a*	60S ribosomal protein L18a (Fragment)	-0.2
P61255	*Rpl26*	60S ribosomal protein L26	-0.2
Q8CIE6	*Copa*	Coatomer subunit alpha	-0.2
P16045	*Lgals1*	Galectin-1	-0.2
Q99JX3	*Gorasp2*	Golgi reassembly-stacking protein 2	-0.2
Q8JZN5	*Acad9*	Acyl-CoA dehydrogenase family member 9, mitochondrial	0.2
Q8QZT2	*Ccsap*	Centriole, cilia and spindle-associated protein	0.2
P47753	*Capza1*	F-actin-capping protein subunit alpha-1	0.2
Q8CIB5	*Fermt2*	Fermitin family homolog 2	0.2
Q9ERL9	*Gucy1a1*	Guanylate cyclase soluble subunit alpha-1	0.2

Table A3.3 (cont'd)

P63158	*Hmgb1*	High mobility group protein B1	0.2
P70699	*Gaa*	Lysosomal alpha-glucosidase	0.2
O55022	*Pgrmc1*	Membrane-associated progesterone receptor component 1	0.2
P04370	*Mbp*	Myelin basic protein (Fragment)	0.2
O09114	*Ptgds*	Prostaglandin-H2 D-isomerase	0.2
Q80UJ7	*Rab3gap1*	Rab3 GTPase-activating protein catalytic subunit	0.2
Q9D031	*Rsu1*	Ras suppressor protein 1	0.2
Q9R1Z7	*Pts*	6-pyruvoyl tetrahydrobiopterin synthase	0.21
Q9D7S9	*Chmp5*	Charged multivesicular body protein 5	0.21
P62897	*Cycs*	Cytochrome c, somatic	0.21
Q8R3R8	*Gabarapl1*	Gamma-aminobutyric acid receptor-associated protein-like 1	0.21
Q99PU5	*Acsbg1*	Long-chain-fatty-acid--CoA ligase ACSBG1	0.21
Q6RHR9	*Magi1*	Membrane-associated guanylate kinase, WW and PDZ domain-containing protein 1	0.21
Q9D6Y7	*Msra*	Mitochondrial peptide methionine sulfoxide reductase	0.21
Q9DBG5	*Plin3*	Perilipin-3	0.21
Q8JZP2	*Syn3*	Synapsin-3	0.21
Q9JJQ6	*F8a*	Factor 8-associated gene A	0.22
P97807	*Fh*	Fumarate hydratase, mitochondrial	0.22
P54071	*Idh2*	Isocitrate dehydrogenase [NADP], mitochondrial	0.22
Q8BTG7	*Ndrg4*	Isoform 3 of Protein NDRG4	0.22
Q9DC07	*Nebl*	LIM zinc-binding domain-containing Nebulette	0.22
Q8CGK3	*Lonp1*	Lon protease homolog, mitochondrial	0.22
Q9DCL9	*Paics*	Multifunctional protein ADE2	0.22
P60761	*Nrgn*	Neurogranin	0.22
P52196	*Tst*	Thiosulfate sulfurtransferase	0.22
P68033	*Actc1*	Actin, alpha cardiac muscle 1	0.23
P56480	*Atp5f1b*	ATP synthase subunit beta, mitochondrial	0.23
Q9D172	*D10Jhu81e*	ES1 protein homolog, mitochondrial	0.23
B1AQZ2	*Kif3a*	Kinesin-like protein	0.23
Q9WVL0	*Gstz1*	Maleylacetoacetate isomerase	0.23
P29758	*Oat*	Ornithine aminotransferase, mitochondrial	0.23
Q91YM2	*Arhgap35*	Rho GTPase-activating protein 35	0.23
Q8BJI1	*Slc6a17*	Sodium-dependent neutral amino acid transporter SLC6A17	0.23

Table A3.3 (cont'd)

Q8VBT9	*Aspscr1*	Tether containing UBX domain for GLUT4	0.23
Q91YR1	*Twf1*	Twinfilin-1	0.23
Q9CX80	*Cygb*	Cytoglobin	0.24
Q99LC5	*Etfa*	Electron transfer flavoprotein subunit alpha, mitochondrial	0.24
P0C0S6	*H2afz*	Histone H2A.Z	0.24
Q9Z0S1	*Bpnt1*	3'(2'),5'-bisphosphate nucleotidase 1	0.25
Q8BWT1	*Acaa2*	3-ketoacyl-CoA thiolase, mitochondrial	0.25
P60710	*Actb*	Actin, cytoplasmic 1	0.25
Q03265	*Atp5f1a*	ATP synthase subunit alpha, mitochondrial	0.25
Q06770	*Serpina6*	Corticosteroid-binding globulin	0.25
Q9JHI5	*Ivd*	Isovaleryl-CoA dehydrogenase, mitochondrial	0.25
Q9DCM0	*Ethe1*	Persulfide dioxygenase ETHE1, mitochondrial	0.25
P52760	*Rida*	2-iminobutanoate/2-iminopropanoate deaminase	0.26
O55137	*Acot1*	Acyl-coenzyme A thioesterase 1	0.26
Q8BGB7	*Enoph1*	Enolase-phosphatase E1	0.26
P26443	*Glud1*	Glutamate dehydrogenase 1, mitochondrial	0.26
Q9CX00	*Ist1*	IST1 homolog	0.26
Q9Z2I8	*Suclg2*	Succinate--CoA ligase [GDP-forming] subunit beta, mitochondrial	0.26
Q8QZS1	*Hibch*	3-hydroxyisobutyryl-CoA hydrolase, mitochondrial	0.27
Q9WTN0	*Ggps1*	Geranylgeranyl pyrophosphate synthase	0.27
Q8K4Z3	*Naxe*	NAD(P)H-hydrate epimerase	0.27
P55302	*Lrpap1*	Alpha-2-macroglobulin receptor-associated protein	0.28
Q9DCW4	*Etfb*	Electron transfer flavoprotein subunit beta	0.28
Q9CQZ1	*Hsbp1*	Heat shock factor-binding protein 1	0.28
P85094	*Isoc2a*	Isochorismatase domain-containing protein 2A	0.28
A2AP18	*Plch2*	Isoform 3 of 1-phosphatidylinositol 4,5-bisphosphate phosphodiesterase eta-2	0.28
P47757	*Capzb*	Isoform 3 of F-actin-capping protein subunit beta	0.28
Q9D0K2	*Oxct1*	Succinyl-CoA:3-ketoacid coenzyme A transferase 1, mitochondrial	0.28
Q9DCT1	*Akr1e2*	1,5-anhydro-D-fructose reductase	0.29
Q8QZT1	*Acat1*	Acetyl-CoA acetyltransferase, mitochondrial	0.29
P06728	*Apoa4*	Apolipoprotein A-IV	0.29
Q99L13	*Hibadh*	3-hydroxyisobutyrate dehydrogenase, mitochondrial	0.3
Q8VCW8	*Acsf2*	Acyl-CoA synthetase family member 2, mitochondrial	0.3

Table A3.3 (cont'd)

P70236	*Map2k6*	Dual specificity mitogen-activated protein kinase kinase 6	0.3
Q9QYG0	*Ndrg2*	Protein NDRG2	0.3
Q64433	*Hspe1*	10 kDa heat shock protein, mitochondrial	0.31
P42125	*Eci1*	Enoyl-CoA delta isomerase 1, mitochondrial	0.31
P13020	*Gsn*	Isoform 2 of Gelsolin	0.31
Q61771	*Kif3b*	Kinesin-like protein KIF3B	0.31
A2AG50	*Map7d2*	MAP7 domain-containing protein 2	0.31
Q99K01	*Pdxdc1*	MCG129810, isoform CRA_c	0.32
Q68FH4	*Galk2*	N-acetylgalactosamine kinase	0.32
Q3UGX2	*Sptb*	Spectrin beta chain	0.32
P97797	*Sirpa*	Tyrosine-protein phosphatase non-receptor type substrate 1	0.32
Q99KI0	*Aco2*	Aconitate hydratase, mitochondrial	0.33
Q8BFZ3	*Actbl2*	Beta-actin-like protein 2	0.33
Q3TC72	*Fahd2a*	Fumarylacetoacetate hydrolase domain-containing 2A	0.33
Q9EQ20	*Aldh6a1*	Methylmalonate-semialdehyde dehydrogenase [acylating], mitochondrial	0.33
Q8BKZ9	*Pdhx*	Pyruvate dehydrogenase protein X component, mitochondrial	0.33
Q8BH57	*Wdr48*	WD repeat-containing protein 48	0.33
P05202	*Got2*	Aspartate aminotransferase, mitochondrial	0.34
Q9CZU6	*Cs*	Citrate synthase, mitochondrial	0.34
P10518	*Alad*	Delta-aminolevulinic acid dehydratase	0.34
D3Z7P3	*Gls*	Glutaminase kidney isoform, mitochondrial	0.34
Q9WUT3	*Rps6ka2*	Ribosomal protein S6 kinase alpha-2	0.34
P38647	*Hspa9*	Stress-70 protein, mitochondrial	0.34
P09671	*Sod2*	Superoxide dismutase [Mn], mitochondrial	0.34
Q60597	*Ogdh*	Isoform 3 of 2-oxoglutarate dehydrogenase, mitochondrial	0.35
P08249	*Mdh2*	Malate dehydrogenase, mitochondrial	0.35
Q9JLZ3	*Auh*	Methylglutaconyl-CoA hydratase, mitochondrial	0.35
E9QPD7	*Pcx*	Pyruvate carboxylase	0.35
P20108	*Prdx3*	Thioredoxin-dependent peroxide reductase, mitochondrial	0.35
Q9JKK7	*Tmod2*	Tropomodulin-2	0.35
P61922	*Abat*	4-aminobutyrate aminotransferase, mitochondrial	0.36
Q9CQR4	*Acot13*	Acyl-coenzyme A thioesterase 13	0.36

Table A3.3 (cont'd)

Q9D3D9	*Atp5f1d*	ATP synthase subunit delta, mitochondrial	0.36
Q8BMF3	*Me3*	NADP-dependent malic enzyme, mitochondrial	0.36
Q922B2	*Dars*	Aspartate--tRNA ligase, cytoplasmic	0.37
Q9CQN1	*Trap1*	Heat shock protein 75 kDa, mitochondrial	0.37
Q9Z2I9	*Sucla2*	Succinate--CoA ligase [ADP-forming] subunit beta, mitochondrial	0.37
Q63932	*Map2k2*	Dual specificity mitogen-activated protein kinase kinase 2	0.38
Q9D051	*Pdhb*	Pyruvate dehydrogenase E1 component subunit beta, mitochondrial	0.38
Q8BWF0	*Aldh5a1*	Succinate-semialdehyde dehydrogenase, mitochondrial	0.38
P47738	*Aldh2*	Aldehyde dehydrogenase, mitochondrial	0.39
Q8R5L1	*C1qbp*	Complement component 1 Q subcomponent-binding protein, mitochondrial	0.39
Q7TMG8	*Nipsnap2*	Glioblastoma amplified sequence	0.39
P70404	*Idh3g*	Isocitrate dehydrogenase [NAD] subunit gamma 1, mitochondrial	0.39
Q6ZWY8	*Tmsb10*	Thymosin beta-10	0.39
Q8BH44	*Coro2b*	Coronin-2B	0.4
B2RXT3	*Ogdhl*	Ogdhl protein	0.4
Q9CR21	*Ndufab1*	Acyl carrier protein, mitochondrial	0.42
Q9QYG0	*Ndrg2*	Isoform 2 of Protein NDRG2	0.42
O08749	*Dld*	Dihydrolipoyl dehydrogenase, mitochondrial	0.43
Q91VA7	*Idh3b*	Isocitrate dehydrogenase [NAD] subunit, mitochondrial	0.43
D3Z0Y2	*Prdx6*	Peroxiredoxin-6	0.43
Q9DB15	*Mrpl12*	39S ribosomal protein L12, mitochondrial	0.45
P63038	*Hspd1*	60 kDa heat shock protein, mitochondrial	0.45
P20065	*Tmsb4x*	Thymosin beta-4	0.45
Q8BMF4	*Dlat*	Dihydrolipoyllysine-residue acetyltransferase component of pyruvate dehydrogenase complex, mitochondrial	0.47
Q9D0S9	*Hint2*	Histidine triad nucleotide-binding protein 2, mitochondrial	0.48
Q9WUM5	*Suclg1*	Succinate--CoA ligase [ADP/GDP-forming] subunit alpha, mitochondrial	0.49
Q9D2G2	*Dlst*	Dihydrolipoyllysine-residue succinyltransferase component of 2-oxoglutarate dehydrogenase complex, mitochondrial	0.51

Q9D6R2	*Idh3a*	Isocitrate dehydrogenase [NAD] subunit, mitochondrial	0.51
O08756	*Hsd17b10*	3-hydroxyacyl-CoA dehydrogenase type-2	0.52
Q9WTP7	*Ak3*	GTP:AMP phosphotransferase AK3, mitochondrial	0.52
P35486	*Pdha1*	Pyruvate dehydrogenase E1 component subunit alpha, somatic form, mitochondrial	0.54
Q8BFR5	*Tufm*	Elongation factor Tu, mitochondrial	0.55
O89023	*Tpp1*	Tripeptidyl-peptidase 1	0.55
Q61425	*Hadh*	Hydroxyacyl-coenzyme A dehydrogenase, mitochondrial	0.56
Q8BH95	*Echs1*	Enoyl-CoA hydratase, mitochondrial	0.57
Q8R071	*Itpka*	Inositol-trisphosphate 3-kinase A	0.59
Q99KY4	*Gak*	Cyclin-G-associated kinase	0.6
Q8K1Z0	*Coq9*	Ubiquinone biosynthesis protein COQ9, mitochondrial	0.61
O88696	*Clpp*	ATP-dependent Clp protease proteolytic subunit, mitochondrial	0.62
P33173	*Kif1a*	Kinesin-like protein KIF1A	0.62
Q6GSS7	*Hist2h2aa1*	Histone H2A type 2-A	0.64
P01867	*Igh-3*	Ig gamma-2B chain C region	0.65
Q9QXS6	*Dbn1*	Drebrin	0.66
Q9CQX8	*Mrps36*	28S ribosomal protein S36, mitochondrial	0.68
P60670	*Nploc4*	Nuclear protein localization protein 4 homolog	0.7
P62322	*Lsm5*	U6 snRNA-associated Sm-like protein LSm5	0.76
Q9CYW4	*Hdhd3*	Haloacid dehalogenase-like hydrolase domain-containing protein 3	0.8
D3YUE4	*Fam151b*	Family with sequence similarity 151, member B	0.91
Q8CHT0	*Aldh4a1*	Delta-1-pyrroline-5-carboxylate dehydrogenase, mitochondrial	1.03
Q64288	*Omp*	Olfactory marker protein	1.12
Q02105	*C1qc*	Complement C1q subcomponent subunit C	1.26

Table A3.4 List of proteins whose abundance changed in the hindbrain of *Efhd2⁻/⁻*

Accession ID	Gene	Protein Description	Abundance Ratio (log2): (KO) / (WT)
Q9D8Y9	EFhd2	EF-hand domain-containing protein D2	-2.14
A8DUK4	*Hbb-bs*	Beta-globin	-1.6
Q3UFY7	*Nt5c3b*	7-methylguanosine phosphate-specific 5'-nucleotidase	-1.44
Q9Z2H5	*Epb41l1*	Band 4.1-like protein 1	-1
Q9D8L5	*Ccdc91*	Coiled-coil domain-containing protein 91	-0.86
Q63932	*Map2k2*	Dual specificity mitogen-activated protein kinase kinase 2	-0.81
Q9JKF1	*Iqgap1*	Ras GTPase-activating-like protein IQGAP1	-0.76
O35250	*Exoc7*	Exocyst complex component 7	-0.71
Q9Z1W8	*Atp12a*	Potassium-transporting ATPase alpha chain 2	-0.68
O88398	*Avil*	Advillin	-0.67
Q8BR90	*Rimoc1*	UPF0600 protein C5orf51 homolog	-0.65
Q8R010	*Aimp2*	Aminoacyl tRNA synthase complex-interacting multifunctional protein 2	-0.63
Q80TL7	*Mon2*	Protein MON2 homolog	-0.63
Q8CHW4	*Eif2b5*	Translation initiation factor eIF-2B subunit epsilon	-0.62
Q8R0H9	*Gga1*	ADP-ribosylation factor-binding protein GGA1	-0.61
Q8CFV9	*Rfk*	Riboflavin kinase	-0.61
Q9Z2E4	*Ppp1r17*	Protein phosphatase 1 regulatory subunit 17	-0.59
Q8VI75	*Ipo4*	Importin-4	-0.58
Q19LI2	*A1bg*	Alpha-1B-glycoprotein	-0.57
P04247	*Mb*	Myoglobin	-0.57
Q9Z0P4	*Palm*	Paralemmin-1	-0.57
Q9D708	*S100a16*	Protein S100-A16	-0.57
P62761	*Vsnl1*	Visinin-like protein 1	-0.57
Q8R2R9	*Ap3m2*	AP-3 complex subunit mu-2	-0.56
P28658	*Atxn10*	Ataxin-10	-0.56
O54865	*Gucy1b1*	Guanylate cyclase soluble subunit beta-1	-0.56
Q6P2B1	*Tnpo3*	Isoform 2 of Transportin-3	-0.54

Table A3.4 (cont'd)

P29391	*Ftl1*	Ferritin light chain 1	-0.52
E9PV58	*Tnpo2*	Transportin-2	-0.52
Q9ERK4	*Cse1l*	Exportin-2	-0.5
P97352	*S100a13*	Protein S100-A13	-0.5
Q8VE09	*Ttc39c*	RIKEN cDNA 2810439F02	-0.5
Q8R3R8	*Gabarapl1*	Gamma-aminobutyric acid receptor-associated protein-like 1	-0.49
Q63ZW7	*Patj*	InaD-like protein	-0.49
Q8R123	*Flad1*	Isoform 2 of FAD synthase	-0.49
Q9DCG9	*Trmt112*	Multifunctional methyltransferase subunit TRM112-like protein	-0.49
Q91X97	*Ncald*	Neurocalcin-delta	-0.49
Q91YS4	*Klc2*	Kinesin light chain 2	-0.48
Q9Z0E0	*Ncdn*	Neurochondrin	-0.48
Q9JLB0	*Mpp6*	MAGUK p55 subfamily member 6	-0.46
O88737	*Bsn*	Protein bassoon	-0.46
Q9D031	*Rsu1*	Ras suppressor protein 1	-0.46
Q8BYR5	*Cadps2*	Calcium-dependent secretion activator 2	-0.45
Q60737	*Csnk2a1*	Casein kinase II subunit alpha	-0.45
Q8K3H0	*Appl1*	DCC-interacting protein 13-alpha	-0.45
Q6P5F9	*Xpo1*	Exportin-1	-0.45
P48320	*Gad2*	Glutamate decarboxylase 2	-0.45
Q8BKC5	*Ipo5*	Importin-5	-0.45
Q91YE6	*Ipo9*	Importin-9	-0.45
Q8CI71	*Vps50*	Syndetin	-0.45
Q9JME5	*Ap3b2*	AP-3 complex subunit beta-2	-0.44
Q91YI0	*Asl*	Argininosuccinate lyase	-0.44
Q9D868	*Ppih*	Isoform 2 of Peptidyl-prolyl cis-trans isomerase H	-0.44
P07310	*Ckm*	Creatine kinase M-type	-0.43
J3QNT7	*Epn2*	Epsin-2	-0.43
F8VQK3	*Gucy1a2*	Guanylate cyclase 1, soluble, alpha 2	-0.43
Q9Z2H5	*Epb41l1*	Band 4.1-like protein 1 (Fragment)	-0.42
P68404	*Prkcb*	Protein kinase C beta type	-0.42
Q91VW3	*Sh3bgrl3*	SH3 domain-binding glutamic acid-rich-like protein 3	-0.42
O08599	*Stxbp1*	Syntaxin-binding protein 1	-0.42
P70290	*Mpp1*	55 kDa erythrocyte membrane protein	-0.41

Table A3.4 (cont'd)

P61205	*Arf3*	ADP-ribosylation factor 3	-0.41
Q3UHL1	*Camkv*	CaM kinase-like vesicle-associated protein	-0.41
P84228	*Hist2h3c1*	Histone H3.2	-0.41
E9PVY8	*Macf1*	Microtubule-actin cross-linking factor 1	-0.41
Q8R1N4	*Nudcd3*	NudC domain-containing protein 3	-0.41
E9PUL5	*Prrt2*	Proline-rich transmembrane protein 2	-0.41
Q62159	*Rhoc*	Rho-related GTP-binding protein RhoC	-0.41
Q5SSL4	*Abr*	Isoform 2 of Active breakpoint cluster region-related protein	-0.4
Q5SRX1	*Tom1l2*	Isoform 2 of TOM1-like protein 2	-0.4
G3X9A7	*Plcxd3*	MCG49978	-0.4
P10637	*Mapt*	Microtubule-associated protein	-0.4
Q3TYX3	*Smyd5*	SET and MYND domain-containing protein 5	-0.4
Q8VC30	*Tkfc*	Triokinase/FMN cyclase	-0.4
Q9CXW3	*Cacybp*	Calcyclin-binding protein	-0.39
E9PUD2	*Dnm1l*	Dynamin-1-like protein	-0.39
Q62420	*Sh3gl2*	Endophilin-A1	-0.39
Q8K394	*Plcl2*	Inactive phospholipase C-like protein 2	-0.39
Q9WV34	*Mpp2*	Isoform 2 of MAGUK p55 subfamily member 2	-0.39
Q80TJ1	*Cadps*	Isoform 4 of Calcium-dependent secretion activator 1	-0.39
P06837	*Gap43*	Neuromodulin	-0.39
P61294	*Rab6b*	Ras-related protein Rab-6B	-0.39
A2AH85	*Eftud2*	116 kDa U5 small nuclear ribonucleoprotein component	-0.38
P11031	*Sub1*	Activated RNA polymerase II transcriptional coactivator p15	-0.38
F8WHW6	*Pip5k1c*	Phosphatidylinositol 4-phosphate 5-kinase type-1 gamma	-0.38
P54227	*Stmn1*	Stathmin	-0.38
Q9ES56	*Trappc4*	Trafficking protein particle complex subunit 4	-0.38
O08529	*Capn2*	Calpain-2 catalytic subunit	-0.37
A2AWI7	*Sh3glb2*	Endophilin-B2	-0.37
P60521	*Gabarapl2*	Gamma-aminobutyric acid receptor-associated protein-like 2	-0.37
Q99JX3	*Gorasp2*	Golgi reassembly-stacking protein 2	-0.37

Table A3.4 (cont'd)

P62806	*Hist1h4a*	Histone H4	-0.37
Q8BHL8	*Psmf1*	Proteasome inhibitor PI31 subunit	-0.37
Q8C8N2	*Scai*	Protein SCAI	-0.37
Q08642	*Padi2*	Protein-arginine deiminase type-2	-0.37
P20065	*Tmsb4x*	Thymosin beta-4	-0.37
P61089	*Ube2n*	Ubiquitin-conjugating enzyme E2 N	-0.37
P84084	*Arf5*	ADP-ribosylation factor 5	-0.36
P48036	*Anxa5*	Annexin A5	-0.36
E9PX52	*Asap2*	Arf-GAP with SH3 domain, ANK repeat and PH domain-containing protein 2	-0.36
O88545	*Cops6*	COP9 signalosome complex subunit 6	-0.36
Q8BIW1	*Prune1*	Exopolyphosphatase PRUNE1	-0.36
Q9CQC9	*Sar1b*	GTP-binding protein SAR1b	-0.36
P61082	*Ube2m*	NEDD8-conjugating enzyme Ubc12	-0.36
P84075	*Hpca*	Neuron-specific calcium-binding protein hippocalcin	-0.36
Q3UYC0	*Ppm1h*	Protein phosphatase 1H	-0.36
P31750	*Akt1*	RAC-alpha serine/threonine-protein kinase	-0.36
P48428	*Tbca*	Tubulin-specific chaperone A	-0.36
Q9WUL7	*Arl3*	ADP-ribosylation factor-like protein 3	-0.35
Q8BGW1	*Fto*	Alpha-ketoglutarate-dependent dioxygenase FTO	-0.35
Q99KK7	*Dpp3*	Dipeptidyl peptidase 3	-0.35
Q5U3K5	*Rabl6*	Rab-like protein 6	-0.35
Q7TQD2	*Tppp*	Tubulin polymerization-promoting protein	-0.35
Q8R464	*Cadm4*	Cell adhesion molecule 4	-0.34
Q3TCH7	*Cul4a*	Cullin-4A	-0.34
Q8BWY3	*Etf1*	Eukaryotic peptide chain release factor subunit 1	-0.34
P48318	*Gad1*	Glutamate decarboxylase 1	-0.34
Q9JHQ5	*Lztfl1*	Leucine zipper transcription factor-like protein 1	-0.34
Q8BUK6	*Hook3*	Protein Hook homolog 3	-0.34
P48453	*Ppp3cb*	Serine/threonine-protein phosphatase 2B catalytic subunit beta isoform	-0.34
G5E866	*Sf3b1*	Splicing factor 3B subunit 1	-0.34
Q6PEV3	*Wipf2*	WAS/WASL-interacting protein family member 2	-0.34

Table A3.4 (cont'd)

Q8BK64	*Ahsa1*	Activator of 90 kDa heat shock protein ATPase homolog 1	-0.33
Q8BHE3	*Atcay*	Caytaxin	-0.33
Q9Z1Z0	*Uso1*	General vesicular transport factor p115	-0.33
P53612	*Rabggtb*	Geranylgeranyl transferase type-2 subunit beta	-0.33
P68404	*Prkcb*	Isoform Beta-II of Protein kinase C beta type	-0.33
Q9DBG5	*Plin3*	Perilipin-3	-0.33
Q9JIF0	*Prmt1*	Protein arginine N-methyltransferase 1	-0.33
Q8JZS0	*Lin7a*	Protein lin-7 homolog A	-0.33
P50114	*S100b*	Protein S100-B	-0.33
Q9CR09	*Ufc1*	Ubiquitin-fold modifier-conjugating enzyme 1	-0.33
Q9QZB7	*Actr10*	Actin-related protein 10	-0.32
G3UXW9	*Gps1*	COP9 signalosome complex subunit 1	-0.32
Q6P1Y9	*Exoc1*	Exocyst complex component 1	-0.32
P08752	*Gnai2*	Guanine nucleotide-binding protein G(i) subunit alpha-2	-0.32
Q9CQZ1	*Hsbp1*	Heat shock factor-binding protein 1	-0.32
Q9D0B6	*Pbdc1*	Protein PBDC1	-0.32
P13439	*Umps*	Uridine 5'-monophosphate synthase	-0.32
Q00897	*Serpina1d*	Alpha-1-antitrypsin 1-4	-0.31
O55042	*Snca*	Alpha-synuclein	-0.31
P14824	*Anxa6*	Annexin A6	-0.31
Q68FF6	*Git1*	ARF GTPase-activating protein GIT1	-0.31
P28651	*Ca8*	Carbonic anhydrase-related protein	-0.31
P84086	*Cplx2*	Complexin-2	-0.31
P31938	*Map2k1*	Dual specificity mitogen-activated protein kinase kinase 1	-0.31
Q61035	*Hars*	Histidine--tRNA ligase, cytoplasmic	-0.31
Q9D967	*Mdp1*	Magnesium-dependent phosphatase 1	-0.31
Q80XU3	*Nucks1*	Nuclear ubiquitous casein and cyclin-dependent kinase substrate 1	-0.31
Q91XL9	*Osbpl1a*	Oxysterol-binding protein-related protein 1	-0.31
O55091	*Impact*	Protein IMPACT	-0.31
Q9DBB8	*Dhdh*	Trans-1,2-dihydrobenzene-1,2-diol dehydrogenase	-0.31
P12382	*Pfkl*	ATP-dependent 6-phosphofructokinase, liver type	-0.3

Table A3.4 (cont'd)

O88456	*Capns1*	Calpain small subunit 1	-0.3
Q8BZA9	*Tigar*	Fructose-2,6-bisphosphatase TIGAR	-0.3
P16045	*Lgals1*	Galectin-1	-0.3
Q9CQM9	*Glrx3*	Glutaredoxin-3	-0.3
P60335	*Pcbp1*	Poly(rC)-binding protein 1	-0.3
A2ADY9	*Ddi2*	Protein DDI1 homolog 2	-0.3
Q8BHZ0	*Fam49a*	Protein FAM49A	-0.3
P35282	*Rab21*	Ras-related protein Rab-21	-0.3
Q5SSM3	*Arhgap44*	Rho GTPase-activating protein 44	-0.3
F6Q8A4	*Rps6ka1*	Ribosomal protein S6 kinase alpha-1 (Fragment)	-0.3
P63328	*Ppp3ca*	Serine/threonine-protein phosphatase 2B catalytic subunit alpha isoform	-0.3
Q71LX4	*Tln2*	Talin-2	-0.3
F8WHQ1	*Tpd52*	Tumor protein D52	-0.3
Q9QXG4	*Acss2*	Acetyl-coenzyme A synthetase, cytoplasmic	-0.29
O54774	*Ap3d1*	AP-3 complex subunit delta-1	-0.29
O35864	*Cops5*	COP9 signalosome complex subunit 5	-0.29
O88712	*Ctbp1*	C-terminal-binding protein 1	-0.29
Q9D1P4	*Chordc1*	Cysteine and histidine-rich domain-containing protein 1	-0.29
Q9Z0Y1	*Dctn3*	Dynactin subunit 3	-0.29
Q8K1M6	*Dnm1l*	Dynamin-1-like protein	-0.29
O09172	*Gclm*	Glutamate--cysteine ligase regulatory subunit	-0.29
P47791	*Gsr*	Glutathione reductase, mitochondrial	-0.29
P60469	*Ppfia3*	Liprin-alpha-3	-0.29
D3Z656	*Synj1*	Synaptojanin-1	-0.29
P10711	*Tcea1*	Transcription elongation factor A protein 1	-0.29
Q99KC8	*Vwa5a*	von Willebrand factor A domain-containing protein 5A	-0.29
P54923	*Adprh*	[Protein ADP-ribosylarginine] hydrolase	-0.28
Q8VHQ9	*Acot11*	Acyl-coenzyme A thioesterase 11	-0.28
A2AFQ0	*Huwe1*	E3 ubiquitin-protein ligase HUWE1	-0.28
Q3TDK6	*Rogdi*	Isoform 2 of Protein rogdi homolog	-0.28
Q9WTU6	*Mapk9*	Mitogen-activated protein kinase 9	-0.28
P28665	*Mug1*	Murinoglobulin-1	-0.28

Table A3.4 (cont'd)

G3X8Y3	*Naa15*	N-alpha-acetyltransferase 15, NatA auxiliary subunit	-0.28
Q9EPN1	*Nbea*	Neurobeachin	-0.28
P61971	*Nutf2*	Nuclear transport factor 2	-0.28
Q8CGA0	*Ppm1f*	Protein phosphatase 1F	-0.28
Q9JLI6	*Scly*	Selenocysteine lyase	-0.28
B7ZC46	*Sept8*	Septin-8	-0.28
Q9Z1W9	*Stk39*	STE20/SPS1-related proline-alanine-rich protein kinase	-0.28
Q9Z1F9	*Uba2*	SUMO-activating enzyme subunit 2	-0.28
Q80YX1	*Tnc*	Tenascin	-0.28
E9QKC6	*Trim2*	Tripartite motif-containing protein 2	-0.28
Q8VCT3	*Rnpep*	Aminopeptidase B	-0.27
P63248	*Pkia*	cAMP-dependent protein kinase inhibitor alpha	-0.27
P63040	*Cplx1*	Complexin-1	-0.27
A2A432	*Cul4b*	Cullin-4B	-0.27
P11440	*Cdk1*	Cyclin-dependent kinase 1	-0.27
P39053	*Dnm1*	Dynamin-1	-0.27
Q8VE33	*Gdap1l1*	Ganglioside-induced differentiation-associated protein 1-like 1	-0.27
Q9R257	*Hebp1*	Heme-binding protein 1	-0.27
Q8CD76	*Klc1*	Kinesin light chain 1	-0.27
Q9CZ30	*Ola1*	Obg-like ATPase 1	-0.27
Q9R0Q7	*Ptges3*	Prostaglandin E synthase 3	-0.27
Q91V89	*Ppp2r5d*	Serine/threonine-protein phosphatase 2A 56 kDa regulatory subunit	-0.27
Q3V2H3	*Snx12*	Sorting nexin-12	-0.27
P63046	*Sult4a1*	Sulfotransferase 4A1	-0.27
P61087	*Ube2k*	Ubiquitin-conjugating enzyme E2 K	-0.27
Q6ZQ38	*Cand1*	Cullin-associated NEDD8-dissociated protein 1	-0.26
Q9EQF6	*Dpysl5*	Dihydropyrimidinase-related protein 5	-0.26
Q9JI46	*Nudt3*	Diphosphoinositol polyphosphate phosphohydrolase 1	-0.26
Q8BZ98	*Dnm3*	Dynamin-3	-0.26
Q6ZWX6	*Eif2s1*	Eukaryotic translation initiation factor 2 subunit 1	-0.26

Table A3.4 (cont'd)

Q80XI3	*Eif4g3*	Eukaryotic translation initiation factor 4 gamma 3	-0.26
Q61081	*Cdc37*	Hsp90 co-chaperone Cdc37	-0.26
P70168	*Kpnb1*	Importin subunit beta-1	-0.26
Q5SWU9	*Acaca*	Isoform 2 of Acetyl-CoA carboxylase 1	-0.26
Q8BFU3	*Rnf214*	Isoform 4 of RING finger protein 214	-0.26
P29595	*Nedd8*	NEDD8	-0.26
Q9D1X0	*Nol3*	Nucleolar protein 3	-0.26
Q61206	*Pafah1b2*	Platelet-activating factor acetylhydrolase IB subunit beta	-0.26
Q9QYX7	*Pclo*	Protein piccolo	-0.26
P62823	*Rab3c*	Ras-related protein Rab-3C	-0.26
Q60996	*Ppp2r5c*	Serine/threonine-protein phosphatase 2A 56 kDa regulatory subunit gamma isoform	-0.26
O54988	*Slk*	STE20-like serine/threonine-protein kinase	-0.26
Q9CRB6	*Tppp3*	Tubulin polymerization-promoting protein family member 3	-0.26
Q78JW9	*Ubfd1*	Ubiquitin domain-containing protein UBFD1	-0.26
Q7TQI3	*Otub1*	Ubiquitin thioesterase OTUB1	-0.26
Q9CQV8	*Ywhab*	14-3-3 protein beta/alpha	-0.25
P68510	*Ywhah*	14-3-3 protein eta	-0.25
P68254	*Ywhaq*	14-3-3 protein theta (Fragment)	-0.25
Q99JI4	*Psmd6*	26S proteasome non-ATPase regulatory subunit 6	-0.25
O35841	*Api5*	Apoptosis inhibitor 5	-0.25
Q62048	*Pea15*	Astrocytic phosphoprotein PEA-15	-0.25
Q01065	*Pde1b*	Calcium/calmodulin-dependent 3',5'-cyclic nucleotide phosphodiesterase 1B	-0.25
P67871	*Csnk2b*	Casein kinase II subunit beta	-0.25
P23198	*Cbx3*	Chromobox protein homolog 3	-0.25
O88544	*Cops4*	COP9 signalosome complex subunit 4	-0.25
Q8K3G9	*Appl2*	DCC-interacting protein 13-beta	-0.25
Q9D7X3	*Dusp3*	Dual-specificity protein phosphatase 3	-0.25
Q8VD62	*AI837181*	Expressed sequence AI837181	-0.25
Q9QUH0	*Glrx*	Glutaredoxin-1	-0.25
Q9DCZ1	*Gmpr*	GMP reductase 1	-0.25
P07901	*Hsp90aa1*	Heat shock protein HSP 90-alpha	-0.25

Table A3.4 (cont'd)

Q05BC3	*Eml1*	Isoform 3 of Echinoderm microtubule-associated protein-like 1	-0.25
Q8R001	*Mapre2*	Microtubule-associated protein RP/EB family member 2	-0.25
Q9D997	*Nagk*	N-acetyl-D-glucosamine kinase	-0.25
Q69ZK0	*Prex1*	Phosphatidylinositol 3,4,5-trisphosphate-dependent Rac exchanger 1 protein	-0.25
P27612	*Plaa*	Phospholipase A-2-activating protein	-0.25
Q8VE70	*Pdcd10*	Programmed cell death protein 10	-0.25
P12815	*Pdcd6*	Programmed cell death protein 6	-0.25
P63011	*Rab3a*	Ras-related protein Rab-3A	-0.25
P35279	*Rab6a*	Ras-related protein Rab-6A	-0.25
E9PYT0	*Arhgap5*	Rho GTPase-activating protein 5	-0.25
Q9JLN9	*Mtor*	Serine/threonine-protein kinase mTOR	-0.25
Q8CIN4	*Pak2*	Serine/threonine-protein kinase PAK 2	-0.25
Q80TB8	*Vat1l*	Synaptic vesicle membrane protein VAT-1 homolog-like	-0.25
Q8C1A5	*Thop1*	Thimet oligopeptidase	-0.25
Q9JKB1	*Uchl3*	Ubiquitin carboxyl-terminal hydrolase isozyme L3	-0.25
P68037	*Ube2l3*	Ubiquitin-conjugating enzyme E2 L3	-0.25
Q8C7R4	*Uba6*	Ubiquitin-like modifier-activating enzyme 6	-0.25
Q9WTL7	*Lypla2*	Acyl-protein thioesterase 2	-0.24
P61750	*Arf4*	ADP-ribosylation factor 4	-0.24
Q9WTQ5	*Akap12*	A-kinase anchor protein 12	-0.24
O08739	*Ampd3*	AMP deaminase	-0.24
Q7TQF7	*Amph*	Amphiphysin	-0.24
Q07076	*Anxa7*	Annexin	-0.24
P35585	*Ap1m1*	AP-1 complex subunit mu-1	-0.24
Q91ZZ3	*Sncb*	Beta-synuclein	-0.24
Q8R016	*Blmh*	Bleomycin hydrolase	-0.24
Q63810	*Ppp3r1*	Calcineurin subunit B type 1	-0.24
Q9DB16	*Cab39l*	Calcium-binding protein 39-like	-0.24
Q9D4H8	*Cul2*	Cullin-2	-0.24
O08788	*Dctn1*	Dynactin subunit 1	-0.24
Q9QXY6	*Ehd3*	EH domain-containing protein 3	-0.24
Q7TPM6	*Fsd1*	Fibronectin type III and SPRY domain-containing protein 1	-0.24

Table A3.4 (cont'd)

Q99JP6	*Homer3*	Isoform 2 of Homer protein homolog 3	-0.24
P32921-2	*Wars*	Isoform 2 of Tryptophan--tRNA ligase, cytoplasmic	-0.24
Q99LB6	*Mat2b*	Methionine adenosyltransferase 2 subunit beta	-0.24
O08539	*Bin1*	Myc box-dependent-interacting protein 1	-0.24
Q4VAA2	*Cdv3*	Protein CDV3	-0.24
P52480	*Pkm*	Pyruvate kinase PKM	-0.24
Q9CQK7	*Rwdd1*	RWD domain-containing protein 1	-0.24
Q9CWK8	*Snx2*	Sorting nexin-2	-0.24
Q9CQW1	*Ykt6*	Synaptobrevin homolog YKT6	-0.24
Q61187	*Tsg101*	Tumor susceptibility gene 101 protein	-0.24
Q8VE47	*Uba5*	Ubiquitin-like modifier-activating enzyme 5	-0.24
Q8CCB4	*Vps53*	Vacuolar protein sorting-associated protein 53 homolog	-0.24
Q9CVB6	*Arpc2*	Actin-related protein 2/3 complex subunit 2	-0.23
Q64010	*Crk*	Adapter molecule crk	-0.23
Q9Z2A5	*Ate1*	Arginyl-tRNA--protein transferase 1	-0.23
Q80YN3	*Bcas1*	Breast carcinoma-amplified sequence 1 homolog	-0.23
Q91YS8	*Camk1*	Calcium/calmodulin-dependent protein kinase type 1	-0.23
Q06138	*Cab39*	Calcium-binding protein 39	-0.23
Q61548	*Snap91*	Clathrin coat assembly protein AP180	-0.23
G3X914	*Cul5*	Cullin-5	-0.23
Q9DBE0	*Csad*	Cysteine sulfinic acid decarboxylase	-0.23
P48024	*Eif1*	Eukaryotic translation initiation factor 1	-0.23
Q9Z0N1	*Eif2s3x*	Eukaryotic translation initiation factor 2 subunit 3, X-linked	-0.23
P06745	*Gpi*	Glucose-6-phosphate isomerase	-0.23
Q5PR73	*Diras2*	GTP-binding protein Di-Ras2	-0.23
P11499	*Hsp90ab1*	Heat shock protein HSP 90-beta	-0.23
P68181	*Prkacb*	Isoform 4 of cAMP-dependent protein kinase catalytic subunit beta	-0.23
P39053	*Dnm1*	Isoform 4 of Dynamin-1	-0.23
P52480	*Pkm*	Isoform M1 of Pyruvate kinase PKM	-0.23
O35226	*Psmd4*	Isoform Rpn10B of 26S proteasome non-ATPase regulatory subunit 4	-0.23
Q63844	*Mapk3*	Mitogen-activated protein kinase 3	-0.23

Table A3.4 (cont'd)

Q4KMM3	*Oxr1*	Oxidation resistance protein 1	-0.23
Q8K0S0	*Phyhip*	Phytanoyl-CoA hydroxylase-interacting protein	-0.23
Q9WU78	*Pdcd6ip*	Programmed cell death 6-interacting protein	-0.23
Q91VC7	*Ppp1r14a*	Protein phosphatase 1 regulatory subunit 14A	-0.23
Q9CX34	*Sugt1*	Protein SGT1 homolog	-0.23
Q9Z2Q6	*Sept5*	Septin-5	-0.23
F8VPQ4	*Srgap3*	SLIT-ROB Rho GTPase-activating protein 3	-0.23
Q8BJU0	*Sgta*	Small glutamine-rich tetratricopeptide repeat-containing protein alpha	-0.23
Q9Z172	*Sumo3*	Small ubiquitin-related modifier 3	-0.23
Q91VZ6	*Smap1*	Stromal membrane-associated protein 1	-0.23
P54797	*Tango2*	Transport and Golgi organization 2 homolog	-0.23
P17751	*Tpi1*	Triosephosphate isomerase	-0.23
Q8R5H1	*Usp15*	Ubiquitin carboxyl-terminal hydrolase 15	-0.23
O08759	*Ube3a*	Ubiquitin-protein ligase E3A	-0.23
P62259	*Ywhae*	14-3-3 protein epsilon	-0.22
P59999	*Arpc4*	Actin-related protein 2/3 complex subunit 4	-0.22
O70318	*Epb41l2*	Band 4.1-like protein 2	-0.22
E9PZD8	*Cp*	Ceruloplasmin	-0.22
P61202	*Cops2*	COP9 signalosome complex subunit 2	-0.22
Q9Z140	*Cpne6*	Copine-6	-0.22
Q9WTX6	*Cul1*	Cullin-1	-0.22
Q9QZ73	*Dcun1d1*	DCN1-like protein 1	-0.22
Q5EBJ4	*Ermn*	Ermin	-0.22
P51880	*Fabp7*	Fatty acid-binding protein, brain	-0.22
Q9CR41	*Hypk*	Huntingtin-interacting protein K	-0.22
O35343	*Kpna4*	Importin subunit alpha-3	-0.22
Q9EPL8	*Ipo7*	Importin-7	-0.22
Q9CZ04	*Cops7a*	Isoform 2 of COP9 signalosome complex subunit 7a	-0.22
Q8C078	*Camkk2*	Isoform 5 of Calcium/calmodulin-dependent protein kinase kinase 2	-0.22
P28738	*Kif5c*	Kinesin heavy chain isoform 5C	-0.22
P70202	*Lxn*	Latexin	-0.22
Q9ESJ4	*Nckipsd*	NCK-interacting protein with SH3 domain	-0.22

Table A3.4 (cont'd)

Q8BHW2	*Oscp1*	Organic solute carrier protein 1 isoform	-0.22
P53810	*Pitpna*	Phosphatidylinositol transfer protein alpha isoform	-0.22
Q9JJV2	*Pfn2*	Profilin-2	-0.22
P49722	*Psma2*	Proteasome subunit alpha type-2	-0.22
Q61239	*Fnta*	Protein farnesyltransferase/geranylgeranyltransferase type-1 subunit alpha	-0.22
Q9D394	*Rufy3*	Protein RUFY3	-0.22
E0CYV0	*Pcmt1*	Protein-L-isoaspartate O-methyltransferase	-0.22
Q91XF0	*Pnpo*	Pyridoxine-5'-phosphate oxidase	-0.22
Q9CT10	*Ranbp3*	Ran-binding protein 3	-0.22
O70338	*Rnh1*	Ribonuclease inhibitor	-0.22
P62141	*Ppp1cb*	Serine/threonine-protein phosphatase PP1-beta catalytic subunit	-0.22
O55060	*Tpmt*	Thiopurine S-methyltransferase	-0.22
Q9QZ06	*Tollip*	Toll-interacting protein	-0.22
P61961	*Ufm1*	Ubiquitin-fold modifier 1	-0.22
Q6P5E4	*Uggt1*	UDP-glucose:glycoprotein glucosyltransferase 1	-0.22
P97765	*Wbp2*	WW domain-binding protein 2	-0.22
P61982	*Ywhag*	14-3-3 protein gamma	-0.21
P63101	*Ywhaz*	14-3-3 protein zeta/delta	-0.21
Q8CBB7	*Ap1g1*	AP-1 complex subunit gamma	-0.21
E9PY16	*Adap1*	ArfGAP with dual PH domains 1	-0.21
Q61024	*Asns*	Asparagine synthetase [glutamine-hydrolyzing]	-0.21
Q04447	*Ckb*	Creatine kinase B-type	-0.21
Q8VDK1	*Nit1*	Deaminated glutathione amidase	-0.21
O08553	*Dpysl2*	Dihydropyrimidinase-related protein 2	-0.21
Q9WVK4	*Ehd1*	EH domain-containing protein 1	-0.21
P03995	*Gfap*	Glial fibrillary acidic protein	-0.21
Q9R111	*Gda*	Guanine deaminase	-0.21
Q3UMA3	*Hgs*	Hepatocyte growth factor-regulated tyrosine kinase substrate	-0.21
Q8VIM9	*Irgq*	Immunity-related GTPase family Q protein	-0.21
Q91V64	*Isoc1*	Isochorismatase domain-containing protein 1	-0.21

Table A3.4 (cont'd)

P63087	*Ppp1cc*	Isoform 2 of Serine/threonine-protein phosphatase PP1-gamma catalytic subunit	-0.21
P10637	*Mapt*	Isoform Tau-A of Microtubule-associated protein tau	-0.21
Q7M6Y3	*Picalm*	Phosphatidylinositol-binding clathrin assembly protein	-0.21
Q61990	*Pcbp2*	Poly(rC)-binding protein 2	-0.21
P57722	*Pcbp3*	Poly(rC)-binding protein 3	-0.21
P47199	*Cryz*	Quinone oxidoreductase	-0.21
Q61598	*Gdi2*	Rab GDP dissociation inhibitor beta	-0.21
A2ALS4	*Rap1gap*	Rap1 GTPase-activating protein 1	-0.21
P61021	*Rab5b*	Ras-related protein Rab-5B	-0.21
P35278	*Rab5c*	Ras-related protein Rab-5C	-0.21
Q76MZ3	*Ppp2r1a*	Serine/threonine-protein phosphatase 2A 65 kDa regulatory subunit A alpha isoform	-0.21
Q78YZ6	*Scoc*	Short coiled-coil protein	-0.21
P70297	*Stam*	Signal transducing adapter molecule 1	-0.21
Q9Z1N5	*Ddx39b*	Spliceosome RNA helicase Ddx39b	-0.21
Q9JMH6	*Txnrd1*	Thioredoxin reductase 1, cytoplasmic	-0.21
Q9JMA1	*Usp14*	Ubiquitin carboxyl-terminal hydrolase 14	-0.21
Q9R0Q6	*Arpc1a*	Actin-related protein 2/3 complex subunit 1A	-0.2
P40124	*Cap1*	Adenylyl cyclase-associated protein 1	-0.2
Q9CYT6	*Cap2*	Adenylyl cyclase-associated protein 2	-0.2
P61164	*Actr1a*	Alpha-centractin	-0.2
O88533	*Ddc*	Aromatic-L-amino-acid decarboxylase	-0.2
Q8BWG8	*Arrb1*	Beta-arrestin-1	-0.2
O88587	*Comt*	Catechol O-methyltransferase	-0.2
P18760	*Cfl1*	Cofilin-1	-0.2
Q68ED7	*Crtc1*	CREB-regulated transcription coactivator 1	-0.2
P47941	*Crkl*	Crk-like protein	-0.2
Q9CX80	*Cygb*	Cytoglobin	-0.2
P97427	*Crmp1*	Dihydropyrimidinase-related protein 1	-0.2
Q99KJ8	*Dctn2*	Dynactin subunit 2	-0.2
Q66JS6	*Eif3j2*	Eukaryotic translation initiation factor 3 subunit J-B	-0.2
P09528	*Fth1*	Ferritin heavy chain	-0.2

A2AEY2	*Fhl1*	Four and a half LIM domains 1, isoform CRA_c	-0.2
Q9Z0F7	*Sncg*	Gamma-synuclein	-0.2
Q61768	*Kif5b*	Kinesin-1 heavy chain	-0.2
P10637	*Mapt*	Microtubule-associated protein	-0.2
P62774	*Mtpn*	Myotrophin	-0.2
O35685	*Nudc*	Nuclear migration protein nudC	-0.2
Q61838	*Pzp*	Pregnancy zone protein	-0.2
P63318	*Prkcg*	Protein kinase C gamma type	-0.2
P61027	*Rab10*	Ras-related protein Rab-10	-0.2
Q99J08	*Sec14l2*	SEC14-like protein 2	-0.2
G3X972	*Sec24c*	SEC24 related gene family, member C (S. cerevisiae), isoform CRA_a	-0.2
Q6P1F6	*Ppp2r2a*	Serine/threonine-protein phosphatase 2A 55 kDa regulatory subunit B alpha isoform	-0.2
Q6NZD2	*Snx1*	Sorting nexin 1	-0.2
P08228	*Sod1*	Superoxide dismutase [Cu-Zn]	-0.2
Q91ZJ5	*Ugp2*	UTP--glucose-1-phosphate uridylyltransferase	-0.2
P62301	*Rps13*	40S ribosomal protein S13	0.2
Q3UHB1	*Nt5dc3*	5'-nucleotidase domain-containing protein 3	0.2
Q922B2	*Dars*	Aspartate--tRNA ligase, cytoplasmic	0.2
E9Q557	*Dsp*	Desmoplakin	0.2
Q8BPU7	*Elmo1*	Engulfment and cell motility protein 1	0.2
P23116	*Eif3a*	Eukaryotic translation initiation factor 3 subunit A	0.2
D3Z5G7	*Ces1b*	Carboxylic ester hydrolase	0.21
Q6A065	*Cep170*	Centrosomal protein of 170 kDa	0.21
Q91W50	*Csde1*	Cold shock domain-containing protein E1	0.21
Q9DCW4	*Etfb*	Electron transfer flavoprotein subunit beta	0.21
Q8BTM8	*Flna*	Filamin-A	0.21
Q9CQN1	*Trap1*	Heat shock protein 75 kDa, mitochondrial	0.21
P14602	*Hspb1*	Heat shock protein beta-1	0.21
Q7TMK9	*Syncrip*	Heterogeneous nuclear ribonucleoprotein Q	0.21
P09405	*Ncl*	Nucleolin	0.21
Q8BH04	*Pck2*	Phosphoenolpyruvate carboxykinase [GTP], mitochondrial	0.21
Q62277	*Syp*	Synaptophysin	0.21

Table A3.4 (cont'd)

Q9ER00	*Stx12*	Syntaxin-12	0.21
P63044	*Vamp2*	Vesicle-associated membrane protein 2	0.21
P63082	*Atp6v0c*	V-type proton ATPase 16 kDa proteolipid subunit	0.21
Q9D8B3	*Chmp4b*	Charged multivesicular body protein 4b	0.22
P62897	*Cycs*	Cytochrome c, somatic	0.22
P10854	*Hist1h2bm*	Histone H2B type 1-M	0.22
Q8CGK3	*Lonp1*	Lon protease homolog, mitochondrial	0.22
Q7TSJ2	*Map6*	Microtubule-associated protein 6	0.22
G3X8R0	*Reep5*	Receptor expression-enhancing protein	0.22
Q8BH80	*Vapb*	Vesicle-associated membrane protein, associated protein B and C	0.22
Q9Z1G4	*Atp6v0a1*	V-type proton ATPase subunit a	0.22
P51863	*Atp6v0d1*	V-type proton ATPase subunit d 1	0.22
Q9DCT1	*Akr1e2*	1,5-anhydro-D-fructose reductase	0.23
P62267	*Rps23*	40S ribosomal protein S23	0.23
Q80X90	*Flnb*	Filamin-B	0.23
Q6GSS7	*Hist2h2aa1*	Histone H2A type 2-A	0.23
A2AG50	*Map7d2*	MAP7 domain-containing protein 2	0.23
Q8VDD5	*Myh9*	Myosin-9	0.23
Q99NF7	*Ppm1b*	Ppm1b protein	0.23
P70663	*Sparcl1*	SPARC-like protein 1	0.23
P37804	*Tagln*	Transgelin	0.23
O35350	*Capn1*	Calpain-1 catalytic subunit	0.24
P23953	*Ces1c*	Carboxylesterase 1C	0.24
Q9CQB4	*Uqcrb*	Cytochrome b-c1 complex subunit 7	0.24
Q9CQJ6	*Denr*	Density-regulated protein	0.24
Q9QX60	*Dguok*	Deoxyguanosine kinase, mitochondrial	0.24
Q60973	*Rbbp7*	Histone-binding protein RBBP7	0.24
Q61545	*Ewsr1*	RNA-binding protein EWS	0.24
Q62261	*Sptbn1*	Spectrin beta chain, non-erythrocytic 1	0.24
Q9JIS5	*Sv2a*	Synaptic vesicle glycoprotein 2A	0.24
P14148	*Rpl7*	60S ribosomal protein L7	0.25
P12960	*Cntn1*	Contactin-1	0.25
Q9WUM4	*Coro1c*	Coronin-1C	0.25

Table A3.4 (cont'd)

Q8BGN3	*Enpp6*	Ectonucleotide pyrophosphatase/phosphodiesterase family member 6	0.25
Q9D6S7	*Mrrf*	Ribosome-recycling factor, mitochondrial	0.25
P62320	*Snrpd3*	Small nuclear ribonucleoprotein Sm D3	0.25
Q9Z2I8	*Suclg2*	Succinate--CoA ligase [GDP-forming] subunit beta, mitochondrial	0.25
Q62318	*Trim28*	Transcription intermediary factor 1-beta	0.25
Q8VEK3	*Hnrnpu*	Heterogeneous nuclear ribonucleoprotein U	0.26
Q9JLZ3	*Auh*	Methylglutaconyl-CoA hydratase, mitochondrial	0.26
P07724	*Alb*	Serum albumin	0.26
Q8BYI9	*Tnr*	Tenascin-R	0.26
P42669	*Pura*	Transcriptional activator protein Pur-alpha	0.26
Q62442	*Vamp1*	Vesicle-associated membrane protein 1	0.26
P62754	*Rps6*	40S ribosomal protein S6	0.27
Q61247	*Serpinf2*	Alpha-2-antiplasmin	0.27
Q6PHZ2	*Camk2d*	Calcium/calmodulin-dependent protein kinase type II subunit delta	0.27
O08677	*Kng1*	Kininogen-1	0.27
Q9D5V6	*Syap1*	Synapse-associated protein 1	0.27
O55100	*Syngr1*	Synaptogyrin-1	0.27
O35295	*Purb*	Transcriptional activator protein Pur-beta	0.27
Q6IRU2	*Tpm4*	Tropomyosin alpha-4 chain	0.27
Q9WV55	*Vapa*	Vesicle-associated membrane protein-associated protein A	0.27
Q9QZE5	*Copg1*	Coatomer subunit gamma-1	0.28
P63037	*Dnaja1*	DnaJ homolog subfamily A member 1	0.28
P54071	*Idh2*	Isocitrate dehydrogenase [NADP], mitochondrial	0.28
Q91UZ1	*Plcb4*	Phosphoinositide phospholipase C	0.28
P60122	*Ruvbl1*	RuvB-like 1	0.28
Q8K021	*Scamp1*	Secretory carrier-associated membrane protein 1	0.28
Q9CZX8	*Rps19*	40S ribosomal protein S19	0.29
P62900	*Rpl31*	60S ribosomal protein L31	0.29
Q8JZN5	*Acad9*	Acyl-CoA dehydrogenase family member 9, mitochondrial	0.29
Q3U0V1	*Khsrp*	Far upstream element-binding protein 2	0.29

Table A3.4 (cont'd)

Q60668	*Hnrnpd*	Heterogeneous nuclear ribonucleoprotein D0	0.29
Q9D1I5	*Mcee*	Methylmalonyl-CoA epimerase, mitochondrial	0.29
Q8R326	*Pspc1*	Paraspeckle component 1	0.29
Q99KP6	*Prpf19*	Pre-mRNA-processing factor 19	0.29
P62835	*Rap1a*	Ras-related protein Rap-1A	0.29
Q68FG2	*Sptbn2*	Spectrin beta chain	0.29
Q8K4Z5	*Sf3a1*	Splicing factor 3A subunit 1	0.29
P52196	*Tst*	Thiosulfate sulfurtransferase	0.29
Q8R0F8	*Fahd1*	Acylpyruvase FAHD1, mitochondrial	0.3
P56135	*Atp5j2*	ATP synthase subunit f, mitochondrial	0.3
Q9DCH4	*Eif3f*	Eukaryotic translation initiation factor 3 subunit F	0.3
Q8C2Q7	*Hnrnph1*	Heterogeneous nuclear ribonucleoprotein H	0.3
Q8VDM6	*Hnrnpul1*	Heterogeneous nuclear ribonucleoprotein U-like protein 1	0.3
Q9DCM0	*Ethe1*	Persulfide dioxygenase ETHE1, mitochondrial	0.3
O35286	*Dhx15*	Pre-mRNA-splicing factor ATP-dependent RNA helicase DHX15	0.3
Q8BWT1	*Acaa2*	3-ketoacyl-CoA thiolase, mitochondrial	0.31
P62918	*Rpl8*	60S ribosomal protein L8	0.31
Q9QYR9	*Acot2*	Acyl-coenzyme A thioesterase 2, mitochondrial	0.31
Q9WTP6	*Ak2*	Adenylate kinase 2, mitochondrial	0.31
Q60902	*Eps15l1*	Epidermal growth factor receptor substrate 15-like 1	0.31
C0HKE4	*Hist1h2ae*	Histone H2A type 1-E	0.31
G3XA53	*Omg*	Oligodendrocyte-myelin glycoprotein	0.31
Q62059	*Vcan*	Versican core protein	0.31
Q6ZWN5	*Rps9*	40S ribosomal protein S9	0.32
Q3TC72	*Fahd2a*	Fumarylacetoacetate hydrolase domain-containing 2A	0.32
P13020	*Gsn*	Isoform 2 of Gelsolin	0.32
P51174	*Acadl*	Long-chain specific acyl-CoA dehydrogenase, mitochondrial	0.32
Q91YJ3	*Thyn1*	Thymocyte nuclear protein 1	0.32
P63325	*Rps10*	40S ribosomal protein S10	0.33
P62717	*Rpl18a*	60S ribosomal protein L18a (Fragment)	0.33
P47911	*Rpl6*	60S ribosomal protein L6	0.33

Table A3.4 (cont'd)

P29758	*Oat*	Ornithine aminotransferase, mitochondrial	0.33
P97379	*G3bp2*	Ras GTPase-activating protein-binding protein 2	0.33
A3KGU9	*Sptan1*	Spectrin alpha chain, non-erythrocytic 1	0.33
P60879	*Snap25*	Synaptosomal-associated protein 25	0.33
P53026	*Rpl10a*	60S ribosomal protein L10a	0.34
P61924	*Copz1*	Coatomer subunit zeta-1	0.34
P10518	*Alad*	Delta-aminolevulinic acid dehydratase	0.34
P04370	*Mbp*	Myelin basic protein (Fragment)	0.34
Q61937	*Npm1*	Nucleophosmin	0.34
Q9QXT0	*Cnpy2*	Protein canopy homolog 2	0.34
P07309	*Ttr*	Transthyretin	0.34
Q6ZWZ7	*Rpl17*	60S ribosomal protein L17	0.35
O35943	*Fxn*	Frataxin, mitochondrial	0.35
P61979	*Hnrnpk*	Isoform 2 of Heterogeneous nuclear ribonucleoprotein K	0.35
P08249	*Mdh2*	Malate dehydrogenase, mitochondrial	0.35
P60202	*Plp1*	Myelin proteolipid protein	0.35
P24369	*Ppib*	Peptidyl-prolyl cis-trans isomerase B	0.35
Q8R164	*Bphl*	Valacyclovir hydrolase	0.35
P50544	*Acadvl*	Very long-chain specific acyl-CoA dehydrogenase, mitochondrial	0.35
P62245	*Rps15a*	40S ribosomal protein S15a	0.36
P61922	*Abat*	4-aminobutyrate aminotransferase, mitochondrial	0.36
P62751	*Rpl23a*	60S ribosomal protein L23a	0.36
P14115	*Rpl27a*	60S ribosomal protein L27a	0.36
Q9D172	*D10Jhu81e*	ES1 protein homolog, mitochondrial	0.36
P62317	*Snrpd2*	Small nuclear ribonucleoprotein Sm D2	0.36
Q921F2	*Tardbp*	TAR DNA-binding protein 43	0.36
Q8QZS1	*Hibch*	3-hydroxyisobutyryl-CoA hydrolase, mitochondrial	0.37
P25444	*Rps2*	40S ribosomal protein S2	0.37
P16332	*Mut*	Methylmalonyl-CoA mutase, mitochondrial	0.37
P46097	*Syt2*	Synaptotagmin II	0.37
Q7TMG8	*Nipsnap2*	Glioblastoma amplified sequence	0.38
Q9EQ20	*Aldh6a1*	Methylmalonate-semialdehyde dehydrogenase [acylating], mitochondrial	0.38
Q8C5H8	*Nadk2*	NAD kinase 2, mitochondrial	0.38

Table A3.4 (cont'd)

Q9EP69	*Sacm1l*	Phosphatidylinositide phosphatase SAC1	0.38
P63321	*Rala*	Ras-related protein Ral-A	0.38
Q8VCW8	*Acsf2*	Acyl-CoA synthetase family member 2, mitochondrial	0.39
Q9CQR4	*Acot13*	Acyl-coenzyme A thioesterase 13	0.39
P06728	*Apoa4*	Apolipoprotein A-IV	0.39
P70333	*Hnrnph2*	Heterogeneous nuclear ribonucleoprotein H2	0.39
P45952	*Acadm*	Medium-chain specific acyl-CoA dehydrogenase, mitochondrial	0.39
P63323	*Rps12*	40S ribosomal protein S12	0.4
P63276	*Rps17*	40S ribosomal protein S17	0.4
P35980	*Rpl18*	60S ribosomal protein L18	0.4
Q8BP67	*Rpl24*	60S ribosomal protein L24	0.4
Q9CZU6	*Cs*	Citrate synthase, mitochondrial	0.4
Q3UGB5	*Dazap1*	DAZ associated protein 1, isoform CRA_b	0.4
P42125	*Eci1*	Enoyl-CoA delta isomerase 1, mitochondrial	0.4
P97807	*Fh*	Fumarate hydratase, mitochondrial	0.4
Q99LP6	*Grpel1*	GrpE protein homolog 1, mitochondrial	0.4
Q71RI9	*Kyat3*	Kynurenine--oxoglutarate transaminase 3	0.4
Q8BMF3	*Me3*	NADP-dependent malic enzyme, mitochondrial	0.4
P32848	*Pvalb*	Parvalbumin alpha	0.4
Q5XG69	*Fam169a*	Soluble lamin-associated protein of 75 kDa	0.4
Q78PY7	*Snd1*	Staphylococcal nuclease domain-containing protein 1	0.4
O89023	*Tpp1*	Tripeptidyl-peptidase 1	0.4
P62281	*Rps11*	40S ribosomal protein S11	0.41
P62852	*Rps25*	40S ribosomal protein S25	0.41
Q91Z31	*Ptbp2*	Isoform 2 of Polypyrimidine tract-binding protein 2	0.41
Q8BWF0	*Aldh5a1*	Succinate-semialdehyde dehydrogenase, mitochondrial	0.41
P62908	*Rps3*	40S ribosomal protein S3	0.42
P99027	*Rplp2*	60S acidic ribosomal protein P2	0.42
P57780	*Actn4*	Alpha-actinin-4	0.42
P85094	*Isoc2a*	Isochorismatase domain-containing protein 2A	0.42
Q60605	*Myl6*	Myosin light polypeptide 6	0.42
Q9DCC4	*Pycr3*	Pyrroline-5-carboxylate reductase 3	0.42

Table A3.4 (cont'd)

P68040	*Rack1*	Receptor of activated protein C kinase 1	0.42
Q8BG13	*Rbm3*	RNA-binding protein 3	0.42
Q99L13	*Hibadh*	3-hydroxyisobutyrate dehydrogenase, mitochondrial	0.43
P97461	*Rps5*	40S ribosomal protein S5	0.43
Q9D8E6	*Rpl4*	60S ribosomal protein L4	0.43
Q8K310	*Matr3*	Matrin-3	0.43
Q3UEB3	*Puf60*	Poly(U)-binding-splicing factor PUF60	0.43
O08756	*Hsd17b10*	3-hydroxyacyl-CoA dehydrogenase type-2	0.44
P62264	*Rps14*	40S ribosomal protein S14	0.44
P47738	*Aldh2*	Aldehyde dehydrogenase, mitochondrial	0.44
Q8BH95	*Echs1*	Enoyl-CoA hydratase, mitochondrial	0.44
Q61425	*Hadh*	Hydroxyacyl-coenzyme A dehydrogenase, mitochondrial	0.44
P13595	*Ncam1*	Neural cell adhesion molecule 1 (Fragment)	0.44
Q99JF8	*Psip1*	PC4 and SFRS1-interacting protein	0.44
O55125	*Nipsnap1*	Protein NipSnap homolog 1	0.44
O35633	*Slc32a1*	Vesicular inhibitory amino acid transporter	0.44
Q9JK42	*Pdk2*	[Pyruvate dehydrogenase (acetyl-transferring)] kinase isozyme 2, mitochondrial	0.45
Q99KI0	*Aco2*	Aconitate hydratase, mitochondrial	0.45
Q8R4N0	*Clybl*	Citramalyl-CoA lyase, mitochondrial	0.45
P43277	*Hist1h1d*	Histone H1.3	0.45
Q6PB66	*Lrpprc*	Leucine-rich PPR motif-containing protein, mitochondrial	0.45
P62849	*Rps24*	40S ribosomal protein S24	0.46
P62082	*Rps7*	40S ribosomal protein S7	0.46
P14206	*Rpsa*	40S ribosomal protein SA	0.46
Q9D0S9	*Hint2*	Histidine triad nucleotide-binding protein 2, mitochondrial	0.46
O08583	*Alyref*	THO complex subunit 4	0.46
Q8CCJ4	*Amer2*	APC membrane recruitment protein 2	0.47
Q80WM4	*Hapln4*	Hyaluronan and proteoglycan link protein 4	0.47
P45878	*Fkbp2*	Peptidyl-prolyl cis-trans isomerase FKBP2	0.47
Q62093	*Srsf2*	Serine/arginine-rich splicing factor 2	0.47
Q8K2C9	*Hacd3*	Very-long-chain (3R)-3-hydroxyacyl-CoA dehydratase 3	0.47
P63038	*Hspd1*	60 kDa heat shock protein, mitochondrial	0.48

Table A3.4 (cont'd)

P09103	*P4hb*	Protein disulfide-isomerase	0.48
Q9D0K2	*Oxct1*	Succinyl-CoA:3-ketoacid coenzyme A transferase 1, mitochondrial	0.48
P05202	*Got2*	Aspartate aminotransferase, mitochondrial	0.49
Q8C522	*Endod1*	Endonuclease domain-containing 1 protein	0.49
P57759	*Erp29*	Endoplasmic reticulum resident protein 29	0.49
P27773	*Pdia3*	Protein disulfide-isomerase A3	0.49
Q9JKD3	*Scamp5*	Secretory carrier-associated membrane protein 5	0.49
P09671	*Sod2*	Superoxide dismutase [Mn], mitochondrial	0.49
Q64433	*Hspe1*	10 kDa heat shock protein, mitochondrial	0.5
P14211	*Calr*	Calreticulin	0.5
Q91ZA3	*Pcca*	Propionyl-CoA carboxylase alpha chain, mitochondrial	0.5
Q9Z2I9	*Sucla2*	Succinate--CoA ligase [ADP-forming] subunit beta, mitochondrial	0.5
Q8VDJ3	*Hdlbp*	Vigilin	0.5
P61255	*Rpl26*	60S ribosomal protein L26	0.51
Q60865	*Caprin1*	Caprin-1	0.51
P26443	*Glud1*	Glutamate dehydrogenase 1, mitochondrial	0.51
Q5EBP8	*Hnrnpa1*	Heterogeneous nuclear ribonucleoprotein A1	0.51
Q91VA7	*Idh3b*	Isocitrate dehydrogenase [NAD] subunit, mitochondrial	0.51
P62075	*Timm13*	Mitochondrial import inner membrane translocase subunit Tim13	0.51
Q922R8	*Pdia6*	Protein disulfide-isomerase A6	0.51
P14231	*Atp1b2*	Sodium/potassium-transporting ATPase subunit beta-2	0.51
D3Z0Y2	*Prdx6*	Peroxiredoxin-6	0.52
P08003	*Pdia4*	Protein disulfide-isomerase A4	0.52
Q3UNZ8	*Cryzl2*	Quinone oxidoreductase-like protein 2	0.53
Q8VDN2	*Atp1a1*	Sodium/potassium-transporting ATPase subunit alpha-1	0.53
Q8VIJ6	*Sfpq*	Splicing factor, proline- and glutamine-rich	0.53
Q9JKK7	*Tmod2*	Tropomodulin-2	0.53
P08113	*Hsp90b1*	Endoplasmin	0.54
P11881	*Itpr1*	Inositol 1,4,5-trisphosphate receptor type 1	0.54
Q99MR8	*Mccc1*	Methylcrotonoyl-CoA carboxylase subunit alpha, mitochondrial	0.54
Q91V14	*Slc12a5*	Solute carrier family 12 member 5	0.54

Table A3.4 (cont'd)

P62702	*Rps4x*	40S ribosomal protein S4, X isoform	0.55
E9Q8N8	*Slc4a4*	Anion exchange protein	0.55
Q62167	*Ddx3x*	ATP-dependent RNA helicase DDX3X	0.55
Q9D6R2	*Idh3a*	Isocitrate dehydrogenase [NAD] subunit, mitochondrial	0.55
Q99KE1	*Me2*	NAD-dependent malic enzyme, mitochondrial	0.55
Q9WUM5	*Suclg1*	Succinate--CoA ligase [ADP/GDP-forming] subunit alpha, mitochondrial	0.55
Q8VBT9	*Aspscr1*	Tether containing UBX domain for GLUT4	0.55
P60867	*Rps20*	40S ribosomal protein S20	0.56
D3YZP9	*Ccdc6*	Coiled-coil domain-containing protein 6	0.56
P70404	*Idh3g*	Isocitrate dehydrogenase [NAD] subunit gamma 1, mitochondrial	0.56
O55022	*Pgrmc1*	Membrane-associated progesterone receptor component 1	0.56
Q8VHC3	*Selenom*	Selenoprotein M	0.56
P38647	*Hspa9*	Stress-70 protein, mitochondrial	0.56
Q91W90	*Txndc5*	Thioredoxin domain-containing protein 5	0.57
P62242	*Rps8*	40S ribosomal protein S8	0.58
P35564	*Canx*	Calnexin	0.59
Q8QZT1	*Acat1*	Acetyl-CoA acetyltransferase, mitochondrial	0.6
P56564	*Slc1a3*	Excitatory amino acid transporter 1	0.6
Q9CXY6	*Ilf2*	Interleukin enhancer-binding factor 2	0.6
Q8BHN3	*Ganab*	Isoform 2 of Neutral alpha-glucosidase AB	0.6
Q5SVJ0	*Camk2b*	Calcium/calmodulin-dependent protein kinase II, beta, isoform CRA_b	0.61
Q8BIJ6	*Iars2*	Isoleucine--tRNA ligase, mitochondrial	0.61
P62855	*Rps26*	40S ribosomal protein S26	0.62
Q8R5L1	*C1qbp*	Complement component 1 Q subcomponent-binding protein, mitochondrial	0.62
Q91WC3	*Acsl6*	Isoform 2 of Long-chain-fatty-acid--CoA ligase 6	0.62
Q8K1Z0	*Coq9*	Ubiquinone biosynthesis protein COQ9, mitochondrial	0.62
P14131	*Rps16*	40S ribosomal protein S16	0.63
Q3U741	*Ddx17*	DEAD (Asp-Glu-Ala-Asp) box polypeptide 17, isoform CRA_a	0.64
Q9CYW4	*Hdhd3*	Haloacid dehalogenase-like hydrolase domain-containing protein 3	0.64

Table A3.4 (cont'd)

Q60749	*Khdrbs1*	KH domain-containing, RNA-binding, signal transduction-associated protein 1	0.64
Q9CY58	*Serbp1*	Plasminogen activator inhibitor 1 RNA-binding protein	0.64
E9QPD7	*Pcx*	Pyruvate carboxylase	0.64
Q60930	*Vdac2*	Voltage-dependent anion-selective channel protein 2	0.64
Q60597	*Ogdh*	2-oxoglutarate dehydrogenase, mitochondrial	0.65
P62843	*Rps15*	40S ribosomal protein S15	0.65
Q99MN9	*Pccb*	Propionyl-CoA carboxylase beta chain, mitochondrial	0.65
Q8BH44	*Coro2b*	Coronin-2B	0.66
D3Z7P3	*Gls*	Glutaminase kidney isoform, mitochondrial	0.66
P97300	*Nptn*	Neuroplastin	0.67
B2RXT3	*Ogdhl*	Ogdhl protein	0.67
Q9DBL1	*Acadsb*	Short/branched chain-specific acyl-CoA dehydrogenase, mitochondrial	0.67
O35143	*Atpif1*	ATPase inhibitor, mitochondrial	0.68
Q9DB72	*Btbd17*	BTB/POZ domain-containing protein 17	0.68
F8WHB1	*Atp2b2*	Calcium-transporting ATPase	0.68
Q9CPT4	*Mydgf*	Myeloid-derived growth factor	0.68
O08795	*Prkcsh*	Isoform 2 of Glucosidase 2 subunit beta	0.69
Q8VCE0	*Atp1a3*	Sodium/potassium-transporting ATPase subunit alpha	0.69
P62315	*Snrpd1*	Small nuclear ribonucleoprotein Sm D1	0.7
O88696	*Clpp*	ATP-dependent Clp protease proteolytic subunit, mitochondrial	0.71
Q3THE2	*Myl12b*	Myosin regulatory light chain 12B	0.71
P35802	*Gpm6a*	Neuronal membrane glycoprotein M6-a	0.71
O08749	*Dld*	Dihydrolipoyl dehydrogenase, mitochondrial	0.72
Q9CR21	*Ndufab1*	Acyl carrier protein, mitochondrial	0.73
Q9JKR6	*Hyou1*	Hypoxia up-regulated protein 1	0.74
Q9JHI5	*Ivd*	Isovaleryl-CoA dehydrogenase, mitochondrial	0.74
Q9QXS6	*Dbn1*	Drebrin	0.75
Q9D3D9	*Atp5f1d*	ATP synthase subunit delta, mitochondrial	0.76
P20029	*Hspa5*	Endoplasmic reticulum chaperone BiP	0.76
Q8K2B3	*Sdha*	Succinate dehydrogenase [ubiquinone] flavoprotein subunit, mitochondrial	0.76

Table A3.4 (cont'd)

Q8BKZ9	*Pdhx*	Pyruvate dehydrogenase protein X component, mitochondrial	0.77
Q6PIE5	*Atp1a2*	Sodium/potassium-transporting ATPase subunit alpha-2	0.77
P01831	*Thy1*	Thy-1 membrane glycoprotein	0.77
P20108	*Prdx3*	Thioredoxin-dependent peroxide reductase, mitochondrial	0.78
P56480	*Atp5f1b*	ATP synthase subunit beta, mitochondrial	0.79
Q02819	*Nucb1*	Nucleobindin-1	0.79
O55143	*Atp2a2*	Sarcoplasmic/endoplasmic reticulum calcium ATPase 2	0.79
Q3UH59	*Myh10*	Myosin-10	0.8
P17095	*Hmga1*	High mobility group protein HMG-I/HMG-Y	0.82
P14094	*Atp1b1*	Sodium/potassium-transporting ATPase subunit beta-1	0.82
Q8BTS0	*Ddx5*	DEAD (Asp-Glu-Ala-Asp) box polypeptide 5	0.83
Q3ULD5	*Mccc2*	Methylcrotonoyl-CoA carboxylase beta chain, mitochondrial	0.83
Q8BFR5	*Tufm*	Elongation factor Tu, mitochondrial	0.84
Q9CQF3	*Nudt21*	Cleavage and polyadenylation specificity factor subunit 5	0.85
Q9D2G2	*Dlst*	Dihydrolipoyllysine-residue succinyltransferase component of 2-oxoglutarate dehydrogenase complex, mitochondrial	0.85
Q9CQ62	*Decr1*	2,4-dienoyl-CoA reductase, mitochondrial	0.87
H3BJW3	*Cpsf6*	Cleavage and polyadenylation-specificity factor subunit 6	0.88
P01867	*Igh-3*	Ig gamma-2B chain C region	0.9
Q9CQQ7	*Atp5f1*	ATP synthase F(0) complex subunit B1, mitochondrial	0.93
Q03265	*Atp5f1a*	ATP synthase subunit alpha, mitochondrial	0.93
P43006	*Slc1a2*	Excitatory amino acid transporter 2	0.94
Q9D051	*Pdhb*	Pyruvate dehydrogenase E1 component subunit beta, mitochondrial	0.94
P56959	*Fus*	RNA-binding protein FUS	0.94
O88569	*Hnrnpa2b1*	Heterogeneous nuclear ribonucleoproteins A2/B1	0.96
Q8BG05	*Hnrnpa3*	Heterogeneous nuclear ribonucleoprotein A3	0.97

Table A3.4 (cont'd)

Q99K48	*Nono*	Non-POU domain-containing octamer-binding protein	0.97
Q91VR2	*Atp5f1c*	ATP synthase subunit gamma, mitochondrial	0.99
Q9D6J6	*Ndufv2*	NADH dehydrogenase [ubiquinone] flavoprotein 2, mitochondrial	1
Q8CHT0	*Aldh4a1*	Delta-1-pyrroline-5-carboxylate dehydrogenase, mitochondrial	1.04
P84104	*Srsf3*	Serine/arginine-rich splicing factor 3	1.04
P35486	*Pdha1*	Pyruvate dehydrogenase E1 component subunit alpha, somatic form, mitochondrial	1.07
Q8R081	*Hnrnpl*	Heterogeneous nuclear ribonucleoprotein L (Fragment)	1.12
Q9DB15	*Mrpl12*	39S ribosomal protein L12, mitochondrial	1.23
Q9CQX8	*Mrps36*	28S ribosomal protein S36, mitochondrial	1.24
P12787	*Cox5a*	Cytochrome c oxidase subunit 5A, mitochondrial	1.28
P46660	*Ina*	Alpha-internexin	1.3
Q8BMF4	*Dlat*	Dihydrolipoyllysine-residue acetyltransferase component of pyruvate dehydrogenase complex, mitochondrial	1.3
Q9WVA2	*Timm8a1*	Mitochondrial import inner membrane translocase subunit Tim8 A	1.3
P08553	*Nefm*	Neurofilament medium polypeptide	1.31
Q60932	*Vdac1*	Voltage-dependent anion-selective channel protein 1	1.35
P48962	*Slc25a4*	ADP/ATP translocase 1	1.38
P19246	*Nefh*	Neurofilament heavy polypeptide	1.41
P08551	*Nefl*	Neurofilament light polypeptide	1.43
Q9DCX2	*Atp5h*	ATP synthase subunit d, mitochondrial	1.53
Q9DB77	*Uqcrc2*	Cytochrome b-c1 complex subunit 2, mitochondrial	1.55
P00405	*Mtco2*	Cytochrome c oxidase subunit 2	1.67
P30275	*Ckmt1*	Creatine kinase U-type, mitochondrial	1.81

Table A3.5. Validation of EFhd2-associated proteins in the forebrain using targeted mass spectrometry

Accession ID	Protein Name	Selected peptide	WT_Forebrain _IP-Total Area Fragment	KO_Forebrain_ IP-Total Area Fragment	Forebrain_WT /KO Relative Abundance Ratio
Q9JKK7	TMOD2	Peptide 1	5585690	596687	9.361173
Q9JKK7	TMOD2	Peptide 2	4068702	195804	20.77946
Q9QXS6	DREB	Peptide 1	12702598	1266471	10.02992
Q9QXS6	DREB	Peptide 2	12760502	1100825	11.59176
Q61545	EWS	Peptide 1	807956	130080	6.211224
Q61545	EWS	Peptide 2	12194448	5939145	2.053233
Q61545	EWS	Peptide 3	2729809	804376	3.393698
P47754	CAZA2	Peptide 1	13764217	1419424	9.697044
P47754	CAZA2	Peptide 2	13755381	1333528	10.31503
Q9R1Q8	TAGL3	Peptide 1	4553320	0	4553320
Q9R1Q8	TAGL3	Peptide 2	4816439	0	4816439
Q8BH44	COR2B	Peptide 1	4817364	0	4817364
Q8BH44	COR2B	Peptide 2	3352290	0	3352290
Q8VDD5	MYH9	Peptide 1	16207324	1613512	10.04475
Q8VDD5	MYH9	Peptide 2	4098568	420089	9.756428
Q61879	MYH10	Peptide 1	8671644	866189	10.01126
Q61879	MYH10	Peptide 2	8278301	1312563	6.306974

Table A3.6. Validation of EFhd2-associated proteins in the hindbrain using targeted mass spectrometry

Accession ID	Protein Name	Selected peptide	WT_Hindbrain_IP-Total Area Fragment	KO_Hindbrain_IP-Total Area Fragment	Hindbrain_WT/KO Relative Abundance Ratio
Q9JKK7	TMOD2	Peptide 1	1599469	98798	16.1892852
Q9JKK7	TMOD2	Peptide 2	1461946	0	1461946
Q9QXS6	DREB	Peptide 1	1146429	292153	3.92407061
Q9QXS6	DREB	Peptide 2	1767624	0	1767624
Q61545	EWS	Peptide 1	728110	179892	4.04748405
Q61545	EWS	Peptide 2	19693132	11083950	1.77672508
Q61545	EWS	Peptide 3	3194845	1744581	1.83129645
P47754	CAZA2	Peptide 1	4676086	752719	6.21225982
P47754	CAZA2	Peptide 2	3874584	922770	4.19886212
Q9R1Q8	TAGL3	Peptide 1	1526660	0	1526660
Q9R1Q8	TAGL3	Peptide 2	1032914	96782	10.6725837
Q8BH44	COR2B	Peptide 1	990570	0	990570
Q8BH44	COR2B	Peptide 2	894720	4	223680
Q8VDD5	MYH9	Peptide 1	5805187	1292660	4.49088469
Q8VDD5	MYH9	Peptide 2	1642165	147803	11.1104984
Q61879	MYH10	Peptide 1	2555404	247579	10.3215701
Q61879	MYH10	Peptide 2	3016662	349774	8.62460332

Chapter Four: Investigating the role of EFhd2 protein in modulating tau pathology in a Tau_{P301L} mouse model

Abstract

Accumulation of abnormally aggregated tau is the main pathological hallmark in tauopathies, including Alzheimer's disease (AD), frontotemporal dementia (FTD), and progressive supranuclear palsy (PSP). A growing number of researchers share the view that early pretangle oligomeric tau aggregates potentially exert neurotoxicity and insidiously promote neurodegeneration. In contrast, the formation of neurofibrillary tangles could represent a neuroprotective response that possibly delays cellular demise. A multitude of *in vitro* studies have endorsed the low propensity of tau protein to aggregate without an external aggregation inducer that mostly acts as a nucleation factor seeding tau aggregation. These insights prompted scientists to ferret out molecular factors that could drive tau aggregation during pathology. Among these factors, tau mutations have a profound impact on tau aggregation. Research has shown that mutant tau is more prone to self-aggregation than wild type. In fact, tau mutations cause a subset of familial tauopathies that merely constitute a small proportion of tauopathy cases. Therefore, mutations cannot explain the biogenesis of pathological aggregates in sporadic tauopathies such as AD. Studying tau-interacting proteins has garnered research attention in the last decade as a potential factor that engages in pathological tau aggregation. Our research group has identified EFhd2 protein as a tau-associated protein in JNPL3 mouse model (that overexpresses P301L mutant human tau) and postmortem tauopathies tissues. Furthermore, we conducted *in vitro* studies where we demonstrated that EFhd2 associates with tau, promotes β-sheet formation, and alters its dynamic properties. Accordingly, we hypothesized that EFhd2 might contribute to tau-mediated neurodegeneration by promoting the formation of pathological and toxic tau aggregates. To test this hypothesis, we examined the impact of deleting *Efhd2* gene *in vivo* on the progressive pathological phenotype and neuropathological changes of tau in Tau_{P301L} expressing mice. The results showed a marginal change in the lifespan of Tau_{P301L} expressing mice in the absence of EFhd2 and in the pathological phenotype. In addition, we detected a medium-large reduction of pSer422 and PHF1 positive tau (markers of late aggregation events) in the absence of EFhd2 in the cortex of old mice. We also quantified Alz50 tau, which detects early conformational changes of tau that associate with pathology. The deletion of *Efhd2* induced higher accumulation of Alz50 tau compared to wild type mice. These findings suggest that the absence of EFhd2 induced the accumulation of early pathological

pretangle tau aggregates accompanied by a reduction of markers of late aggregation events. Further experiments are warranted to further understand the role of EFhd2 in tau pathology.

Introduction

Prior research has demonstrated the link between the relatively novel protein EFhd2 and a number of neurological disorders and neurodegenerative diseases (Martins-de-Souza et al., 2009; Martins-de-Souza et al., 2010; Kekesi et al., 2012; Vega, 2016; Mielenz et al., 2018; Broniarczyk-Czarniak & Gałecki, 2019; Kogias et al., 2020). Our group primarily has shown the association of EFhd2 and pathological changes in tauopathies using animal models and human brains. Tauopathies encompass highly diverse neurodegenerative disorders, including AD, FTD, and PSP, and the major pathological hallmark thereof is aberrant aggregates of tau protein (Chung et al., 2021; Sexton et al., 2022). In fact, the major differences among tauopathies largely consist in affected brain regions, cellular inclusions, tau aggregates, and clinical presentation (Chung et al., 2021; Sexton et al., 2022). However, they all converge on the abnormal transformation of tau from a highly dynamic protein to a static protein with great tendency for self-aggregation (Wang & Mandelkow, 2016; Chung et al., 2021). It has become clear that abnormal tau aggregation follows a similar trajectory in all tauopathies (Kuret et al., 2005; Wang & Mandelkow, 2016; Chung et al., 2021; Limorenko & Lashuel, 2022). Abnormal conformational changes of tau promote the formation of early dimers, trimers, and oligomers. Then these oligomeric species further aggregate to tau filaments and fibrils leading to ultimate high molecular weight aggregates e.g., neurofibrillary tangles (NFTs) in AD (Kuret et al., 2005; Chung et al., 2021; Limorenko & Lashuel, 2022). Evolving insights deem the early pretangle oligomeric aggregates as the true perpetrator causing neurotoxicity and neurodegeneration (Berger et al., 2007; Brunden et al., 2008; Spires-Jones et al., 2009; Kayed, 2010; Lasagna-Reeves et al., 2011; Patterson et al., 2011; Lasagna-Reeves et al., 2012). On the other hand, the formation of neurofibrillary tangles could represent a neuroprotective response that possibly delays cellular demise (Gomez-Isla et al., 1997; Morsch et al., 1999; Wittmann et al., 2001; Santacruz et al., 2005; Spires et al., 2006; Sydow et al., 2011; Cowan & Mudher, 2013; Kuchibhotla et al., 2014). Therefore, years of extensive research have been fully dedicated to unraveling the molecular mechanisms that govern abnormal tau conformations and aggregation.

In familial tauopathies, such as frontotemporal dementia and parkinsonism linked to chromosome 17 (FTDP-17), mutations of *MAPT* gene (that encodes tau) predispose tau to adopt aberrant conformations leading to the formation of aggregates (Hutton et al., 1998; Wang & Mandelkow, 2016; Strang et al., 2019; Kanaan et al., 2020). Although the mechanism remains

unknown, a number of *in vitro* studies have shown the capacity of mutant tau to self-aggregate in the absence of external inducers as opposed to wild type tau. In this vein, transgenic tauopathy models that overexpress human mutant tau exhibit progressive pathological aggregation and neurodegeneration modeling some aspects of human diseases. However, in sporadic tauopathies, such as AD and corticobasal degeneration (CBD), where autosomal mutations are lacking, scientists have proposed some factors that might lead to tau pathology. For instance, tau undergoes a large array of post-translational modifications (PTMs). Imbalance in regulating these PTMs disrupts tau structure and promotes its aggregation (Kanaan et al., 2011; Tiernan et al., 2016; Wang & Mandelkow, 2016). A recent surge of interest has been drawn to study tau-interacting proteins as another molecular factor that could impact pathological tau accumulation in tauopathies (Kavanagh et al., 2022; Prikas et al., 2022; Tracy et al., 2022; Betters et al., 2023; Griffin et al., 2023; Younas et al., 2024).

We first reported the association between EFhd2 and pathological tau in a tauopathy model JNPL3 that overexpresses human tau with P301L mutation linked to FTDP-17 (Hutton et al., 1998; Rizzu et al., 1999; Lewis et al., 2000; Vega et al., 2008). EFhd2 is a relatively novel calcium-binding protein that was first uniquely identified in CD8^{+} T-Cells (Vuadens et al., 2004; Vega, 2016; Kogias et al., 2019). Pioneering structural studies of EFhd2 protein determined three major domains: N-terminus, calcium-binding motif, and coiled-coil domain. The N-terminus domain includes 6-9 alanine residues forming a PolyA tail and a low-complexity flexible region (Avramidou et al., 2007; Ferrer-Acosta et al., 2013a; Kogias et al., 2019). Consistently, initial studies suggested that EFhd2, due to its dynamicity, does not adopt a well-defined tertiary structure (Dyson & Wright, 2005; Ferrer-Acosta et al., 2013a). In fact, this feature characterizes a large group of neurodegeneration-linked proteins, such as tau, α-Synuclein, and TDP-43 (Avila et al., 2016; Lim et al., 2016; Bisi et al., 2021). Calcium-binding domain of EFhd2 comprises two EF-hand motifs that typify other calcium-binding proteins (Vuadens et al., 2004; Hagen et al., 2012; Ferrer-Acosta et al., 2013a). A considerable amount of research bears out that EFhd2 binds to intracellular calcium and regulates downstream signaling pathways (Nelson et al., 2002; Avramidou et al., 2007; Kroczek et al., 2010; Hagen et al., 2012; Park et al., 2017). In addition, the coiled-coil domain (C-C) at the C-terminus mediates EFhd2 self-oligomerization and protein-protein interactions, thereby classifying EFhd2 as an amyloid protein (Liu et al., 2006; Ferrer-Acosta et al., 2013a; Ferrer-Acosta et al., 2013b; Park et al., 2017; Szczepaniak et al., 2021).

Furthermore, we have shown that EFhd2 phase separates *in vitro* in the presence of a crowding agent into static solid-like structures (Vega et al., 2019). In the presence of calcium, these structures transform into more dynamic droplets. Regardless of the presence of calcium, C-C domain seemed necessary for phase separation of EFhd2, and not the N-terminus (Vega et al., 2019).

EFhd2 exhibits a widespread expression in the body with the highest abundance in the central nervous system (CNS) (Avramidou et al., 2007; Vega et al., 2008). In addition, EFhd2 expression is not homogenous in the brain. In particular, a higher expression levels of EFhd2 were reported in the cortex, limbic system, and basal ganglia whereas it exists at lower levels in brains stem and cerebellum (Vega et al., 2008; Purohit et al., 2014).

We identified a progressive accumulation of EFhd2 with pathological tau aggregates in an age-dependent manner (Vega et al., 2008). Furthermore, EFhd2 exclusively co-purified with sarkosyl-insoluble pathological tau species extracted from animals with severe behavioral phenotype, whereas EFhd2 was not detected with tau in younger mice. These findings were corroborated in postmortem tauopathies brain of AD and FTD (Vega et al., 2008; Ferrer-Acosta et al., 2013b). Along similar lines, EFhd2 and PHF1 tau (phosphorylated tau at Ser396/404) colocalized in the somatodendritic compartment in the frontal cortex of AD (Ferrer-Acosta et al., 2013b). Moreover, we identified higher EFhd2 levels in AD brains compared to controls. A recent study proposed that this increase in EFhd2 levels in AD is due to downregulation of miR-126a, a microRNA that regulates EFhd2 expression in the brain (Ferrer-Acosta et al., 2013b; Xue et al., 2022).

Given these findings, we hypothesized that EFhd2 contributes to the biogenesis of pathological tau aggregation. To test this hypothesis, we first assessed the level of β-sheet formation by incubating EFhd2 with microtubule-binding repeat K19 fragment of tau and measuring thioflavin S (ThS) (Vega et al., 2018). We noticed a significant increase in ThS signal when EFhd2 and K19 tau co-incubated in the absence of external aggregation inducer as heparin. Interestingly, ThS signal remarkably diminished upon deleting C-C domain from EFhd2 (Vega et al., 2018). Considering the liquid-liquid phase separation (LLPS) phenomenon of tau, we tested whether EFhd2 could impact tau's demixing capabilities. Our previous findings evinced that EFhd2 transforms the dynamic tau liquid droplets into static solid-like structures (Vega et al., 2019). Again, EFhd2's C-C domain mediated the observed changes on tau's dynamics.

185

Our previous findings sparked the hypothesis that EFhd2 plays a neurodegenerative role in tauopathies by driving abnormal tau aggregation and, hence, neurotoxicity. As such, reducing EFhd2 might protect against tau-mediated neurodegeneration. To test this hypothesis, we developed the Tau$_{P301L}$/*Efhd2$^{-/-}$* mouse model by crossing JNPL3 (that overexpresses P301L mutant human tau) with *Efhd2$^{-/-}$*. The absence of EFhd2 induced a marginal change in the age-dependent behavioral phenotype of Tau$_{P301L}$ expressing mice compared to wild type mice. In addition, we evaluated pathological tau markers in 6- and 12-months female mice and identified a large age-dependent increase in these markers. Moreover, we identified a region-specific effect of *Efhd2* deletion on pSer422 and PHF1 markers in old mice. Specifically, Tau$_{P301L}$/*Efhd2$^{-/-}$* old mice showed a medium-large decline in pSer422 and PHF1 markers in the cortex compared to wild type mice. In contrast, the results demonstrated a medium and large increase in Alz50 positive tau in old Tau$_{P301L}$/*Efhd2$^{-/-}$* mice compared to wild type mice in both brainstem and cortex, respectively. The data imply that the absence of EFhd2 led to the accumulation of pretangle (Alz50 positive) tau aggregates along with obvious reduction in the markers of later aggregates (pSer422 and PHF1). These compelling findings necessitate more studies to understand whether the effect of EFhd2 on the biogenesis of pathological tau aggregates has a direct or indirect impact on associated neurodegeneration. In this regard, our new Tau$_{P301L}$/*Efhd2$^{-/-}$* mouse model will help disentangle the contribution of EFhd2 to tau-mediated neurodegeneration.

Materials and Methods

Animals

All experiments were conducted in compliance with federal, state, and institutional guidelines and approved by the Michigan State University Institutional Animal Care and Use Committee (Protocol #PROTO202400017). *Efhd2$^{-/-}$* mice were generated as delineated in Chapter Three (Materials and Methods section). JNPL3 mice (Tau$_{P301L}$) overexpressing human 0N4R tau that harbors P301L mutation under mouse prion promoter ((Tg(Prnp-MAPT*P301L) were maintained in a heterozygous state and backcrossed to Swiss Webster (SWR) inbred strain (Lewis et al., 2000). JNPL3 mice were bred with *Efhd2$^{-/-}$* mice producing pups with heterozygous endogenous mouse *Efhd2* allele (*Efhd2$^{+/-}$*) and either transgenic (Tau$_{P301L}$) or non-transgenic (Non-Tg). Pups from F1 generation were then bred to generate littermates Non-Tg/*Efhd2$^{+/+}$*, Non-Tg/*Efhd2$^{-/-}$*, Tau$_{P301L}$/*Efhd2$^{+/+}$*, and Tau$_{P301L}$/*Efhd2$^{-/-}$* that were then used in

this study as illustrated in Figure 4.1. In this study, neither Non-Tg/*Efhd2*$^{+/-}$ nor Tau$_{P301L}$/*Efhd2*$^{+/-}$ were analyzed. Since the progeny have mixed strains of SWR and C57BL/6, a specific breeding strategy was then followed throughout generations to produce the required sample size of mice with identical homogenous background. To assess genomic background, we used the genomic marker developed by DartMouse^{TM}. This approach utilizes single-nucleotide polymorphisms (SNP) spread throughout the genome to determine the contribution of genomic DNA when different mouse strains are crossed, providing greater efficiency towards reaching a homogenous genomic background colony. Based on genomic markers data, the mouse colony shows a stable mixed SWR/C57BL/6 genomic background (Figure A4.1A). The background was assessed every few generations to ensure background homogeneity. In that way, confounding effects due to a predominant background that could impact data interpretation was avoided. Mice were socially housed (up to 5 mice per cage) without enrichments in a 12-h light/dark cycle with food and water provided *ad libitum*. Mice were transferred to a clean cage with food and water weekly.
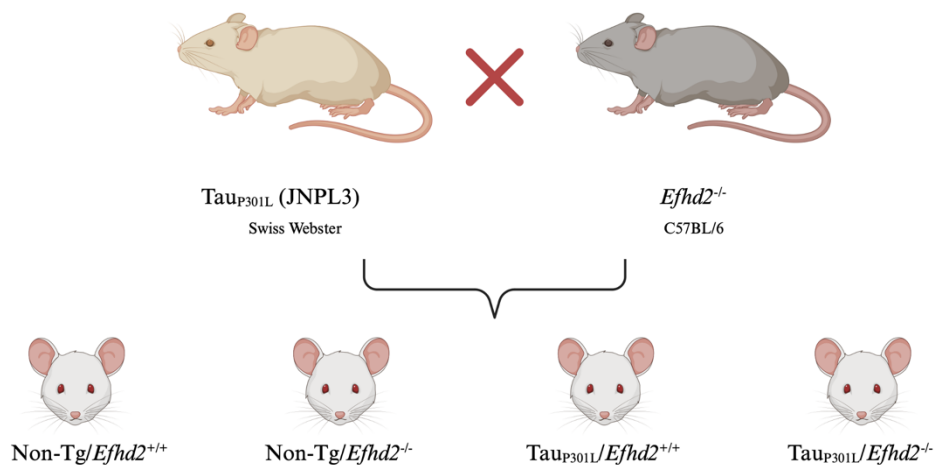
Figure 4.1. Developing Tau$_{P301L}$/*Efhd2*$^{-/-}$ model. JNPL3 (Tau$_{P301L}$ expressing) mouse model that overexpresses human tau bearing missense mutation P301L under the control of mouse prion has been maintained in Swiss Webster (SWR) background. JNPL3 was bred with *Efhd2*$^{-/-}$ developed on C57BL/6. The progeny includes mixed genotypes either Non-Tg (no Tau$_{P301L}$) or Tau$_{P301L}$ with either *Efhd2*$^{+/+}$, *Efhd2*$^{-/-}$, or *Efhd2*$^{+/-}$. In this study *Efhd2*$^{+/-}$ was not included due to sample size limitation. No behavioral differences were detected between *Efhd2*$^{-/-}$ and *Efhd2*$^{+/-}$. Figure was created with Biorender.com.

Genotyping

DNA was extracted from ear punches at weaning (21 days) using Kappa Mouse Genotyping Kit (GE cat #KK7352) according to manufacturers' recommendations. Amplification of the LacZ gene was performed using the 3' Uni *Neo* (*5′-GCAGCCTCTGTTCCACATACACTTCA-3′*) and Reg 10032R1 (*5′-GCCTATAGTTAAGGGGAGTTGGGTGG-3′*) primers. For the *Efhd2* gene, Fwd (*5′-CTTGGCCTCGAAGAAGTTCTTGG-3′*) and Rev (*5′-GCCCTCTAAGGCTTTGTGAATGC-3′*) primers were used. For *Mapt* gene, Exon 9 Fwd (*5′-CACTGAGAACCTGAAGIACCAG-3′*) and Exon 13 Rev (*5′-AGACACCACTGGCGACTTGTAC-3′*) primers were used. Amplification of the three genes was performed using cycling conditions recommended by the KOMP consortium. The PCR reaction constitutes 12.5 μl 2x Kappa Fast genotyping, 1.25 μl Primer Fwd (100ng/ μl), 1.25 μl primer Rev (100 ng/ μl), 1 μl extracted DNA and 9 μl ddH$_2$0. The amplified DNA was then separated on 1% agarose and visualized with 0.005% ethidium bromide using Bio-Rad Imager as shown in Figure A4.1B. Positive control represents a verified *Tau$_{P301L}$/Efhd2$^{+/-}$* whereas the negative control is the master mix (including the primers) without DNA sample (Figure A4.1B).

Sample size

A priori power analysis was conducted using G*Power software (Faul et al., 2007; Kang, 2021). First, preliminary behavioral data were used to calculate effect size with PASS 2020 Power Analysis and Sample size Calculation. The power analysis did not include sex as a factor. Hence, males and females are not statistically compared in this study. The calculated sample size for longitudinal behavioral assessment using effect size 0.44 for repeated measures ANOVA (RM-ANOVA), 80% power and α 0.05 was 11 mice/ genotype/sex. Given the potential for attrition and to ensure adequate power, we aimed for 16 mice/genotype/sex as depicted in Figure 4.2. By the end of the study, the sample size was actually 12-16/group. The sample size for cross-sectional study (Figure 4.2) was estimated according to previous experiments and published research (Apicco et al., 2018). According to effect size of 0.4 for two-way ANOVA, 80% power, and α 0.05, the calculated sample size was 4/genotype/age/sex. We aimed for 6/ group to compensate for untoward technical issues (Figure 4.2). Collectively, sample size determined for the entire study was approximately 320 mice.

It is important to note that randomization was not possible in this study; however, experimenters were blind to the genotype of each mouse. After data collection, genotypes were decoded.

Behavioral testing

Figure 4.2 summarizes the experimental design for the longitudinal and cross-sectional analysis. In the longitudinal section, mice were aged at 12 months whereby behavioral assessment was undertaken every three months starting at the age 3 months (Figure 4.2). In the cross-sectional behavioral and pathological analysis, separate cohorts of mice were aged at 3, 6,9, and 12 months Immediately after the behavioral assessment of each age, mice were euthanized, and tissues were collected as shown in Figure 4.2.
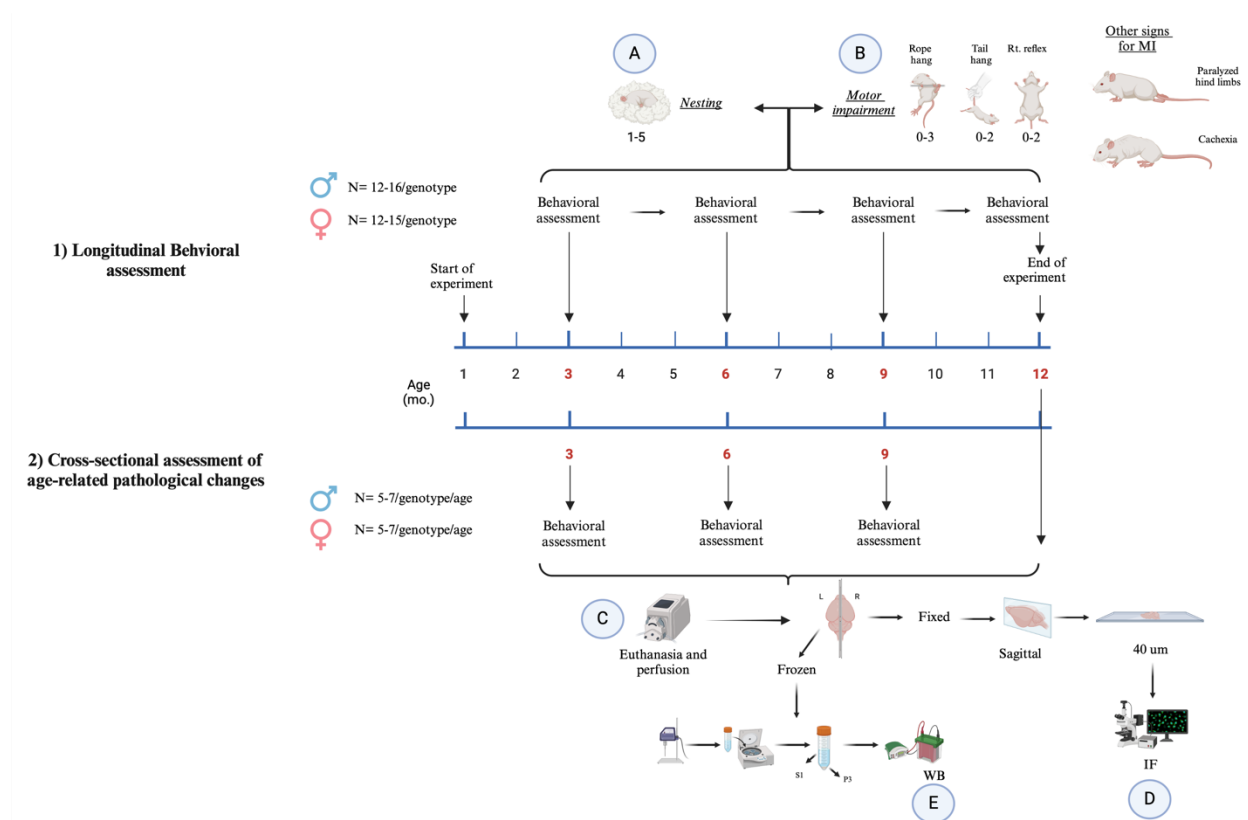
Figure 4.2. Experimental design and workflow. To investigate the impact of deleting *Efhd2* on tau pathology, we designed a two-pronged study: (**1**) longitudinal behavioral assessment, (**2**) cross-sectional assessment of age-related pathological changes. For the longitudinal behavioral assessment, we used four genotypes Non-Tg/*Efhd2*$^{+/+}$, Non-Tg/*Efhd2*$^{-/-}$, Tau$_{P301L}$/*Efhd2*$^{+/+}$, and Tau$_{P301L}$/*Efhd2*$^{-/-}$ males and females. Sample size was calculated according to a priori power analysis n=12-16 per group. Behavioral assessment was conducted every 3 months starting at 3 months of age until 12 months The behavioral tests included (**A**) Nesting behavior and (**B**) motor impairment. Other signs of motor dysfunction were noted, such as hind limbs paralysis and cachexia, which indicate severe illness and impending death. Mice were euthanized after

189

Figure 4.2 (cont'd)
behavioral assessment at 12 months in (**2**) cross-sectional study, females and males from the four genotypes with n= 5-7/group were assessed for behavior and euthanized immediately afterwards at 3, 6, 9, and 12 months In (**C**) mice were euthanized and brains were collected. The right hemisphere was fixed for (**D**) immunofluorescence processing, and the left hemisphere was frozen for further homogenization for biochemical analysis by western blot (**E**). Figure was created with Biorender.com.

1- *Motor function assessment*

Tau$_{P301L}$ mice overexpress human 0N4R tau with P301L mutation under the control mouse prion promoter (Lewis et al., 2000). The original JNPL3 model was developed after the initial discovery of FTDP-17-related missense mutations (Hutton et al., 1998). The progressive pathological tau accumulation starts in the brainstem and spinal cord before later propagation to other brain regions; primarily the cortex, hypothalamus, and basal ganglia (Lewis et al., 2000; Sahara et al., 2002). In this model, less pathology is noted in the hippocampus. As a result, the principal behavioral phenotype in this model is motor impairment exhibited as progressive dystonia of hind limbs, abnormal escape extension, hunched posture, and inability to righting. This motor phenotype does not represent all human tauopathies but overlaps with progressive supranuclear palsy (PSP), FTD-ALS, and FTDP-17. In fact, the severity of motor impairment increases with advanced age in JNPL3 mice and correlates with pathological tau depositions and neurodegeneration.

As shown in Figure A4.2 B and C, motor phenotype was represented by motor impairment score (MIS) that was assessed according to three tests: tail hang (scale 0-2), righting reflex (score 0-2), and rope hand (score 0-2) (Lewis & McGowan, 2005). Rope hang test is performed twice. Each score was given according to a rubric summarized in Figure A4.2B. The scores of the three tests were combined and converted to a final MIS, which equates to the respective stage of neurodegeneration (Figure A4.2C) (Lewis & McGowan, 2005). Each mouse was evaluated by two independent raters, and the average of the two scores was used for analysis. The assessment of motor function was conducted after the nesting test. In addition to MIS, other signs of motor dysfunction were monitored weekly starting at 6 months, including slouched posture, conjunctivitis, dystonia, paralyzed hind limbs, and cachexia. These signs typically indicate severe illness followed by death. The mice that died before the end of the study (12 months) due to motor phenotype were given score 30 of MIS and score 1 for nesting and are calculated as death events for survival analysis.

2- Nesting

As mentioned earlier, the main behavioral phenotype in the Tau_{P301L} model is age-dependent motor dysfunction. That weakens the reliability of traditional maze-based behavioral tests, such as water maze or Y-maze, to assess cognitive domain in this model. Alternatively, in this study we assessed nesting behavior as a substitute to evaluate impaired activities of daily living that reflect cognitive function (Deacon, 2006; Neely et al., 2019). All mice for longitudinal and cross-sectional experiments were evaluated for nesting performance as depicted in Figure 4.2-point A. Evaluating nesting performance was adopted from previously described protocol (Deacon, 2006). Briefly, mice were transferred to a clean cage individually without any enrichment except standard Neslets 5 cm^2 cotton batting 24 h before the test. On day 2, nesting construction was evaluated according to the 5-point scale shown in Figure A4.2A. Each mouse was assessed by three independent blind raters; then, the average score was used for subsequent analysis.

Combined phenotype score

We sought to create a combined score that represents nesting and motor phenotype for each mouse. We developed the combined score for two reasons. The first reason is that, with aging, nesting behavior could be impacted to some extent by the level of motor dysfunction. The second reason is to make the data parametric that allows adequate statistical analysis. To this end, we first normalized each of nesting score (NS) and MIS using traditional, minimum-maximum normalization methods as follows:

$$Normalized\ MIS = \frac{30 - score}{30}$$

$$Normalized\ NS = \frac{score - 1}{4}$$

Then we combined them in an equation to calculate the final phenotype score:

$$Combined\ phenotype\ score = (Normalized\ MIS * 0.5) + (Normalized\ NS * 0.5)$$

In this equation, 0.5 denotes the weight that each of NS and MIS contribute to the final phenotype. The combined phenotype score could reside between 0-1 where 0 indicates severe illness and behavioral phenotype whereas 1 indicates normal phenotype.

Tissue collection and processing

At the age of sacrifice, mice were administered intraperitoneally an overdose of Fatal Plus solution ($\geq$100 mg/kg). Mice were transcardially perfused with 0.9% saline containing

heparin (10,000 units/L) at rate 2 ml/min for 20 min. Brains were then removed and the right hemisphere was post-fixed in 4% paraformaldehyde overnight at 4 ºC. For cryoprotection, brains were then immersed first in a 15% sucrose solution for 24 h (until sinking to the bottom of the vial), followed by a 30% sucrose solution. The left hemisphere was removed and flash frozen on dry ice for downstream biochemical analysis. Using a freezing stage and sliding knife microtome, the right hemisphere was sliced into 40 μm sagittal sections. Brain sections were stored in a cryoprotectant solution at 4 ºC (30% sucrose + 30% ethylene glycol in PBS) for subsequent histological analysis.

Immunofluorescence

Initial tittering experiments were conducted to determine optimal primary antibodies dilution. DAPI, a nuclear marker (Thermo Scientific cat #D1306) was stored as a stock solution of 5 mg/ml in DMSO (Sigma cat #D8418) and frozen at -20 °C. Immunofluorescence was undertaken according to established protocols (Combs et al., 2016). The 40-μm free floating tissues were washed in 0.1%Triton-X (Thermo Scientific cat #A16046) in TBS for 6 times x 10 min. Then, tissues were blocked in 10% goat serum/2% BSA/0.4% Triton-X/TBS for 1.5 h at room temperature (goat serum: Gibco cat #16210-072; BSA: Bioreagents cat #BP1600). Primary antibodies were diluted in 2% goat serum/0.1% Triton-X/TBS: pSer422 (1:2K; Abcam cat #ab79415), Alz50 (1:2K, RRID:AB_2313937), and PHF1(1:500, RRID: AB_2315150) (Wolozin et al., 1986; Ksiezak-Reding et al., 1988; Goedert et al., 1991; Greenberg et al., 1992; Otvos et al., 1994; Ksiezak-Reding et al., 1995; Carmel et al., 1996). After blocking, tissues were incubated with the primary antibody overnight at 4 ºC. Then the tissues were washed in 0.1% Triton-X/TBS 6 times x 10 min. Afterwards, tissues were incubated with secondary antibody 1:500: AlexaFluor goat anti-mouse IgG1 (H + L) 488 (Invitrogen, cat #A-21121), AlexaFluor goat anti-mouse IgM (H + L) 488 (Invitrogen, cat #A-21042), and AlexaFluor goat anti-rabbit IgG (H + L) 488 (Invitrogen, cat #A-11008) for 2 h at room temperature. The first wash after secondary antibody contained DAPI at a final concentration of 0.5 ng/μl in 0.1% Triton-X/TBS followed by 5 washes x 10 min. Sections were then mounted on microscope slides and allowed to air dry overnight. To block autofluorescence, mounted sections were stained with Sudan Black (Thermo Scientific, cat #BP109). Briefly, slides were rinsed in water by 3 dips followed by equilibration in 70% ethanol for 2 min. Then the slides were covered with 2% Sudan Black/70% ethanol for 5 min. Immediately afterwards, the slides were rinsed with 3 dips of 70% ethanol

followed by 3 quick dips in water. Finally, slides were washed in water twice x 1 min. Slides were quickly coverslipped with Vectashield aqueous mounting media (Vector laboratories, #H-1000). All slides were stored in the dark at 4 ºC until ready for imaging.

Immunofluorescence (IF) images were acquired with Zeiss AxioScan 7 using the appropriate fluorescence filter for each fluorophore. Area of positive stain was quantified using Halo (Indica Labs), Area Quantification FL v2.3.3 module. Using Allen Brain Atlas, three sections per animal were selected encompassing the brainstem, hippocampus, and cortex. These three regions were quantified separately for positive stain area. Negative controls Non-Tg brain sections were used to determine the background and ensure antibodies specificity.

Western blotting

Left brain hemispheres were weighed and homogenized in 5 volumes (w/v) ice-cold Buffer A (25 mM Tris–HCl, pH7.4/150 mM NaCl/1 mM EDTA/1 mM EGTA/5 mM sodium pyrophosphate/30 mM β-glycerophosphate/30 mM sodium fluoride/1 mM phenylmethylsulfonyl fluoride (PMSF) with 1X Halt protease inhibitors cocktail (Thermo Scientific, cat #78430). Subsequently, the homogenates were centrifuged using Sorvall MTX 150 Micro-Ultracentrifuge at 110,000 x g (rotor S120-AT2) at 4 °C for 15 min. The supernatant (S1) fraction was carefully transferred to clean tubes. Pellets (P1) were resuspended in 5 volumes (w/v) ice-cold Buffer B (20 mM Tris-Base pH 7.4/800 mM NaCl/1 mM EDTA/1 mM EGTA/1 mM PMSF/5 mM sodium pyrophosphate/10 mM β-glycerophosphate/30 mM sodium fluoride/10% sucrose) and sonicated using Misonix XL-2000 set at 4 on ice 3 times with 3 s pulses. Homogenates were then ultracentrifuged at 110,000 x g at 4 °C for 15 min. With great caution, the supernatants (S2) were transferred to clean tubes. Sarkosyl (Acros Organics cat #61207-5000) (10% w/v) was added to the S2 fractions to a final concentration of 1%, vortexed, and incubated at 37°C for 1 h. Then S2 fraction was ultracentrifuged at 110,000 x g for 30 min at 4 °C. Supernatants (S3) were carefully removed and stored at -80 °C. The pellets (P3, sarkosyl-insoluble fraction) were resuspended in 50 μl Buffer A. Protein concentration of S1 fraction was determined using Pierce BCA Protein Assay Kit (cat #23225). To avoid repetitive freeze-thaw cycles, separate aliquots of S1 and P3 were prepared and stored at -80 C until immunoblotting.

For all P3 samples, 3 μl were mixed with 2X SDS loading buffer. The amount of protein loading for S1 samples varied according to each primary antibody ranging from 1.5-10 μg protein mixed 2X SDS loading buffer. Protein was separated on 4–15% Criterion TGX Stain-

Free gels (Bio-Rad cat #5678084) and transferred to pure nitrocellulose membrane (0.45μm Bio-Rad cat #1620115). The membrane was blocked using 5% dry-milk solution in 1x TBST (2.5mM Tris-Base/15mM NaCl/30mM KCL/0.02% Tween 20 detergent) for 1h at room temperature. Then the membrane was incubated with the primary antibodies overnight at 4 °C. The primary antibodies used are: mouse monoclonal anti-Tau13 (1:100k, Biolegend, cat #835201), mouse monoclonal anti-PHF1 (1:1000, RRID: AB_2315150), mouse monoclonal anti-EFhd2, clone 10D6 (1:5000, prepared by Kanaan lab as explained in detail in Chapter Three), and rabbit monoclonal pSer422 (1:1000, Abcam cat #Ab79415). The next day, the membrane is washed 3 times x 5 min in 1x TBS-T before incubation with secondary antibodies: goat anti-rabbit IRDye 680 (LiCor cat #926–68021) and goat anti-mouse IRDye 800 (LiCor cat #926–32210) at 1:2000. Afterwards, the membrane is washed 3 times x 5 min in TBS-T and imaged by Li-COR Odyssey Imaging System, using Image Studio Software (v5.2).

Statistical analysis

All data were analyzed using GraphPad Prism v10.2.2 (San Diego, www.graphpad.com, RRID:SCR_002798). Repeated measures mixed factor ANOVA (RM-ANOVA) was conducted to assess the differences among groups in the longitudinal behavioral assessment. Tukey's post hoc test was conducted for pairwise comparison to determine differences among groups. Likewise, two-way ANOVA was used to determine the differences in cross-sectional histological and biochemical analysis. Holm-Šídák test was pursued for pairwise comparison. For two-way- and repeated measures ANOVA, partial eta squared (η^2_p) was calculated to determine the magnitude of main effects and interaction (Maher et al., 2013). According to (Cohen, 2013), guidelines to interpret η^2_p will be negligible (<0.01), small (0.01), medium (0.06), or large (0.14) effect. To determine the magnitude of effect between certain groups with post hoc analysis, Hedge's g was calculated and interpreted according to widely accepted guidelines (Lakens, 2013; Maher et al., 2013). Hedge's g value of 0.2, 0.5, and 0.8 corresponds to small, medium, and large effects. Correlations between phenotype scores and various tau markers were established by using the Spearman rank test. The criteria followed to determine strength of Spearman correlation is modified from published guides (Akoglu, 2018; Schober et al., 2018). Strictly speaking, Spearman r_s is weak (0-0.39), moderate (0.4-0.59), strong (0.6-0.79), or very strong (0.8-1). In all analysis, p values were calculated with a 95% confidence interval. *$p < 0.05$, **$p < 0.01$, ***$p < 0.001$, ****$p < 0.0001$. Data are shown as mean ± SEM. Kaplan-Meier

survival analysis was conducted to compare survival percentage among groups. Log-rank Mantel-Cox test was chosen to report the difference between survival curves with family wise p =0.05. Two pairwise comparisons were conducted using Bonferroni's corrected p value of 0.025 for each comparison.

Results

Survival analysis of Tau$_{P301L}$/*Efhd2$^{-/-}$* mice

In this study, we sought to investigate the impact of EFhd2 on progressive pathology and behavioral deficit induced by tau. To this end, we bred *Efhd2$^{-/-}$* mice with JNPL3 (Tau$_{P301L}$) mice. The JNPL3 transgenic mouse model overexpresses 0R4N human tau that harbors P301L mutation under the control of mouse prion promoter (Lewis et al., 2000). Pathological tau accumulation in the form of neurofibrillary tangles (NFTs) and pretangles in addition to neuronal loss predominate primarily in spinal cord, brainstem, and telencephalon (Lewis et al., 2000; Lewis & McGowan, 2005). Therefore, motor impairment is the principal pathological phenotype in this Tau$_{P301L}$ expressing mouse model. That motor phenotype indeed overlaps with motor symptoms in a few tauopathies as PSP, FTDP, and ALS (Lewis & McGowan, 2005). Several studies have established the sex difference in mice expressing Tau$_{P301L}$ where females develop tau pathology and exhibit the impaired motor phenotype approximately 6 months earlier than males (Sahara et al., 2002; Lewis & McGowan, 2005). Furthermore, the severity of motor impairment correlates with the neuronal burden of tau aggregates and increases with advanced aging.

Shorter lifespan due to severe motor impairment characterizes Tau$_{P301L}$ mice. Particularly, the mice become moribund within 4-8 weeks from initial signs of motor impairment (Lewis et al., 2000). In this study, we conducted Kaplan-Meier survival analysis to examine whether the absence of EFhd2 changed the lifespan of Tau$_{P301L}$ expressing mice. In addition to collecting NS and MIS every three months, mice were monitored for other motor impairment signs, including dystonia, hunched posture, conjunctivitis, and cachexia. The progression of these signs ultimately hindered the mice from properly reaching water and food, leading to death.

Kaplan-Meier survival curves are shown in Figure 4.3 for females and males. Log-rank (Mantel-Cox test) detected an overall difference (p=0.043) among survival curves of females (Figure 4.3A). Pairwise comparison revealed a difference in the percent survival between Non-Tg/*Efhd2$^{+/+}$* and Tau$_{P301L}$/*Efhd2$^{+/+}$* (p=0.072). We noticed from Figure 4.3A that death events

due to motor impairment started earlier in Tau$_{P301L}$/*Efhd2*$^{+/+}$ (8 months) compared to Tau$_{P301L}$/*Efhd2*$^{-/-}$ (9 months). In addition, the percentage of Tau$_{P301L}$/*Efhd2*$^{-/-}$ that survived to 12 months was 72.2% compared to 78.5% in Tau$_{P301L}$/*Efhd2*$^{+/+}$ (p=0.72). By closely looking at percent survival of Non-Tg/*Efhd2*$^{+/+}$ and Non-Tg/*Efhd2*$^{-/-}$, we can see that the deletion of *Efhd2* gene did not change the lifespan or induce early death events (Purohit et al., 2014). Therefore, early death events reported in Tau$_{P301L}$/*Efhd2*$^{-/-}$ mice are solely ascribed to mutant tau overexpression and not *Efhd2* gene deletion. In Figure 4.3B, no death events due to motor phenotype were reported in males. These findings perfectly align with previous research demonstrating that males usually develop overt pathological phenotype between 12-15 months of age later than females.

Overall, survival analysis accords with other studies showing that mutant tau overexpression causes shorter lifespan in mice. Importantly, the data indicate that the absence of EFhd2 did not cause a large change in percent survival and lifespan in either males or females.

A
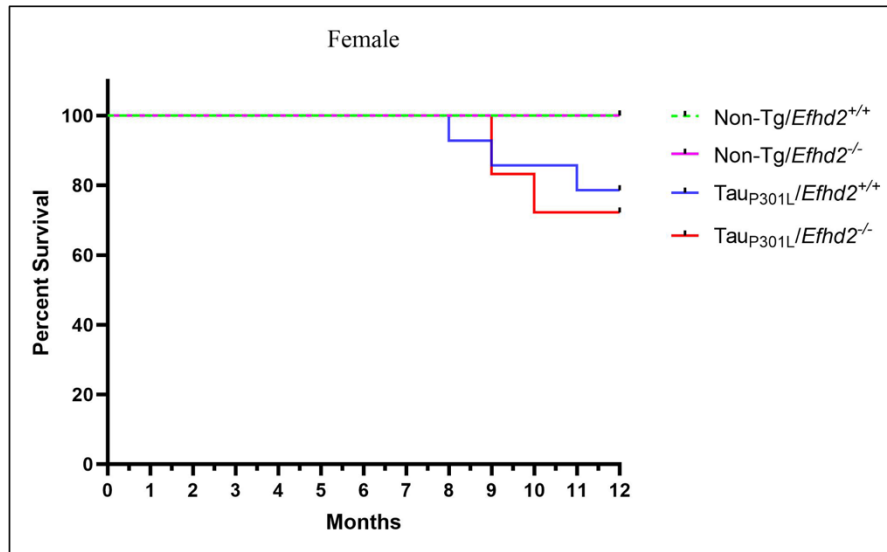
B
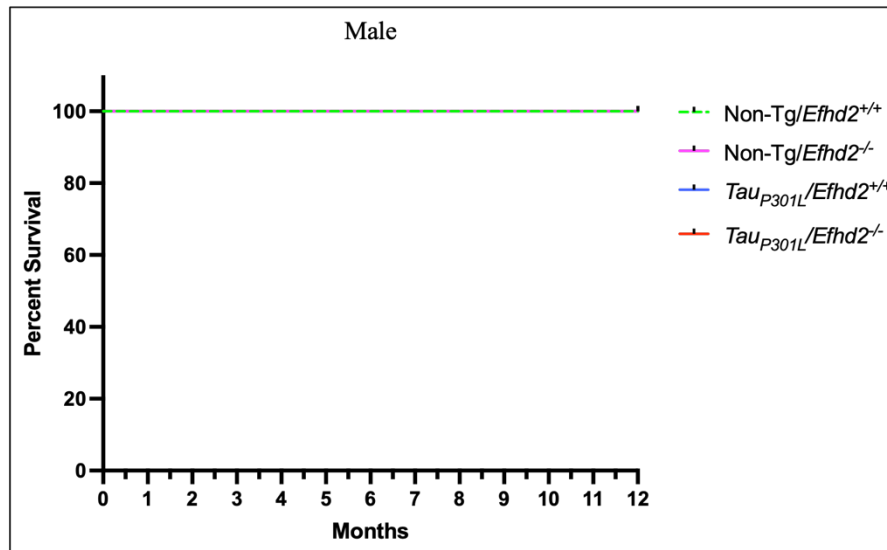
Figure 4.3. Deleting *Efhd2* gene did not change the lifespan of Tau$_{P301L}$ mice. (**A**) Kaplan–Meier survival curve of females indicated the difference in percent survival among groups by the log-rank (Mantel–Cox test) (p= 0.0431). Pairwise comparison revealed a reduction in percent survival of Tau$_{P301L}$/*Efhd2$^{+/+}$* mice compared to Non-Tg/*Efhd2$^{+/+}$* mice (p=0.0719). Likewise, comparing the survival curve of Tau$_{P301L}$/*Efhd2$^{+/+}$* and Tau$_{P301L}$/*Efhd2$^{-/-}$* mice by log-rank (Mantel–Cox test) detected a difference (p= 0.7219). At 12 months, the percent survival of Tau$_{P301L}$/*Efhd2$^{-/-}$* mice was 72.2% vs 78.5 % in Tau$_{P301L}$/*Efhd2$^{+/+}$* mice. Non-Tg mice did not face any death events until the end of the study, indicating the deleting *Efhd2* gene did not provoke early death. Non-Tg/*Efhd2$^{+/+}$* n=14, Non-Tg/*Efhd2$^{-/-}$* n=14, Tau$_{P301L}$/*Efhd2$^{+/+}$*n=14, Tau$_{P301L}$/*Efhd2$^{-/-}$* n=18. (**B**) Visualization of lifespan of male mice. Herein, Kaplan–Meier

Figure 4.3 (cont'd)

survival curve analysis of males was not feasible due to the absence of death events. Until the end of the study at 12 months no neurodegeneration-related death event was recorded.

<u>Behavioral assessment of Tau$_{P301L}$/*Efhd2$^{-/-}$* mice</u>

Longitudinal assessment of motor function and nesting was executed every three months starting at 3 months as described in the methods section, NS and MIS were normalized and combined to a final phenotype score that provides a holistic evaluation of phenotypic abnormalities in the mice. It is important to note that the mice that died before the end of the study due to severe motor dysfunction were considered terminally ill and given MIS and NS representing severe disease stage. Figure 4.4 demonstrates data analysis for the combined pathological phenotype score using RM-ANOVA to detect the differences among groups in females and males. A large number of studies reported invariably sex differences in regard to pathological phenotype in Tau$_{P301L}$; hence, we conducted a separate analysis for males and females. We can observe from Figure 4.4A an overall decline in the phenotype score in both Tau$_{P301L}$/*Efhd2$^{+/+}$* and Tau$_{P301L}$/*Efhd2$^{-/-}$* compared to their Non-Tg littermates. Mixed factor RM-ANOVA revealed a large interaction effect between genotype and age ($F_{(9, 153)} = 4.649$, $p<0.0001$, $\eta^2_p = 0.21$). The analysis also detected a large age effect on phenotype scores ($F_{(2.118, 108.0)} = 12.80$ $p<0.0001$, $\eta^2_p = 0.2$). Likewise, a large main genotype effect was identified ($F_{(3, 51)} = 3.937$ $p=0.0133$, $\eta^2_p = 0.18$). By isolating simple main effects, we detected a large effect of age in Tau$_{P301L}$/*Efhd2$^{+/+}$* ($F_{(1.595, 17.54)} = 6.854$ $p=0.0092$, $\eta^2_p = 0.38$) and Tau$_{P301L}$/*Efhd2$^{-/-}$* mice ($F_{(1.707, 22.19)} = 9.527$ $p=0.0016$, $\eta^2_p = 0.42$). In regard to Non-Tg mice, the analysis detected a negligible effect of age on the pathological phenotype of Non-Tg/*Efhd2$^{+/+}$* mice ($F_{(2.671, 37.39)} = 0.06706$ $p=0.9680$, $\eta^2_p <0.01$). Furthermore, we noticed a medium age effect on phenotype score of Non-Tg/*Efhd2$^{-/-}$* mice ($F_{(2.868, 37.28)} = 1.19$ $p=0.3249$, $\eta^2_p = 0.08$). Tukey's Pairwise comparisons confirmed a negligible reduction in the phenotype scores of Tau$_{P301L}$/*Efhd2$^{+/+}$* mice between 3 and 6 months ($p=0.9996$, Hedge's g<0.2). Obvious reduction of phenotype scores was noticed upon comparing 12-month-old to each 3 ($p=0.0361$, Hege's g= 1.2), 6 ($p=0.0388$, Hedge's g=1.2), and 9 months-old mice ($p=0.023$, Hedge's g= 0.6) (blue asterisk Figure 4.4A). Likewise, the analysis showed a small difference in phenotype scores between 3 and 6 months of Tau$_{P301L}$/*Efhd2$^{-/-}$* mice ($p= 0.8949$, Hedge's g= 0.2). A consistent age-dependent decline in phenotype scores was detected with the largest decline at 12 months in comparison to 3 ($p=0.0171$, Hedge's g=1.1), 6 ($p=0.0171$, Hedge's g=1.2), and 9

months (p=0.0359, Hedge's g=0.74) (red asterisk Figure 4.4A). We analyzed also the simple main effect of genotype to determine the difference in phenotype scores in each age group. The results indicated a marginal genotype effect at 3 ($F_{(3, 51)} = 0.08690$ p=0.9669, η^2_p=0.01) and 6 months ($F_{(3, 51)} = 0.354$ p=0.7861, η^2_p= 0.02). At 9 months, we noticed a medium effect among the four genotypes in phenotype scores ($F_{(3, 51)} = 2.582$ p=0.0635, η^2_p= 0.13). As anticipated, the largest difference in phenotype scores was identified at 12 months ($F_{(3, 51)} = 6.556$ p=0.0008, η^2_p= 0.28). Post hoc Tukey's analysis demonstrated a large reduction in the phenotype scores at 12 months Tau$_{P301L}$/*Efhd2*$^{+/+}$ mice compared to 12 months Non-Tg/*Efhd2*$^{+/+}$ mice (p= 0.0233, Hedge's g= 1.2) and Non-Tg/*Efhd2*$^{-/-}$ mice (p=0.0135, Hedge's g= 1.4) (blue caret in Figure 4.4A). Likewise, at 12 months, Tau$_{P301L}$/*Efhd2*$^{-/-}$ mice exhibited a large decline in the phenotype score compared to Non-Tg/*Efhd2*$^{+/+}$ (p=0.0164, Hedge's g=1) and Non-Tg/*Efhd2*$^{-/-}$ mice (p=0.0092, Hedge's g=1.2) (red caret in Figure 4.4A). However, we detected a negligible difference at 12 months between the mean phenotype score of Tau$_{P301L}$/*Efhd2*$^{+/+}$ and Tau$_{P301L}$/*Efhd2*$^{-/-}$ mice (p>0.9999, Hedge's g<0.2). Taken together, the data indicate a consistent age-dependent pathological phenotype in both Tau$_{P301L}$/*Efhd2*$^{+/+}$ and Tau$_{P301L}$/*Efhd2*$^{-/-}$ mice. The findings also show that the absence of EFhd2 did not induce noticeable changes on the temporal appearance of phenotypic signs of neurodegeneration.

Figure 4.4B illustrates the analysis of longitudinal pathological phenotype scores in males among the four genotypes. Mixed factor RM-ANOVA detected a medium interaction effect between age and genotype ($F_{(9, 153)} = 2.328$ p=0.0174, η^2_p=0.12) . A small main effect of genotype ($F_{(3, 51)} = 0.8907$ p=0.4523, η^2_p=0.04) and age ($F_{(2.519, 128.5)} = 1.310$ p=0.2747, η^2_p=0.03) were identified among groups. Upon isolating simple main effects, we determined a negligible effect of age on phenotype scores in Non-Tg/*Efhd2*$^{+/+}$ mice ($F_{(2.711, 29.82)} = 0.01666$ p=0.995, η^2_p <0.01). Similarly, age effect was small in Non-Tg/*Efhd2*$^{-/-}$ mice ($F_{(2.267, 38.53)} = 0.7981$ p=0.47151, η^2_p= 0.04). However, the data analysis revealed a large age effect on phenotype scores in both Tau$_{P301L}$/*Efhd2*$^{+/+}$ ($F_{(1.587, 17.46)} = 2.803$ p=0.0973, η^2_p= 0.2) and Tau$_{P301L}$/*Efhd2*$^{-/-}$ mice ($F_{(2.632, 31.59)} = 2.311$ p=0.1021, η^2_p=0.16). By looking at Figure 4.4B, we can observe that the large age effect detected in Tau$_{P301L}$/*Efhd2*$^{+/+}$ and Tau$_{P301L}$/*Efhd2*$^{-/-}$ mice phenotype scores could be driven by phenotype scores at 6 months. That was confirmed when we analyzed the simple main effect of genotype at each age group. We noticed a medium genotype difference at 6 months ($F_{(3, 51)} = 2.164$ p=0.1037, η^2_p=0.11). As expected, data

analysis also showed a medium genotype effect at 12 months ($F_{(3, 51)} = 2.585$ p=0.0632, η^2_p=0.13). Corresponding to what is shown in Figure 4.4B, genotype effect was small at both 3 months ($F_{(3, 51)} = 0.2788$ p=0.8404, η^2_p=0.02) and 9 months ($F_{(3, 51)} = 0.7849$ p=0.5079, η^2_p=0.04). Interestingly, we observed a large drop in phenotype score in Tau$_{P301L}$/*Efhd2$^{-/-}$* compared to Tau$_{P301L}$/*Efhd2$^{+/+}$* mice at 6 months (p= 0.1068, Hedge's g= 0.87). In contrast, at 12 months we noticed a medium rise in phenotype scores in Tau$_{P301L}$/*Efhd2$^{-/-}$* compared to Tau$_{P301L}$/*Efhd2$^{+/+}$* mice (p= 0.3474, Hedge's g=0.5). In general, the behavioral assessment in males highlights a different longitudinal pattern when juxtaposed to female mice, which is consistent with the literature (Lewis et al., 2001; Sahara et al., 2002; Lewis & McGowan, 2005). Prior studies have shown that male Tau$_{P301L}$ mice exhibit prominent pathological phenotype beyond 12 months, whereas females typically develop neurodegeneration phenotype between 6-8 months. That largely illustrates sex-driven differences in the penetrance of P301L mutant tau. Some studies have unraveled genomic variations between male and female mice brains that plausibly underlie behavioral differences (Knoedler et al., 2022; Levy et al., 2023). In this section, we examined how the deletion of *Efhd2* gene could change the penetrance of P301L tau in males and females. The results by and large endorse a consistent age-dependent pathological phenotype in females with minimal difference between Tau$_{P301L}$/*Efhd2$^{+/+}$* and Tau$_{P301L}$/*Efhd2$^{-/-}$* mice. On the other hand, a highly variable pathological phenotype of male Tau$_{P301L}$ mice was detected in the absence of EFhd2. The marked deviation of age-dependent pathological phenotype between males and females merits further examination to determine whether a possible interaction between the deletion of *Efhd2* gene and sex exists.

A
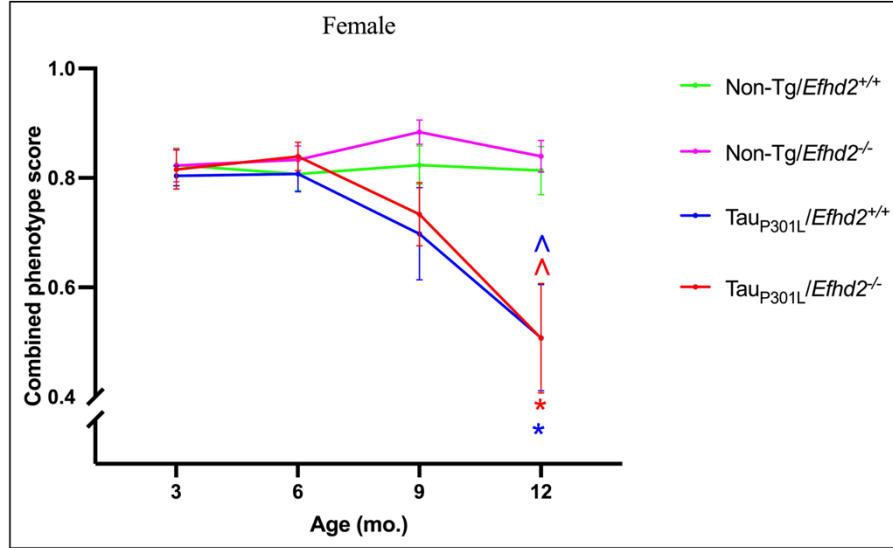
B
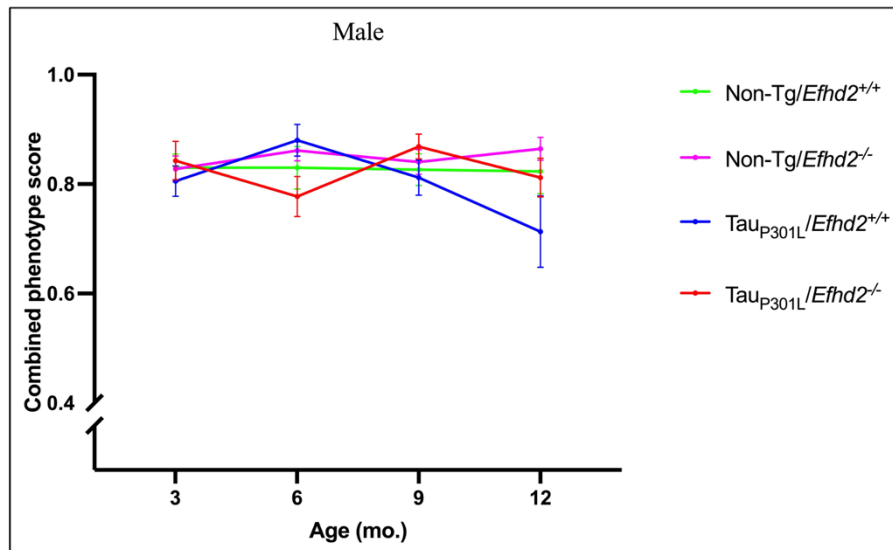
Figure 4.4. The penetrance of P301L mutant tau showed a small change with deleting *Efhd2* in females and a more variable phenotype was observed in males. NS and MIS were normalized and combined to generate a combined phenotype score (Materials and Methods). (**A**) Mixed factor RM-ANOVA for female mice detected a large interaction between genotype and age (F (9, 153) = 4.649, p<0.0001, η^2_p=0.21). By isolating simple main effects of genotype and age, Tukey's pairwise comparison detected a large reduction of phenotype scores at 12 months compared to 3 (p=0.0361, Hege's g= 1.2), 6 (p=0.0388, Hedge's g=1.2), and 9 months (p=0.023, Hedge's g= 0.6) Tau$_{P301L}$/*Efhd2*$^{+/+}$ mice (blue asterisk). Similarly, in Tau$_{P301L}$/*Efhd2*$^{-/-}$ mice, the phenotype score of 12 months was lower than each 3 (p=0.0171, Hedge's g=1.1), 6 (p=0.0171, Hedge's g=1.2), and 9 months (p=0.0359, Hedge's g=0.74. (red asterisk). Negligible (p=0.9680, η^2_p <0.01) and medium (p=0.3249, η^2_p= 0.08) differences were identified within

Figure 4.4 (cont'd)

Non-Tg/*Efhd2*$^{+/+}$ and Non-Tg/*Efhd2*$^{-/-}$, respectively, which further supports that the absence of EFhd2 does not induce age-dependent behavioral phenotype. Furthermore, at 12 months, phenotype score of Tau$_{P301L}$/*Efhd2*$^{+/+}$ mice was lower compared to Non-Tg/*Efhd2*$^{+/+}$ mice (p= 0.0233, Hedge's g= 1.2) and Non-Tg/*Efhd2*$^{-/-}$ mice (p=0.0135, Hedge's g= 1.4) (blue caret) by Tukey's post hoc analysis. Moreover, 12 months Tau$_{P301L}$/*Efhd2*$^{-/-}$ mice exhibited a large decrease in phenotype score compared to Non-Tg/*Efhd2*$^{+/+}$ mice (p=0.0164, Hedge's g=1) and Non-Tg/*Efhd2*$^{-/-}$ mice (p=0.0092, Hedge's g=1.2) (red caret). The absence of EFhd2, hence, did not change temporal decline of behavioral phenotype in Tau$_{P301L}$ mice. n=12-15. (**B**) Mixed factor RM-ANOVA for male mice detected a medium interaction between genotype and age (F$_{(9, 153)}$ = 4.649, p=0.0174, η^2_p=0.12). Isolating simple main effects revealed a medium difference at 6 months among the four genotypes (F$_{(3, 51)}$ = 2.164 p=0.1037, η^2_p=0.11). Furthermore, data analysis showed a medium genotype effect at 12 months (F$_{(3, 51)}$ = 2.585 p=0.0632, η^2_p=0.13). Tukey's post hoc analysis detected a large reduction in pathological phenotype score in Tau$_{P301L}$/*Efhd2*$^{-/-}$ compared to Tau$_{P301L}$/*Efhd2*$^{+/+}$ mice at 6 months (p= 0.1068, Hedge's g= 0.87). In contrast, at 12 months we noticed a medium rise in phenotype scores in Tau$_{P301L}$/*Efhd2*$^{-/-}$ compared to Tau$_{P301L}$/*Efhd2*$^{+/+}$ mice (p= 0.3474, Hedge's g=0.5). The results confirm that Tau$_{P301L}$ mice manifest a largely variable age-dependent pathological phenotype before 12 months induced by deleting Efhd2. n=12-16. Error bars indicate mean ± SEM.

Assessment of pathological tau markers in Tau$_{P301L}$/*Efhd2*$^{-/-}$ mice

In this section, we investigated neuropathological changes in the absence of EFhd2 in Tau$_{P301L}$ mice. We decided to assess pathological tau markers in female mice given their consistent age-dependent pathological phenotype (Figure 4.4A) as opposed to the males that exhibited a variable longitudinal phenotype (Figure 4.4B). In doing so, we evaluated whether the effect of EFhd2 on the age-dependent pathological phenotype aligns with molecular pathological changes. We conducted histological and biochemical analysis for pathological tau markers at 6 and 12 months of female Tau$_{P301L}$/*Efhd2*$^{+/+}$ and Tau$_{P301L}$/*Efhd2*$^{-/-}$ mice. We particularly chose these two age groups for further analysis because they could model pathological events that take place in human tauopathies. In particular, scientists and clinicians agree that pathological accumulation of tau aggregates precede clinical symptoms by years or even decades. As such, by investigating pathological tau markers at 6 months (unnoticeable neurodegenerative phenotype) and 12 months (prominent neurodegenerative phenotype), we will gain deeper insights on the influence of the absence of EFhd2 on the progressive tau accumulation.

First, we investigated a well-known disease-specific phosphorylated tau marker, pSer422, using IF and western blot (Figures 4.5 and 4.6). pSer422, as the name denotes, is a C-terminal phosphorylation site at serine residue 422 (Morishima-Kawashima et al., 1995). Previous studies

have suggested that pSer422 modified tau hardly exists in normal brains, whereas its level remarkably increases in tauopathies brains (Hasegawa et al., 1996; Bussiere et al., 1999). Thus, pSer422 is a disease-specific pathological tau marker. Furthermore, pSer422 tau level correlates with disease progression and cognitive decline (Vana et al., 2011; Mufson et al., 2014; Kanaan et al., 2016). Immunohistochemistry-based studies on human tauopathy brains and other P301L expressing mice models substantiate pSer422 tau as a marker for intermediate and late aggregation stages (Kimura et al., 1996; Bussiere et al., 1999; Götz et al., 2001; Augustinack et al., 2002; Deters et al., 2008; Neddens et al., 2018). Strictly speaking, in the linear model of NFTs maturity, phosphorylation of tau at Ser422 reflects fibrillar and mature tangles formation with unnoticeable detection in the pretangle neurons. Typically, pretangle neurons stained by phosphorylated tau markers appear as granular or diffuse perinuclear labeling (Bancher et al., 1989; Duong et al., 1993; Braak et al., 1994).

As noted earlier, pathological tau accumulation predominates primarily in spinal cord and brainstem region along with diencephalon and telencephalon regions (Lewis et al., 2000; Lewis & McGowan, 2005). With advanced age, NFTs become the main pathological feature in brainstem and spinal cord. In addition, tau depositions akin to pretangle aggregates develop later in cortex, hippocampus, and basal ganglia (Lewis et al., 2000). In our study, we confirmed that the deletion of *Efhd2* gene did not change the selective vulnerability of brain regions as seen in Figure A4.3. By comparing Tau$_{P301L}$/*Efhd2*$^{+/+}$ and Tau$_{P301L}$/*Efhd2*$^{-/-}$ mice, we observed no differences in the pervasion of tau depositions in different brain regions. The absence of differences in brain region vulnerability was also affirmed with other pathological tau markers tested in this study.

Then, to analyze differences in stained areas, we quantified brainstem (BS) and cortex (CTX). Figure 4.5 represents fluorescent staining of pSer422 tau in 6 and 12 months Tau$_{P301L}$/*Efhd2*$^{+/+}$ and Tau$_{P301L}$/*Efhd2*$^{-/-}$ mice in BS and CTX. We observed minimal pSer422 tau reactivity in BS of 6 months mice with imperceptible difference between Tau$_{P301L}$/*Efhd2*$^{-/-}$ and Tau$_{P301L}$/*Efhd2*$^{+/+}$ tissues (Figure 4.5A). pSer422 appears as sparse staining in this age group. In contrast, pervasive pSer422 staining nearly covers the entire BS region of 12 months Tau$_{P301L}$/*Efhd2*$^{+/+}$ and Tau$_{P301L}$/*Efhd2*$^{-/-}$ mice as presented in Figure 4.5B. pSer422 staining was quantified as percent of stained area and analyzed to evaluate the differences among groups (Figure 4.5C). Two-way ANOVA detected a small interaction between age and genotype (F (1,

18) = 0.4025 p=0.5338, η^2_p=0.02) in pSer422 staining percent area. Furthermore, data analysis confirmed a large main effect of age (F (1, 18) = 10.06 p=0.0053, η^2_p=0.36). In contrast, the main effect of genotype was small (F (1, 18) = 0.3682 p=0.5515, η^2_p= 0.02). Post hoc pairwise analysis by Holm-Šídák indicated that pSer422 percent staining area rose at 12 months Tau$_{P301L}$/*Efhd2*$^{+/+}$ mice compared to 6 months group (p= 0.0641, Hegde's g=1.7) (Figure 4.5C). By the same token, we noticed a large increase in pSer422 reactivity in 12 months Tau$_{P301L}$/*Efhd2*$^{-/-}$ mice compared to 6 months group (p= 0.2327, Hedge's g=1.1). As we can see in Figure 4.5C, the absence of EFhd2 induced a small change in pSer422 staining area in 6 months (p= 0.9859, Hedge's g=0.2) and 12 months (p= 0.3438, Hedge's g=0.4). Hence, the absence of EFhd2 did not cause a marked change in the extent of pSer422 staining area neither at 6 months nor at 12 months age groups of Tau$_{P301L}$ expressing mice.

We also collected cross-sectional behavioral data from the 6- and 12-months mice (Figure 4.2). Since motor function is principally regulated by BS, we conducted a correlation analysis between MIS of Tau$_{P301L}$/*Efhd2*$^{+/+}$ mice and pSer422 staining area in BS. The analysis yielded a very strong correlation (r= 0.94, p<0.0001). This result aligns with previously published reports on Tau$_{P301L}$ mice demonstrating an association between motor impairment and increased pathology with age (Lewis et al., 2000; Lewis et al., 2001; Sahara et al., 2002; Lewis & McGowan, 2005). However, Spearman correlation analysis indicated a medium correlation between MIS and pSer422 staining area in the BS of Tau$_{P301L}$/*Efhd2*$^{-/-}$ mice (r= 0.5353, p= 0.0926). Interestingly, the data suggest that deleting *Efhd2* gene weakened the relation between pSer422 tau and motor impairment.

In the CTX, pSer422 follows a different pattern than what was observed in the BS. In Figure 4.5D, we can see pSer422 staining in the CTX of 6 months age group as puncta. Moreover, neuronal soma and processes show reactivity to pSer422 in the CTX of 12 months as demonstrated in Figure 4.5E. To analyze the difference among groups in pSer422 staining percent area, two-way ANOVA was conducted (Figure 4.5F). The results showed a small interaction between age and genotype (F (1, 18) = 0.7881 p=0.3864, η^2_p=0.04). Furthermore, the analysis detected a large main effect of age (F (1, 18) = 3.673 p=0.0713, η^2_p=0.17). On the other hand, we noticed a medium genotype effect (F (1, 18) = 1.270 p=0.2746, η^2_p=0.07) on pSer422 percent area in the CTX (Figure 4.5F). Further data analysis demonstrated that age-dependent increase of pSer422 staining area is maintained in Tau$_{P301L}$/*Efhd2*$^{+/+}$ mice (p= 0.2421, Hedge's

g=0.9) and Tau$_{P301L}$/*Efhd2*$^{-/-}$ mice (p= 0.9203, Hedge's g=1). Furthermore, the findings indicate a large reduction of the pSer422 staining area at 6 months in the CTX of Tau$_{P301L}$/*Efhd2*$^{-/-}$ compared to Tau$_{P301L}$/*Efhd2*$^{+/+}$ mice (p= 0.9998, Hedge's g= 0.9). Importantly, a medium-large reduction of pSer422 staining area in the CTX of Tau$_{P301L}$/*Efhd2*$^{-/-}$ mice was detected in comparison to Tau$_{P301L}$/*Efhd2*$^{+/+}$ mice (p= 0.4323, Hedge's g= 0.69). By looking at Figures 4.5C and 4.5F, we can deduce a differential effect of deleting *Efhd2* gene on pSer422 tau in BS and CTX. According to a previous report, EFhd2 has higher expression in the CTX (Purohit et al., 2014). That may explain why we noticed a more noticeable effect on pSer422 tau due to deleting *Efhd2* in the CTX.

Nesting performance is regulated by cortical and hippocampal regions. Hence, we conducted a correlation analysis between NS and pSer422 staining area in the CTX. Analogous to correlation results of BS, NS are strongly correlated with pSer422 positive area in the CTX of Tau$_{P301L}$/*Efhd2*$^{+/+}$ mice (r= -0.7426, p= 0.0114). Yet, the results confirmed a weak correlation between NS and pSer422 positive area in the CTX of Tau$_{P301L}$/*Efhd2*$^{-/-}$ mice (r= -0.2655, p= 0.4268). Clearly, the strong correlation between the behavioral performance (motor function and nesting) and pSer422 staining area in both BS and CTX is disrupted by deleting *Efhd2* gene in Tau$_{P301L}$/*Efhd2*$^{-/-}$ mice.
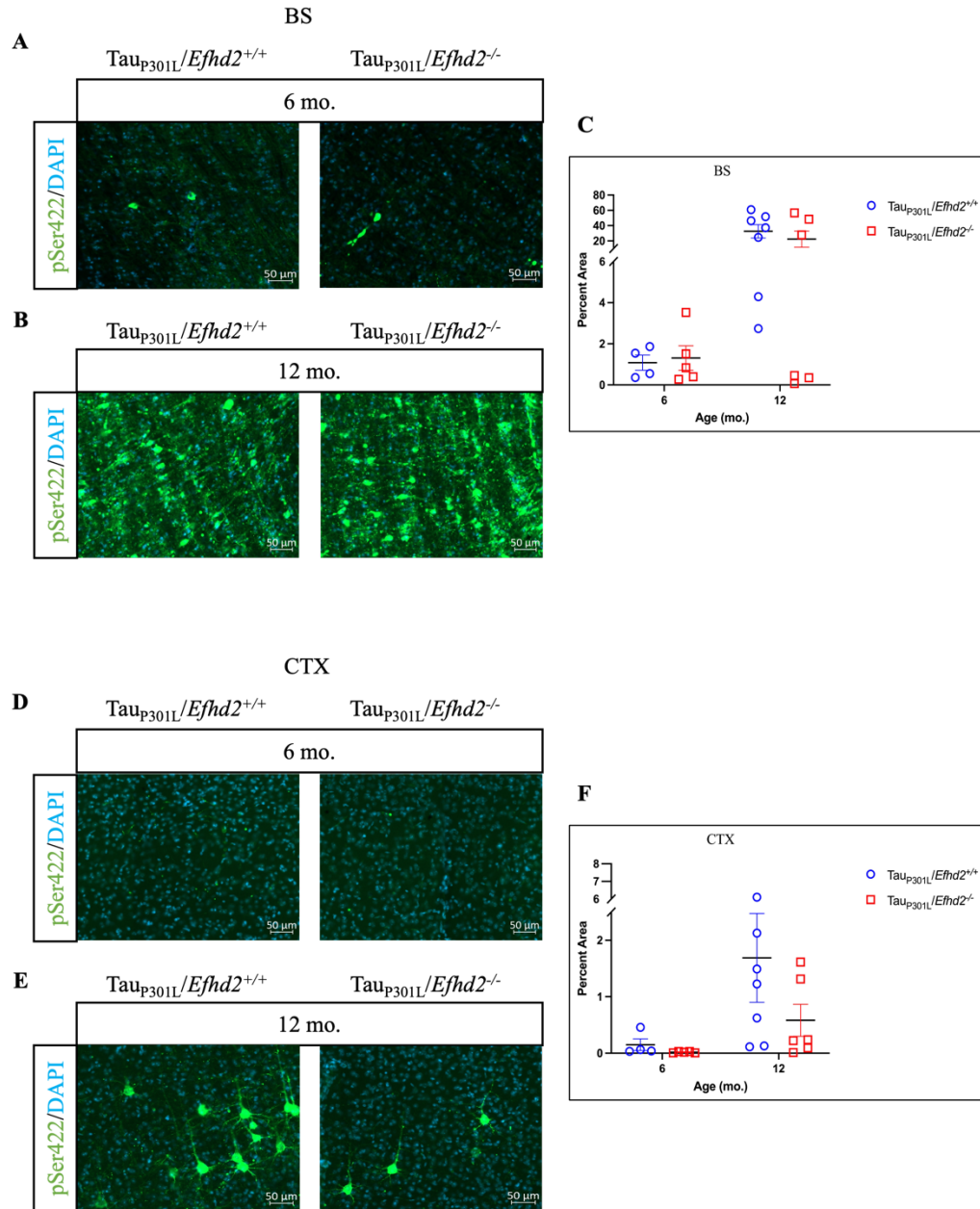
Figure 4.5. The absence of EFhd2 induced a brain-region specific effect on pSer422 tau staining area. Right hemispheres from 6- and 12-month-old females Tau$_{P301L}$/*Efhd2*$^{+/+}$ and Tau$_{P301L}$/*Efhd2*$^{-/-}$ mice (n= 4-7/group) were processed for immunofluorescence analysis of pSer422 modified tau marker (green) and DAPI (blue) in brainstem (BS) panels A and B and cortex (CTX) panels D and E. (**A**) Representative pSer422 immunofluorescent images for 6-month-old female Tau$_{P301L}$/*Efhd2*$^{+/+}$ and Tau$_{P301L}$/*Efhd2*$^{-/-}$ mice BS. (**B**) Representative pSer422 immunofluorescent images in BS of 12-month-old female Tau$_{P301L}$/*Efhd2*$^{+/+}$ and Tau$_{P301L}$/*Efhd2*$^{-/-}$ mice. (**C**) Quantification of pSer422 immunofluorescence was completed using HALO software and statistical analysis was conducted using two-way ANOVA that showed a small interaction between age and genotype (F (1, 18) = 0.4025 p=0.5338, η^2_p=0.02). The analysis showed a large main effect of age is significant (F (1, 18) = 10.06 p=0.0053, η^2_p=0.36) and a small main effect of genotype on percent area (F (1, 18) = 0.3682 p=0.5515, η^2_p=0.02).

206

Figure 4.5 (cont'd)
Holm-Šídák post hoc analysis indicated an increase in the percent area of pSer422 staining in Tau$_{P301L}$/*Efhd2*$^{+/+}$ 12 months in comparison to 6 months mice (p= 0.0641, Hegde's g=1.7). pSer422 percent area in Tau$_{P301L}$/*Efhd2*$^{-/-}$ 12 months mice was also higher than 6 months (p= 0.2327, Hedge's g=1.1). (**D**) Representative pSer422 immunofluorescent images for 6-month-old female Tau$_{P301L}$/*Efhd2*$^{+/+}$and Tau$_{P301L}$/*Efhd2*$^{-/-}$ mice in the CTX. (**E**) Representative pSer422 immunofluorescent images in CTX of 12-month-old female Tau$_{P301L}$/*Efhd2*$^{+/+}$ and Tau$_{P301L}$/*Efhd2*$^{-/-}$ mice. (**F**) Two-way ANOVA analysis for pSer422 percent area in the CTX: small interaction between age and genotype (F (1, 18) = 0.7881 p=0.3864, η^2_p=0.04). Furthermore, a large main effect of age (F (1, 18) = 3.673 p=0.0713, η^2_p=0.17) and a medium genotype effect (F (1, 18) = 1.270 p=0.2746, η^2_p=0.07) were confirmed. A large age-dependent increased pSer422 reactivity was detected in Tau$_{P301L}$/*Efhd2*$^{+/+}$ (p= 0.2421, Hedge's g=0.9) and Tau$_{P301L}$/*Efhd2*$^{-/-}$ mice (p= 0.9203, Hedge's g=1). pSer422 staining area was lower at 6 months Tau$_{P301L}$/*Efhd2*$^{-/-}$ mice than Tau$_{P301L}$/*Efhd2*$^{+/+}$ mice (p= 0.9998, Hedge's g= 0.9). At 12 months, pSer422 staining area moderately declined in the CTX of Tau$_{P301L}$/*Efhd2*$^{-/-}$ compared to Tau$_{P301L}$/*Efhd2*$^{+/+}$ mice (p= 0.4323, Hedge's g= 0.69). Error bars indicate mean ± SEM.

In addition to histological assessment of pSer422 tau, we conducted biochemical analysis by western blot on the entire left hemisphere. We showed before the association between EFhd2 and sarkosyl-insoluble high molecular weight tau aggregates (Vega et al., 2008; Ferrer-Acosta et al., 2013b). Moreover, our previous studies provided evidence that this association is not contingent upon phosphorylation states of tau (Vega et al., 2008; Ferrer-Acosta et al., 2013b; Vega et al., 2018; Vega et al., 2019). Therefore, in this study, we used western blotting to biochemically characterize the impact of the absence of EFhd2 on these tau species. First, we measured total tau using the Tau13 antibody in 6 and 12 months as shown in Figure 4.6. We did not observe a difference in 55 kDa tau species in S1 (soluble tau fraction) among all mice in 6 and 12 months (Figure 4.6A and B). That further supports that deleting *Efhd2* gene did not influence basal level of tau protein. However, 64 kDa tau that is predominantly detected in P3 fraction, shows a stronger intensity in 12 months compared to 6 months mice (arrowheads in Figure 4.6A and B). In fact, the 64 kDa tau represents higher order multimeric and filamentous pathological tau species that accumulate with aging and correlate with behavioral deficit in JNPL3 mice and human tauopathies (Sahara et al., 2002; Berger et al., 2007; Ren & Sahara, 2013). Herein, we quantified the 64 kDa species in the P3 fraction of Tau13. Statistical analysis of 64 kDa total tau by two-way ANOVA showed a small interaction between age and genotype (F (1, 18) = 0.9325 p=0.3470, η^2_p=0.05). A large main effect of age on the signal of 64 kDa total tau was detected (F (1, 18) = 18.83 p=0.0004, η^2_p=0.51). The analysis also demonstrated a medium main effect of genotype (F (1, 18) = 2.417 p=0.1374, η^2_p= 0.12). Holm-Šídák post hoc

pairwise comparison revealed a large increase in 64 kDa tau in 12 months Tau_{P301L}/*Efhd2*$^{+/+}$ mice in comparison to 6 months group (p= 0.0067, Hedge's g=2.2) as seen in Figure 4.6C. Likewise, 12 months Tau_{P301L}/*Efhd2*$^{-/-}$ mice showed higher signal of 64 kDa tau compared to 6 months group (p= 0.0757, Hedge's g=1.5) (Figure 4.6C.). Moreover, the data analysis points to a large reduction of 64 kDa tau at 6 months in Tau_{P301L}/*Efhd2*$^{-/-}$ mice compared to Tau_{P301L}/*Efhd2*$^{+/+}$ mice (p=0.7065, Hedge's g=1.2). This reduction seemed consistent at 12 months Tau_{P301L}/*Efhd2*$^{-/-}$ mice when compared to Tau_{P301L}/*Efhd2*$^{+/+}$ mice (p= 0.1238, Hedge's g=0.8).

Western blotting of pSer422 tau indicated the absence of either 55 or 64 kDa tau species in all 6 months mice (Figure 4.6A). In contrast, 64 kDa of pSer422 tau was identified in the P3 fraction of a few mice at 12 months (Figure 4.6B arrowheads). Indeed, these data recapitulate previous findings on JNPL3 mice showing the absence of 55 or 64 kDa pSer422 at young ages in S1 fraction (Sahara et al., 2002). We can see in Figure 4.6 that not all higher order 64 kDa tau species depicted as Tau13 contain pSer422 positive tau species. In simpler terms, pathological tau aggregates are an ensemble of different phases of aggregation events and possibly different levels of neurotoxicity. Two-way ANOVA was conducted to compare the 64 kDa pSer422 among groups, and a negligible interaction between age and genotype was confirmed (F (1, 18) = 0.009426 p=0.9237, η^2_p <0.01). Moreover, we detected a large main effect of age (F (1, 18) = 3.865 p=0.0649, η^2_p=0.18) . However, a negligible genotype effect was detected (F (1, 18) = 0.009426 p=0.9237, η^2_p <0.01). The difference between Tau_{P301L}/*Efhd2*$^{+/+}$ and Tau_{P301L}/*Efhd2*$^{-/-}$ mice at 12 months was negligible (p= 0.9858, Hedge's g=0.06).

To summarize, histological and biochemical analysis substantiated age-dependent increase in pSer422 tau in both Tau_{P301L}/*Efhd2*$^{+/+}$ and Tau_{P301L}/*Efhd2*$^{-/-}$ mice. In addition, the absence of EFhd2 led to a conspicuous reduction in pSer422 staining area in the cortex of old Tau_{P301L}/*Efhd2*$^{-/-}$ mice compared to wild type littermates. Consistently, the data showed a large decrease in insoluble Tau13 species in old Tau_{P301L}/*Efhd2*$^{-/-}$ mice. All in all, the absence of EFhd2 may have reduced pathological tau markers that label later aggregation events.
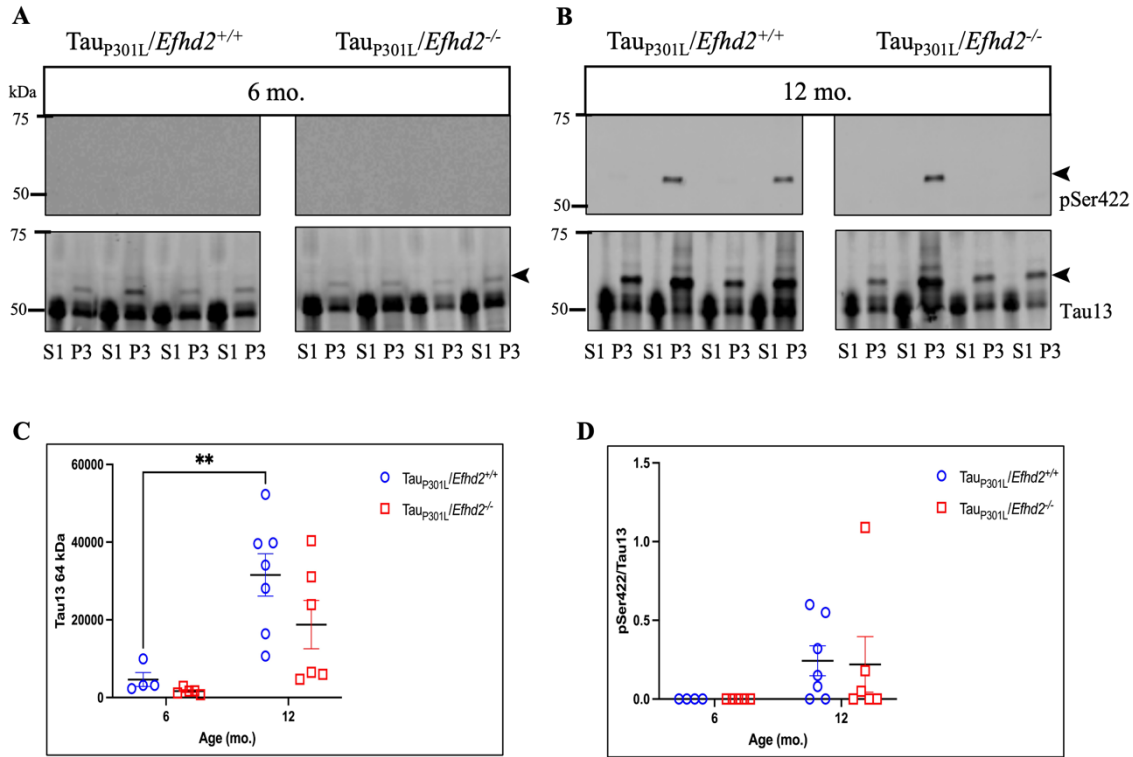
Figure 4.6. The absence of EFhd2 induced a large reduction of insoluble Tau13 species in old mice with no detectable change in pSer422 tau. Left hemisphere of females Tau$_{P301L}$/*Efhd2$^{+/+}$* and Tau$_{P301L}$/*Efhd2$^{-/-}$* mice at 6 months (panel A) and 12 months (panel B) were homogenized . S1 soluble and P3 sarkosyl-insoluble fraction were analyzed by western blot (n=4-7). (**A**) Western blot for Tau$_{P301L}$/*Efhd2$^{+/+}$* and Tau$_{P301L}$/*Efhd2$^{-/-}$* mice at 6 months probed for pSer422 top and Tau13 bottom. Arrowhead denotes 64 kDa pathological tau species emerging in P3. (**B**) Western blot for Tau$_{P301L}$/*Efhd2$^{+/+}$* and Tau$_{P301L}$/*Efhd2$^{-/-}$* mice at 12 months probed for pSer422 top and tau13 bottom. Arrowhead denotes 64 kDa pathological tau species. (**C**) quantification of Tau13 64 kDa in P3 fraction as absolute arbitrary units. Analysis by two-way ANOVA showed a small interaction (F (1, 18) = 0.9325 p=0.3470, η^2_p=0.05). A large main effect of age on the signal of 64 kDa total tau was detected (F (1, 18) = 18.83 p=0.0004, η^2_p=0.51) along with a medium main effect of genotype (F (1, 18) = 2.417 p=0.1374, η^2_p= 0.12). Holm-Šídák post hoc analysis revealed a higher 64 kDa signal in Tau$_{P301L}$/*Efhd2$^{+/+}$* mice at 12 months than 6 months (p= 0.0067, Hedge's g=2.2). The 64 kDa Tau13 was also higher in 12 months Tau$_{P301L}$/*Efhd2$^{-/-}$* mice compared to 6 months (p= 0.0757, Hedge's g=1.5). Moreover, 64 kDa tau at 6 months in Tau$_{P301L}$/*Efhd2$^{-/-}$* mice reduced compared to Tau$_{P301L}$/*Efhd2$^{+/+}$* mice (p=0.7065, Hedge's g=1.2). Similarly, at 12 months 64 kDa signal showed a large decline in Tau$_{P301L}$/*Efhd2$^{-/-}$* when compared to Tau$_{P301L}$/*Efhd2$^{+/+}$* mice (p=0.1238, Hedge's g=0.8). (**D**) quantification of pSer422/Tau13 64 kDa in P3 as relative arbitrary units analyzed by two-way ANOVA a small interaction between age and genotype was confirmed (F (1, 18) = 0.009426 p=0.9237, η^2_p <0.01). The main effect of age was large (F (1, 18) = 3.865 p=0.0649, η^2_p=0.18). However, a negligible genotype effect was detected (F (1, 18) = 0.009426 p=0.9237, η^2_p <0.01). The analysis demonstrated a negligible difference between Tau$_{P301L}$/*Efhd2$^{+/+}$* and Tau$_{P301L}$/*Efhd2$^{-/-}$* mice at 12 months (p= 0.9858, Hedge's g=0.06). p **<0.01. Error bars indicate mean ± SEM. Immunoblots were cropped.

To further characterize the accumulation of pathological tau, we also investigated the difference in age-dependent accumulation of PHF1 between $Tau_{P301L}/Efhd2^{-/-}$ and $Tau_{P301L}/Efhd2^{+/+}$ mice by IF and western blot. Physiologically, PHF1 (phosphorylated serine 396 and 404) tau exists at certain levels in normal brains, but it shows marked increase in tauopathies (Greenberg et al., 1992; Otvos et al., 1994; Hasegawa et al., 1996; Kyalu Ngoie Zola et al., 2023). Some studies demonstrated that PHF1 positive tau emerges later than pSer422 labeling NFTs and to a less extent the ghost tangles (Kimura et al., 1996; Augustinack et al., 2002; Moloney et al., 2021). It is widely accepted that PHF1 signal correlates with later stages of pathological tau accumulation (Moloney et al., 2021).

In line with pSer422 tau, IF for PHF1 in BS indicates the difference between the 6- and 12-months groups. As anticipated, at 6 months, PHF1 is hardly detected in BS (Figure 4.7A). We statistically analyzed PHF1 staining percent area to determine whether a difference between $Tau_{P301L}/Efhd2^{+/+}$ and $Tau_{P301L}/Efhd2^{-/-}$ mice exists. Two-way ANOVA revealed a small interaction between age and genotype ($F_{(1, 18)} = 0.5867$ p=0.4536, η^2_p=0.03). Additionally, the analysis demonstrated a large main effect of age in PHF1 staining ($F_{(1, 18)} = 5.036$ p=0.0376, η^2_p=0.22). Accordingly, Holm-Šídák pairwise comparison confirmed that PHF1 in $Tau_{P301L}/Efhd2^{+/+}$ mice exhibited a large increase in reactivity at 12 months compared to 6 month-group (Figure 4.7C) (p=0.1883, Hedge's g=1.55). Similarly, statistical comparison between $Tau_{P301L}/Efhd2^{-/-}$ 6- and 12-months mice (Figure 4.7B) detected a medium difference in PHF1 staining percent area (p=0.6593, Hedge's g=0.57). Importantly, the analysis demonstrated a negligible main effect of genotype ($F_{(1, 18)} = 0.006050$ p=0.9389, η^2_p <0.01). That indicates that the absence of EFhd2 did not alter the level of PHF1 staining in the BS of Tau_{P301L} mice. Correlation analysis between MIS of $Tau_{P301L}/Efhd2^{+/+}$ mice and PHF1 staining area in BS revealed a strong correlation (r= 0.79, p= 0.0068). Likewise, a strong correlation between MIS and PHF1 staining area in the BS of $Tau_{P301L}/Efhd2^{-/-}$ (r= 0.67, p= 0.0292) was detected. Unlike pSer422, deleting *Efhd2* gene did not largely affect the relation between PHF1 and motor impairment.

We also quantified PHF1 staining percent area in the CTX as shown in Figure 4.7D-F. We noticed little to no PHF1 positive staining in CTX of 6 months of both genotypes (Figure 4.7D). By statistically analyzing PHF1 staining percent area using two-way ANOVA, we detected a small interaction between age and genotype ($F_{(1, 18)} = 0.8084$ p=0.3805, η^2_p=0.04).

Furthermore, the analysis demonstrated a medium main effect of age ((F (1, 18) = 1.625 p=0.218, η^2_p=0.08) among groups. Similar to BS, genotype main effect of PHF1 staining area was small (F (1, 18) = 0.7560 p=0.3960, η^2_p=0.04) as illustrated in Figure 4.7F. Further analysis detected a large increase in PHF1 staining area in the CTX of Tau$_{P301L}$/*Efhd2*$^{-/-}$ mice at 12months compared to 6 months (p= 0.9559, Hedge's g=0.96). In addition, PHF1 staining area in the CTX of 12 months Tau$_{P301L}$/*Efhd2*$^{+/+}$ mice exhibited a medium increase than the 6 months group (p=0.4733, Hedge's g=0.67). A medium-large reduction in PHF1 staining was revealed comparing Tau$_{P301L}$/*Efhd2*$^{-/-}$ to Tau$_{P301L}$/*Efhd2*$^{+/+}$ mice at 12 months (p= 0.4733, Hedge's g=0.6). Additionally, we determined a strong correlation between NS and PHF1 staining area in the CTX of Tau$_{P301L}$/*Efhd2*$^{+/+}$ (r= -0.6333, p= 0.0407). By contrast, the results showed a weak correlation between NS and PHF1 positive area in the CTX of Tau$_{P301L}$/*Efhd2*$^{-/-}$ (r= -0.3387, p= 0.3058). The findings indicate that deleting the *Efhd2* gene weakened the correlation between nesting performance and PHF1 staining area in the CTX.

Western blot analysis of the PHF1 signal age-dependent difference in PHF1 signal in 64 kDa pathological tau species in P3 fraction (Figure 4.8). The PHF1 signal in the S1 fraction was comparable across all mice. Previously, it was reported that 64 kDa PHF1 in P3 are low in young mice with normal behavior but progressively rises with age and advancing neurodegeneration (Sahara et al., 2002; Kametani et al., 2020). We quantified and analyzed the difference in PHF1 64 kDa in P3 using two-way ANOVA. The analysis revealed a small interaction between age and genotype (F (1, 18) = 0.1296 p=0.7230, η^2_p=0.01). Furthermore, a large main effect of age existed among groups (F (1, 18) = 10.29 p=0.0049, η^2_p=0.36). Holm-Šídák pairwise comparison showed a large increase of PHF1 signal in 12 months Tau$_{P301L}$/*Efhd2*$^{+/+}$ mice compared to 6 months group (p= 0.0897, Hedge's g=1.9) (Figure 4.8C). In Tau$_{P301L}$/*Efhd2*$^{-/-}$ mice, PHF1 signal at 12 months was higher than that observed in 6 months mice (p=0.0553) (Figure 4.8C). Given the undetectable signal of PHF1 in 6 months Tau$_{P301L}$/*Efhd2*$^{-/-}$ mice, we could not calculate Hedge's g effect size. Moreover, the analysis detected a small main effect of genotype (F (1, 18) = 0.2214 p=0.6436, η^2_p=0.01). In essence, the age-dependent accumulation of PHF1 tau compares well with previous studies. Consistent with pSer422 positive tau, PHF1 tau declined in old Tau$_{P301L}$/*Efhd2*$^{-/-}$ compared to wildtype, thereby pointing to a possible reduced formation of late tangles.
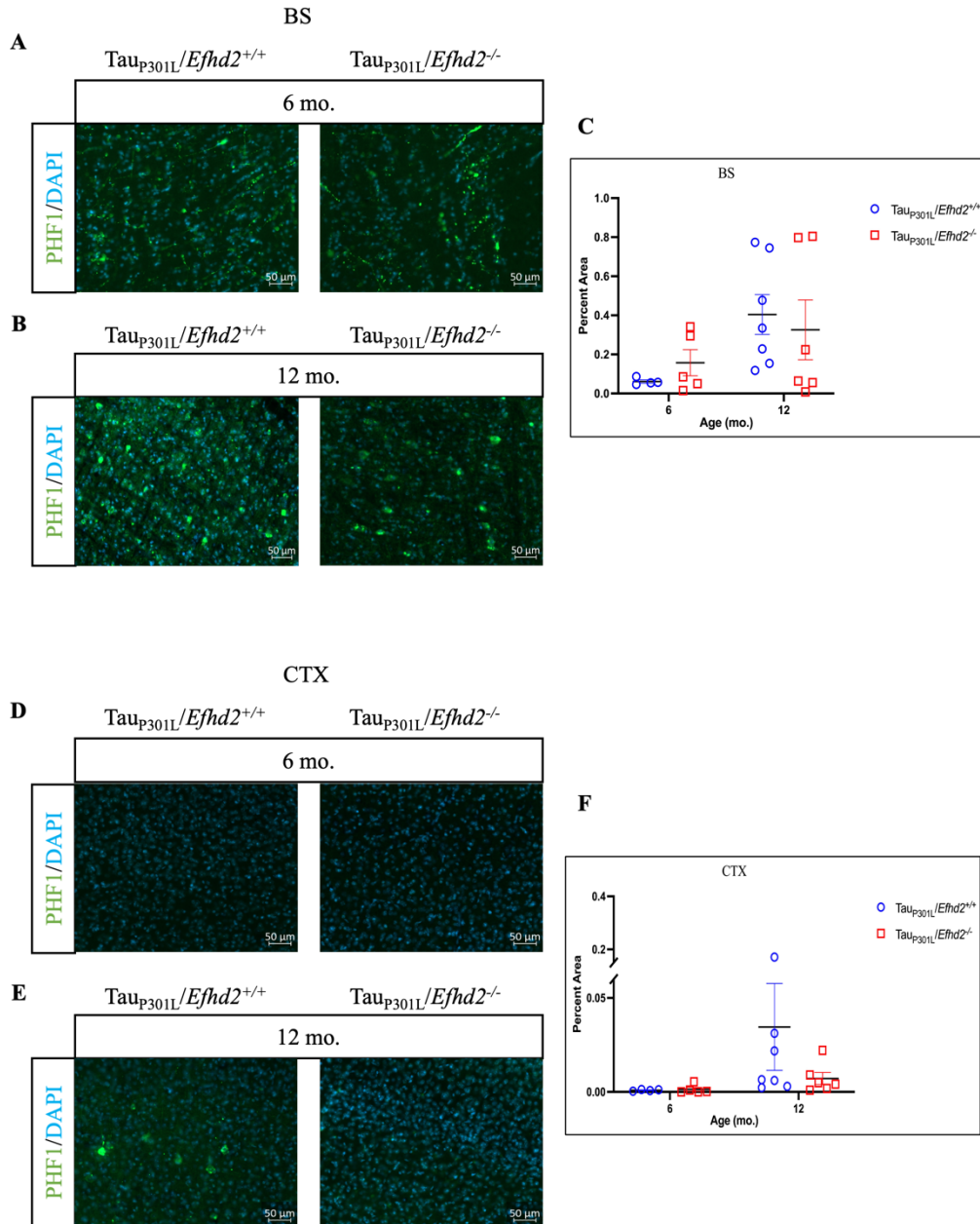
Figure 4.7. *Efhd2* **deletion caused a medium-large reduction of PHF1 staining area in the cortex of old Tau$_{P301L}$ mice**. Right hemispheres from 6- and 12-month-old females Tau$_{P301L}$/*Efhd2$^{+/+}$* and Tau$_{P301L}$/*Efhd2$^{-/-}$* mice (n= 4-7/group) were processed for immunofluorescence analysis of PHF1 modified tau marker (green) and DAPI (blue) in brainstem (BS) panels A and B and cortex (CTX) panels D and E. (**A**) Representative PHF1 immunofluorescent images for 6-month-old female Tau$_{P301L}$/*Efhd2$^{+/+}$*and Tau$_{P301L}$/*Efhd2$^{-/-}$* mice in BS. (**B**) Representative PHF1 immunofluorescent images in BS of 12-month-old female Tau$_{P301L}$/*Efhd2$^{+/+}$* and Tau$_{P301L}$/*Efhd2$^{-/-}$* mice. (**C**) Quantification of PHF1 immunofluorescence was completed using HALO software and statistical analysis was conducted using two-way ANOVA showed a small interaction between age and genotype

Figure 4.7 (cont'd)

$(F (1, 18) = 0.5867$ p=0.4536, η^2_p=0.03). Additionally, we observed a large main effect of age in PHF1 staining $(F (1, 18) = 5.036$ p=0.0376, η^2_p=0.22). Holm-Šídák pairwise comparison confirmed that PHF1 in $Tau_{P301L}/Efhd2^{+/+}$ mice exhibited higher PHF1reactivity at 12 months compared to 6 months (p= 0.1883, Hedge's g=1.55). Similarly, PHF1 staining percent area is higher in 12 months $Tau_{P301L}/Efhd2^{-/-}$ mice than at 6 month- group (p= 0.6593, Hedge's g=0.57). Importantly, the analysis demonstrated a negligible main effect of genotype $(F (1, 18) = 0.006050$ p=0.9389, η^2_p <0.01). (**D**) Representative PHF1 immunofluorescent images for 6-month-old female $Tau_{P301L}/Efhd2^{+/+}$and $Tau_{P301L}/Efhd2^{-/-}$ mice in CTX. (**E**) Representative PHF1 immunofluorescent images in CTX of 12-month-old female $Tau_{P301L}/Efhd2^{+/+}$ and $Tau_{P301L}/Efhd2^{-/-}$ mice. (**F**) Two-way ANOVA analysis for PHF1 percent area in the CTX: small interaction between age and genotype $(F (1, 18) = 0.8084$ p=0.3805, η^2_p=0.04), a medium main effect of age $(F (1, 18) = 1.625$ p=0.218, η^2_p=0.08), and small genotype main effect $(F (1, 18) = 0.7560$ p=0.3960, η^2_p=0.04). PHF1 staining area in the CTX of $Tau_{P301L}/Efhd2^{-/-}$ mice at 12 months is larger than 6 months group (p= 0.9559, Hedge's g=0.96). In addition, PHF1 staining area in the CTX of 12 months $Tau_{P301L}/Efhd2^{+/+}$ mice exhibited a medium increase compared to 6 months group (p= 0.4733, Hedge's g=0.67). Error bars indicate mean ± SEM.
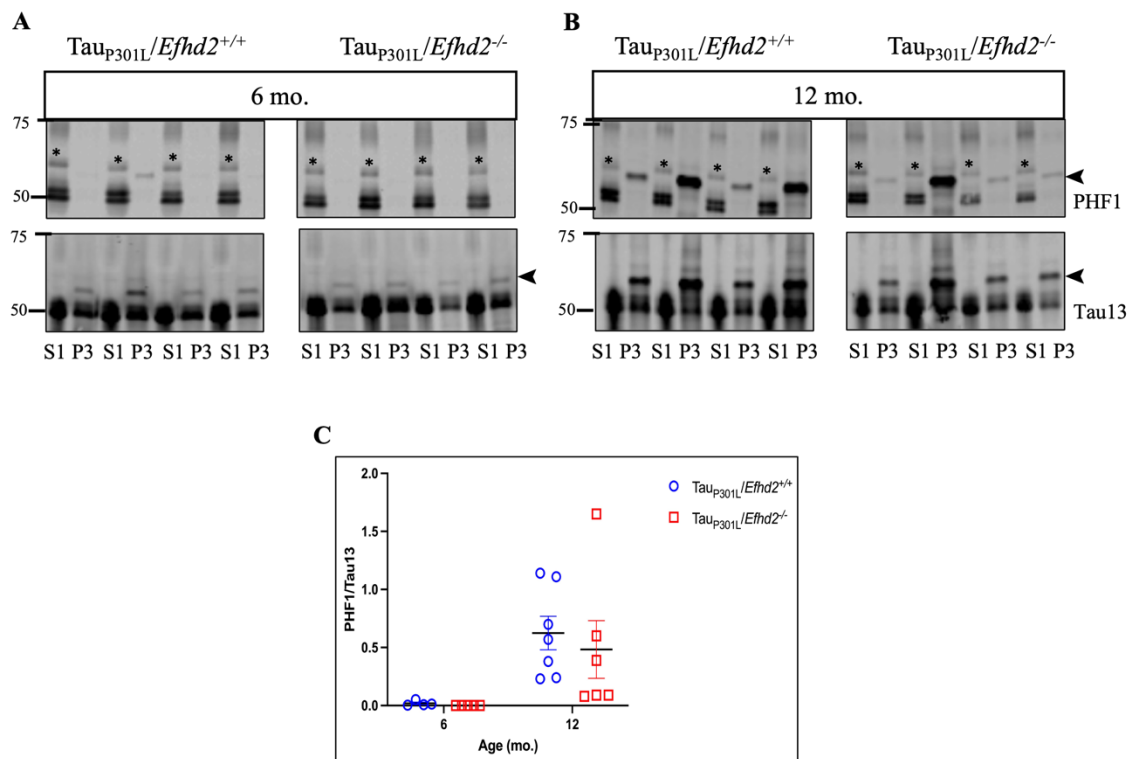
Figure 4.8. The absence of EFhd2 did not change the progressive accumulation of pathological tau species of PHF1. Left hemisphere of females $Tau_{P301L}/Efhd2^{+/+}$ and $Tau_{P301L}/Efhd2^{-/-}$ 6 months (panel A) and 12 months (panel B) were homogenized . S1 soluble and P3 sarkosyl-insoluble fraction were analyzed by western blot (n=4-7). (**A**) Western blot for $Tau_{P301L}/Efhd2^{+/+}$ and $Tau_{P301L}/Efhd2^{-/-}$ mice at 6 months probed for PHF1 top and Tau13 bottom. Arrowhead denotes 64 kDa pathological tau species emerging in P3. (**B**) Western blot for $Tau_{P301L}/Efhd2^{+/+}$ and $Tau_{P301L}/Efhd2^{-/-}$ mice at 12 months probed for PHF1 top and Tau13 bottom. Arrowhead denotes 64 kDa pathological tau species. (**C**) Quantification of PHF1/Tau13

Figure 4.8 (cont'd)
64 kDa P3 fraction as relative arbitrary unit. The analysis by two-way ANOVA showed a small interaction between age and genotype (F (1, 18) = 0.1296 p=0.7230, η^2_p=0.01). A large main effect of age existed among groups (F (1, 18) = 10.29 p=0.0049, η^2_p=0.36). PHF1 signal was higher in 12 months Tau$_{P301L}$/*Efhd2*$^{+/+}$ mice than 6 month-group (p= 0.0897, Hedge's g=1.9). In Tau$_{P301L}$/*Efhd2*$^{-/-}$ mice, we observed increased PHF1 signal at 12 months in contrast to 6 months mice (p= 0.1568). Calculating effect size was not feasible due to the very low PHF1 signal at 6 months Moreover, the analysis detected a small main effect of genotype (F (1, 18) = 0.2214 p=0.6436, η^2_p=0.01). Asterisk on PHF1 blots indicates nonspecific band due to secondary antibody binding. Error bars indicate mean ± SEM. Immunoblots were cropped.

Lastly, we interrogated changes in pathological tau conformation induced by the absence of EFhd2. In particular, we examined Alz50 positive tau inclusions. Alz50 is a conformational tau antibody that detects a discontinuous epitope formed by the folding of the N-terminus over microtubule-binding repeat domains of tau(Wolozin et al., 1986; Ksiezak-Reding et al., 1988; Goedert et al., 1991; Ksiezak-Reding et al., 1995; Carmel et al., 1996). It is widely accepted that Alz50 positive tau signifies early conformational changes that precede other modifications and aggregation events (Guillozet-Bongaarts et al., 2005). Hence, Alz50 is largely considered an early marker of pretangle aggregates (Luna-Muñoz et al., 2007; Moloney et al., 2021). Fluorescent staining for Alz50 indicated a perceptible difference between 6- and 12-month-age groups, especially in the BS (Figure 4.9). In addition, we noticed more Alz50 staining in 12 months of Tau$_{P301L}$/*Efhd2*$^{-/-}$ mice compared to 6 months in the BS (Figure 4.9A and B). In contrast, Alz50 staining is nearly comparable in 6 and 12 months Tau$_{P301L}$/*Efhd2*$^{+/+}$ mice (Figure 4.9A and B). Notably, Alz50 reactivity mostly resided in neuronal somata with almost nonexistent neuronal processes staining in both 6 and 12 months (Figure 4.9). To determine whether the noticeable difference in Alz50 staining is statistically different, we conducted two-way ANOVA to compare Alz50 staining percent area across groups. In the BS, the analysis yielded a small interaction between age and genotype ((F (1, 17) = 0.7526, p=0.3977, η^2_p=0.04). Moreover, the analysis showed a large main effect of age (F (1, 17) = 2.661 p=0.1212, η^2_p=0.14) (Figure 4.9C). The results also highlighted a medium main effect of genotype (F (1, 17) = 1.170 p=0.2945, η^2_p=0.06). The largest age-dependent increase in Alz50 staining area lies in the difference detected between 6 and 12 months Tau$_{P301L}$/*Efhd2*$^{-/-}$ mice (p=0.3338, Hedge's g=0.9) (Figure 4.9C). On the other hand, we noted a small increase in Alz50 staining area comparing 6 and 12 months Tau$_{P301L}$/*Efhd2*$^{+/+}$ mice (p= 0.8355, Hedge's g=0.46). An interesting finding was the medium uptick of Alz50 staining area in BS in Tau$_{P301L}$/*Efhd2*$^{-/-}$ mice at 12 months compared

to wild type littermates (p= 0.4002, Hedge's g=0.7). We noticed also that the visible accumulation of Alz50 staining at 6 months $\text{Tau}_{\text{P301L}}$/*Efhd2*$^{-/-}$ mice was small (p= 0.8887, Hedge's g=0.2) (Figure 4.9C).

    In the CTX, statistical analysis by two-way ANOVA revealed a small interaction between age and genotype ($F_{(1, 17)}$ = 1.890 p=0.1871, η^2_p=0.01). Moreover, a medium main effect of age ($F_{(1, 17)}$ = 0.3921 p=0.5395, η^2_p=0.13) was detected. The analysis revealed a small main effect of genotype ($F_{(1, 17)}$ = 0.8832 p=0.3605, η^2_p=0.01). A distinct increase of Alz50 staining area in 12 months $\text{Tau}_{\text{P301L}}$/*Efhd2*$^{-/-}$ mice in comparison to 6 months was detected (Figure 4.9D and E) (p= 0.5686, Hedge's g=0.93). By comparing $\text{Tau}_{\text{P301L}}$/*Efhd2*$^{+/+}$ 6- and 12-months mice, we can see a medium increase in Alz50 reactivity (Figure 4.9D and E) (p= 0.7712, Hedge's g=0.52). From Figures 4.9C and F, we can observe perceptible increase of Alz50 staining area at 12 months $\text{Tau}_{\text{P301L}}$/*Efhd2*$^{-/-}$ compared to $\text{Tau}_{\text{P301L}}$/*Efhd2*$^{+/+}$ mice. Statistically that increase was small-medium due to skewedness of $\text{Tau}_{\text{P301L}}$/*Efhd2*$^{+/+}$ Alz50 staining area (p= 0.7712, Hedge's g=0.4). Similarly, the analysis endorsed a moderately higher Alz50 reactivity at 6 months in $\text{Tau}_{\text{P301L}}$/*Efhd2*$^{-/-}$ mice than $\text{Tau}_{\text{P301L}}$/*Efhd2*$^{+/+}$ mice (p= 0.7773, Hedge's g=0.63).

    In contrast to pSer422 and PHF1 positive tau, weak correlation was detected between Alz50 staining area in BS and MIS in $\text{Tau}_{\text{P301L}}$/*Efhd2*$^{+/+}$ mice (r= -0.1593, p= 0.6362). Data analysis indicated a medium correlation between Alz50 staining area in BS and MIS in $\text{Tau}_{\text{P301L}}$/*Efhd2*$^{-/-}$ mice (r= 0.5207, p= 0.1255). The correlation between NS and Alz50 staining area in the CTX was weak in both $\text{Tau}_{\text{P301L}}$/*Efhd2*$^{+/+}$ and $\text{Tau}_{\text{P301L}}$/*Efhd2*$^{-/-}$ mice (r= 0.2050, p= 0.5432) (r= -0.2134, p= 0.5513), respectively.

    These contrasting results, using different pathological tau markers, underscore the need for further studies to understand the differential toxicity of various pathological tau species and its relation to phenotype presentation.
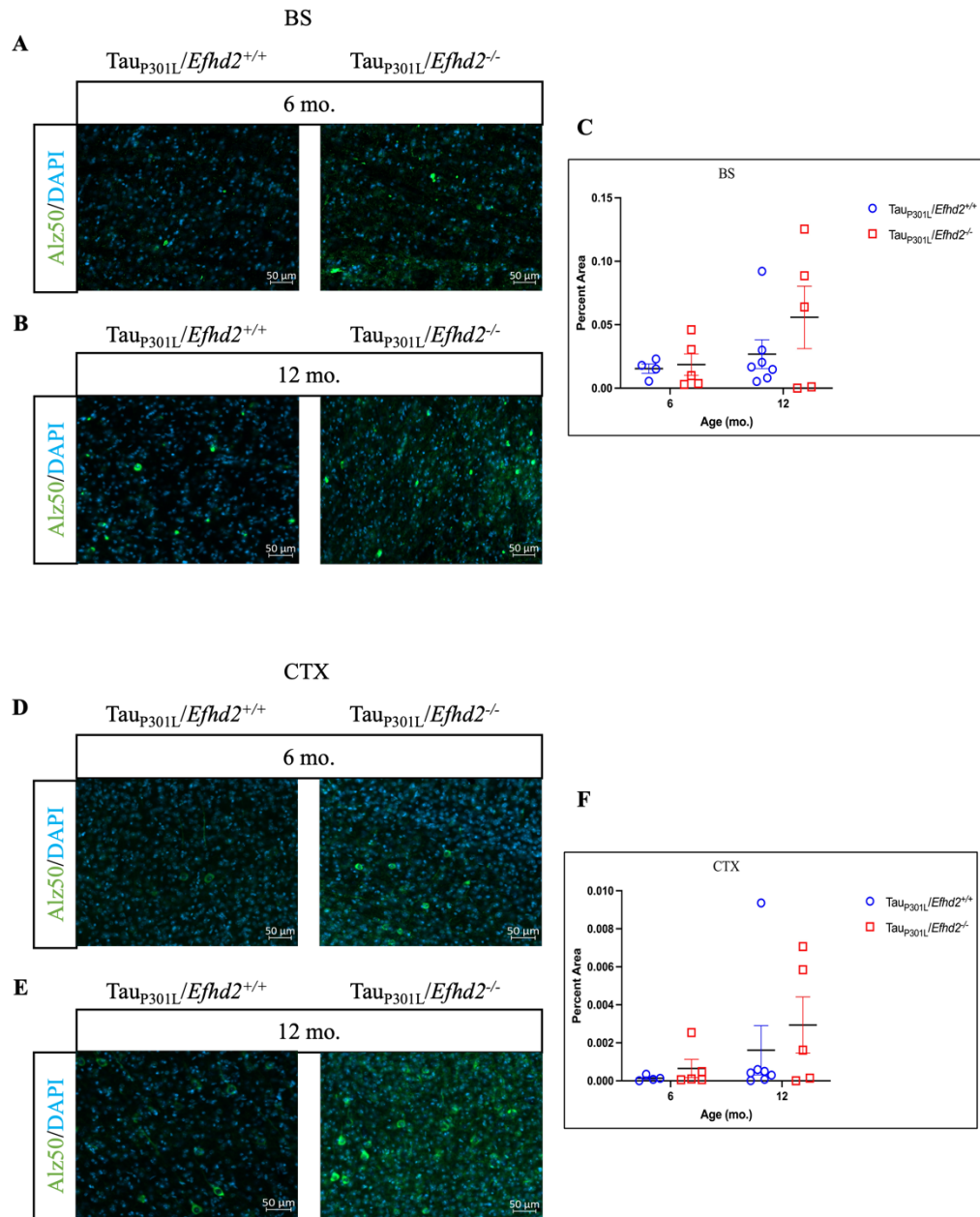
Figure 4.9. Deleting *Efhd2* gene induced a small-moderate rise in the level of Alz50 tau conformation. Right hemispheres from 6- and 12-month-old females Tau$_{P301L}$/*Efhd2$^{+/+}$* and Tau$_{P301L}$/*Efhd2$^{-/-}$* mice (n= 4-7/group) were processed for immunofluorescence analysis of Alz50 modified tau marker (green) and DAPI (blue) in brainstem (BS) panels A and B, and cortex (CTX) panels D and E. (**A**) Representative Alz50 immunofluorescent images for 6-month-old female Tau$_{P301L}$/*Efhd2$^{+/+}$*and Tau$_{P301L}$/*Efhd2$^{-/-}$* mice BS. (**B**) Representative Alz50 immunofluorescent images in BS of 12-month-old female Tau$_{P301L}$/*Efhd2$^{+/+}$* and Tau$_{P301L}$/*Efhd2$^{-/-}$* mice. (**C**) Quantification of Alz50 immunofluorescence was completed using HALO software and statistical analysis was conducted using two-way ANOVA showing a small interaction between age and genotype ((F (1, 17) = 0.7526, p=0.3977, η^2$_p$=0.04). The main effect of age detected was large (F (1, 17) = 2.661 p=0.1212, η^2$_p$=0.14). The results illustrated a medium main effect of genotype (F (1, 17) = 1.170 p=0.2945, η^2$_p$=0.06). The analysis pointed out that

216

Figure 4.9 (cont'd)

the largest age-dependent increase in Alz50 staining area lies between 6 and 12 months Tau$_{P301L}$/*Efhd2$^{-/-}$* mice (p= 0.3338, Hedge's g=0.9). A small increase in Alz50 staining area was noted comparing 6 and 12 months Tau$_{P301L}$/*Efhd2$^{+/+}$* mice (p= 0.8355, Hedge's g=0.46). Alz50 staining area in BS in Tau$_{P301L}$/*Efhd2$^{-/-}$* mice at 12 months was moderately higher than wild type littermates (p= 0.4002, Hedge's g=0.7). We noticed that the visible accumulation of Alz50 staining at 6 months Tau$_{P301L}$/*Efhd2$^{-/-}$* mice was small (p= 0.8887, Hedge's g=0.2). (**D**) Representative Alz50 immunofluorescent images for 6-month-old female Tau$_{P301L}$/*Efhd2$^{+/+}$* and Tau$_{P301L}$/*Efhd2$^{-/-}$* mice in the CTX. (**E**) Representative Alz50 immunofluorescent images in CTX of 12-month-old female Tau$_{P301L}$/*Efhd2$^{+/+}$* and Tau$_{P301L}$/*Efhd2$^{-/-}$* mice. (**F**) Two-way ANOVA analysis for Alz50 percent area in the CTX: a small interaction between age and genotype (F (1, 17) = 1.890 p=0.1871, η^2_p=0.01), a medium main effect of age (F (1, 17) = 0.3921 p=0.5395, η^2_p=0.13), and a small main effect of genotype (F (1, 17) = 0.8832 p=0.3605, η^2_p=0..01). Higher Alz50 staining area in 12 months Tau$_{P301L}$/*Efhd2$^{-/-}$* mice in comparison to 6 months was detected (p= 0.5686, Hedge's g=0.93). In Tau$_{P301L}$/*Efhd2$^{+/+}$* mice, a medium increase in Alz50 reactivity in 12 months compared to 6 months was detected (p= 0.7712, Hedge's g=0.52). A small-medium increase in Alz50 reactivity in Tau$_{P301L}$/*Efhd2$^{-/-}$* mice at 12 months in comparison to Tau$_{P301L}$/*Efhd2$^{+/+}$* mice exists (p= 0.7712, Hedge's g=0.4). We noticed a moderately higher Alz50 reactivity at 6 months in Tau$_{P301L}$/*Efhd2$^{-/-}$* than Tau$_{P301L}$/*Efhd2$^{+/+}$* mice (p= 0.7773, Hedge's g=0.63). Error bars indicate mean ± SEM.

Discussion

In our previous research, we provided evidence for the association of EFhd2 with pathological tau, especially NFTs, in JNPL3 mouse model and postmortem tauopathies brains (Vega et al., 2008; Ferrer-Acosta et al., 2013b; Vega, 2016). Furthermore, we conducted several *in vitro* studies indicating that EFhd2 modulates the dynamic properties of tau and possibly promotes its aggregation (Vega et al., 2018; Vega et al., 2019). Hence, we hypothesized that EFhd2 might contribute to tau-mediated neurodegeneration by enhancing the formation of pathological tau aggregates. In this study, we sought to test this hypothesis *in vivo* by deleting *Efhd2* gene in Tau$_{P301L}$ expressing mice, thereby investigating to what extent the absence of EFhd2 could impact the formation and progression of tau pathology. Using our novel Tau$_{P301L}$/*Efhd2$^{-/-}$* model, we show, for the first time, that the absence of EFhd2 differentially affects specific pathological tau markers without changing selective brain region vulnerability or the progression of neurodegeneration. The most compelling finding in this study is the heightened accumulation of early pretangle tau markers along with reduced late tangle makers in a brain region-specific manner. That suggests a potential role of EFhd2 in driving oligomeric tau into the later mature tangles. The molecular factors that could drive the transition of filamentous tau into mature tangles has eluded the field for a long time. A litany of studies has elucidated the

molecular factors that might contribute to early pathological conformational changes of tau that lead to aberrant oligomerization, which incessantly progresses to tangle formation. Among those factors are PTMs, mutations, and tau-interacting proteins. Thus, this study proposes EFhd2 as a potential tau-interacting protein that may govern, at least partly, mature tangle formation. Accordingly, future studies that include EFhd2 overexpression are needed to test the proposed role of EFhd2 in NFTs formation and how that could impact the neurodegeneration phenotype in mice.

We first evaluated the outcome of deleting *Efhd2* gene through longitudinal behavioral assessment to monitor changes in the behavioral phenotype (represented by motor function and nesting). We determined that the absence of EFhd2 did not greatly alter the onset of neurodegeneration phenotype. In general, Tau_{P301L} expressing mice develop a pronounced neurodegeneration phenotype around 7 to 8 months in females and beyond 12 months in males (Lewis et al., 2000; Sahara et al., 2002; Lewis & McGowan, 2005). Our results are in line with established reports of Tau_{P301L} expressing mice. By comparing Tau_{P301L}/*Efhd2*$^{+/+}$ and Tau_{P301L}/*Efhd2*$^{-/-}$ mice, neurodegeneration phenotype onset did not greatly change in females and males.

The age-dependent decline in behavioral phenotype of Tau_{P301L}/*Efhd2*$^{-/-}$ mice cannot be ascribed to *Efhd2* gene deletion given the negligible difference between Non-Tg/*Efhd2*$^{+/+}$ and Non-Tg/*Efhd2*$^{-/-}$. A previous study showed that EFhd2 might regulate adult hippocampal neurogenesis and synaptic integrity (Regensburger et al., 2018). In that study, markedly impaired dendritic morphology and reduced synaptic markers predominated in *Efhd2*$^{-/-}$ mice brains. It should be noted that the authors of that study did not conduct behavioral assessments to examine the functional implications of impaired hippocampal neurogenesis induced by deleting the *Efhd2* gene. Another study has recently demonstrated that overexpressing EFhd2 in the brain adversely affected hippocampus-dependent memory consolidation (Xue et al., 2022). That effect was reversed by *Efhd2* knock down. Although the seemingly discrepant findings, the confluence of the two studies attests to the possible role of EFhd2 in hippocampus-dependent memory formation, aside from its role in pathological tau aggregation. Notwithstanding, that warrants more studies to unravel mechanistically the physiological and pathological significance of EFhd2 in the hippocampus.

In this study, we evaluated nesting behavior as a surrogate measurement for hippocampus function. The analysis of individual nesting results did not reveal a difference between Non-Tg/*Efhd2*$^{-/-}$ and Non-Tg/*Efhd2*$^{+/+}$ mice as shown in Figure A4.4. In general, *Efhd2*$^{-/-}$ mice exhibited normal phenotype without behavioral anomalies. One may speculate that nesting assessment does not have the required sensitivity to detect impaired hippocampus function induced by the absence of EFhd2. While other memory assessment tasks such as maze-dependent tests and fear conditioning might afford more robust measurements of hippocampus-dependent memory, these tasks require intact motor function. Tau$_{P301L}$ mice develop extensive pathological tau accumulation mainly in the spinal cord and brainstem along with motor neurons degeneration (Lewis et al., 2000; Lewis & McGowan, 2005). Hence, motor impairment is the major behavioral phenotype in this model whose severity increases with age and correlates with the level of tau pathology. As such, other memory assessment tests are not adequate, especially at older ages. Therefore, we opted to compare between Non-Tg/*Efhd2*$^{+/+}$ and Non-Tg/*Efhd2*$^{-/-}$ using nesting performance as a baseline for transgenic mice. Another reason we chose nesting in this study is that it has been shown that Tau$_{P301L}$ mice exhibited poor nesting performance with aging (Rao et al., 2014). It follows that the observed neurodegeneration phenotype (nesting and motor function) in Tau$_{P301L}$/*Efhd2*$^{-/-}$ mice is primarily driven by the mutant tau overexpression.

Second, we investigated neuropathological changes due to the absence of EFhd2. We particularly assessed pSer422 and PHF1 as two post-translationally modified tau markers in addition to Alz50 as a conformation tau marker. In fact, numerous studies have shown repeatedly that pSer422 and PHF1 mark later phases of NFTs maturity. Hence, detecting these two markers potentially indicates intermediate/late mature tangles (Kimura et al., 1996; Bussiere et al., 1999; Götz et al., 2001; Augustinack et al., 2002; Deters et al., 2008; Neddens et al., 2018; Moloney et al., 2021). On the other hand, Alz50 recognizes one of the early conformational changes of tau, labeling pretangle forms (Luna-Muñoz et al., 2007; Moloney et al., 2021). Herein, we detected a brain-region specific effect on PHF1 and pSer422 staining areas in Tau$_{P301L}$/*Efhd2*$^{-/-}$ mice. In particular, in the BS region of old Tau$_{P301L}$/*Efhd2*$^{-/-}$ mice, we noted a small reduction in PHF1 and pSer422 staining areas compared to wild type controls. A more appreciable decrease in the area covered by these two markers was detected in the CTX of Tau$_{P301L}$/*Efhd2*$^{-/-}$ mice. Taken together, EFhd2 absence caused a reduction in pSer422 and PHF1 staining areas in BS and CTX. We can speculate that the reduction is more prominent in the CTX due to higher EFhd2

expression in forebrain regions than hindbrain regions as reported before (Purohit et al., 2014). Future studies should dissect brain region-specific effects of EFhd2 on the biogenesis of tau aggregates.

Previously, we showed the association of EFhd2 with pathological tau aggregates in sarkosyl-insoluble fraction in AD and Tau$_{P301L}$ mice (Vega et al., 2008; Ferrer-Acosta et al., 2013b). Therefore, we undertook biochemical analysis of pSer422, PHF1, and Tau13 by western blot to assess the influence of EFhd2 absence on the accumulation of sarkosyl-insoluble tau species, especially 64 kDa tau species. Broadly speaking, 64 kDa tau species represent high molecular weight pathological tau (Berger et al., 2007). The results showed a large reduction in Tau13 64 kDa in P3 extracted from Tau$_{P301L}$/*Efhd2*$^{-/-}$ mice brains when compared with wild type. However, the reduction in pSer422 and PHF1 64 kDa species was small in Tau$_{P301L}$/*Efhd2*$^{-/-}$ mice. According to many scholars, 64 kDa and higher molecular weight tau signal advanced events of tau aggregation that follows early phases of pretangle formation and increases with age. Together, histological assessment of pSer422 and PHF1 (as later tangle markers) along with biochemical assessment of sarkosyl-insoluble tau species highlight the effect of deleting the *Efhd2* gene on tau fibrillar and tangles maturity.

We also observed an overall tendency of Alz50 tau to accumulate in Tau$_{P301L}$/*Efhd2*$^{-/-}$ mice brain compared to controls. In fact, the age-dependent increase of Alz50 tau is more pronounced in Tau$_{P301L}$/*Efhd2*$^{-/-}$ mice. Importantly, statistical analysis, including effect size, endorses the appreciable rise of Alz50 tau in Tau$_{P301L}$/*Efhd2*$^{-/-}$ mice at 12 months in comparison to Tau$_{P301L}$/*Efhd2*$^{+/+}$. As noted earlier, Alz50 primarily signifies pretangle tau aggregates. It is proposed that the detection of Alz50 decreases as the accumulation of tangles increases because another conformational change leads to N-terminus cleavage and the loss of Alz50 epitope in later fibrils and tangle aggregates (Guillozet-Bongaarts et al., 2005; Moloney et al., 2021). In other words, pathological progression and neurodegeneration might not necessarily correlate with the number of Alz50 positive neurons. In essence, the neuropathological changes induced by deleting *Efhd2* gene in Tau$_{P301L}$ expressing mice endorse the potential unique capacity of EFhd2 to regulate the transition of early and intermediate filamentous tau into mature tangles. This finding has not been reported before in regard to other tau-interacting proteins that influence tau aggregation and related neurotoxicity.

For instance, T-cell intracellular antigen 1 (TIA1), an RNA-binding protein that nucleates RNA stress granules (Cruz et al., 2019; Jiang et al., 2019), has the capacity to interact with tau and induce its aberrant folding and neurodegeneration. TIA1 colocalized with aggregated tau in a tauopathy mouse model that overexpresses human P301S mutant tau, PS19 model (Vanderweyde et al., 2016; Jiang et al., 2019). Using the same approach we used, reducing TIA1 in heterozygous knockout of TIA1 bred with PS19 exhibited improved cognitive performance in Y-maze and novel object recognition test (Apicco et al., 2018). Moreover, reducing TIA1 prolonged survival lifespan of PS19. Above all, lower levels of TIA1 led to reduced pretangle oligomeric tau aggregates along with enhanced accumulation of high molecular weight fibrillar tau shown in PS19/*TIA1*$^{+/-}$ mice. Further *in vitro* experiments supported the role of TIA1 in promoting the accumulation of oligomeric pretangle tau forms, and not fibrillar tau (Jiang et al., 2019; Ash et al., 2021). Collectively, these findings indicate that increased TIA1 abundance might exact a toll on neuronal integrity and cognitive performance by sustaining the formation of oligomeric tau and reducing fibrillar tau and NFTs (Maziuk et al., 2018).

Bassoon is another tau-interacting protein that regulates normal synaptic functions and networks (Annamneedi et al., 2018). Recently, bassoon co-purified with seed-competent misfolded and aggregated tau extracted from AD and PS19 brains (Martinez et al., 2022). Consistently, bassoon enhanced tau misfolding and seeding. Moreover, knocking down bassoon in PS19 mice halted tau seeding and propagation. In addition, reducing bassoon levels PS19 mice has rescued behavioral deficit, especially the motor dysfunction (Martinez et al., 2022). Apropos of pathological tau markers, Martinez, et al reported that knocking down bassoon resulted in significant reduction in PHF1 and MC1(Martinez et al., 2022). It is noteworthy that MC1 antibody recognizes the same tau conformational change detected by Alz50. The results suggest that bassoon stabilizes oligomeric tau and induces neurotoxic effect.

Reputed researchers have agreed that the formation of tau fibrils and tangles potentially represent an innocuous response in the pathological trajectory of tauopathies. Several studies have unfailingly shown that higher order tangles do not exert neurotoxicity. Hence, more attention has been directed to pretangle oligomeric tau species demonstrating that these early tau aggregates could be the true perpetrator in tau-mediated neurodegeneration. In view of this, TIA1 and bassoon interfere with tau aggregation by enhancing the accumulation of oligomeric tau structures; thus, reducing their levels rescued behavioral deficit and increased higher

molecular weight tau forms. Comparatively, our data allude to possible increased accumulation of pretangle oligomeric forms (Alz50 positive) and reduced pSer422 and PHF1 (later tangle markers) upon deleting *Efhd2* gene at old age. Previously, we discovered EFhd2 as a tau-associated protein in sarkosyl-insoluble fraction (Vega et al., 2008). Furthermore, immunogold labeling confirmed the colocalization of EFhd2 and tau in sarkosyl-insoluble tangles (Ferrer-Acosta et al., 2013b). The presented data, together with our previous research, imply that EFhd2 uniquely impacts the biogenesis of pathological tau aggregates by driving the formation of higher order tangle forms.

Several points should be considered before we can deduce a consequent neuroprotective or neurodegenerative role for EFhd2 in tau pathology. In this study, we did not measure other pretangle oligomeric markers that have been linked to neurotoxicity, such as TOC1, TOMA1, AT8, and PAD-exposure. Pretangle oligomers are ensemble of diverse populations of tau aggregates with differential neurotoxicity. Therefore, in a future study we will assess a larger panel for these pretangle markers that will undergird the effect of EFhd2 absence on their levels. In addition, pSer422 and PHF1 herein were used as a surrogate measure for late tangles. However, we should precisely quantify the levels of tangle-bearing neurons and assess the changes associated with EFhd2 absence. One way to do this is by immunogold labeling and high-resolution electron microscopy to evaluate neuronal morphology of pSer422 and PHF1 positive neurons. These studies will advance our understanding of the role of EFhd2 in the biogenesis of pathological tau aggregates and associated neurotoxicity.

One might wonder why the observed effect of *Efhd2* gene deletion on pathological tau markers was not reflected in the behavioral phenotype. In other words, we would expect a worsened or accelerated neurodegeneration phenotype driven by the accumulation of pretangle tau aggregates. One explanation could be tau-independent factors induced by deleting *Efhd2* gene that might contribute to the phenotype. This explanation seems plausible due to the differential correlation between these markers and behavior deficit in Tau$_{P301L}$/*Efhd2*$^{+/+}$ vs Tau$_{P301L}$/*Efhd2*$^{-/-}$. Particularly, the strong correlation between pSer422 and PHF1 with motor function and nesting largely waned in Tau$_{P301L}$/*Efhd2*$^{-/-}$ mice. Interestingly, we noticed a weak correlation between Alz50 and motor impairment in wild type mice, which is slightly increased in Tau$_{P301L}$/*Efhd2*$^{-/-}$ mice. These data suggest that deleting *Efhd2* gene possibly changed the cellular milieu whereby other factors, not merely tau aggregation, contribute to the phenotype.

Another possibility for the lack of detectable change in the behavioral phenotype is that the Tau_{P301L} mouse model develops robust age-dependent behavioral deficit and pathology, which could create a ceiling effect and reach a maximum level of pathology beyond which no further worsening or progression could be detected. Taking these points on board, we should be wary in concluding whether EFhd2 plays a neuroprotective role.

In conclusion, the results provide evidence that EFhd2 could regulate the biogenesis of pathological tau aggregates towards NFTs formation. A future comprehensive characterization $Tau_{P301L}/Efhd2^{-/-}$ mouse model represents an essential next step to gain deeper insights on how the absence of EFhd2 impacts tau-mediated neurodegeneration. Particularly, other conformational tau markers are worth investigating along with structural analysis to verify changes in NFTs formation. Furthermore, histological and biochemical analysis for tau pathology will be examined at 3 and 9 months to provide a holistic description of the model. It will be important to investigate neuropathological changes in male $Tau_{P301L}/Efhd2^{-/-}$ mice, especially at 6 and 12 months that showed a large fluctuating phenotype compared to wild type mice. Given the stark variability seen among mice of the same age and genotype, it would be also interesting to run proteomic analysis and determine the factors rendering some mice more resilient to pathology than others. These future experiments will verify the applicability of $Tau_{P301L}/Efhd2^{-/-}$ model to identify the precise mechanism by which EFhd2 influences tau pathology.

REFERENCES

Akoglu, H. (2018). User's guide to correlation coefficients. *Turk J Emerg Med*, *18*(3), 91-93. https://doi.org/10.1016/j.tjem.2018.08.001

Annamneedi, A., Caliskan, G., Muller, S., Montag, D., Budinger, E., Angenstein, F., Fejtova, A., Tischmeyer, W., Gundelfinger, E. D., & Stork, O. (2018). Ablation of the presynaptic organizer Bassoon in excitatory neurons retards dentate gyrus maturation and enhances learning performance. *Brain Struct Funct*, *223*(7), 3423-3445. https://doi.org/10.1007/s00429-018-1692-3

Apicco, D. J., Ash, P. E. A., Maziuk, B., LeBlang, C., Medalla, M., Al Abdullatif, A., Ferragud, A., Botelho, E., Ballance, H. I., Dhawan, U., Boudeau, S., Cruz, A. L., Kashy, D., Wong, A., Goldberg, L. R., Yazdani, N., Zhang, C., Ung, C. Y., Tripodis, Y., . . . Wolozin, B. (2018). Reducing the RNA binding protein TIA1 protects against tau-mediated neurodegeneration in vivo. *Nat Neurosci*, *21*(1), 72-80. https://doi.org/10.1038/s41593-017-0022-z

Ash, P. E. A., Lei, S., Shattuck, J., Boudeau, S., Carlomagno, Y., Medalla, M., Mashimo, B. L., Socorro, G., Al-Mohanna, L. F. A., Jiang, L., Ozturk, M. M., Knobel, M., Ivanov, P., Petrucelli, L., Wegmann, S., Kanaan, N. M., & Wolozin, B. (2021). TIA1 potentiates tau phase separation and promotes generation of toxic oligomeric tau. *Proc Natl Acad Sci U S A*, *118*(9). https://doi.org/10.1073/pnas.2014188118

Augustinack, J. C., Schneider, A., Mandelkow, E. M., & Hyman, B. T. (2002). Specific tau phosphorylation sites correlate with severity of neuronal cytopathology in Alzheimer's disease. *Acta Neuropathol*, *103*(1), 26-35. https://doi.org/10.1007/s004010100423

Avila, J., Jimenez, J. S., Sayas, C. L., Bolos, M., Zabala, J. C., Rivas, G., & Hernandez, F. (2016). Tau Structures. *Front Aging Neurosci*, *8*, 262. https://doi.org/10.3389/fnagi.2016.00262

Avramidou, A., Kroczek, C., Lang, C., Schuh, W., Jack, H. M., & Mielenz, D. (2007). The novel adaptor protein Swiprosin-1 enhances BCR signals and contributes to BCR-induced apoptosis. *Cell Death Differ*, *14*(11), 1936-1947. https://doi.org/10.1038/sj.cdd.4402206

Bancher, C., Brunner, C., Lassmann, H., Budka, H., Jellinger, K., Seitelberger, F., Grundke-Iqbal, I., Iqbal, K., & Wisniewski, H. M. (1989). Tau and ubiquitin immunoreactivity at different stages of formation of Alzheimer neurofibrillary tangles. *Prog Clin Biol Res*, *317*, 837-848. https://www.ncbi.nlm.nih.gov/pubmed/2557644

Berger, Z., Roder, H., Hanna, A., Carlson, A., Rangachari, V., Yue, M., Wszolek, Z., Ashe, K., Knight, J., Dickson, D., Andorfer, C., Rosenberry, T. L., Lewis, J., Hutton, M., & Janus, C. (2007). Accumulation of pathological tau species and memory loss in a conditional model of tauopathy. *J Neurosci*, *27*(14), 3650-3662. https://doi.org/10.1523/JNEUROSCI.0587-07.2007

Betters, R. K., Luhmann, E., Gottschalk, A. C., Xu, Z., Shin, M. R., Ptak, C. P., Fiock, K. L., Radoshevich, L. C., & Hefti, M. M. (2023). Characterization of the Tau Interactome in Human Brain Reveals Isoform-Dependent Interaction with 14-3-3 Family Proteins. *eNeuro*, *10*(3). https://doi.org/10.1523/ENEURO.0503-22.2023

Bisi, N., Feni, L., Peqini, K., Perez-Pena, H., Ongeri, S., Pieraccini, S., & Pellegrino, S. (2021). alpha-Synuclein: An All-Inclusive Trip Around its Structure, Influencing Factors and Applied Techniques. *Front Chem*, *9*, 666585. https://doi.org/10.3389/fchem.2021.666585

Braak, E., Braak, H., & Mandelkow, E. M. (1994). A sequence of cytoskeleton changes related to the formation of neurofibrillary tangles and neuropil threads. *Acta Neuropathol*, *87*(6), 554-567. https://doi.org/10.1007/bf00293315

Broniarczyk-Czarniak, M., & Gałecki, P. (2019). Is the EFHD2/Swiprosin-1 protein linked to Alzheimer's disease? [journal article]. *Postępy Psychiatrii i Neurologii*, *28*(3), 220-224. https://doi.org/10.5114/ppn.2019.89137

Brunden, K. R., Trojanowski, J. Q., & Lee, V. M. (2008). Evidence that non-fibrillar tau causes pathology linked to neurodegeneration and behavioral impairments. *J Alzheimers Dis*, *14*(4), 393-399. https://doi.org/10.3233/jad-2008-14406

Bussiere, T., Hof, P. R., Mailliot, C., Brown, C. D., Caillet-Boudin, M. L., Perl, D. P., Buee, L., & Delacourte, A. (1999). Phosphorylated serine422 on tau proteins is a pathological epitope found in several diseases with neurofibrillary degeneration. *Acta Neuropathol*, *97*(3), 221-230. https://doi.org/10.1007/s004010050978

Carmel, G., Mager, E. M., Binder, L. I., & Kuret, J. (1996). The structural basis of monoclonal antibody Alz50's selectivity for Alzheimer's disease pathology. *J Biol Chem*, *271*(51), 32789-32795. https://doi.org/10.1074/jbc.271.51.32789

Chung, D. C., Roemer, S., Petrucelli, L., & Dickson, D. W. (2021). Cellular and pathological heterogeneity of primary tauopathies. *Mol Neurodegener*, *16*(1), 57. https://doi.org/10.1186/s13024-021-00476-x

Cohen, J. (2013). *Statistical Power Analysis for the Behavioral Sciences* (2nd Edition ed.). Routledge. https://doi.org/10.4324/9780203771587

Combs, B., Hamel, C., & Kanaan, N. M. (2016). Pathological conformations involving the amino terminus of tau occur early in Alzheimer's disease and are differentially detected by monoclonal antibodies. *Neurobiol Dis*, *94*, 18-31. https://doi.org/10.1016/j.nbd.2016.05.016

Cowan, C. M., & Mudher, A. (2013). Are tau aggregates toxic or protective in tauopathies? *Front Neurol*, *4*, 114. https://doi.org/10.3389/fneur.2013.00114

Cruz, A., Verma, M., & Wolozin, B. (2019). The Pathophysiology of Tau and Stress Granules in Disease. *Adv Exp Med Biol*, *1184*, 359-372. https://doi.org/10.1007/978-981-32-9358-8_26

Deacon, R. M. (2006). Assessing nest building in mice. *Nat Protoc*, *1*(3), 1117-1119. https://doi.org/10.1038/nprot.2006.170

Deters, N., Ittner, L. M., & Götz, J. (2008). Divergent phosphorylation pattern of tau in P301L tau transgenic mice. *Eur J Neurosci*, *28*(1), 137-147. https://doi.org/10.1111/j.1460-9568.2008.06318.x

Duong, T., Doucette, T., Zidenberg, N. A., Jacobs, R. W., & Scheibel, A. B. (1993). Microtubule-associated proteins tau and amyloid P component in Alzheimer's disease. *Brain Res*, *603*(1), 74-86. https://doi.org/10.1016/0006-8993(93)91301-8

Dyson, H. J., & Wright, P. E. (2005). Intrinsically unstructured proteins and their functions. *Nat Rev Mol Cell Biol*, *6*(3), 197-208. https://doi.org/10.1038/nrm1589

Faul, F., Erdfelder, E., Lang, A. G., & Buchner, A. (2007). G*Power 3: a flexible statistical power analysis program for the social, behavioral, and biomedical sciences. *Behav Res Methods*, *39*(2), 175-191. https://doi.org/10.3758/bf03193146

Ferrer-Acosta, Y., Rodriguez Cruz, E. N., Vaquer Adel, C., & Vega, I. E. (2013a). Functional and structural analysis of the conserved EFhd2 protein. *Protein Pept Lett*, *20*(5), 573-583. https://doi.org/10.2174/0929866511320050011

Ferrer-Acosta, Y., Rodriguez-Cruz, E. N., Orange, F., De Jesus-Cortes, H., Madera, B., Vaquer-Alicea, J., Ballester, J., Guinel, M. J., Bloom, G. S., & Vega, I. E. (2013b). EFhd2 is a novel amyloid protein associated with pathological tau in Alzheimer's disease. *J Neurochem*, *125*(6), 921-931. https://doi.org/10.1111/jnc.12155

Goedert, M., Spillantini, M. G., & Jakes, R. (1991). Localization of the Alz-50 epitope in recombinant human microtubule-associated protein tau. *Neurosci Lett*, *126*(2), 149-154. https://doi.org/10.1016/0304-3940(91)90541-z

Gomez-Isla, T., Hollister, R., West, H., Mui, S., Growdon, J. H., Petersen, R. C., Parisi, J. E., & Hyman, B. T. (1997). Neuronal loss correlates with but exceeds neurofibrillary tangles in Alzheimer's disease. *Ann Neurol*, *41*(1), 17-24. https://doi.org/10.1002/ana.410410106

Götz, J., Chen, F., van Dorpe, J., & Nitsch, R. M. (2001). Formation of neurofibrillary tangles in P301l tau transgenic mice induced by Abeta 42 fibrils. *Science*, *293*(5534), 1491-1495. https://doi.org/10.1126/science.1062097

Greenberg, S. G., Davies, P., Schein, J. D., & Binder, L. I. (1992). Hydrofluoric acid-treated tau PHF proteins display the same biochemical properties as normal tau. *J Biol Chem*, *267*(1), 564-569. https://doi.org/10.1016/S0021-9258(18)48531-6

Griffin, T. A., Schnier, P. D., Cleveland, E. M., Newberry, R. W., Becker, J., & Carlson, G. A. (2023). Fibril treatment changes protein interactions of tau and alpha-synuclein in human neurons. *J Biol Chem*, *299*(3), 102888. https://doi.org/10.1016/j.jbc.2023.102888

Guillozet-Bongaarts, A. L., Garcia-Sierra, F., Reynolds, M. R., Horowitz, P. M., Fu, Y., Wang, T., Cahill, M. E., Bigio, E. H., Berry, R. W., & Binder, L. I. (2005). Tau truncation during neurofibrillary tangle evolution in Alzheimer's disease. *Neurobiol Aging*, *26*(7), 1015-1022. https://doi.org/10.1016/j.neurobiolaging.2004.09.019

Hagen, S., Brachs, S., Kroczek, C., Furnrohr, B. G., Lang, C., & Mielenz, D. (2012). The B cell receptor-induced calcium flux involves a calcium mediated positive feedback loop. *Cell Calcium*, *51*(5), 411-417. https://doi.org/10.1016/j.ceca.2012.01.004

Hasegawa, M., Jakes, R., Crowther, R. A., Lee, V. M., Ihara, Y., & Goedert, M. (1996). Characterization of mAb AP422, a novel phosphorylation-dependent monoclonal antibody against tau protein. *FEBS Lett*, *384*(1), 25-30. https://doi.org/10.1016/0014-5793(96)00271-2

Hutton, M., Lendon, C. L., Rizzu, P., Baker, M., Froelich, S., Houlden, H., Pickering-Brown, S., Chakraverty, S., Isaacs, A., Grover, A., Hackett, J., Adamson, J., Lincoln, S., Dickson, D., Davies, P., Petersen, R. C., Stevens, M., de Graaff, E., Wauters, E., . . . Heutink, P. (1998). Association of missense and 5'-splice-site mutations in tau with the inherited dementia FTDP-17. *Nature*, *393*(6686), 702-705. https://doi.org/10.1038/31508

Jiang, L., Ash, P. E. A., Maziuk, B. F., Ballance, H. I., Boudeau, S., Abdullatif, A. A., Orlando, M., Petrucelli, L., Ikezu, T., & Wolozin, B. (2019). TIA1 regulates the generation and response to toxic tau oligomers. *Acta Neuropathol*, *137*(2), 259-277. https://doi.org/10.1007/s00401-018-1937-5

Kametani, F., Yoshida, M., Matsubara, T., Murayama, S., Saito, Y., Kawakami, I., Onaya, M., Tanaka, H., Kakita, A., Robinson, A. C., Mann, D. M. A., & Hasegawa, M. (2020). Comparison of Common and Disease-Specific Post-translational Modifications of Pathological Tau Associated With a Wide Range of Tauopathies. *Front Neurosci*, *14*, 581936. https://doi.org/10.3389/fnins.2020.581936

Kanaan, N. M., Cox, K., Alvarez, V. E., Stein, T. D., Poncil, S., & McKee, A. C. (2016). Characterization of Early Pathological Tau Conformations and Phosphorylation in Chronic Traumatic Encephalopathy. *J Neuropathol Exp Neurol*, *75*(1), 19-34. https://doi.org/10.1093/jnen/nlv001

Kanaan, N. M., Hamel, C., Grabinski, T., & Combs, B. (2020). Liquid-liquid phase separation induces pathogenic tau conformations in vitro. *Nat Commun*, *11*(1), 2809. https://doi.org/10.1038/s41467-020-16580-3

Kanaan, N. M., Morfini, G. A., LaPointe, N. E., Pigino, G. F., Patterson, K. R., Song, Y., Andreadis, A., Fu, Y., Brady, S. T., & Binder, L. I. (2011). Pathogenic forms of tau inhibit kinesin-dependent axonal transport through a mechanism involving activation of axonal phosphotransferases. *J Neurosci*, *31*(27), 9858-9868. https://doi.org/10.1523/JNEUROSCI.0560-11.2011

Kang, H. (2021). Sample size determination and power analysis using the G*Power software. *J Educ Eval Health Prof*, *18*, 17. https://doi.org/10.3352/jeehp.2021.18.17

Kavanagh, T., Halder, A., & Drummond, E. (2022). Tau interactome and RNA binding proteins in neurodegenerative diseases. *Mol Neurodegener*, *17*(1), 66. https://doi.org/10.1186/s13024-022-00572-6

Kayed, R. (2010). Anti-tau oligomers passive vaccination for the treatment of Alzheimer disease. *Hum Vaccin*, *6*(11), 931-935. https://doi.org/10.4161/hv.6.11.12689

Kekesi, K. A., Juhasz, G., Simor, A., Gulyassy, P., Szego, E. M., Hunyadi-Gulyas, E., Darula, Z., Medzihradszky, K. F., Palkovits, M., Penke, B., & Czurko, A. (2012). Altered functional

protein networks in the prefrontal cortex and amygdala of victims of suicide. *PLoS One*, *7*(12), e50532. https://doi.org/10.1371/journal.pone.0050532

Kimura, T., Ono, T., Takamatsu, J., Yamamoto, H., Ikegami, K., Kondo, A., Hasegawa, M., Ihara, Y., Miyamoto, E., & Miyakawa, T. (1996). Sequential changes of tau-site-specific phosphorylation during development of paired helical filaments. *Dementia*, *7*(4), 177-181. https://doi.org/10.1159/000106875

Knoedler, J. R., Inoue, S., Bayless, D. W., Yang, T., Tantry, A., Davis, C. H., Leung, N. Y., Parthasarathy, S., Wang, G., Alvarado, M., Rizvi, A. H., Fenno, L. E., Ramakrishnan, C., Deisseroth, K., & Shah, N. M. (2022). A functional cellular framework for sex and estrous cycle-dependent gene expression and behavior. *Cell*, *185*(4), 654-671.e622. https://doi.org/10.1016/j.cell.2021.12.031

Kogias, G., Kornhuber, J., Reimer, D., Mielenz, D., & Muller, C. P. (2019). Swiprosin-1/ EFhd2: from Immune Regulator to Personality and Brain Disorders. *Neurosignals*, *27*(S1), 1-19. https://doi.org/10.33594/000000179

Kogias, G., Zheng, F., Kalinichenko, L. S., Kornhuber, J., Alzheimer, C., Mielenz, D., & Muller, C. P. (2020). Swiprosin1/EFhd2 is involved in the monoaminergic and locomotor responses of psychostimulant drugs. *J Neurochem*, *154*(4), 424-440. https://doi.org/10.1111/jnc.14959

Kroczek, C., Lang, C., Brachs, S., Grohmann, M., Dutting, S., Schweizer, A., Nitschke, L., Feller, S. M., Jack, H. M., & Mielenz, D. (2010). Swiprosin-1/EFhd2 controls B cell receptor signaling through the assembly of the B cell receptor, Syk, and phospholipase C gamma2 in membrane rafts. *J Immunol*, *184*(7), 3665-3676. https://doi.org/10.4049/jimmunol.0903642

Ksiezak-Reding, H., Davies, P., & Yen, S. H. (1988). Alz 50, a monoclonal antibody to Alzheimer's disease antigen, cross-reacts with tau proteins from bovine and normal human brain. *J Biol Chem*, *263*(17), 7943-7947. https://doi.org/10.1016/S0021-9258(18)68425-X

Ksiezak-Reding, H., Leibowitz, R. L., Bowser, R., & Davies, P. (1995). Binding of Alz 50 depends on Phe8 in tau synthetic peptides and varies between native and denatured tau proteins. *Brain Res*, *697*(1-2), 63-75. https://doi.org/10.1016/0006-8993(95)00785-o

Kuchibhotla, K. V., Wegmann, S., Kopeikina, K. J., Hawkes, J., Rudinskiy, N., Andermann, M. L., Spires-Jones, T. L., Bacskai, B. J., & Hyman, B. T. (2014). Neurofibrillary tangle-bearing neurons are functionally integrated in cortical circuits in vivo. *Proc Natl Acad Sci U S A*, *111*(1), 510-514. https://doi.org/10.1073/pnas.1318807111

Kuret, J., Chirita, C. N., Congdon, E. E., Kannanayakal, T., Li, G., Necula, M., Yin, H., & Zhong, Q. (2005). Pathways of tau fibrillization. *Biochim Biophys Acta*, *1739*(2-3), 167-178. https://doi.org/10.1016/j.bbadis.2004.06.016

Kyalu Ngoie Zola, N., Balty, C., Pyr Dit Ruys, S., Vanparys, A. A. T., Huyghe, N. D. G., Herinckx, G., Johanns, M., Boyer, E., Kienlen-Campard, P., Rider, M. H., Vertommen, D., & Hanseeuw, B. J. (2023). Specific post-translational modifications of soluble tau protein

distinguishes Alzheimer's disease and primary tauopathies. *Nat Commun*, *14*(1), 3706. https://doi.org/10.1038/s41467-023-39328-1

Lakens, D. (2013). Calculating and reporting effect sizes to facilitate cumulative science: a practical primer for t-tests and ANOVAs. *Front Psychol*, *4*, 863. https://doi.org/10.3389/fpsyg.2013.00863

Lasagna-Reeves, C. A., Castillo-Carranza, D. L., Sengupta, U., Clos, A. L., Jackson, G. R., & Kayed, R. (2011). Tau oligomers impair memory and induce synaptic and mitochondrial dysfunction in wild-type mice. *Mol Neurodegener*, *6*, 39. https://doi.org/10.1186/1750-1326-6-39

Lasagna-Reeves, C. A., Castillo-Carranza, D. L., Sengupta, U., Sarmiento, J., Troncoso, J., Jackson, G. R., & Kayed, R. (2012). Identification of oligomers at early stages of tau aggregation in Alzheimer's disease. *Faseb j*, *26*(5), 1946-1959. https://doi.org/10.1096/fj.11-199851

Levy, D. R., Hunter, N., Lin, S., Robinson, E. M., Gillis, W., Conlin, E. B., Anyoha, R., Shansky, R. M., & Datta, S. R. (2023). Mouse spontaneous behavior reflects individual variation rather than estrous state. *Curr Biol*, *33*(7), 1358-1364 e1354. https://doi.org/10.1016/j.cub.2023.02.035

Lewis, J., Dickson, D. W., Lin, W. L., Chisholm, L., Corral, A., Jones, G., Yen, S. H., Sahara, N., Skipper, L., Yager, D., Eckman, C., Hardy, J., Hutton, M., & McGowan, E. (2001). Enhanced neurofibrillary degeneration in transgenic mice expressing mutant tau and APP. *Science*, *293*(5534), 1487-1491. https://doi.org/10.1126/science.1058189

Lewis, J., & McGowan, E. (2005). Rodent Models of Tauopathies. In M. LeDoux (Ed.), *Animal Models of Movement Disorders* (pp. 529-539). Academic Press. https://doi.org/10.1016/b978-012088382-0/50048-7

Lewis, J., McGowan, E., Rockwood, J., Melrose, H., Nacharaju, P., Van Slegtenhorst, M., Gwinn-Hardy, K., Paul Murphy, M., Baker, M., Yu, X., Duff, K., Hardy, J., Corral, A., Lin, W. L., Yen, S. H., Dickson, D. W., Davies, P., & Hutton, M. (2000). Neurofibrillary tangles, amyotrophy and progressive motor disturbance in mice expressing mutant (P301L) tau protein. *Nat Genet*, *25*(4), 402-405. https://doi.org/10.1038/78078

Lim, L., Wei, Y., Lu, Y., & Song, J. (2016). ALS-Causing Mutations Significantly Perturb the Self-Assembly and Interaction with Nucleic Acid of the Intrinsically Disordered Prion-Like Domain of TDP-43. *PLoS Biol*, *14*(1), e1002338. https://doi.org/10.1371/journal.pbio.1002338

Limorenko, G., & Lashuel, H. A. (2022). Revisiting the grammar of Tau aggregation and pathology formation: how new insights from brain pathology are shaping how we study and target Tauopathies. *Chem Soc Rev*, *51*(2), 513-565. https://doi.org/10.1039/d1cs00127b

Liu, J., Zheng, Q., Deng, Y., Cheng, C. S., Kallenbach, N. R., & Lu, M. (2006). A seven-helix coiled coil. *Proc Natl Acad Sci U S A*, *103*(42), 15457-15462. https://doi.org/10.1073/pnas.0604871103

Luna-Muñoz, J., Mena, R., Chávez-Macías, L., & García-Sierra, F. (2007). Earliest stages of tau conformational changes are related to the appearance of a sequence of specific phospho-dependent tau epitopes in Alzheimer's disease [Article]. *Journal of Alzheimer's Disease*, *12*(4), 365-375-375. https://doi.org/10.3233/JAD-2007-12410

Maher, J. M., Markey, J. C., & Ebert-May, D. (2013). The other half of the story: effect size analysis in quantitative research. *CBE Life Sci Educ*, *12*(3), 345-351. https://doi.org/10.1187/cbe.13-04-0082

Martinez, P., Patel, H., You, Y., Jury, N., Perkins, A., Lee-Gosselin, A., Taylor, X., You, Y., Viana Di Prisco, G., Huang, X., Dutta, S., Wijeratne, A. B., Redding-Ochoa, J., Shahid, S. S., Codocedo, J. F., Min, S., Landreth, G. E., Mosley, A. L., Wu, Y. C., . . . Lasagna-Reeves, C. A. (2022). Bassoon contributes to tau-seed propagation and neurotoxicity. *Nat Neurosci*, *25*(12), 1597-1607. https://doi.org/10.1038/s41593-022-01191-6

Martins-de-Souza, D., Gattaz, W. F., Schmitt, A., Rewerts, C., Maccarrone, G., Dias-Neto, E., & Turck, C. W. (2009). Prefrontal cortex shotgun proteome analysis reveals altered calcium homeostasis and immune system imbalance in schizophrenia. *Eur Arch Psychiatry Clin Neurosci*, *259*(3), 151-163. https://doi.org/10.1007/s00406-008-0847-2

Martins-de-Souza, D., Maccarrone, G., Wobrock, T., Zerr, I., Gormanns, P., Reckow, S., Falkai, P., Schmitt, A., & Turck, C. W. (2010). Proteome analysis of the thalamus and cerebrospinal fluid reveals glycolysis dysfunction and potential biomarkers candidates for schizophrenia. *J Psychiatr Res*, *44*(16), 1176-1189. https://doi.org/10.1016/j.jpsychires.2010.04.014

Maziuk, B. F., Apicco, D. J., Cruz, A. L., Jiang, L., Ash, P. E. A., da Rocha, E. L., Zhang, C., Yu, W. H., Leszyk, J., Abisambra, J. F., Li, H., & Wolozin, B. (2018). RNA binding proteins co-localize with small tau inclusions in tauopathy. *Acta Neuropathol Commun*, *6*(1), 71. https://doi.org/10.1186/s40478-018-0574-5

Mielenz, D., Reichel, M., Jia, T., Quinlan, E. B., Stockl, T., Mettang, M., Zilske, D., Kirmizi-Alsan, E., Schonberger, P., Praetner, M., Huber, S. E., Amato, D., Schwarz, M., Purohit, P., Brachs, S., Spranger, J., Hess, A., Buttner, C., Ekici, A. B., . . . Muller, C. P. (2018). EFhd2/Swiprosin-1 is a common genetic determinator for sensation-seeking/low anxiety and alcohol addiction. *Mol Psychiatry*, *23*(5), 1303-1319. https://doi.org/10.1038/mp.2017.63

Moloney, C. M., Lowe, V. J., & Murray, M. E. (2021). Visualization of neurofibrillary tangle maturity in Alzheimer's disease: A clinicopathologic perspective for biomarker research. *Alzheimers Dement*, *17*(9), 1554-1574. https://doi.org/10.1002/alz.12321

Morishima-Kawashima, M., Hasegawa, M., Takio, K., Suzuki, M., Yoshida, H., Titani, K., & Ihara, Y. (1995). Proline-directed and non-proline-directed phosphorylation of PHF-tau. *J Biol Chem*, *270*(2), 823-829. https://doi.org/10.1074/jbc.270.2.823

Morsch, R., Simon, W., & Coleman, P. D. (1999). Neurons may live for decades with neurofibrillary tangles. *J Neuropathol Exp Neurol*, *58*(2), 188-197. https://doi.org/10.1097/00005072-199902000-00008

Mufson, E. J., Ward, S., & Binder, L. (2014). Prefibrillar tau oligomers in mild cognitive impairment and Alzheimer's disease. *Neurodegener Dis*, *13*(2-3), 151-153. https://doi.org/10.1159/000353687

Neddens, J., Temmel, M., Flunkert, S., Kerschbaumer, B., Hoeller, C., Loeffler, T., Niederkofler, V., Daum, G., Attems, J., & Hutter-Paier, B. (2018). Phosphorylation of different tau sites during progression of Alzheimer's disease. *Acta Neuropathol Commun*, *6*(1), 52. https://doi.org/10.1186/s40478-018-0557-6

Neely, C. L. C., Pedemonte, K. A., Boggs, K. N., Flinn, J. M., Neely, C. L. C., Pedemonte, K. A., & Flinn, J. M. (2019). Nest Building Behavior as an Early Indicator of Behavioral Deficits in Mice. *JoVE*(152), e60139. https://doi.org/10.3791/60139

Nelson, M. R., Thulin, E., Fagan, P. A., Forsen, S., & Chazin, W. J. (2002). The EF-hand domain: a globally cooperative structural unit. *Protein Sci*, *11*(2), 198-205. https://doi.org/10.1110/ps.33302

Otvos, L., Jr., Feiner, L., Lang, E., Szendrei, G. I., Goedert, M., & Lee, V. M. (1994). Monoclonal antibody PHF-1 recognizes tau protein phosphorylated at serine residues 396 and 404. *J Neurosci Res*, *39*(6), 669-673. https://doi.org/10.1002/jnr.490390607

Park, K. R., An, J. Y., Kang, J. Y., Lee, J. G., Lee, Y., Mun, S. A., Jun, C. D., Song, W. K., & Eom, S. H. (2017). Structural mechanism underlying regulation of human EFhd2/Swiprosin-1 actin-bundling activity by Ser183 phosphorylation. *Biochem Biophys Res Commun*, *483*(1), 442-448. https://doi.org/10.1016/j.bbrc.2016.12.124

Patterson, K. R., Remmers, C., Fu, Y., Brooker, S., Kanaan, N. M., Vana, L., Ward, S., Reyes, J. F., Philibert, K., Glucksman, M. J., & Binder, L. I. (2011). Characterization of prefibrillar Tau oligomers in vitro and in Alzheimer disease. *J Biol Chem*, *286*(26), 23063-23076. https://doi.org/10.1074/jbc.M111.237974

Prikas, E., Paric, E., Asih, P. R., Stefanoska, K., Stefen, H., Fath, T., Poljak, A., & Ittner, A. (2022). Tau target identification reveals NSF-dependent effects on AMPA receptor trafficking and memory formation. *Embo j*, *41*(18), e10242. https://doi.org/10.15252/embj.2021110242

Purohit, P., Perez-Branguli, F., Prots, I., Borger, E., Gunn-Moore, F., Welzel, O., Loy, K., Wenzel, E. M., Gromer, T. W., Brachs, S., Holzer, M., Buslei, R., Fritsch, K., Regensburger, M., Bohm, K. J., Winner, B., & Mielenz, D. (2014). The Ca2+ sensor protein swiprosin-1/EFhd2 is present in neurites and involved in kinesin-mediated transport in neurons. *PLoS One*, *9*(8), e103976. https://doi.org/10.1371/journal.pone.0103976

Rao, M. V., McBrayer, M. K., Campbell, J., Kumar, A., Hashim, A., Sershen, H., Stavrides, P. H., Ohno, M., Hutton, M., & Nixon, R. A. (2014). Specific calpain inhibition by calpastatin prevents tauopathy and neurodegeneration and restores normal lifespan in tau P301L mice. *J Neurosci*, *34*(28), 9222-9234. https://doi.org/10.1523/JNEUROSCI.1132-14.2014

Regensburger, M., Prots, I., Reimer, D., Brachs, S., Loskarn, S., Lie, D. C., Mielenz, D., & Winner, B. (2018). Impact of Swiprosin-1/Efhd2 on Adult Hippocampal Neurogenesis. *Stem Cell Reports*, *10*(2), 347-355. https://doi.org/10.1016/j.stemcr.2017.12.010

Ren, Y., & Sahara, N. (2013). Characteristics of tau oligomers. *Front Neurol*, *4*, 102. https://doi.org/10.3389/fneur.2013.00102

Rizzu, P., Van Swieten, J. C., Joosse, M., Hasegawa, M., Stevens, M., Tibben, A., Niermeijer, M. F., Hillebrand, M., Ravid, R., Oostra, B. A., Goedert, M., van Duijn, C. M., & Heutink, P. (1999). High prevalence of mutations in the microtubule-associated protein tau in a population study of frontotemporal dementia in the Netherlands. *Am J Hum Genet*, *64*(2), 414-421. https://doi.org/10.1086/302256

Sahara, N., Lewis, J., DeTure, M., McGowan, E., Dickson, D. W., Hutton, M., & Yen, S. H. (2002). Assembly of tau in transgenic animals expressing P301L tau: alteration of phosphorylation and solubility. *J Neurochem*, *83*(6), 1498-1508. https://doi.org/10.1046/j.1471-4159.2002.01241.x

Santacruz, K., Lewis, J., Spires, T., Paulson, J., Kotilinek, L., Ingelsson, M., Guimaraes, A., DeTure, M., Ramsden, M., McGowan, E., Forster, C., Yue, M., Orne, J., Janus, C., Mariash, A., Kuskowski, M., Hyman, B., Hutton, M., & Ashe, K. H. (2005). Tau suppression in a neurodegenerative mouse model improves memory function. *Science*, *309*(5733), 476-481. https://doi.org/10.1126/science.1113694

Schober, P., Boer, C., & Schwarte, L. A. (2018). Correlation Coefficients: Appropriate Use and Interpretation. *Anesth Analg*, *126*(5), 1763-1768. https://doi.org/10.1213/ANE.0000000000002864

Sexton, C., Snyder, H., Beher, D., Boxer, A. L., Brannelly, P., Brion, J. P., Buee, L., Cacace, A. M., Chetelat, G., Citron, M., DeVos, S. L., Diaz, K., Feldman, H. H., Frost, B., Goate, A. M., Gold, M., Hyman, B., Johnson, K., Karch, C. M., . . . Carrillo, M. C. (2022). Current directions in tau research: Highlights from Tau 2020. *Alzheimers Dement*, *18*(5), 988-1007. https://doi.org/10.1002/alz.12452

Spires, T. L., Orne, J. D., SantaCruz, K., Pitstick, R., Carlson, G. A., Ashe, K. H., & Hyman, B. T. (2006). Region-specific dissociation of neuronal loss and neurofibrillary pathology in a mouse model of tauopathy. *Am J Pathol*, *168*(5), 1598-1607. https://doi.org/10.2353/ajpath.2006.050840

Spires-Jones, T. L., Stoothoff, W. H., de Calignon, A., Jones, P. B., & Hyman, B. T. (2009). Tau pathophysiology in neurodegeneration: a tangled issue. *Trends Neurosci*, *32*(3), 150-159. https://doi.org/10.1016/j.tins.2008.11.007

Strang, K. H., Golde, T. E., & Giasson, B. I. (2019). MAPT mutations, tauopathy, and mechanisms of neurodegeneration. *Lab Invest*, *99*(7), 912-928. https://doi.org/10.1038/s41374-019-0197-x

Sydow, A., Van der Jeugd, A., Zheng, F., Ahmed, T., Balschun, D., Petrova, O., Drexler, D., Zhou, L., Rune, G., Mandelkow, E., D'Hooge, R., Alzheimer, C., & Mandelkow, E. M. (2011). Tau-induced defects in synaptic plasticity, learning, and memory are reversible in transgenic mice after switching off the toxic Tau mutant. *J Neurosci*, *31*(7), 2511-2525. https://doi.org/10.1523/JNEUROSCI.5245-10.2011

Szczepaniak, K., Bukala, A., da Silva Neto, A. M., Ludwiczak, J., & Dunin-Horkawicz, S. (2021). A library of coiled-coil domains: from regular bundles to peculiar twists. *Bioinformatics*, *36*(22-23), 5368-5376. https://doi.org/10.1093/bioinformatics/btaa1041

Tiernan, C. T., Combs, B., Cox, K., Morfini, G., Brady, S. T., Counts, S. E., & Kanaan, N. M. (2016). Pseudophosphorylation of tau at S422 enhances SDS-stable dimer formation and impairs both anterograde and retrograde fast axonal transport. *Exp Neurol*, *283*(Pt A), 318-329. https://doi.org/10.1016/j.expneurol.2016.06.030

Tracy, T. E., Madero-Perez, J., Swaney, D. L., Chang, T. S., Moritz, M., Konrad, C., Ward, M. E., Stevenson, E., Huttenhain, R., Kauwe, G., Mercedes, M., Sweetland-Martin, L., Chen, X., Mok, S. A., Wong, M. Y., Telpoukhovskaia, M., Min, S. W., Wang, C., Sohn, P. D., . . . Gan, L. (2022). Tau interactome maps synaptic and mitochondrial processes associated with neurodegeneration. *Cell*, *185*(4), 712-728 e714. https://doi.org/10.1016/j.cell.2021.12.041

Vana, L., Kanaan, N. M., Ugwu, I. C., Wuu, J., Mufson, E. J., & Binder, L. I. (2011). Progression of tau pathology in cholinergic Basal forebrain neurons in mild cognitive impairment and Alzheimer's disease. *Am J Pathol*, *179*(5), 2533-2550. https://doi.org/10.1016/j.ajpath.2011.07.044

Vanderweyde, T., Apicco, D. J., Youmans-Kidder, K., Ash, P. E. A., Cook, C., Lummertz da Rocha, E., Jansen-West, K., Frame, A. A., Citro, A., Leszyk, J. D., Ivanov, P., Abisambra, J. F., Steffen, M., Li, H., Petrucelli, L., & Wolozin, B. (2016). Interaction of tau with the RNA-Binding Protein TIA1 Regulates tau Pathophysiology and Toxicity. *Cell Rep*, *15*(7), 1455-1466. https://doi.org/10.1016/j.celrep.2016.04.045

Vega, I. E. (2016). EFhd2, a Protein Linked to Alzheimer's Disease and Other Neurological Disorders. *Front Neurosci*, *10*, 150. https://doi.org/10.3389/fnins.2016.00150

Vega, I. E., Sutter, A., Parks, L., Umstead, A., & Ivanova, M. I. (2018). Tau's Three-Repeat Domain and EFhd2 Co-incubation Leads to Increased Thioflavin Signal. *Front Neurosci*, *12*, 879. https://doi.org/10.3389/fnins.2018.00879

Vega, I. E., Traverso, E. E., Ferrer-Acosta, Y., Matos, E., Colon, M., Gonzalez, J., Dickson, D., Hutton, M., Lewis, J., & Yen, S. H. (2008). A novel calcium-binding protein is associated with tau proteins in tauopathy. *J Neurochem*, *106*(1), 96-106. https://doi.org/10.1111/j.1471-4159.2008.05339.x

Vega, I. E., Umstead, A., & Kanaan, N. M. (2019). EFhd2 Affects Tau Liquid-Liquid Phase Separation. *Front Neurosci*, *13*, 845. https://doi.org/10.3389/fnins.2019.00845

Vuadens, F., Rufer, N., Kress, A., Corthesy, P., Schneider, P., & Tissot, J. D. (2004). Identification of swiprosin 1 in human lymphocytes. *Proteomics*, *4*(8), 2216-2220. https://doi.org/10.1002/pmic.200300779

Wang, Y., & Mandelkow, E. (2016). Tau in physiology and pathology. *Nat Rev Neurosci*, *17*(1), 5-21. https://doi.org/10.1038/nrn.2015.1

Wittmann, C. W., Wszolek, M. F., Shulman, J. M., Salvaterra, P. M., Lewis, J., Hutton, M., & Feany, M. B. (2001). Tauopathy in Drosophila: neurodegeneration without neurofibrillary tangles. *Science*, *293*(5530), 711-714. https://doi.org/10.1126/science.1062382

Wolozin, B. L., Pruchnicki, A., Dickson, D. W., & Davies, P. (1986). A neuronal antigen in the brains of Alzheimer patients. *Science*, *232*(4750), 648-650. https://doi.org/10.1126/science.3083509

Xue, B., Qu, Y., Zhang, X., & Xu, X. F. (2022). miRNA-126a-3p participates in hippocampal memory via alzheimer's disease-related proteins. *Cereb Cortex*, *32*(21), 4763-4781. https://doi.org/10.1093/cercor/bhab515

Younas, A., Younas, N., Iqbal, M. J., Ferrer, I., & Zerr, I. (2024). Comparative interactome mapping of Tau-protein in classical and rapidly progressive Alzheimer's disease identifies subtype-specific pathways. *Neuropathol Appl Neurobiol*, *50*(1), e12964. https://doi.org/10.1111/nan.12964

A
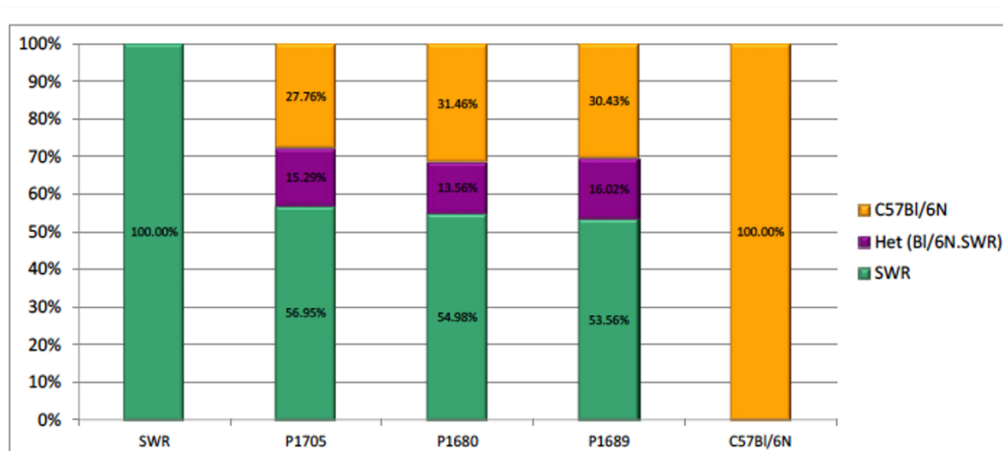
B
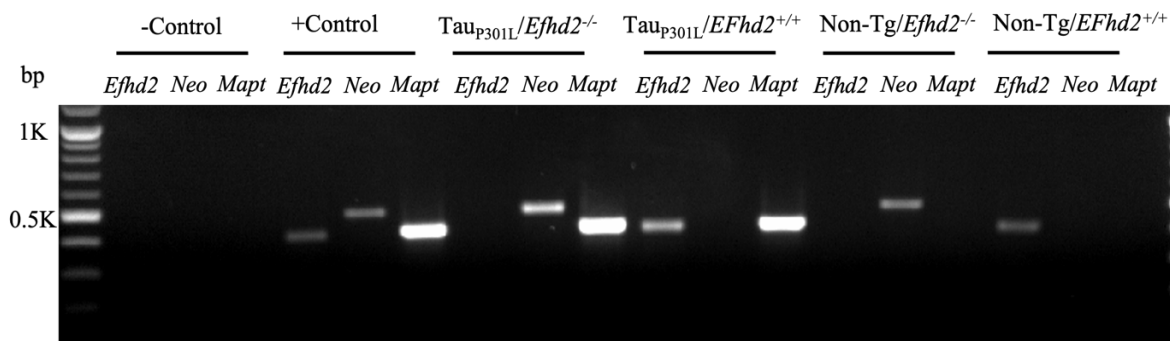
Figure A4.1. Genomic marker background assessment – SNPs and genotyping. (A) Illustrates the SNPs associated to either Swiss Webster (SWR), C57BL/6J or Mixed (Het(Sw.B6) genomic background. Mice were selected randomly (n=3). The number assigned to each mouse is listed on the graph. The mice maintained a stable homogeneous genomic background. (**B**) PCR-based genotyping. It shows the presence of *Efhd2* in the wild type (*Efhd2*$^{+/+}$) while detection of the Neomycin cassette (*Neo*) verifies the knockout (*Efhd2*$^{-/-}$). In addition, the presence of *MAPT* confirms Tau$_{P301L}$ and its absence indicates Non-Tg (no tau). Positive and negative controls were included in each genotyping cycle for verification. (bp) denotes DNA base pair.
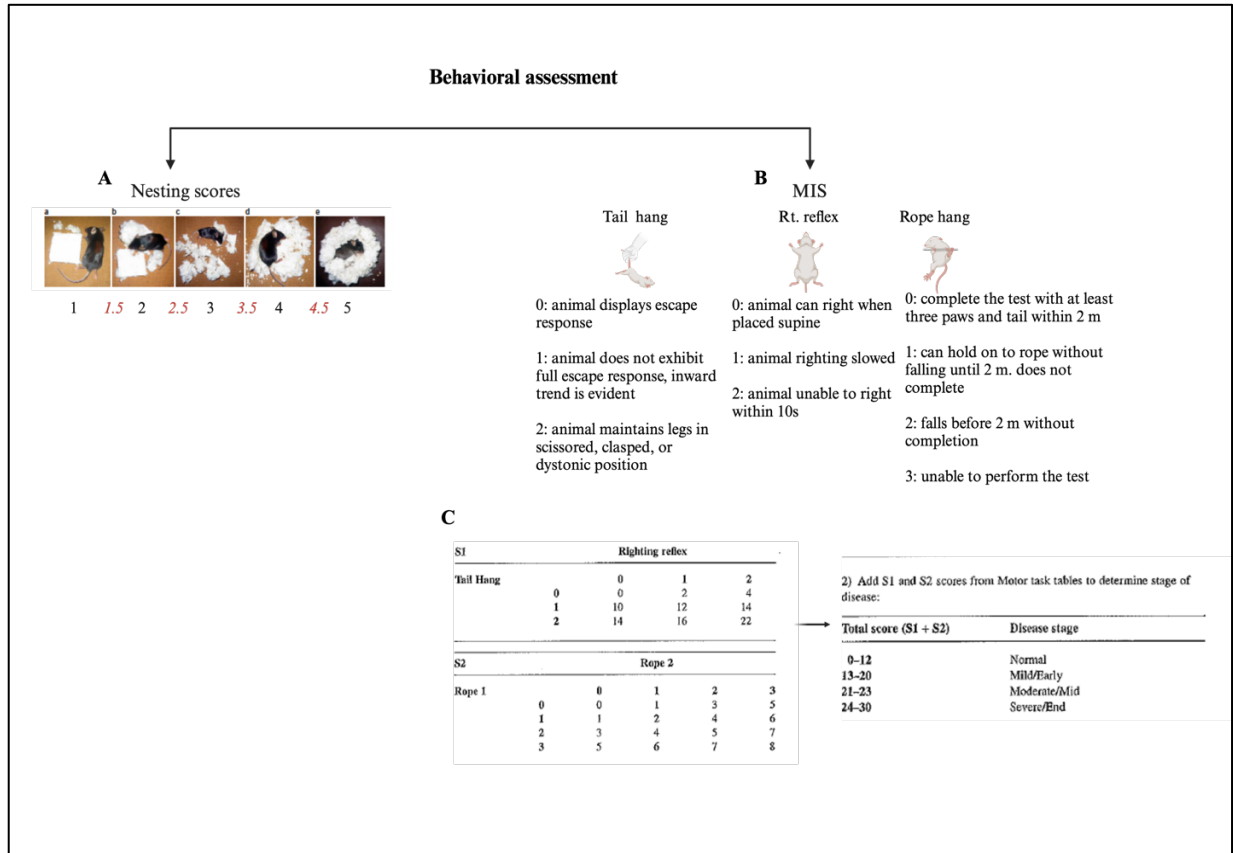
Figure A4.2. Nesting and motor impairment scoring. (**A**) Mice were singly housed for 24 h with nestlets. The next day the nest of each mouse was evaluated by three independent blind raters. The average of the three scores was used for analysis. Nesting scoring (NS) was adopted from (Deacon, 2006). Scores from 1 to 5 with 0.5 increments were used whereby 1 indicates poorest nesting behavior, and 5 indicates normal nesting behavior. (**B**) motor impairment scoring (MIS) was adopted from (Lewis & McGowan, 2005). Motor function of each mouse was evaluated by three sub-assessments: tail hang, righting reflex, and rope hang. Each of these tests are given a separate score according to the rubric. Rope hang test is done twice for each mouse. (**C**) The combination of righting reflex score and tail hang will be converted to S1 score. Likewise, the two rope hang tests will be merged into S2 score according to a conversion table. Adding S1 and S2 yields a final MIS for each mouse representing progressive disease stages. Motor assessment was conducted by two independent blind raters. Figure was created with Biorender.com.
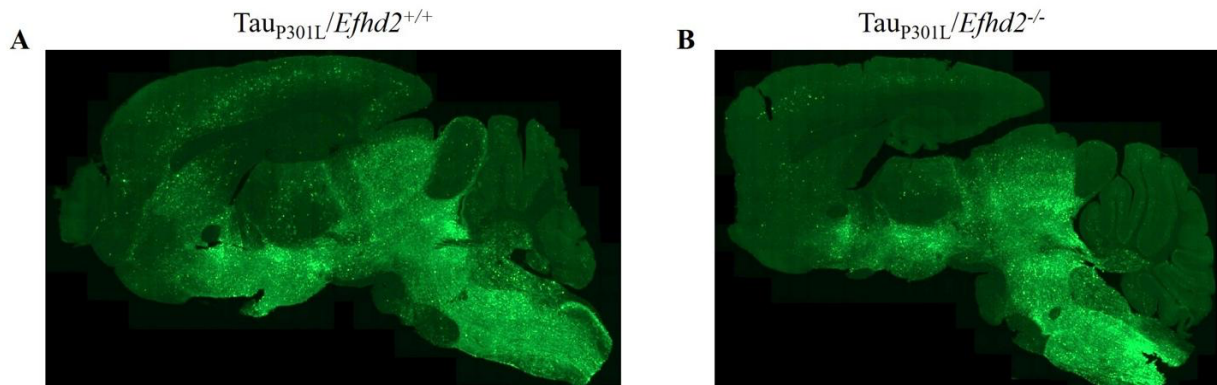
Figure A4.3. The deletion of *Efhd2* did not change selective vulnerability of brain regions. Sagittal brain sections of 12 months Tau$_{P301L}$/*Efhd2*$^{+/+}$ (**A**) and Tau$_{P301L}$/*Efhd2*$^{-/-}$ (**B**) stained with pSer422. Consistent with the literature, accumulation of tau pathology pervades brainstem, hypothalamus, basal ganglia, and the cortex with minimal accumulation in the hippocampus. The absence of EFhd2 in Tau$_{P301L}$ (JNPL3) mice did not change tau propagation to these brain regions.

A
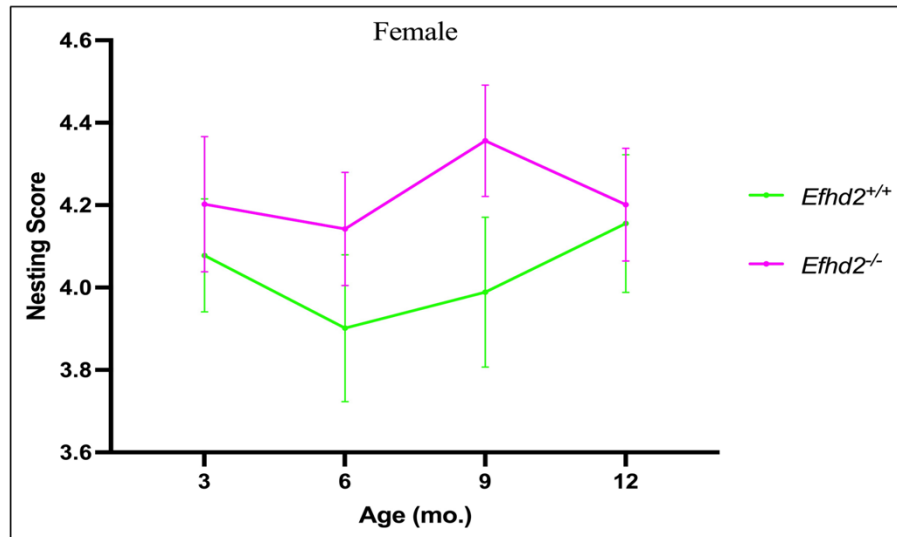
B
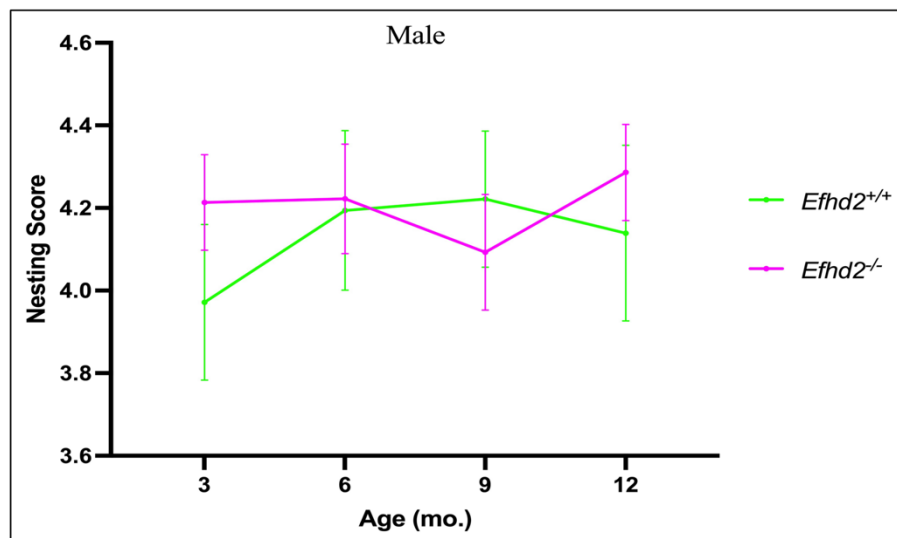
Figure A4.4. No difference in nesting scores between *Efhd2$^{+/+}$* and *Efhd2$^{-/-}$*. (**A**) Mixed factor RM-ANOVA analysis of longitudinal nesting scores of female mice revealed a small interaction (F $(3, 81) = 0.4828$ p$=0.6951$, $\eta^2_p=0.02$). Both the genotype (F $(1, 27) = 2.047$ p$=0.1639$, $\eta^2_p=0.04$) and age (F $(2.793, 75.40) = 0.5212$ p$=0.6561$, $\eta^2_p=0.02$) main effects were small. N$=$ 14-15. (**B**) Mixed factor RM-ANOVA analysis for male nesting scores also showed a small interaction between genotype and age (F $(3, 84) = 0.6541$ p$=0.5826$, $\eta^2_p=0.02$). Likewise, a small genotype effect (F $(1, 28) = 0.2750$ p$=0.6042$, $\eta^2_p=0.01$) and age effect (F $(2.566, 71.84) = 0.3215$ p$=0.7785$, $\eta^2_p=0.01$) were detected. N$=$ 12-18. Error bars indicate mean $\pm$ SEM.

Chapter Five: Conclusions

Overview

The last two decades have witnessed a dramatic increase in studies that primarily focused on tauopathies (Chung et al., 2021; Limorenko & Lashuel, 2022; Sexton et al., 2022; Zhang et al., 2022). Indeed, reputed research groups have devoted much effort to demystify the molecular mechanisms that govern the biogenesis of pathological tau aggregates and associated progressive neurodegeneration. These efforts aim ultimately to achieve better diagnostic and therapeutic strategies for people living with tauopathies (Chung et al., 2021; Limorenko & Lashuel, 2022; Sexton et al., 2022; Zhang et al., 2022). Nonetheless, this is not an easy task given the growing evidence indicating a striking heterogeneity among different tauopathies(Chung et al., 2021).

Tauopathies diverge with respect to brain regions vulnerability, cellular inclusions, and propagation patterns of tau aggregates (Chung et al., 2021; Limorenko & Lashuel, 2022). In addition, the diversity among tauopathies extends to include the distinctive aggregation of different tau structures e.g., neuronal neurofibrillary tangles (NFTs) in Alzheimer's disease (AD), tufted astrocytes and oligodendroglial coiled bodies in progressive supranuclear palsy (PSP), and Pick's bodies in Pick's disease (PiD) in specific brain regions (Chung et al., 2021; Limorenko & Lashuel, 2022; Sexton et al., 2022; Zhang et al., 2022). This remarkably diverse neuropathological features translate into differences in the clinical phenotype of each disorder showing a wide spectrum of symptoms that distinguish impacted domains (cognitive, motion, and language) (Chung et al., 2021; Limorenko & Lashuel, 2022; Sexton et al., 2022; Zhang et al., 2022). A multitude of studies have also endorsed the structural differences of filamentous tau aggregates across tauopathies (Ksiezak-Reding et al., 1996; Ksiezak-Reding et al., 1998; King et al., 2001; Ksiezak-Reding & Wall, 2005; Alhadidy & Kanaan, 2024). These studies collectively indicate unique aberrant tau conformations constituting the core of the pathological hallmark aggregates in each tauopathy (Fitzpatrick et al., 2017; Falcon et al., 2018a; Falcon et al., 2018b; Falcon et al., 2019; Zhang et al., 2020). Hence, many scientists adhere to the view that different molecular factors probably drive tau aggregation across different tauopathies (Chung et al., 2021; Sexton et al., 2022; Zhang et al., 2022; Alhadidy & Kanaan, 2024).

Akin to other neurodegenerative disorders, the major challenge that faces the tauopathy field is the paucity of reliable therapeutic approaches. With the unknown etiology for most of tauopathies (except inherited frontotemporal dementia (FTD) and chronic traumatic encephalopathy (CTE)), developing disease-modifying therapy has attracted a considerable

interest in the field (Sexton et al., 2022; Zhang et al., 2022). Attempts to rescue disturbed tau-related physiological function or to target directly tau aggregation have either failed or remained under active investigation (Zhang et al., 2022). Against this backdrop, unraveling the molecular factors that govern the abnormal transition of tau into pathological aggregates has become fundamental to eventually develop effective therapeutic approaches (Limorenko & Lashuel, 2022). As mentioned earlier, these molecular factors are not anticipated to be the same across tauopathies, which imply the need for tauopathy-specific therapy in the future.

It is widely accepted that pathological tau aggregation starts with aberrant tau conformations that aggregate to form dimers, trimers, and oligomers (Kuret et al., 2005; Wang & Mandelkow, 2016; Chung et al., 2021). Then those oligomeric species further aggregate to form filamentous tau that coalesce forming higher order ultrastructure, e.g., NFTs in AD (Kuret et al., 2005; Wang & Mandelkow, 2016; Chung et al., 2021). A growing number of scholars agree that early pretangle oligomeric tau aggregates are the true culprit that induces propagation and neurodegeneration as opposed to later tau filaments and tangles (Gomez-Isla et al., 1997; Wittmann et al., 2001; Santacruz et al., 2005; Spires et al., 2006; Berger et al., 2007; Brunden et al., 2008; Spires-Jones et al., 2009; Kayed, 2010; Lasagna-Reeves et al., 2011; Patterson et al., 2011; Sydow et al., 2011; Lasagna-Reeves et al., 2012; Cowan & Mudher, 2013). The basic tenet considers the later tangles as a protective cellular response whereby they halt further propagation and transmission of toxic pretangle aggregates that seed further tau aggregation in other regions (Gomez-Isla et al., 1997; Wittmann et al., 2001; Santacruz et al., 2005; Spires et al., 2006; Berger et al., 2007; Brunden et al., 2008; Spires-Jones et al., 2009; Kayed, 2010; Lasagna-Reeves et al., 2011; Patterson et al., 2011; Sydow et al., 2011; Lasagna-Reeves et al., 2012; Cowan & Mudher, 2013). As such, it became imperative to study the factors that could initiate, enhance, or inhibit aberrant tau aggregation. Tau mutations, post-translational modifications (PTMs), and truncations have been suggested to predispose tau to oligomerize and further aggregate (Wang & Mandelkow, 2016). Furthermore, studying tau interactome has become an interesting area of research to gain more insights into tau's role in health and disease by dissecting its connecting network (Kavanagh et al., 2022; Limorenko & Lashuel, 2022; Tracy et al., 2022). Several tau interacting proteins could have significant impact on tau aggregation leading to the accumulation of certain pathological tau forms at the expense of others

(Vanderweyde et al., 2016; Apicco et al., 2018; Maziuk et al., 2018; Jiang et al., 2019; Ash et al., 2021; Moreira et al., 2021; Martinez et al., 2022).

This dissertation endeavor expands our research group's work regarding the interaction between EFhd2 and tau (Vega et al., 2008; Ferrer-Acosta et al., 2013a; Ferrer-Acosta et al., 2013b; Vazquez-Rosa et al., 2014; Vega, 2016; Vega et al., 2018; Vega et al., 2019). Previously, we discovered EFhd2 as a tau-associated protein in JNPL3 mice and postmortem tauopathy brains (Vega et al., 2008; Ferrer-Acosta et al., 2013b). EFhd2 accumulation with pathological tau aggregates increased with aging (Vega et al., 2008). Furthermore, we identified higher EFhd2 protein level in AD compared to normal aging (Ferrer-Acosta et al., 2013b). Importantly, we discovered that EFhd2 impacts tau dynamics and promotes β-sheet formation *in vitro* (Vega et al., 2018; Vega et al., 2019). These findings instigated the question "What is the role of EFhd2 in the biogenesis of pathological tau aggregates?" In this dissertation research, we sought to address this question by testing the overarching hypothesis that EFhd2 has a neurodegenerative role by inducing the formation of pathological tau aggregates.

Main findings and key insights

Previous studies demonstrated that EFhd2 co-purify and co-aggregate with pathological tau in AD. Our results highlight the distinct capacity of EFhd2 to interact with monomeric and filamentous tau *in vitro* inducing the formation of unique larger aggregates (Chapter Two). The extent of EFhd2-tau aggregation was more pronounced with filamentous tau compared to monomeric tau (Chapter Two). Strikingly, EFhd2 entangled tau filaments into structures that are largely reminiscent of higher order pathological tangles formed in AD (Chapter Two). Importantly, the results showed that adding EFhd2 after the formation of tau filaments significantly reduced the area of entangled aggregate structures. In contrast, the presence of EFhd2 and tau together before inducing tau fibrillization (with arachidonic acid (ARA)) did not elicit significant change in the area of those aggregates (Chapter Two). In essence, these data suggest a dynamic relation between EFhd2 and tau that influences subsequent aggregate formation. In particular, we can infer from the results that EFhd2 largely does not perturb or preclude the formation of tau filaments/oligomers; instead, EFhd2 transforms them into entangled structures (Chapter Two).

As noted before, EFhd2 protein levels are elevated in AD brains (Ferrer-Acosta et al., 2013b). However, the temporal changes in tau-EFhd2 association and in EFhd2 protein levels

during different disease stages remain unknown. Given the presented findings in Chapter Two, we could postulate that the timing of EFhd2-tau interaction during the sequential events of tau aggregation could critically impact the extent of tangle formation *in vivo.* This explanation merits further investigation to uncover the role that EFhd2-induced tau aggregation plays in tau pathology.

Our results imply that EFhd2 entanglement of tau filaments into large aggregates reduces the exposure of Alz50 epitope (Chapter Two). Coinciding with that conclusion, neuropathological assessment of Tau_{P301L}/*Efhd2*$^{-/-}$ mouse model revealed a distinct increase in Alz50 staining area along with reduced pSer422 and PHF1 tau (Chapter Four). Interestingly, that change was more predominant in the cortex than the brainstem area. Since Alz50 indicates pretangle aggregates whereas pSer422 and PHF1 tau mostly indicate later fibrillar and mature tangles, we can infer that the absence of EFhd2 led to a reduction in the NFTs maturity towards tangles formation accompanied by accumulation of pretangle aggregates. Together, Chapter Two (*in vitro*) and Chapter Four (*in vivo*) propose a plausible scenario for the role of EFhd2 in tau pathology. EFhd2's prominent role during pathological trajectory manifests in later stages of tau aggregation enhancing higher order tangles formation without impacting the prior phases of aggregation.

As discussed earlier, numerous studies have shown that the formation of tau tangles potentially holds a neuroprotective response against cellular demise and pathological propagation (Gomez-Isla et al., 1997; Wittmann et al., 2001; Santacruz et al., 2005; Spires et al., 2006; Berger et al., 2007; Brunden et al., 2008; Spires-Jones et al., 2009; Kayed, 2010; Lasagna-Reeves et al., 2011; Patterson et al., 2011; Sydow et al., 2011; Lasagna-Reeves et al., 2012; Cowan & Mudher, 2013). Conversely, pretangle tau aggregates have been associated with neuronal death and spreading of pathology throughout the brain (Gomez-Isla et al., 1997; Wittmann et al., 2001; Santacruz et al., 2005; Spires et al., 2006; Berger et al., 2007; Brunden et al., 2008; Spires-Jones et al., 2009; Kayed, 2010; Lasagna-Reeves et al., 2011; Patterson et al., 2011; Sydow et al., 2011; Lasagna-Reeves et al., 2012; Cowan & Mudher, 2013). In light of the presented findings, however, proposing that EFhd2 plays a neuroprotective role solely because it may promote the transformation of the neurotoxic tau aggregates to the less toxic tangle aggregates requires more research. The reason for that is the lack of detectable change in the age-dependent neurodegeneration phenotype of Tau_{P301L}/*Efhd2*$^{-/-}$ compared to wild type mice.

Indeed, one might ask why the absence of EFhd2 did not exacerbate the behavioral phenotype since early "neurotoxic" pretangle aggregates increased in Tau$_{P301L}$/*Efhd2*$^{-/-}$ mice. That could be interpreted by many ways. Tau$_{P301L}$ mouse model exhibits progressive robust age-dependent pathology and neurodegeneration, thereby creating a ceiling effect that could obscure further worsening. Furthermore, the literature is replete with several studies showing a degree of asynchrony between neuropathological changes of tau aggregates and the phenotype (Heinonen et al., 1995; Gómez-Isla et al., 1996; Gómez-Isla & Frosch, 2022). Hence, the presence of pathological aggregates does not necessarily impart immediate changes on the phenotype.

In fact, the discussion so far has focused on the tau-related aspect of EFhd2; nevertheless, a putative tau-independent effect for EFhd2 could contribute to the neurodegeneration phenotype. Specifically, changes in cellular milieu induced by deleting the *Efhd2* gene could define the neurotoxic or neuroprotective outcomes and the consequent phenotype upon introducing additional insult, such as pathological tau accumulation (Mielenz et al., 2018; Tu et al., 2018; Zhang et al., 2018; Kogias et al., 2020; Tong et al., 2021). From this stance, we examined the proteome changes in the brain of *Efhd2*$^{-/-}$ mice using mass spectrometry (MS) in Chapter Three. The significance of this study is twofold: 1) gain further insights into the understudied role of EFhd2 in the central nervous system (CNS) by unraveling the biological processes changed by its absence, 2) provide the biological context wherein tau pathology emerges in the Tau$_{P301L}$/*Efhd2*$^{-/-}$ mice. In other words, by understanding the proteome changes induced by the absence of EFhd2, we could better understand its biological function and deduce the indirect effect of EFhd2 on tau pathology.

MS-Label-free quantification (MS-LFQ) identified differential abundance of several proteins that regulate diverse cellular processes. For example, we detected higher abundance of tumor necrosis factor receptor-associated protein 1 (TRAP1) in *Efhd2*$^{-/-}$ mice brain. Amazingly, TRAP1 is down regulated in AD brains (Dekker & Rüdiger, 2021). TRAP1 is a mitochondrial HSP90 protein whose main function is to protect against oxidative stress by decreasing reactive oxygen species (ROS) (Dekker & Rüdiger, 2021). It is important to note that the association between low TRAP1 levels and AD pathology remains elusive. However, based on its normal function, we can postulate that lower TRAP1 levels could lead to ROS accumulation, unfettered oxidative stress, and, subsequently, mitochondrial dysfunction. Lower TRAP1 levels also deteriorated synaptic connections (Dekker & Rüdiger, 2021). Therefore, preliminary evidence

suggests that higher levels of TRAP1 may maintain synaptic integrity and neuronal health in the disease (Ramos Rego et al., 2021). By extrapolating this knowledge to our data, we can assume that increased TRAP1 level in Tau$_{P301L}$/$Efhd2^{-/-}$ mice brain contemporaneously with the accumulation of pathological tau resulted in indistinguishable neurodegenerative phenotype compared to Tau$_{P301L}$/$Efhd2^{+/+}$ mice despite the accumulation of pretangle Alz50 positive tau. In simpler terms, deleting the $Efhd2$ gene led to enhanced levels of TRAP1, which, in turn, may protect against the neurotoxic effect of tau aggregates. A compelling future experiment to assess TRAP1 protein levels in Tau$_{P301L}$/$Efhd2^{-/-}$ mice brains will verify this hypothesis.

Of interest, a recently established tau-interacting protein, bassoon, showed a diminished protein level in $Efhd2^{-/-}$ mice brain. Bassoon is a scaffolding pre-synaptic protein that was identified as an interactor with seeding-competent oligomeric tau. The study soundly showed that bassoon could exacerbate oligomeric tau seeding and the resultant neurotoxicity *in vitro* and *in vivo* (Martinez et al., 2022). Furthermore, knocking down Bsn in a tauopathy model rescued behavioral deficits, improved synaptic integrity, and attenuated tau spreading. In fact, bassoon does not seem to impact the formation or the composition of high molecular weight tau aggregates. Rather, bassoon primarily stabilizes seeding competency of tau oligomers and enhances their toxicity. The abundance changes of bassoon in $Efhd2^{-/-}$ mice brains imply a genetic linkage with $Efhd2$. Still, we should determine bassoon protein levels in Tau$_{P301L}$/$Efhd2^{-/-}$ mice brains. An anticipated increase in bassoon levels may indicate a direct response to Tau$_{P301L}$ overexpression and explain the observed changes in the pathological markers.

Additionally, we detected lower abundance of the low-density lipoprotein (LDL) receptor-related protein 1 in $Efhd2^{-/-}$ mice brain compared to wild type. LRP1 is an endocytic protein that regulates endocytosis and trafficking of several ligands by delivering them to lysosomes for degradation (Cooper et al., 2021). Few years ago, a research group proposed that LRP1 controls tau internalization and subsequent spread (Rauch et al., 2020). Despite the limited data, it has been postulated that LRP1 binds to monomeric and pathogenic aggregated tau (Rauch et al., 2020; Cooper et al., 2021). Upon binding with monomeric tau, LRP1 internalizes and delivers tau for lysosomes for degradation. Thence, physiologically, LRP1 may maintain normal tau protein turnover in the cell. However, LRP1 role becomes detrimental when it binds to aggregated tau because it enhances the propagation of tau pathology from cell to another without directing these pathogenic forms to degradation. Knocking down *LRP1 in vitro* and *in vivo*

halted aggregated tau spreading. Still, more studies should verify the role of LRP1 in tauopathy. Its reduction in *Efhd2*$^{-/-}$ mice brain possibly explain the decline of pSer422 and PHF1 tau area in Tau$_{P301L}$/*Efhd2*$^{-/-}$ mice. In short, the potential link between EFhd2 and both bassoon and LRP1 demands further research to determine how these proteins in concert with EFhd2 impact tau aggregation and associated neurodegeneration.

Another approach whereby we examined potential physiological function of EFhd2 in the CNS was mapping its interactome (Chapter Three). The data illustrate a striking similarity between EFhd2 and tau interactome (Kavanagh et al., 2022). Common biological processes that were enriched in tau and EFhd2 interactome networks include vesicle localization, synaptic vesicle cycling, cytoskeletal organization, and mitochondrial regulation (Soliman et al., 2021; Kavanagh et al., 2022; Prikas et al., 2022; Tracy et al., 2022) (Chapter Three). Furthermore, tau and EFhd2 are associated with heat shock proteins (HSPs) and RNA-binding proteins (RBPs). These findings strongly indicate that EFhd2 and tau possibly share the same physiological significance in the brain. In line with this notion, both *Efhd2*$^{-/-}$ and tau knockout (TKO) mice do not exhibit a behavioral phenotype or developmental anomalies (Harada et al., 1994; Purohit et al., 2014). However, studies showed changes at the molecular level where adult hippocampal neurogenesis was impaired in TKO and *Efhd2*$^{-/-}$ mice (Fuster-Matanzo et al., 2009; Hong et al., 2010; Borger et al., 2014).

EFhd2 interactome also include proteins that play a role in tau pathology, such as Camk4 and O-GlcNAc transferase (OGT) (Okuyama & Marshall, 2003; Sałaciak et al., 2021; Zuliani et al., 2021; Martinez et al., 2022) (Chapter Three). Importantly, bassoon was identified in the EFhd2 interactome, which underscores the association between these two proteins. Collectively, EFhd2 brain interactome undergirds its role in several disparate biological processes and cellular pathways that could help demystify its putative role in tau pathology and other neurological disorders.

Concluding this section, the most important contribution of this research is the unique capacity of EFhd2 to interact with early tau aggregates transforming them into later tangles and the biological network of EFhd2 in the brain. Whether EFhd2 plays a neuroprotective or neurotoxic role in tauopathies, the answer probably lies somewhere between these two poles. Hence, the results presented in this dissertation suggest a number of new avenues for research:

1) EFhd2, a friend or a foe?

Our findings point to a direct effect of EFhd2 on biogenesis of tau aggregates along with indirect effect on pathological propagation and neuronal health. The direct effect of EFhd2 on tau suggests its propensity to drive late tangle formation raising a possible neuroprotective role of EFhd2 in tau pathology. An approach to test that is by overexpressing EFhd2 in a tauopathy model and monitoring whether high levels of EFhd2 would alleviate behavioral deficit, maintain neuronal and synaptic integrity, and lessen neuronal burden of pathological tau. Since we propose that EFhd2 might interact with accumulating oligomeric and filamentous tau aggregates to transform them into larger less propagating tangles, it could be more beneficial to overexpress EFhd2 during initial phases of pathology (young age before overt phenotype develops). In that way, neurons would express EFhd2 at levels that suffice to interact promptly with ensuing tau fibrils and form tangles. If EFhd2 overexpression takes place at later ages after incessant neurodegeneration and behavioral deficit emerged, EFhd2 may not have the capacity to stop or rescue neurodegeneration. Nonetheless, that merits further investigation by overexpressing EFhd2 at different stages of pathology in a tauopathy model and assessing behavioral, biochemical, and histological changes.

EFhd2 may indirectly contribute to progressive tau-mediated neurodegeneration through pathological propagation (bassoon and LRP1) and neuronal survival (TRAP1). That indirect effect emanates from the genetic linkage we observed between *Efhd2* expression and these proteins. However, more studies using cellular and animal models should be executed to determine functional consequences of this genetic linkage. We suggest using human tau knock-in (MAPT KI) mouse model to determine functional association of EFhd2 with the aforementioned proteins and resultant impact on behavior and neuronal function. In MAPT KI model, murine *Mapt* gene was replaced by human *MAPT* gene expressing the six isoforms of tau at endogenous levels. Several studies extensively characterized this model showing the absence of overt pathology, behavioral deficit, or neurodegeneration. Therefore, through genetic manipulations, MAPT KI model affords a practical tool to investigate the functional implications for the association of EFhd2 with those proteins in tau-mediated neurodegeneration.

We reported high levels of EFhd2 in AD brains of Braak stages above IV (Ferrer-Acosta et al., 2013b; Vazquez-Rosa et al., 2014). Furthermore, miR-126a that regulates *Efhd2* gene expression in the brain is downregulated in the gray matter of AD brains, which underpins the

increased level of EFhd2 (Wang et al., 2011; Xue et al., 2022). We should bear in mind that the temporal changes of EFhd2 levels in AD or other tauopathies remain unclear. Based on our results, EFhd2 does not preclude early events of tau oligomerization. We propose that the presence of EFhd2 while these early tau aggregates are formed favors their transition to the less toxic tangle aggregates. That shows a clear need for investigating whether EFhd2 and miR-126a levels are disrupted in early or later stages of the disease. Conducting a cross-sectional study to assess EFhd2 and miR-126a levels at different Braak stages will support our proposal for overexpressing EFhd2 at different stages of tau pathology *in vivo.* Alternatively, we could knock down miR-126a in Tau$_{P301L}$/*Efhd2*$^{+/+}$ brain to enhance EFhd2 levels and examine subsequent behavioral and neuropathological changes. Moreover, upstream factors that reduce miR-126a during pathology need further investigation.

Studying tau-interacting proteins has garnered research attention in the past decade. That indeed has prompted new ways of looking at tau pathological trajectory wherein other factors could have profound impact on its aggregation. The combinatorial effect of multiple proteins on tau aggregation and related neurodegeneration has not been explored. Take TIA1 for example; it is an RBP that interacts with tau and enhances the formation of oligomeric tau accumulation and resultant neurotoxicity and seeding (Vanderweyde et al., 2016; Apicco et al., 2018; Maziuk et al., 2018; Jiang et al., 2019; Ash et al., 2021). Furthermore, TIA1 reduced fibrils and tangles formation (Vanderweyde et al., 2016; Apicco et al., 2018; Maziuk et al., 2018; Jiang et al., 2019; Ash et al., 2021). Reducing TIA1 in a PS19 tauopathy model (PS19/*TIA1*$^{+/-}$) reduced oligomeric aggregates accumulation with increased buildup of fibrillar and tangle aggregates. In addition, seeding and pathological spreading were diminished upon reducing TIA1. In light of those findings, we are impelled to scrutinize the association of EFhd2 with tau tangles accumulated in the brain of a PS19/*TIA1*$^{+/-}$ (Apicco et al., 2018; Ash et al., 2021). Given our previous and current data, we anticipate the colocalization of EFhd2 and tangles. We posit that tangle accumulation in PS19/*TIA1*$^{+/-}$ is promoted by, at least partly, EFhd2. This hypothesis could be tested by knocking down the *Efhd2* gene in PS19/*TIA1*$^{+/-}$. In this way, TIA1 (that favors oligomeric tau accumulation) and EFhd2 (that favors tangles accumulation) are lacking, so we expect regression in tangles deposition. This experiment will show how the imbalance between different tau-interacting proteins could modulate biogenesis of different pathological aggregates.

2) Does EFhd2 associate with 3R tau isoforms? Does EFhd2 interact with pathological tau in 3R tauopathies?

Tauopathies are classified according to tau isoforms that primarily constitute pathological aggregates into 3R, 4R, and 3R/4R tauopathies (as mentioned in Chapter One). Our previous research affirmed the association of EFhd2 with tau in AD (3R/4R) and FTDP-17 (4R) tauopathies. Furthermore, Tau$_{P301L}$ expressing mice (JNPL3) generally represent 4R tauopathies. In addition, in Chapter Two, we interrogated the impact of EFhd2-tau interaction with filamentous 4R tau isoform. The association between EFhd2 and tau in other 4R tauopathies, such as CTE, PSP, and CBD, is worth exploring. In addition, future experiments to determine the impact of EFhd2 on the biogenesis of tau aggregates in 3R tauopathy (e.g., Pick's disease) should provide a more comprehensive view of the potential role of EFhd2 in tau pathology. Likewise, we can explore the impact of EFhd2 on *in vitro* 3R tau isoforms aggregates (Cox et al., 2016). It is widely accepted by most scientists that the trajectory of tau aggregation diverges across different tauopathies (Chung et al., 2021; Limorenko & Lashuel, 2022; Sexton et al., 2022; Zhang et al., 2022). Hence, it will be valuable to assess whether and/or how EFhd2 contributes to 3R tau aggregation.

3) What is the interactome of EFhd2 in the human brain in health and disease?

By investigating EFhd2 interactome in mouse forebrain and hindbrain (two regions of differential EFhd2 expression (Purohit et al., 2014)), we succeeded in mapping a potential biological network of EFhd2 in the brain. In recent years, investigating a certain protein's interactome has become at the vanguard of protein biology studies. Our findings will be verified in different regions of the human brain to affirm the potential biological role of EFhd2 through its network and, hence, pathological ramifications of its dysregulation. Furthermore, future studies comparing EFhd2 interactome in the brain across different tauopathies could substantiate the effect of EFhd2 in tau-mediated neurodegeneration and its aggregation. In particular, identifying similarities and differences in regard to EFhd2-interacting proteins among tauopathies will enable us to speculate pathways of indirect association between EFhd2 and tau pathology. That will set the foundation to a large array of experiments for further investigation.

We identified abundance changes in bassoon, LRP1, and TRAP1 that are linked to AD pathology. Thus, future experiments investigating abundance changes of these proteins (along with other candidates) in our Tau$_{P301L}$/*Efhd2$^{-/-}$* mouse model would support the association

among these proteins, EFhd2, and pathological tau forms. Furthermore, exploring EFhd2 interactome in Tau$_{P301L}$/*Efhd2*$^{+/+}$ brains would be of interest to validate bassoon as EFhd2-interacting protein in the context of tau pathology. These future experiments will expand our knowledge on the interplay among different factors and their impact on tau pathology.

4) **Does brain EFhd2 hold a pro-inflammatory or anti-inflammatory role in health and neurodegeneration?**

Little is known about the role of EFhd2 with respect to glial function. Early studies focused on the effect of EFhd2 on peripheral immune response both innate and adaptive, especially using *in vitro* systems (Vuadens et al., 2004; Avramidou et al., 2007; Ramesh et al., 2009; Kroczek et al., 2010; Hagen et al., 2012; Huh et al., 2013; Kwon et al., 2013; Tong et al., 2021; Fu et al., 2024). EFhd2 specifically mediates immune response of macrophages and B-cells. In recent years, *Efhd2*$^{-/-}$ mice have been utilized to investigate EFhd2's function in peripheral immune system (Brachs et al., 2014; Tu et al., 2018; Zhang et al., 2018; Fu et al., 2024; Wu et al., 2024; Zhang et al., 2024). EFhd2 has been shown recently to dampen TNF-α-mediated inflammatory response in the intestine by inhibiting the internalization of TNFR (Wu et al., 2024). This effect was ascribed to the association of EFhd2 with cytoskeleton organization and clathrin-dependent endocytosis (Wu et al., 2024). These findings are congruent with our EFhd2 interactome data, wherein we showed that EFhd2 is associated with proteins that regulate vesicle trafficking in the brain (Chapter Three).

Furthermore, EFhd2 regulates NF-κB inflammatory pathway in the intestinal epithelia and B-cells (Avramidou et al., 2007; Wu et al., 2024). These findings highlight the importance of examining whether the role of EFhd2 in regulating immune response peripherally could be extended to CNS with microglia and astrocytes. In this regard, a few *in vitro* studies showed a possible role of EFhd2 in regulating microglia-mediated inflammatory response. A study reported microglial secretion of EFhd2 *in vitro* upon activation with nitrated α-Syn (pathological protein in PD) (Reynolds et al., 2008). Another recent paper has reported that EFhd2 knockdown in BV2 cells (murine microglial cell line) dampened LPS-induced secretion of inflammatory factors such as TNF-α, IL-1β, and iNOS (Bo et al., 2023). The authors also demonstrated that EFhd2 mediates LPS-induced inflammatory response through STAT3 signaling *in vitro* (Bo et al., 2023). Hitherto, no study has provided conclusive evidence of EFhd2 expression and function in glia *in vivo*. Using our *Efhd2*$^{-/-}$ model, we could evaluate pro- vs anti-inflammatory

glial phenotype compared to wild type controls. The evaluation should primarily rely on assessing glial morphology, glial markers, and secreted cytokines. Together, these data will strengthen our understanding about additional possible aspects of EFhd2's function in the brain.

Over the past years, neuroinflammation has been deemed as another pathological hallmark in tauopathies, especially AD (Heneka et al., 2015; Laurent et al., 2018; Saito & Saido, 2018; Langworth-Green et al., 2023). Despite the absence of glial tau lesions in AD brain, heightened inflammatory glial response has been invariably reported in several human and animal model studies. Literature abounds with studies that have shown that activated glia induce neurodegeneration (Heneka et al., 2015; Ransohoff, 2016; Saito & Saido, 2018). As such, many researchers have made laudable attempts to modulate inflammatory response as a therapeutic approach (Zhang et al., 2022). More efforts are ongoing to unravel upstream factors that could promote glia-mediated inflammatory response. It is worth mentioning that neuroinflammation also has been implicated in other neurodegenerative disorders such as PD (Ransohoff, 2016; Cinar et al., 2022). Therefore, it would be interesting to examine glial response in Tau$_{P301L}$/$Efhd2^{-/-}$ and Tau$_{P301L}$/$Efhd2^{+/+}$ mice to gain further insights into the role of EFhd2 on glia-mediated inflammation during tau pathology—an area that was not explored before.

In Chapter Three, we identified complement component 1q (C1q) within EFhd2 interactome in the hindbrain. Interestingly, C1q level increased in the forebrain and hindbrain of $Efhd2^{-/-}$ mice. Activation of complement cascade as an inflammatory response has drawn considerable interest during the past decade (Britschgi et al., 2012; Stephan et al., 2012; Hong et al., 2016; Davies & Spires-Jones, 2018; Dejanovic et al., 2018; Litvinchuk et al., 2018). Activated complement cascade has become evident in neurodegenerative diseases including AD. In fact, activated complement pathway presumably mediates microglia-induced neuronal loss. Several research groups postulate that during the disease, C1q level increases and induces the release of C3 from glia. The interaction of C3 with its synaptic receptor C3aR stimulates microglia to engulf synapses/neurons by phagocytosis (Stephan et al., 2012; Hong et al., 2016; Dejanovic et al., 2018; Litvinchuk et al., 2018). Some reports confirmed high C1q level in postsynapses of human tauopathies brains along with increased C3 (Dejanovic et al., 2018; Litvinchuk et al., 2018). Strikingly, the increase of C1q and C3 levels correlated with cognitive decline and neuronal burden of tau pathology. These findings were borne out in tauopathy models showing that inactivation of complement cascade could ameliorate behavioral deficit and

rescue synaptic loss (Dejanovic et al., 2018; Litvinchuk et al., 2018). Not only does complement activation induce glia-mediated neuronal loss, but also activated complement could enhance tau phosphorylation (Britschgi et al., 2012; Dejanovic et al., 2018; Litvinchuk et al., 2018). Still, active research is ongoing to elaborate the molecular mechanisms linking tau pathology and complement pathway. Herein, the association of EFhd2 and C1q in addition to the abundance change of C1q in *Efhd2*$^{-/-}$ mice brain begs a future question: Does EFhd2 modulate activated complement cascade during tau pathology? In particular, further studies could demonstrate whether EFhd2 induce or inhibit complement activation and, hence, examine pathological outcomes. These future studies will deepen our understanding about other aspects by which EFhd2 influences tau pathology.

5) Does calcium-binding activity of EFhd2 interfere with its role in promoting tau aggregation?

EFhd2 is a calcium-binding protein that possibly acts as a calcium sensor impacting its downstream signaling pathways (Vuadens et al., 2004; Avramidou et al., 2007; Kroczek et al., 2010; Hagen et al., 2012). Furthermore, we reported that calcium prevented EFhd2-induced changes of tau dynamics and LLPS *in vitro* (Vega et al., 2018; Vega et al., 2019). In Chapter Two, we did not include the impact of the presence of calcium on the formation of the entangled EFhd2-tau aggregates. A future set of experiments will closely determine whether adding calcium will induce changes in the aggregate formation.

Investigating the effect of calcium poses a compelling line of research that could enhance our understanding of EFhd2 role in tau pathology. A plethora of studies have established calcium dysregulation as one of the molecular changes occur during pathological trajectory (Pchitskaya et al., 2018; Joshi et al., 2023). Currently, the acceptable hypothesis is that increased internal stores of calcium in endoplasmic reticulum (ER) and mitochondria along with enhanced membrane calcium entry lead to abnormal high cytosolic levels of calcium (Berridge, 2010; Pchitskaya et al., 2018; Joshi et al., 2023). A marked reduction in calcium buffer, calbindin that controls cytosolic calcium levels has been also reported in AD brains (Berridge, 2010). The impact of increased calcium levels is multifold. Dysregulated calcium could disrupt physiological molecular pathways that control synaptic plasticity and, hence, learning and memory processing. In fact, scientists posit that calcium dysregulation potentially underlies early cognitive decline in AD (Berridge, 2010; Pchitskaya et al., 2018; Joshi et al., 2023). Furthermore, upregulated

calcium levels provoke calcium-mediated mitochondrial apoptosis leading to neuronal death and neurodegeneration (Berridge, 2010; Pchitskaya et al., 2018; Joshi et al., 2023). With respect to tau pathology, high levels of neuronal calcium activate several kinases such as PKA, GSK3β, and CamK4 that mediate tau hyperphosphorylation (Berridge, 2010; Wang & Mandelkow, 2016; Sałaciak et al., 2021). A recent study using macaque monkey model of AD demonstrated age-dependent increase in calcium levels and increased PKA activity that subsequently enhanced tau phosphorylation at AD-related sites (Datta et al., 2021). In the same study, the authors reported age-dependent diminished levels of calbindin that could, at least in part, underlie the rise of neuronal calcium (Datta et al., 2021). By and large, calcium dysregulation is a major cellular change that contributes to neurodegeneration in AD and other tauopathies.

As yet, the link between increased calcium levels, high abundance of EFhd2 protein, and tau aggregation *in vivo* remains enigmatic. As noted earlier, we still do not know when EFhd2 levels increase during different stages of tau pathology. Whether it takes place in the early or the late stage needs further investigation. In addition, increased EFhd2 levels in AD could be an outcome of high calcium levels. Prior research suggests that EFhd2 might be a calcium sensor that binds to calcium and controls its downstream effectors (Kroczek et al., 2010; Hagen et al., 2012). The question remains on how the role of EFhd2 as a calcium-binding protein is modulated during tau pathology. Accordingly, we should examine whether and how disrupted calcium levels would impact EFhd2-mediated tau aggregation during pathology. It is worth noting that previously we showed that EFhd2 is phosphorylated by CDK5 (Vazquez-Rosa et al., 2014). Calcium-binding of EFhd2 inhibits it phosphorylation (Vazquez-Rosa et al., 2014). Strikingly, despite the enhanced activity of CDK5 in AD, we detected low phosphorylated EFhd2 in the brain. One might speculate that when EFhd2 increases in AD, it binds to calcium, which subsequently hinders its phosphorylation. It has become clear that further experiments using animal and cellular models of tauopathies preceded by a series of *in vitro* studies are required to unravel the relation between EFhd2, phosphorylated EFhd2, calcium, and tau aggregation.

6) **Does EFhd2 modulate the abnormal aggregation of other amyloid proteins that mediate neurodegenerative disorders?**

Not only is EFhd2 associated with AD and other tauopathies, but also a handful of different studies demonstrated its putative association with other neurodegenerative disorders such as PD and ALS (Vega, 2016). Two studies reported differential abundance of EFhd2 in

transgenic PD mouse model and postmortem brains (Diedrich et al., 2011; Liscovitch & French, 2014). In addition, EFhd2 was identified among the interactome of LRRK2 *in vitro* (Meixner et al., 2011). In ALS, MS-based studies showed the association of EFhd2 with pathological changes (Zhai et al., 2009; May et al., 2014). Our findings on the direct impact of EFhd2 on tau aggregation propel us to inquire whether EFhd2 bears the same capacity to modulate the aggregation of pathological proteins in other neurodegenerative disorders (e.g., α-Syn in PD and TDP-43 in ALS). Moreover, EFhd2 brain interactome indicates a probable association between EFhd2 and these disorders. For instance, in EFhd2 interactome, we identified EWSR1 protein, which belongs to TET-family RBPs (Lee et al., 2019). Missense mutations in *EWSR1* gene associates with ALS and FTD (Lee et al., 2019). Additionally, our MS-LFQ analysis detected a reduced abundance of superoxide dismutase 1 (SOD1) in *Efhd2$^{-/-}$* mice compared to wild type. Autosomal mutations in *SOD1* cause familial ALS (Rosen et al., 1993). MS-based comparison of proteome changes in the spinal lipid raft of G93A mutant SOD1 mice with wild type SOD1 mice showed a noticeable increase of EFhd2 abundance in G93A mice (Zhai et al., 2009). Likewise, we detected low abundance of α-Syn in *Efhd2$^{-/-}$* mice in comparison to wild type. α-Syn is the primary pathological protein in PD (Hodaie et al., 2007). In essence, previous research along with our proteomic data lend further credence to the potential role EFhd2 in other neurodegenerative disorders—an area that warrants further investigation.

Concluding remarks

This research work attempted to answer the central question of what role EFhd2 plays in tau pathology. The studies conducted in Chapters Two and Four provide convincing evidence for the direct role of EFhd2 on driving the formation of higher order tangles. As noted earlier, that direct effect of EFhd2 on NFTs maturity is novel. In addition, Chapter Three shed more light on the possible biological role of EFhd2 in the brain and its association with neurodegeneration. Above all, the presented findings underline a multifaceted role for EFhd2 in tauopathies. This is the first extensive examination of the interplay of EFhd2 and tau pathology using a multidisciplinary approach.

It is important to note that a number of investigators demonstrated the differential abundance of EFhd2 and its association with known pathological proteins in other neurodegenerative diseases, such as PD, ALS, and Huntington's disease. Over the past two decades, it has become clear that EFhd2 is nothing short of the jack-of-all-trades that may be

associated with disparate pathological scenarios. Hence, it is conceivable to assume that dysregulating EFhd2 engenders variable outcomes depending on the biological context. In fact, the growing multidisciplinary interest in studying EFhd2 has stimulated a pressing need to investigate its role in different diseases. Notwithstanding, the field remains short of follow-up studies that can investigate the role of EFhd2 in the pathogenesis of these diseases. Therefore, we are convinced that the results presented in this dissertation open a trove of questions that merit more studies to further uncover the specific pathobiological role of EFhd2 in neurodegenerative disorders, using EFhd2-tau association as a model. These future studies will definitely lay the foundation to determine whether EFhd2 holds a therapeutic and/or diagnostic potential in neurological disorders, especially tauopathies.

REFERENCES

Alhadidy, M. M., & Kanaan, N. M. (2024). Biochemical approaches to assess the impact of post-translational modifications on pathogenic tau conformations using recombinant protein. *Biochem Soc Trans*, *52*(1), 301-318. https://doi.org/10.1042/BST20230596

Apicco, D. J., Ash, P. E. A., Maziuk, B., LeBlang, C., Medalla, M., Al Abdullatif, A., Ferragud, A., Botelho, E., Ballance, H. I., Dhawan, U., Boudeau, S., Cruz, A. L., Kashy, D., Wong, A., Goldberg, L. R., Yazdani, N., Zhang, C., Ung, C. Y., Tripodis, Y., . . . Wolozin, B. (2018). Reducing the RNA binding protein TIA1 protects against tau-mediated neurodegeneration in vivo. *Nat Neurosci*, *21*(1), 72-80. https://doi.org/10.1038/s41593-017-0022-z

Ash, P. E. A., Lei, S., Shattuck, J., Boudeau, S., Carlomagno, Y., Medalla, M., Mashimo, B. L., Socorro, G., Al-Mohanna, L. F. A., Jiang, L., Ozturk, M. M., Knobel, M., Ivanov, P., Petrucelli, L., Wegmann, S., Kanaan, N. M., & Wolozin, B. (2021). TIA1 potentiates tau phase separation and promotes generation of toxic oligomeric tau. *Proc Natl Acad Sci U S A*, *118*(9). https://doi.org/10.1073/pnas.2014188118

Avramidou, A., Kroczek, C., Lang, C., Schuh, W., Jack, H. M., & Mielenz, D. (2007). The novel adaptor protein Swiprosin-1 enhances BCR signals and contributes to BCR-induced apoptosis. *Cell Death Differ*, *14*(11), 1936-1947. https://doi.org/10.1038/sj.cdd.4402206

Berger, Z., Roder, H., Hanna, A., Carlson, A., Rangachari, V., Yue, M., Wszolek, Z., Ashe, K., Knight, J., Dickson, D., Andorfer, C., Rosenberry, T. L., Lewis, J., Hutton, M., & Janus, C. (2007). Accumulation of pathological tau species and memory loss in a conditional model of tauopathy. *J Neurosci*, *27*(14), 3650-3662. https://doi.org/10.1523/JNEUROSCI.0587-07.2007

Berridge, M. J. (2010). Calcium hypothesis of Alzheimer's disease. *Pflugers Arch*, *459*(3), 441-449. https://doi.org/10.1007/s00424-009-0736-1

Bo, X., Xie, F., Zhang, J., Gu, R., Li, X., Li, S., Yuan, Z., & Cheng, J. (2023). Deletion of Calhm2 alleviates MPTP-induced Parkinson's disease pathology by inhibiting EFHD2-STAT3 signaling in microglia. *Theranostics*, *13*(6), 1809-1822. https://doi.org/10.7150/thno.83082

Borger, E., Herrmann, A., Mann, D. A., Spires-Jones, T., & Gunn-Moore, F. (2014). The calcium-binding protein EFhd2 modulates synapse formation in vitro and is linked to human dementia. *J Neuropathol Exp Neurol*, *73*(12), 1166-1182. https://doi.org/10.1097/NEN.0000000000000138

Brachs, S., Turqueti-Neves, A., Stein, M., Reimer, D., Brachvogel, B., Bosl, M., Winkler, T., Voehringer, D., Jack, H. M., & Mielenz, D. (2014). Swiprosin-1/EFhd2 limits germinal center responses and humoral type 2 immunity. *Eur J Immunol*, *44*(11), 3206-3219. https://doi.org/10.1002/eji.201444479

Britschgi, M., Takeda-Uchimura, Y., Rockenstein, E., Johns, H., Masliah, E., & Wyss-Coray, T. (2012). Deficiency of terminal complement pathway inhibitor promotes neuronal tau pathology and degeneration in mice. *J Neuroinflammation*, *9*(1), 220. https://doi.org/10.1186/1742-2094-9-220

Brunden, K. R., Trojanowski, J. Q., & Lee, V. M. (2008). Evidence that non-fibrillar tau causes pathology linked to neurodegeneration and behavioral impairments. *J Alzheimers Dis*, *14*(4), 393-399. https://doi.org/10.3233/jad-2008-14406

Chung, D. C., Roemer, S., Petrucelli, L., & Dickson, D. W. (2021). Cellular and pathological heterogeneity of primary tauopathies. *Mol Neurodegener*, *16*(1), 57. https://doi.org/10.1186/s13024-021-00476-x

Cinar, E., Tel, B. C., & Sahin, G. (2022). Neuroinflammation in Parkinson's Disease and its Treatment Opportunities. *Balkan Med J*, *39*(5), 318-333. https://doi.org/10.4274/balkanmedj.galenos.2022.2022-7-100

Cooper, J. M., Lathuiliere, A., Migliorini, M., Arai, A. L., Wani, M. M., Dujardin, S., Muratoglu, S. C., Hyman, B. T., & Strickland, D. K. (2021). Regulation of tau internalization, degradation, and seeding by LRP1 reveals multiple pathways for tau catabolism. *J Biol Chem*, *296*, 100715. https://doi.org/10.1016/j.jbc.2021.100715

Cowan, C. M., & Mudher, A. (2013). Are tau aggregates toxic or protective in tauopathies? *Front Neurol*, *4*, 114. https://doi.org/10.3389/fneur.2013.00114

Cox, K., Combs, B., Abdelmesih, B., Morfini, G., Brady, S. T., & Kanaan, N. M. (2016). Analysis of isoform-specific tau aggregates suggests a common toxic mechanism involving similar pathological conformations and axonal transport inhibition. *Neurobiol Aging*, *47*, 113-126. https://doi.org/10.1016/j.neurobiolaging.2016.07.015

Datta, D., Leslie, S. N., Wang, M., Morozov, Y. M., Yang, S., Mentone, S., Zeiss, C., Duque, A., Rakic, P., Horvath, T. L., van Dyck, C. H., Nairn, A. C., & Arnsten, A. F. T. (2021). Age-related calcium dysregulation linked with tau pathology and impaired cognition in non-human primates. *Alzheimers Dement*, *17*(6), 920-932. https://doi.org/10.1002/alz.12325

Davies, C., & Spires-Jones, T. L. (2018). Complementing Tau: New Data Show that the Complement System Is Involved in Degeneration in Tauopathies. *Neuron*, *100*(6), 1267-1269. https://doi.org/10.1016/j.neuron.2018.12.003

Deacon, R. M. (2006). Assessing nest building in mice. *Nat Protoc*, *1*(3), 1117-1119. https://doi.org/10.1038/nprot.2006.170

Dejanovic, B., Huntley, M. A., De Maziere, A., Meilandt, W. J., Wu, T., Srinivasan, K., Jiang, Z., Gandham, V., Friedman, B. A., Ngu, H., Foreman, O., Carano, R. A. D., Chih, B., Klumperman, J., Bakalarski, C., Hanson, J. E., & Sheng, M. (2018). Changes in the Synaptic Proteome in Tauopathy and Rescue of Tau-Induced Synapse Loss by C1q Antibodies. *Neuron*, *100*(6), 1322-1336 e1327. https://doi.org/10.1016/j.neuron.2018.10.014

Dekker, F. A., & Rüdiger, S. G. D. (2021). The Mitochondrial Hsp90 TRAP1 and Alzheimer's Disease. *Front Mol Biosci*, *8*, 697913. https://doi.org/10.3389/fmolb.2021.697913

Diedrich, M., Kitada, T., Nebrich, G., Koppelstaetter, A., Shen, J., Zabel, C., Klose, J., & Mao, L. (2011). Brain region specific mitophagy capacity could contribute to selective neuronal vulnerability in Parkinson's disease. *Proteome Sci*, *9*, 59. https://doi.org/10.1186/1477-5956-9-59

Falcon, B., Zhang, W., Murzin, A. G., Murshudov, G., Garringer, H. J., Vidal, R., Crowther, R. A., Ghetti, B., Scheres, S. H. W., & Goedert, M. (2018a). Structures of filaments from Pick's disease reveal a novel tau protein fold. *Nature*, *561*(7721), 137-140. https://doi.org/10.1038/s41586-018-0454-y

Falcon, B., Zhang, W., Schweighauser, M., Murzin, A. G., Vidal, R., Garringer, H. J., Ghetti, B., Scheres, S. H. W., & Goedert, M. (2018b). Tau filaments from multiple cases of sporadic and inherited Alzheimer's disease adopt a common fold. *Acta Neuropathol*, *136*(5), 699-708. https://doi.org/10.1007/s00401-018-1914-z

Falcon, B., Zivanov, J., Zhang, W., Murzin, A. G., Garringer, H. J., Vidal, R., Crowther, R. A., Newell, K. L., Ghetti, B., Goedert, M., & Scheres, S. H. W. (2019). Novel tau filament fold in chronic traumatic encephalopathy encloses hydrophobic molecules. *Nature*, *568*(7752), 420-423. https://doi.org/10.1038/s41586-019-1026-5

Ferrer-Acosta, Y., Rodriguez Cruz, E. N., Vaquer Adel, C., & Vega, I. E. (2013a). Functional and structural analysis of the conserved EFhd2 protein. *Protein Pept Lett*, *20*(5), 573-583. https://doi.org/10.2174/09298665113205050011

Ferrer-Acosta, Y., Rodriguez-Cruz, E. N., Orange, F., De Jesus-Cortes, H., Madera, B., Vaquer-Alicea, J., Ballester, J., Guinel, M. J., Bloom, G. S., & Vega, I. E. (2013b). EFhd2 is a novel amyloid protein associated with pathological tau in Alzheimer's disease. *J Neurochem*, *125*(6), 921-931. https://doi.org/10.1111/jnc.12155

Fitzpatrick, A. W. P., Falcon, B., He, S., Murzin, A. G., Murshudov, G., Garringer, H. J., Crowther, R. A., Ghetti, B., Goedert, M., & Scheres, S. H. W. (2017). Cryo-EM structures of tau filaments from Alzheimer's disease. *Nature*, *547*(7662), 185-190. https://doi.org/10.1038/nature23002

Fu, J. T., Liu, J., Wu, W. B., Chen, Y. T., Lu, G. D., Cao, Q., Meng, H. B., Tong, J., Zhu, J. H., Wang, X. J., Liu, Y., Zhuang, C., Sheng, C., Shen, F. M., Liu, X., Wang, H., Yu, Y., Zhang, Y., Liang, H. Y., . . . Wang, P. (2024). Targeting EFHD2 inhibits interferon-gamma signaling and ameliorates non-alcoholic steatohepatitis. *J Hepatol*. https://doi.org/10.1016/j.jhep.2024.04.009

Fuster-Matanzo, A., de Barreda, E. G., Dawson, H. N., Vitek, M. P., Avila, J., & Hernandez, F. (2009). Function of tau protein in adult newborn neurons. *FEBS Lett*, *583*(18), 3063-3068. https://doi.org/10.1016/j.febslet.2009.08.017

Gómez-Isla, T., & Frosch, M. P. (2022). Lesions without symptoms: understanding resilience to Alzheimer disease neuropathological changes. *Nature Reviews Neurology*, *18*(6), 323-332. https://doi.org/10.1038/s41582-022-00642-9

Gomez-Isla, T., Hollister, R., West, H., Mui, S., Growdon, J. H., Petersen, R. C., Parisi, J. E., & Hyman, B. T. (1997). Neuronal loss correlates with but exceeds neurofibrillary tangles in Alzheimer's disease. *Ann Neurol*, *41*(1), 17-24. https://doi.org/10.1002/ana.410410106

Gómez-Isla, T., Price, J. L., McKeel, D. W., Jr., Morris, J. C., Growdon, J. H., & Hyman, B. T. (1996). Profound loss of layer II entorhinal cortex neurons occurs in very mild Alzheimer's disease. *J Neurosci*, *16*(14), 4491-4500. https://doi.org/10.1523/JNEUROSCI.16-14-04491.1996

Hagen, S., Brachs, S., Kroczek, C., Furnrohr, B. G., Lang, C., & Mielenz, D. (2012). The B cell receptor-induced calcium flux involves a calcium mediated positive feedback loop. *Cell Calcium*, *51*(5), 411-417. https://doi.org/10.1016/j.ceca.2012.01.004

Harada, A., Oguchi, K., Okabe, S., Kuno, J., Terada, S., Ohshima, T., Sato-Yoshitake, R., Takei, Y., Noda, T., & Hirokawa, N. (1994). Altered microtubule organization in small-calibre axons of mice lacking tau protein. *Nature*, *369*(6480), 488-491. https://doi.org/10.1038/369488a0

Heinonen, O., Soininen, H., Sorvari, H., Kosunen, O., Paljarvi, L., Koivisto, E., & Riekkinen, P. J., Sr. (1995). Loss of synaptophysin-like immunoreactivity in the hippocampal formation is an early phenomenon in Alzheimer's disease. *Neuroscience*, *64*(2), 375-384. https://doi.org/10.1016/0306-4522(94)00422-2

Heneka, M. T., Carson, M. J., El Khoury, J., Landreth, G. E., Brosseron, F., Feinstein, D. L., Jacobs, A. H., Wyss-Coray, T., Vitorica, J., Ransohoff, R. M., Herrup, K., Frautschy, S. A., Finsen, B., Brown, G. C., Verkhratsky, A., Yamanaka, K., Koistinaho, J., Latz, E., Halle, A., . . . Kummer, M. P. (2015). Neuroinflammation in Alzheimer's disease. *Lancet Neurol*, *14*(4), 388-405. https://doi.org/10.1016/S1474-4422(15)70016-5

Hodaie, M., Neimat, J. S., & Lozano, A. M. (2007). The dopaminergic nigrostriatal system and Parkinson's disease: molecular events in development, disease, and cell death, and new therapeutic strategies. *Neurosurgery*, *60*(1), 17-28; discussion 28-30. https://doi.org/10.1227/01.NEU.0000249209.11967.CB

Hong, S., Beja-Glasser, V. F., Nfonoyim, B. M., Frouin, A., Li, S., Ramakrishnan, S., Merry, K. M., Shi, Q., Rosenthal, A., Barres, B. A., Lemere, C. A., Selkoe, D. J., & Stevens, B. (2016). Complement and microglia mediate early synapse loss in Alzheimer mouse models. *Science*, *352*(6286), 712-716. https://doi.org/10.1126/science.aad8373

Hong, X. P., Peng, C. X., Wei, W., Tian, Q., Liu, Y. H., Yao, X. Q., Zhang, Y., Cao, F. Y., Wang, Q., & Wang, J. Z. (2010). Essential role of tau phosphorylation in adult hippocampal neurogenesis. *Hippocampus*, *20*(12), 1339-1349. https://doi.org/10.1002/hipo.20712

Huh, Y. H., Kim, S. H., Chung, K. H., Oh, S., Kwon, M. S., Choi, H. W., Rhee, S., Ryu, J. H., Park, Z. Y., Jun, C. D., & Song, W. K. (2013). Swiprosin-1 modulates actin dynamics by regulating the F-actin accessibility to cofilin. *Cell Mol Life Sci*, *70*(24), 4841-4854. https://doi.org/10.1007/s00018-013-1447-5

Jiang, L., Ash, P. E. A., Maziuk, B. F., Ballance, H. I., Boudeau, S., Abdullatif, A. A., Orlando, M., Petrucelli, L., Ikezu, T., & Wolozin, B. (2019). TIA1 regulates the generation and response

to toxic tau oligomers. *Acta Neuropathol*, *137*(2), 259-277. https://doi.org/10.1007/s00401-018-1937-5

Joshi, M., Joshi, S., Khambete, M., & Degani, M. (2023). Role of calcium dysregulation in Alzheimer's disease and its therapeutic implications. *Chem Biol Drug Des*, *101*(2), 453-468. https://doi.org/10.1111/cbdd.14175

Kavanagh, T., Halder, A., & Drummond, E. (2022). Tau interactome and RNA binding proteins in neurodegenerative diseases. *Mol Neurodegener*, *17*(1), 66. https://doi.org/10.1186/s13024-022-00572-6

Kayed, R. (2010). Anti-tau oligomers passive vaccination for the treatment of Alzheimer disease. *Hum Vaccin*, *6*(11), 931-935. https://doi.org/10.4161/hv.6.11.12689

King, M. E., Ghoshal, N., Wall, J. S., Binder, L. I., & Ksiezak-Reding, H. (2001). Structural analysis of Pick's disease-derived and in vitro-assembled tau filaments. *Am J Pathol*, *158*(4), 1481-1490. https://doi.org/10.1016/S0002-9440(10)64099-0

Kogias, G., Zheng, F., Kalinichenko, L. S., Kornhuber, J., Alzheimer, C., Mielenz, D., & Muller, C. P. (2020). Swiprosin1/EFhd2 is involved in the monoaminergic and locomotor responses of psychostimulant drugs. *J Neurochem*, *154*(4), 424-440. https://doi.org/10.1111/jnc.14959

Kroczek, C., Lang, C., Brachs, S., Grohmann, M., Dutting, S., Schweizer, A., Nitschke, L., Feller, S. M., Jack, H. M., & Mielenz, D. (2010). Swiprosin-1/EFhd2 controls B cell receptor signaling through the assembly of the B cell receptor, Syk, and phospholipase C gamma2 in membrane rafts. *J Immunol*, *184*(7), 3665-3676. https://doi.org/10.4049/jimmunol.0903642

Ksiezak-Reding, H., Tracz, E., Yang, L. S., Dickson, D. W., Simon, M., & Wall, J. S. (1996). Ultrastructural instability of paired helical filaments from corticobasal degeneration as examined by scanning transmission electron microscopy. *Am J Pathol*, *149*(2), 639-651. https://www.ncbi.nlm.nih.gov/pubmed/8702002

Ksiezak-Reding, H., & Wall, J. S. (2005). Characterization of paired helical filaments by scanning transmission electron microscopy. *Microsc Res Tech*, *67*(3-4), 126-140. https://doi.org/10.1002/jemt.20188

Ksiezak-Reding, H., Yang, G., Simon, M., & Wall, J. S. (1998). Assembled tau filaments differ from native paired helical filaments as determined by scanning transmission electron microscopy (STEM). *Brain Res*, *814*(1-2), 86-98. https://doi.org/10.1016/s0006-8993(98)01052-x

Kuret, J., Chirita, C. N., Congdon, E. E., Kannanayakal, T., Li, G., Necula, M., Yin, H., & Zhong, Q. (2005). Pathways of tau fibrillization. *Biochim Biophys Acta*, *1739*(2-3), 167-178. https://doi.org/10.1016/j.bbadis.2004.06.016

Kwon, M. S., Park, K. R., Kim, Y. D., Na, B. R., Kim, H. R., Choi, H. J., Piragyte, I., Jeon, H., Chung, K. H., Song, W. K., Eom, S. H., & Jun, C. D. (2013). Swiprosin-1 is a novel actin bundling protein that regulates cell spreading and migration. *PLoS One*, *8*(8), e71626. https://doi.org/10.1371/journal.pone.0071626

Langworth-Green, C., Patel, S., Jaunmuktane, Z., Jabbari, E., Morris, H., Thom, M., Lees, A., Hardy, J., Zandi, M., & Duff, K. (2023). Chronic effects of inflammation on tauopathies. *Lancet Neurol*, *22*(5), 430-442. https://doi.org/10.1016/S1474-4422(23)00038-8

Lasagna-Reeves, C. A., Castillo-Carranza, D. L., Sengupta, U., Clos, A. L., Jackson, G. R., & Kayed, R. (2011). Tau oligomers impair memory and induce synaptic and mitochondrial dysfunction in wild-type mice. *Mol Neurodegener*, *6*, 39. https://doi.org/10.1186/1750-1326-6-39

Lasagna-Reeves, C. A., Castillo-Carranza, D. L., Sengupta, U., Sarmiento, J., Troncoso, J., Jackson, G. R., & Kayed, R. (2012). Identification of oligomers at early stages of tau aggregation in Alzheimer's disease. *Faseb j*, *26*(5), 1946-1959. https://doi.org/10.1096/fj.11-199851

Laurent, C., Buee, L., & Blum, D. (2018). Tau and neuroinflammation: What impact for Alzheimer's Disease and Tauopathies? *Biomed J*, *41*(1), 21-33. https://doi.org/10.1016/j.bj.2018.01.003

Lee, J., Nguyen, P. T., Shim, H. S., Hyeon, S. J., Im, H., Choi, M. H., Chung, S., Kowall, N. W., Lee, S. B., & Ryu, H. (2019). EWSR1, a multifunctional protein, regulates cellular function and aging via genetic and epigenetic pathways. *Biochim Biophys Acta Mol Basis Dis*, *1865*(7), 1938-1945. https://doi.org/10.1016/j.bbadis.2018.10.042

Lewis, J., & McGowan, E. (2005). Rodent Models of Tauopathies. In M. LeDoux (Ed.), *Animal Models of Movement Disorders* (pp. 529-539). Academic Press. https://doi.org/10.1016/b978-012088382-0/50048-7

Limorenko, G., & Lashuel, H. A. (2022). Revisiting the grammar of Tau aggregation and pathology formation: how new insights from brain pathology are shaping how we study and target Tauopathies. *Chem Soc Rev*, *51*(2), 513-565. https://doi.org/10.1039/d1cs00127b

Liscovitch, N., & French, L. (2014). Differential Co-Expression between alpha-Synuclein and IFN-gamma Signaling Genes across Development and in Parkinson's Disease. *PLoS One*, *9*(12), e115029. https://doi.org/10.1371/journal.pone.0115029

Litvinchuk, A., Wan, Y. W., Swartzlander, D. B., Chen, F., Cole, A., Propson, N. E., Wang, Q., Zhang, B., Liu, Z., & Zheng, H. (2018). Complement C3aR Inactivation Attenuates Tau Pathology and Reverses an Immune Network Deregulated in Tauopathy Models and Alzheimer's Disease. *Neuron*, *100*(6), 1337-1353 e1335. https://doi.org/10.1016/j.neuron.2018.10.031

Martinez, P., Patel, H., You, Y., Jury, N., Perkins, A., Lee-Gosselin, A., Taylor, X., You, Y., Viana Di Prisco, G., Huang, X., Dutta, S., Wijeratne, A. B., Redding-Ochoa, J., Shahid, S. S., Codocedo, J. F., Min, S., Landreth, G. E., Mosley, A. L., Wu, Y. C., . . . Lasagna-Reeves, C. A. (2022). Bassoon contributes to tau-seed propagation and neurotoxicity. *Nat Neurosci*, *25*(12), 1597-1607. https://doi.org/10.1038/s41593-022-01191-6

May, S., Hornburg, D., Schludi, M. H., Arzberger, T., Rentzsch, K., Schwenk, B. M., Grasser, F. A., Mori, K., Kremmer, E., Banzhaf-Strathmann, J., Mann, M., Meissner, F., & Edbauer, D. (2014). C9orf72 FTLD/ALS-associated Gly-Ala dipeptide repeat proteins cause neuronal

toxicity and Unc119 sequestration. *Acta Neuropathol, 128*(4), 485-503. https://doi.org/10.1007/s00401-014-1329-4

Maziuk, B. F., Apicco, D. J., Cruz, A. L., Jiang, L., Ash, P. E. A., da Rocha, E. L., Zhang, C., Yu, W. H., Leszyk, J., Abisambra, J. F., Li, H., & Wolozin, B. (2018). RNA binding proteins co-localize with small tau inclusions in tauopathy. *Acta Neuropathol Commun, 6*(1), 71. https://doi.org/10.1186/s40478-018-0574-5

Meixner, A., Boldt, K., Van Troys, M., Askenazi, M., Gloeckner, C. J., Bauer, M., Marto, J. A., Ampe, C., Kinkl, N., & Ueffing, M. (2011). A QUICK screen for Lrrk2 interaction partners--leucine-rich repeat kinase 2 is involved in actin cytoskeleton dynamics. *Mol Cell Proteomics, 10*(1), M110 001172. https://doi.org/10.1074/mcp.M110.001172

Mielenz, D., Reichel, M., Jia, T., Quinlan, E. B., Stockl, T., Mettang, M., Zilske, D., Kirmizi-Alsan, E., Schonberger, P., Praetner, M., Huber, S. E., Amato, D., Schwarz, M., Purohit, P., Brachs, S., Spranger, J., Hess, A., Buttner, C., Ekici, A. B., . . . Muller, C. P. (2018). EFhd2/Swiprosin-1 is a common genetic determinator for sensation-seeking/low anxiety and alcohol addiction. *Mol Psychiatry, 23*(5), 1303-1319. https://doi.org/10.1038/mp.2017.63

Moreira, G. G., Cantrelle, F. X., Quezada, A., Carvalho, F. S., Cristovao, J. S., Sengupta, U., Puangmalai, N., Carapeto, A. P., Rodrigues, M. S., Cardoso, I., Fritz, G., Herrera, F., Kayed, R., Landrieu, I., & Gomes, C. M. (2021). Dynamic interactions and Ca(2+)-binding modulate the holdase-type chaperone activity of S100B preventing tau aggregation and seeding. *Nat Commun, 12*(1), 6292. https://doi.org/10.1038/s41467-021-26584-2

Okuyama, R., & Marshall, S. (2003). UDP-N-acetylglucosaminyl transferase (OGT) in brain tissue: temperature sensitivity and subcellular distribution of cytosolic and nuclear enzyme. *J Neurochem, 86*(5), 1271-1280. https://doi.org/10.1046/j.1471-4159.2003.01939.x

Patterson, K. R., Remmers, C., Fu, Y., Brooker, S., Kanaan, N. M., Vana, L., Ward, S., Reyes, J. F., Philibert, K., Glucksman, M. J., & Binder, L. I. (2011). Characterization of prefibrillar Tau oligomers in vitro and in Alzheimer disease. *J Biol Chem, 286*(26), 23063-23076. https://doi.org/10.1074/jbc.M111.237974

Pchitskaya, E., Popugaeva, E., & Bezprozvanny, I. (2018). Calcium signaling and molecular mechanisms underlying neurodegenerative diseases. *Cell Calcium, 70*, 87-94. https://doi.org/10.1016/j.ceca.2017.06.008

Prikas, E., Paric, E., Asih, P. R., Stefanoska, K., Stefen, H., Fath, T., Poljak, A., & Ittner, A. (2022). Tau target identification reveals NSF-dependent effects on AMPA receptor trafficking and memory formation. *Embo j, 41*(18), e10242. https://doi.org/10.15252/embj.2021110242

Purohit, P., Perez-Branguli, F., Prots, I., Borger, E., Gunn-Moore, F., Welzel, O., Loy, K., Wenzel, E. M., Gromer, T. W., Brachs, S., Holzer, M., Buslei, R., Fritsch, K., Regensburger, M., Bohm, K. J., Winner, B., & Mielenz, D. (2014). The Ca2+ sensor protein swiprosin-1/EFhd2 is present in neurites and involved in kinesin-mediated transport in neurons. *PLoS One, 9*(8), e103976. https://doi.org/10.1371/journal.pone.0103976

Ramesh, T., Kim, Y.-D., Kwon, M.-S., Jun, C.-D., & Kim, S.-W. (2009). Swiprosin-1 regulates cytokine expression of human mast cell line HMC-1 through actin remodeling. *Immune network*, *9*(6), 274-284. https://doi.org/10.4110/in.2009.9.6.274

Ramos Rego, I., Santos Cruz, B., Ambrósio, A. F., & Alves, C. H. (2021). TRAP1 in Oxidative Stress and Neurodegeneration. *Antioxidants (Basel)*, *10*(11). https://doi.org/10.3390/antiox10111829

Ransohoff, R. M. (2016). How neuroinflammation contributes to neurodegeneration. *Science*, *353*(6301), 777-783. https://doi.org/10.1126/science.aag2590

Rauch, J. N., Luna, G., Guzman, E., Audouard, M., Challis, C., Sibih, Y. E., Leshuk, C., Hernandez, I., Wegmann, S., Hyman, B. T., Gradinaru, V., Kampmann, M., & Kosik, K. S. (2020). LRP1 is a master regulator of tau uptake and spread. *Nature*, *580*(7803), 381-385. https://doi.org/10.1038/s41586-020-2156-5

Reynolds, A. D., Kadiu, I., Garg, S. K., Glanzer, J. G., Nordgren, T., Ciborowski, P., Banerjee, R., & Gendelman, H. E. (2008). Nitrated alpha-synuclein and microglial neuroregulatory activities. *J Neuroimmune Pharmacol*, *3*(2), 59-74. https://doi.org/10.1007/s11481-008-9100-z

Rosen, D. R., Siddique, T., Patterson, D., Figlewicz, D. A., Sapp, P., Hentati, A., Donaldson, D., Goto, J., O'Regan, J. P., Deng, H. X., & et al. (1993). Mutations in Cu/Zn superoxide dismutase gene are associated with familial amyotrophic lateral sclerosis. *Nature*, *362*(6415), 59-62. https://doi.org/10.1038/362059a0

Saito, T., & Saido, T. C. (2018). Neuroinflammation in mouse models of Alzheimer's disease. *Clin Exp Neuroimmunol*, *9*(4), 211-218. https://doi.org/10.1111/cen3.12475

Sałaciak, K., Koszałka, A., Żmudzka, E., & Pytka, K. (2021). The Calcium/Calmodulin-Dependent Kinases II and IV as Therapeutic Targets in Neurodegenerative and Neuropsychiatric Disorders. *International Journal of Molecular Sciences*, *22*(9), 4307. https://doi.org/10.3390/ijms22094307

Santacruz, K., Lewis, J., Spires, T., Paulson, J., Kotilinek, L., Ingelsson, M., Guimaraes, A., DeTure, M., Ramsden, M., McGowan, E., Forster, C., Yue, M., Orne, J., Janus, C., Mariash, A., Kuskowski, M., Hyman, B., Hutton, M., & Ashe, K. H. (2005). Tau suppression in a neurodegenerative mouse model improves memory function. *Science*, *309*(5733), 476-481. https://doi.org/10.1126/science.1113694

Sexton, C., Snyder, H., Beher, D., Boxer, A. L., Brannelly, P., Brion, J. P., Buee, L., Cacace, A. M., Chetelat, G., Citron, M., DeVos, S. L., Diaz, K., Feldman, H. H., Frost, B., Goate, A. M., Gold, M., Hyman, B., Johnson, K., Karch, C. M., . . . Carrillo, M. C. (2022). Current directions in tau research: Highlights from Tau 2020. *Alzheimers Dement*, *18*(5), 988-1007. https://doi.org/10.1002/alz.12452

Soliman, A. S., Umstead, A., Grabinski, T., Kanaan, N. M., Lee, A., Ryan, J., Lamp, J., & Vega, I. E. (2021). EFhd2 brain interactome reveals its association with different cellular and molecular processes. *J Neurochem*, *159*(6), 992-1007. https://doi.org/10.1111/jnc.15517

Spires, T. L., Orne, J. D., SantaCruz, K., Pitstick, R., Carlson, G. A., Ashe, K. H., & Hyman, B. T. (2006). Region-specific dissociation of neuronal loss and neurofibrillary pathology in a mouse model of tauopathy. *Am J Pathol*, *168*(5), 1598-1607. https://doi.org/10.2353/ajpath.2006.050840

Spires-Jones, T. L., Stoothoff, W. H., de Calignon, A., Jones, P. B., & Hyman, B. T. (2009). Tau pathophysiology in neurodegeneration: a tangled issue. *Trends Neurosci*, *32*(3), 150-159. https://doi.org/10.1016/j.tins.2008.11.007

Stephan, A. H., Barres, B. A., & Stevens, B. (2012). The complement system: an unexpected role in synaptic pruning during development and disease [Article]. *Annu Rev Neurosci*, *35*, 369-389. https://doi.org/10.1146/annurev-neuro-061010-113810

Sydow, A., Van der Jeugd, A., Zheng, F., Ahmed, T., Balschun, D., Petrova, O., Drexler, D., Zhou, L., Rune, G., Mandelkow, E., D'Hooge, R., Alzheimer, C., & Mandelkow, E. M. (2011). Tau-induced defects in synaptic plasticity, learning, and memory are reversible in transgenic mice after switching off the toxic Tau mutant. *J Neurosci*, *31*(7), 2511-2525. https://doi.org/10.1523/JNEUROSCI.5245-10.2011

Tong, L. C., Wang, Z. B., Zhang, J. Q., Wang, Y., Liu, W. Y., Yin, H., Li, J. C., Su, D. F., Cao, Y. B., Zhang, L. C., & Li, L. (2021). Swiprosin-1 deficiency in macrophages alleviated atherogenesis. *Cell Death Discov*, *7*(1), 344. https://doi.org/10.1038/s41420-021-00739-y

Tracy, T. E., Madero-Perez, J., Swaney, D. L., Chang, T. S., Moritz, M., Konrad, C., Ward, M. E., Stevenson, E., Huttenhain, R., Kauwe, G., Mercedes, M., Sweetland-Martin, L., Chen, X., Mok, S. A., Wong, M. Y., Telpoukhovskaia, M., Min, S. W., Wang, C., Sohn, P. D., . . . Gan, L. (2022). Tau interactome maps synaptic and mitochondrial processes associated with neurodegeneration. *Cell*, *185*(4), 712-728 e714. https://doi.org/10.1016/j.cell.2021.12.041

Tu, Y., Zhang, L., Tong, L., Wang, Y., Zhang, S., Wang, R., Li, L., & Wang, Z. (2018). EFhd2/swiprosin-1 regulates LPS-induced macrophage recruitment via enhancing actin polymerization and cell migration. *Int Immunopharmacol*, *55*, 263-271. https://doi.org/10.1016/j.intimp.2017.12.030

Vanderweyde, T., Apicco, D. J., Youmans-Kidder, K., Ash, P. E. A., Cook, C., Lummertz da Rocha, E., Jansen-West, K., Frame, A. A., Citro, A., Leszyk, J. D., Ivanov, P., Abisambra, J. F., Steffen, M., Li, H., Petrucelli, L., & Wolozin, B. (2016). Interaction of tau with the RNA-Binding Protein TIA1 Regulates tau Pathophysiology and Toxicity. *Cell Rep*, *15*(7), 1455-1466. https://doi.org/10.1016/j.celrep.2016.04.045

Vazquez-Rosa, E., Rodriguez-Cruz, E. N., Serrano, S., Rodriguez-Laureano, L., & Vega, I. E. (2014). Cdk5 phosphorylation of EFhd2 at S74 affects its calcium binding activity. *Protein Sci*, *23*(9), 1197-1207. https://doi.org/10.1002/pro.2499

Vega, I. E. (2016). EFhd2, a Protein Linked to Alzheimer's Disease and Other Neurological Disorders. *Front Neurosci*, *10*, 150. https://doi.org/10.3389/fnins.2016.00150

Vega, I. E., Sutter, A., Parks, L., Umstead, A., & Ivanova, M. I. (2018). Tau's Three-Repeat Domain and EFhd2 Co-incubation Leads to Increased Thioflavin Signal. *Front Neurosci*, *12*, 879. https://doi.org/10.3389/fnins.2018.00879

Vega, I. E., Traverso, E. E., Ferrer-Acosta, Y., Matos, E., Colon, M., Gonzalez, J., Dickson, D., Hutton, M., Lewis, J., & Yen, S. H. (2008). A novel calcium-binding protein is associated with tau proteins in tauopathy. *J Neurochem*, *106*(1), 96-106. https://doi.org/10.1111/j.1471-4159.2008.05339.x

Vega, I. E., Umstead, A., & Kanaan, N. M. (2019). EFhd2 Affects Tau Liquid-Liquid Phase Separation. *Front Neurosci*, *13*, 845. https://doi.org/10.3389/fnins.2019.00845

Vuadens, F., Rufer, N., Kress, A., Corthesy, P., Schneider, P., & Tissot, J. D. (2004). Identification of swiprosin 1 in human lymphocytes. *Proteomics*, *4*(8), 2216-2220. https://doi.org/10.1002/pmic.200300779

Wang, W. X., Huang, Q., Hu, Y., Stromberg, A. J., & Nelson, P. T. (2011). Patterns of microRNA expression in normal and early Alzheimer's disease human temporal cortex: white matter versus gray matter. *Acta Neuropathol*, *121*(2), 193-205. https://doi.org/10.1007/s00401-010-0756-0

Wang, Y., & Mandelkow, E. (2016). Tau in physiology and pathology. *Nat Rev Neurosci*, *17*(1), 5-21. https://doi.org/10.1038/nrn.2015.1

Wittmann, C. W., Wszolek, M. F., Shulman, J. M., Salvaterra, P. M., Lewis, J., Hutton, M., & Feany, M. B. (2001). Tauopathy in Drosophila: neurodegeneration without neurofibrillary tangles. *Science*, *293*(5530), 711-714. https://doi.org/10.1126/science.1062382

Wu, J., Xu, X., Duan, J., Chai, Y., Song, J., Gong, D., Wang, B., Hu, Y., Han, T., Ding, Y., Liu, Y., Li, J., & Cao, X. (2024). EFHD2 suppresses intestinal inflammation by blocking intestinal epithelial cell TNFR1 internalization and cell death. *Nat Commun*, *15*(1), 1282. https://doi.org/10.1038/s41467-024-45539-x

Xue, B., Qu, Y., Zhang, X., & Xu, X. F. (2022). miRNA-126a-3p participates in hippocampal memory via alzheimer's disease-related proteins. *Cereb Cortex*, *32*(21), 4763-4781. https://doi.org/10.1093/cercor/bhab515

Zhai, J., Strom, A. L., Kilty, R., Venkatakrishnan, P., White, J., Everson, W. V., Smart, E. J., & Zhu, H. (2009). Proteomic characterization of lipid raft proteins in amyotrophic lateral sclerosis mouse spinal cord. *Febs j*, *276*(12), 3308-3323. https://doi.org/10.1111/j.1742-4658.2009.07057.x

Zhang, S., Tu, Y., Sun, Y. M., Li, Y., Wang, R. M., Cao, Y., Li, L., Zhang, L. C., & Wang, Z. B. (2018). Swiprosin-1 deficiency impairs macrophage immune response of septic mice. *JCI Insight*, *3*(3). https://doi.org/10.1172/jci.insight.95396

Zhang, W., Chen, L., Lu, X., Dong, X., Feng, M., Tu, Y., & Wang, Z. (2024). EFHD2 regulates T cell receptor signaling and modulates T helper cell activation in early sepsis. *Int Immunopharmacol*, *133*, 112087. https://doi.org/10.1016/j.intimp.2024.112087

Zhang, W., Tarutani, A., Newell, K. L., Murzin, A. G., Matsubara, T., Falcon, B., Vidal, R., Garringer, H. J., Shi, Y., Ikeuchi, T., Murayama, S., Ghetti, B., Hasegawa, M., Goedert, M., & Scheres, S. H. W. (2020). Novel tau filament fold in corticobasal degeneration. *Nature*, *580*(7802), 283-287. https://doi.org/10.1038/s41586-020-2043-0

Zhang, Y., Wu, K. M., Yang, L., Dong, Q., & Yu, J. T. (2022). Tauopathies: new perspectives and challenges. *Mol Neurodegener*, *17*(1), 28. https://doi.org/10.1186/s13024-022-00533-z

Zuliani, I., Lanzillotta, C., Tramutola, A., Francioso, A., Pagnotta, S., Barone, E., Perluigi, M., & Di Domenico, F. (2021). The Dysregulation of OGT/OGA Cycle Mediates Tau and APP Neuropathology in Down Syndrome. *Neurotherapeutics*, *18*(1), 340-363. https://doi.org/10.1007/s13311-020-00978-4